Winter 12-15-2014

The Late Ordovician Biogeochemical Carbon Cycle

John Garrecht Metzger
Washington University in St. Louis

WASHINGTON UNIVERSITY IN ST. LOUIS
Department of Earth and Planetary Sciences

Dissertation Examination Committee:
David A. Fike, Chair
Alexander S. Bradley
Jeffrey G. Catalano
Jill D. Pasteris
Langhorne (Taury) B. Smith

The Late Ordovician Biogeochemical Carbon Cycle

by

J. Garrecht Metzger

A dissertation presented to the
Graduate School of Arts & Sciences
of Washington University in
partial fulfillment of the
requirements for the degree
of Doctor of Philosophy

December 2014
St. Louis, Missouri

Table of Contents

List of Figures

List of Tables

Acknowledgments

When you're a kid there are a lot of things you'd like to be when you "grow up." At different points in time I wanted to be a chemist and a rock star. I guess they've each become partially true, as now I'm a "rock chemist" of sorts. Upon reflection though, the journey to here seems a bit circuitous. Growing up on the ocean hundreds of miles from real rock outcrops, going to college in the foot of the Blue Ridge Mountains and studying water, and finally moving to the middle of the country to study marine rocks. It's also been challenging and at times, grueling, difficult in ways I couldn't have imagined, but still deeply rewarding. Simply put, I could not have made it through this degree without the support and inspiration from so many individuals. Thank you for helping me achieve my goals.

First, I would like to thank my advisor, Dr. David Fike. David's combination of intellect, enthusiasm, generosity, and compassion is a rare occurrence. He has been a rigorous teacher with high expectations, but also patient and instructive. The honesty and dedication with which he approaches his science is inspiring. There is no simple way for me to describe the things I have learned from David. In its place, I will say that it's been a privilege to work for one of my science role models. I look forward to future collaborations.

I would like to thank my committee members, both past and present, for their insightful conversations and willingness to serve as committee members and help me grow as a scientist. Those individuals are Dr. Jeffrey Catalano, Dr. Alex Bradley, Dr. Jill Pasteris, Dr. Robert Criss, Dr. Frédéric Moynier, and Dr. Taury Smith. I would like to thank my collaborators Glenn Robert Osburn, Aaron Addison, Claire Guo, Dr. Samuel Bowring, Dr. Jahan Ramezani, and Dr. Philip Pogge von Strandmann. I would like to thank the staff at the NY, OH, PA, WV, and KY State Geological Surveys for their help with so, so many things.

I would like to thank the staff, instructors, and my classmates of the 2013 International Geobiology Field Course. To live and learn among such a high caliber of scientist was unforgettable. To my classmates and friends in the EPS department: Thank you for knowledge, encouragement, laughs in the good times, and help in the bad times. Specifically: Kun Wang, Pierre Haenacour, Martin Pratt, Brandon Mahan, Michael Zanetti, Torin O'Brien, Margaret Anne Hinkle, Abigail Fraeman, Paul Savage, Stephen Chemtob, Allison Beehr, Rachel Gesserman, Maxwell Thiemans, Jon Lewis, and many more. Special thanks to Rachel Folkerts for two years as an outstanding field assistant. Thanks to the library staff for helping find so many obscure documents. Thanks to the office staff for helping me navigate the world of university forms.

I would like to thank various funding sources and institutions for letting me travel the world doing and disseminating my science. These include the Department of Earth and Planetary Sciences, the Graduate School of Arts and Sciences, the Missouri Space Grant Consortium, the Agouron Institute, the Geological Society of America, DOSECC, the David and Lucile Packard Foundation, the Hanse-Wissenschaftskolleg, the National Science Foundation, and NASA.

I would like to thank my family and friends for their support during this challenging part of my life. Special thanks to Dr. Jessica Whitfield for being such a bright source of encouragement and helping put things in perspective whenever it was needed. This would not have been the same without you. Finally, I'd like to thanks to my sister, Genevieve Metzger, whose advice I cherished and whose natural gifts for science I admire.

J. Garrecht Metzger

Washington University in Saint Louis

November 14th, 2014

This work is dedicated to the scientists and musicians whose works helped me see the world in ways I never would have by myself.

Chapter 1

Introduction

J. Garrecht Metzger

The isotopic composition of the marine dissolved inorganic carbon ($\delta^{13}C_{DIC}$)[1] has been the focus of intense research as marine DIC is the largest reactive pool of carbon on the surface of the Earth. On short time scales ($\leq 10^2$ years) $\delta^{13}C_{DIC}$ changes largely as a function of the rates of biological uptake during photosynthesis and respiration of organic matter (e.g., Patterson & Walter 1994; Gruber et al., 1999). Over longer time scales $\delta^{13}C_{DIC}$ is thought to change largely as a function of the isotopic signatures and fluxes of carbon being delivered to the ocean during weathering, volcanic emissions, and carbon being buried in the ocean as organic carbon and carbonates (*sensu* Kump & Arthur, 1999). Because the ocean is thought to be isotopically well-mixed on the ~1,500 year scale, changes in $\delta^{13}C_{DIC}$ are recorded in sediments deposited synchronously across the ocean. The isotopic fractionation between DIC and carbonate is small so that $\delta^{13}C_{DIC} \approx \delta^{13}C_{DIC}$. Therefore, a carbonate deposited in the Atlantic Basin should record the same $\delta^{13}C_{carb}$ signal in the Pacific Basin. This allows $\delta^{13}C_{carb}$ to be used as a stratigraphic tool that correlates relative time and has given rise to the field of "carbon isotope chemostratigraphy."

[1] $\delta^{13}C_{carb} = [(^{13}C/^{12}C)_{sample} - (^{13}C/^{12}C)_{standard} - 1] \bullet 1{,}000‰$ where $(^{13}C/^{12}C)$ is the abundance ratio in either a sample or standard. The standard, V-PDB, is defined as 0‰. This is analogous to a percent difference from a standard, but in parts per thousand ("per mil") rather than per hundred ("per cent"). Subscript "carb" referes to carbonate.

The first modern study that utilized the stable isotopes of carbonate carbon ($\delta^{13}C_{carb}$) for stratigraphic correlation was Scholle and Arthur (1980). While these authors were not the first to produce a record of $\delta^{13}C_{carb}$ through time, previous workers had sampled at too coarse of a resolution to notice secular (i.e., temporal) changes in $\delta^{13}C_{carb}$, giving rise to the erroneous hypothesis that the isotopic composition of oceanic dissolved inorganic carbon reservoir did not vary significantly through time. The new appreciation for high spatial and temporal resolution data sets that Scholle and Arthur produced gave rise to the field of carbon isotope chemostratigraphy. In the near three and a half decades since the Scholle and Arthur paper was published, carbon isotopes have become one of the main "workhorses" of the stratigrapher and Earth historian (e.g., Saltzman & Thomas, 2012). Intimate links have been made between major biological events – including evolutionary radiations (e.g., Maloof et al. 2010) and mass extinctions (e.g., Kump, 2003) – and environmental events such as glaciations (Kump et al., 1999) and asteroid impacts (D'Hondt, 2005). Despite significant advances in our understanding of the biogeochemical carbon cycle, uncertainty remains in how to interpret much of the $\delta^{13}C_{carb}$ record. Divergent interpretations stem in part from 1) sampling practices and screening methods, 2) an incomplete geological and climate record, 3) poor constraints on carbon cycle model parameters, and 4) the abundance of strata deposited in environments that have no modern analog with which to compare. This dissertation attempts to address points 1-3 and in turn is able to directly test some existing hypotheses about the carbon cycle and stratigraphic correlations. While this dissertation is focused on the Ordovician Period (444-485 Ma) many of the concepts should have general applications to rocks of various ages.

The Ordovician was chosen as the study interval for several reasons. First, Ordovician-aged rocks are widespread on the surface and in the subsurface of the United States of America,

which allowed us to test questions related to spatial variations in $\delta^{13}C_{carb}$ across different depositional environments. Second, there are numerous K-bentonites (altered volcanic ash beds) that are scattered throughout the interval (Kolata et al., 1996), which allows for temporal correlations independent of $\delta^{13}C_{carb}$ and supplies absolute ages using radiometric dating techniques. Third, much of the Late Ordovician of North America is carbonate-rich, which is required for $\delta^{13}C_{carb}$ stratigraphy. Scientifically, the Ordovician is amongst the most important intervals in Earth history. Within this geologic period is the greatest diversification in marine invertebrates in history (Webby et al., 2004), the first of the five major mass extinctions of the Phanerozoic (Sepkowski, 1996), the first major ice age in ~140 Ma and the first glaciation since the evolution of metazoa (animals), some of the largest carbonate platforms of the Phanerozoic (Kiessling et al., 2003), some of the highest relative sea levels of the Phanerozoic (Haq & Shutter, 2008), and two of the largest volcanic ash deposits of the Phanerozoic. These strata have been studied, in many cases, for over a hundred years (e.g., Ulrich, 1904; Ruedemann, 1925; Kay, 1935; Kay, 1937; Martin et al., 1961; Thompson, 1992) and have substantial geologic context already established. This allowed us to employ recent analytical and theoretical advancements to refine the time and nature of environmental change as well as test hypotheses related to the chemical composition of the Ordovician ocean.

Chapter 2 focuses on method development for identifying post-depositional alteration (i.e., diagenesis) of $\delta^{13}C_{carb}$ signals in two outcrop sections from Missouri. This topic is of central interest to stratigraphers and Earth historians because a primary ocean $\delta^{13}C_{carb}$ signal is required for correlations and environmental reconstructions. The chapter focuses specifically on the Guttenberg $\delta^{13}C$ excursion, a globally correlated, positive ~3‰ event that is ~400 kyr in duration. The Guttenberg excursion is one of two globally correlated $\delta^{13}C_{carb}$ excursions in the

Late Ordovician and is found on multiple modern and paleocontinents (e.g., Patzkowsky et al., 1997; Martma, 2005; Ludvigson et al., 2004; Young et al., 2005; Bergström et al., 2010; Munnecke et al, 2011). Observed spatial heterogeneity in $\delta^{13}C_{carb}$ data during the Guttenberg excursion was previously interpreted as primary heterogeneity in $\delta^{13}C$ of the marine inorganic carbon pool (Holmden et al., 1998; Young et al., 2005), the source of carbonate carbon. We use thin section petrography, trace element geochemistry, and stable isotope analyses of C and O to show that differences in the abundance of cements, which contain post-depositional C and O signatures, can produce cm-scale variations in $\delta^{13}C_{carb}$ and $\delta^{18}O_{carb}$. The covariation between petrographic evidence for cement abundance and diagenetic overprint of the primary $\delta^{13}C_{carb}$ and $\delta^{18}O_{carb}$ signal allows the construction of an isotope data filter. Filtering samples increases correlation quality. We find that locations with supposed primary $\delta^{13}C_{carb}$ signals that are different than the global $\delta^{13}C_{carb}$ signal are instead consistent with local diagenetic alteration and are located only short distances from locations $\delta^{13}C_{carb}$ signals that appear to track the global $\delta^{13}C_{carb}$ trend. Consideration of the spatial patterns in $\delta^{13}C_{carb}$ in the new diagenetic framework leads us to conclude there is no evidence for a significant long-distance isotopic gradient and that the isotopic signature of the dissolved inorganic carbon reservoir of the Laurentian epeiric sea was isotopically well-mixed.

Chapter 3 investigates an expanded time interval and spatial scale from that of the previous chapter to demonstrate how $\delta^{13}C_{carb}$ chemostratigraphy can be applied to well cuttings, crushed rock commonly collected from boreholes during subsurface oil and gas exploration. Six cuttings wells and one solid rock core were sampled in New York State and cover at a distance of ~300 km. Unlike solid rock core, which is expensive to collect and store, well cuttings are relatively inexpensive and are therefore collected continuously during exploration rather than in

limited intervals like cores. Unlike outcrops, subsurface samples are not limited by surface exposure and are therefore available in high spatial resolution. This allows us to construct a continuous $\delta^{13}C_{carb}$ record at high spatial *and* temporal resolution. Increased vertical continuity and spatial coverage come at a price, as facies information (e.g., bedding textures, macroscopic fossils) and textural evidence of alteration is greatly reduced; however, the high sampling resolution and close spacing of wells does allow identification of alteration on the regional scale.

While we are not the first to publish $\delta^{13}C_{carb}$ records obtained from well cuttings (e.g., Burns & Matter, 1993; Fike et al., 2006), no study had outlined sampling strategies for these materials, so we tackle this very issue in Chapter 3. We demonstrate that if cuttings are collected over small enough intervals (e.g., 3 m per sample) and in areas of sufficiently rapid sedimentation rate, $\delta^{13}C_{carb}$ records from cuttings suffer little to no loss in fidelity as compared to outcrop or core studies. The sampling of closely spaced wells allowed us to confidently identify $\delta^{13}C_{carb}$ intervals for chemostratigraphic correlation, which were used to construct a refined $\delta^{13}C_{carb}$ reference curve for the Late Ordovician. We also used this high spatial sampling density to identify regional variations in diagenetic alteration, thereby expanding the research goal of identifying diagenetic alteration from Chapter 2 to a new spatial scale. Finally, we were able to unambiguously demonstrate the diachronous facies shift from carbonates to shales across New York State, an issue that geologists and paleontologists have debated for nearly a century.

Chapter 4 takes the sampling methods from the previous chapter and expands the study region to include Pennsylvania, West Virginia, Ohio, and Kentucky while adding 46 new locations. We are able to provide absolute age constraints by measuring U-Pb content in zircons found in K-bentonites. K-bentonites were from taken outcrops in Missouri because in those locations the Guttenberg excursion is tightly bracketed by K-bentonites. With a calibrated

$\delta^{13}C_{carb}$ timeline established, we are able to investigate temporal patterns in sediment accumulation rate and sea level change. The study includes the upper Sandbian and lower Katian Stages, the boundary of which has been hypothesized to represent a shift from "Greenhouse" to "Icehouse" conditions ~10 Myr prior to the End Ordovician Hirnantian glacial maximum (Frakes et al., 1992; Pope & Steffan, 2003; Saltzman & Young, 2005; Page et al., 2007; Loi et al., 2010), an issue that is still being debated (Ettensohn, 2010; Quinton & MacLeod, 2014). The creation of a large $\delta^{13}C_{carb}$ data set obtained from subsurface samples revealed changes in the sediment accumulation rate across the Sandbian-Katian boundary that were not previously identifiable using outcrop data alone. The sedimentation shifts are consistent with a eustatic sea level change, which we interpret as likely glaciogenic. This chapter supplies more stratigraphic evidence that the major climatic shifts that ultimately resulted in the Hirnantian mass extinction began ~10 Myr prior earlier than the event itself, which represents a glacial maximum rather than the initiation of glaciation.

Chapter 5 uses the environmental and temporal constraints supplied in Chapter 4 along with a carbon cycle box model to identify the source of the Guttenberg excursion. The most prevalent theory invokes enhanced burial of organic carbon in the cratonic seas as the result of upwelling of nutrient-rich waters (Patzkowsky et al., 1997; Holmden et al., 1998; Saltzman & Young, 2005; Young et al., 2005). Another competing theory is that the Guttenberg excursion is the result of a change in weathering regime where proportionally more carbonates are weathered during sea level lowstand (Page et al., 2007). Organic carbon burial in cratonic seas is unlikely to quantitatively impact the global carbon budget and therefore upwelling (and burial in general) in the midcontinent is ruled out as a tenable explanation for the source of the excursion. The weathering of carbonates can only drive the excursion if weathering is balanced (i.e., the

absolute flux of weathering is constant, but the relative fraction of carbonates, volcanic input, and organic carbon weathering shifts). This is because any increase in weathering flux additional carbonate weathering will have a negligible effect on $\delta^{13}C_{carb}$ or produce a minor negative excursion. It seems likely that weathering flux does increase when large carbonate platforms are exposed, which makes it much more difficult to drive the excursion by weathering. We suggest that the main driver of the excursion was a rapid increase in the burial of organic matter in marginal and deep marine settings with a gradational drop in organic carbon burial roughly proportional to sea level rise at the end of the excursion. The changes in organic carbon burial may result from the temperature-dependent oxidation of organic matter by marine microorganisms. Tight chronological constraints supplied by K-bentonite ages allow us to directly convert the *stratigraphic expression* (shape) of the $\delta^{13}C_{carb}$ excursion to time. This gives us another level of interpretive power to further constrain the source *and* timing of forces that drove the $\delta^{13}C_{carb}$ excursion. We suggest that rate of change in forcing is rapid during the initial portion of the excursion and declines more gradually during the latter portion.

REFERENCES

Bergstrom, S. M., Agematsu, S., Schmitz, B., 2010, Global Upper Ordovician correlation by means of $\delta^{13}C$ chemostratigraphy: implications of the discovery of the Guttenberg $\delta^{13}C$ excursion (GICE) in Malaysia: Geological Magazine, v. **147**, p. 641-651.

Burns, S. J., Matter, A., 1993, Carbon isotopic record of the latest Proterozoic from Oman: Eclogae Geologicae Helvetiae, v. **86**, p. 595-607.

D'Hondt, S., 2005, Consequences of the Cretaceous/Paleogene mass extinction for marine ecosystems: Annual Review of Ecology, Evolution and Systematics, **v. 36**, p. 295-317.

Ettensohn, F. R., 2010, Origin of Late Ordovician (mid-Mohawkian) temperate-water conditions on southeastern Laurentia: Glacial or tectonic?, *in* Finney, S. C., Berry, W.B.N., ed., GSA Special Paper **466**, p. 163-175.

Fike. D.A., G., J.P., Pratt, L.M., Summons, R.E., 2006, Oxidation of the Ediacaran Ocean: Nature, v. **444**, p. 744-747.

Frakes, L. A., Francis, J.E., Syktus, J.I., 1992, Climate Modes of the Phanerozoic, Great Britian, Press Syndicate of the University of Cambridge, p. 274.

Haq, B. U., Schutter, S.R., 2008, A chronology of Paleozoic sea-level changes: Science, v. **322**, p. 64-68.

Holmden, C., Creaser, R. A., Muehlenbachs, K., Leslie, S. A., and Bergstrom, S. M., 1998, Isotopic evidence for geochemical decoupling between ancient epeiric seas and bordering oceans: Implications for secular curves: Geology, v. **26**, p. 567-570.

Kay, G. M., 1935, Ordovician System of the upper Mississippi Valley, Kansas Geological Society 9th regional field conference, Upper Mississippi River Valley, Kansas Geological Society, p. 281-295.

Kay, G. M., 1937, Stratigraphy of the Trenton Group: Geological Society of America Bulletin, v. **48**, p. 233-302.

Kiessling, W., Flügel, E., Golonka, J., 2003, Patterns of Phanerozoic carbonate platform sedimentation: Lethaia, v. **36**, p. 195-226.

Kolata, D. R., Huff, W.D., Bergström, S.M., 1996, Ordovician K-bentonites of eastern North America: GSA Special Paper **313**, p. 84.

Kump, L., R., Arthur, M.A., 1999, Interpreting carbon-isotope excursions: carbonates and organic matter: Chemical Geology, v. **161**, p. 181-198

Kump, L. R., 2003, The geochemistry of mass extinctions, *in* Mackenzie, F. T., ed., Sediments, Diagenesis, and Sedimentary Rocks, Treatise on Geochemistry Vol. 7: Oxford, England, Elsevier-Pergamon, p. 351-368.

Loi, A., Ghienne, J.L., Dabard, M.P., Paris, F., Botquelen, A., Christ, N., Elaouad-Debbaj, Z., Gorini, A., Vidal, M., Videt, B., Destombes, J., 2010, The Late Ordovician glacio-eustatic record from a high-latitude storm-dominated shelf-succession: The Bou Ingarf

section (Anti-Atlas, Southern Morocco): Palaeogeography Palaeoclimatology Palaeoecology, v. **296**, p. 332-358.

Ludvigson, G. A., Witzke, B.J., Gonzàlez, L.A., Carpenter, S.J., Schneider, C.L., Hasiuk, F., 2004, Late Ordovician (Turnian-Chatfieldian) carbon isotope excursions and their stratigraphic and paleoceanographic significance: Palaeogeography, Palaeoclimatology, Palaeoecology, v. **210**, p. 187-214.

Martma, T., 2005, Ordovician carbon isotopes, *in* Põldvere, A., ed., Estonian Geological Sections, Kerguta (564) Drill Core: Geological Survey of Estonia Bulletin, v. **6**, Estonian Geological Survey, p. 25-30.

Maloof, A. C., Ramezani, J., Bowring, S.A., Fike, D.A., Porter, S.M., Mazouad, M., 2010, Constraints on early Cambrian carbon cycling from the duration of the Nemakit-Daldynian—Tommotian boundary $\delta^{13}C$ shift, Morocco: Geology, v. **38**, p. 623-626.

Martin, J. A., Knight, R.D., Hayes, W.C., 1961, Ordovician System, *in* Koenig, J. W., ed., The stratigraphic succession in Missouri, Volume 40, Missouri Geological Survey and Water Resources, p. 32-35.

Munnecke, A., Zhang, Y. L., Cheng, J., 2011, Stable carbon isotope stratigraphy in the Ordovician of South China: Palaeogeography Palaeoclimatology Palaeoecology, v. 307, p. 17-43.

Page, A. A., Zalasiewicz, J.A., Williams, M., Popov, L.E., 2007, Were transgressive black shales a negative feedback modulating glacioeustasy in the Early Palaeozoic Icehouse?, *in* Williams, M., Haywood, A.M., Gregory, F.J., Schmidt, D.N., ed., Deep-Time Perspectives on Climate Change: Marrying the Signal from Computer Models and Biological Proxies: London, The Geological Society of London, p. 123-156.

Patzkowsky, M. E., Slupik, L.M., Arthur, M.A., Pancost, R.D., Freeman, K.H.,, 1997, Late Middle Ordovician environmental change and extinction: Harbinger of the Late Ordovician or continuation of Cambrian patterns?: Geology, v. **25**, p. 911-914.

Pope, M., Steffan, J.B., 2003, Widespread, prolonged late Middle to Late Ordovician upwelling in North America: A proxy record of glaciation?: Geology, v. **31**, p. 63-66.

Ruedemann, R., 1925, The Utica and Lorraine Formations of New York, Part I: Stratigraphy, New York State Museum Bulletin No. 258, p. 176.

Quinton, P. C., MacLeod, K.G., 2014, Oxygen isotopes from conodont apatite of the midcontinent, US: Implications for Late Ordovician climate evolution: Palaeogeography Palaeoclimatology Palaeoecology, v. **404**, p. 57-66.

Saltzman, M. R., Young, S.A., 2005, Long-lived glaciation in the Late Ordovician? Isotopic and sequence-stratigraphic evidence from western Laurentia: Geology, v. **33**, p. 109-112.

Saltzman, M. R., Thomas, E., 2012, Carbon isotope stratigraphy, *in* Gradstein, F. M., Ogg, J.G., Schmitz, M.D., Ogg, G.M., ed., The Geologic Time Scale 2012, Volume 1: Oxford, England, Elsevier, p. 207-232.

Sepkoski, J. J., 1996, Patterns of Phanerozoic Extinction: A Perspective from Global Data Bases, *in* Walliser, O. H., ed., Global Events and Event Stratigraphy in the Phanerozoic: Berlin, Springer, p. 35-52.

Scholle, P. A., Arthur, M.A., 1980, Carbon isotope fluctuations in Cretaceous Pelagic Limestones: Potential Stratigraphic and Petroleum Exploration Tool: AAPG Bulletin, v. **64**, p. 67-87.

Thompson, T. L., 1991, Paleozoic Successions in Missouri Part 2: Ordovician System, Rolla, Missouri Department of Natural Resources, Division of Geology and Land Survey, Missouri Geological Survey Report of Investigations, v. **2**, p. 282.

Ulrich, E. O., 1904, The quarrying industry of Missouri, *in* Buckley, E. R., Buehler, H.A., ed., v. **2**, Missouri Bureau of Geology and Mines, p. 109-111.

Webby, B. D., Droser, M.L., Paris, F., Percival, I., eds., The Great Ordovician Biodiversification Event, New York, New York, Columbia University Press.

Young, S. A., Saltzman, M.R., Bergström, S.M., 2005, Upper Ordovician (Mohawkian) carbon isotope ($\delta^{13}C$) stratigraphy in eastern and central North America: Regional expression of a perturbation of the global carbon cycle: Palaeogeography, Palaeoclimatology, Palaeoecology, v. **222**, p. 53-76.

Chapter 2

Techniques for Assessing Spatial Heterogeneity of Carbonate $\delta^{13}C$ Values: Implications for Craton-Wide Isotope Gradients

J. Garrecht Metzger & David A. Fike

Department of Earth and Planetary Sciences, Washington University, 1 Brookings Dr., St. Louis, MO 63130 USA; (gmetzger@levee.wustl.edu; dfike@levee.wustl.edu)

Metzger, J.G., Fike, D.A., 2013, Techniques for Assessing Spatial Heterogeneity of Carbonate $\delta^{13}C$ Values: Implications for Craton-Wide Isotope Gradients: Sedimentology, v. 60, p. 1405-1431. doi: 10.1111/sed.12033.

1. ABSTRACT

The sedimentary record of carbonate carbon isotopes ($\delta^{13}C_{carb}$) provides one of the best methods for correlating marine strata and understanding the long-term evolution of the global carbon cycle. This work focuses on the Late Ordovician Guttenberg isotopic carbon excursion, a ~2.5‰ positive $\delta^{13}C_{carb}$ excursion that is found in strata globally. Substantial variability in the apparent magnitude of the Guttenberg excursion and in its stratigraphic morphology between different localities has hampered high-resolution correlations and led to divergent reconstructions of ocean chemistry and the biogeochemical carbon cycle. This work investigates the magnitude, spatial scale, and sources of isotopic variability of the Guttenberg excursion in two sections from

Missouri, USA. Centimetre-scale isotope transects revealed variations in $\delta^{13}C_{carb}$ and $\delta^{18}O_{carb}$ greater than 2‰ across individual beds. Linear $\delta^{13}C_{carb}$–$\delta^{18}O_{carb}$ mixing lines, together with petrographic and elemental abundance data, demonstrate that much of the isotopic scatter in single beds was due to the mixing of isotopically distinct components and allowed objective sample screening to determine the 'least-altered' data. A $\delta^{18}O_{carb}$ filter based on empirical $\delta^{18}O_{carb}$ values of well-preserved carbonate mudstones allowed further sample discrimination. The resulting 'least-altered' $\delta^{13}C_{carb}$ profile improves the understanding of regional as well as continental-scale stratigraphic relationships in this interval. Correlations with other Laurentian sections strongly suggest that: (i) small-scale variability in Guttenberg excursion $\delta^{13}C_{carb}$ values may result in part from local diagenetic overprinting; (ii) peak-Guttenberg excursion $\delta^{13}C_{carb}$ values of the Midcontinent are not distinct from their Taconic equivalents; and (iii) no primary continental-scale spatial gradient in $\delta^{13}C_{carb}$ (e.g., arising from chemically distinct "aquafacies") is required during Guttenberg excursion-time. This study demonstrates the importance of detailed petrographic and geochemical screening of samples to be used for $\delta^{13}C_{carb}$ chemostratigraphy and for enhancing understanding of epeiric ocean chemistry.

2. INTRODUCTION

2.1 General Background

Secular variation in the carbon isotopic composition of marine limestones ($\delta^{13}C_{carb}$)[2] can be used to map the spatial and temporal patterns in sedimentation across basins and link these to environmental and ecological changes. A time-varying $\delta^{13}C$ signal in the marine dissolved inorganic carbon (DIC) reservoir can arise from changes in the flux and isotopic composition of

[2] $\delta^{13}C = [(^{13}C/^{12}C)_{sample})/(^{13}C/^{12}C)_{std} - 1] \bullet 10^3$, measured in permil (‰))

the major sources and sinks of carbon to and from the ocean (Kump & Arthur, 1999). The variation in $\delta^{13}C_{DIC}$ can be captured in coeval sediment as carbonate carbon ($\delta^{13}C_{carb}$) or following biological uptake as organic carbon ($\delta^{13}C_{org}$). The resulting $\delta^{13}C$ data provide a means to correlate sedimentary strata within and between sedimentary basins by aligning their $\delta^{13}C$ chemostratigraphic profiles (e.g., Knoll *et al.,*, 1986; Hayes *et al.,* 1999) revealing stratigraphic information undetectable using conventional lithostratigraphic or biostratigraphic methods. For example, discontinuous changes in $\delta^{13}C_{carb}$ profiles provide a means to identify cryptic hiatal surfaces in sedimentary strata (e.g., Jones *et al.,* 2011) because $\delta^{13}C_{carb}$ should smoothly vary when deposition is continuous. Even when deposition is continuous, various post-depositional processes, such as microbial oxidation of organic carbon (Patterson & Walter, 1994) and meteoric diagenesis (Allan & Matthews, 1982; Joachimski, 1994; Immenhauser et al., 2002), may alter a primary $\delta^{13}C_{carb}$ signal, typically toward more ^{13}C-depleted values. As such, screening for diagenetic alteration is critical when using $\delta^{13}C_{carb}$ data for basinal correlation or for reconstructing the evolution of the global carbon cycle.

The potential utility of $\delta^{13}C_{carb}$ chemostratigraphy for correlations and environmental reconstructions depends on spatial homogeneity in the isotopic composition of the marine DIC reservoir. Recently, it has been suggested that many marine strata, particularly those formed in epeiric settings with uncertain connections to the global ocean, have carbon isotope signatures in which local processes (e.g., aging of the water mass; Immenhauser *et al.*, 2008) variably overprint a global $\delta^{13}C$ signal (Simo *et al.,* 2003; Panchuk *et al.,* 2005; Panchuk *et al.,* 2006; Fanton & Holmden, 2007; Brand *et al.*, 2009), complicating regional- to global-scale correlations and attempts to understand the processes driving carbon cycle variability.

This work focuses on the Guttenberg carbon isotope excursion, a positive ~2.5‰ excursion in $\delta^{13}C_{carb}$ during the Mohawkian Series of the Upper Ordovician, which provides an example where chemostratigraphy has allowed for regional and global correlation of strata from different palaeoenvironments across much of the United States (Patzkowsky *et al.,* 1997; Ludvigson *et al.,* 2000; Ludvigson *et al.,* 2004; Young *et al.,* 2005; Bergström *et al.,* 2010a; Bergström *et al.,* 2010b; Coates *et al.,* 2010), portions of southeastern Canada (Bergström *et al.,* 2010a, Bergström *et al.,* 2010b), Sweden (Bergström *et al.,* 2004), Estonia (Martma, 2005; Kaljo *et al.,* 2007), China (Young *et al.,* 2005; Bergström *et al.,* 2009a), and Malaysia (Bergström *et al.,* 2010c). However, differences in the stratrigraphic expression of the Guttenberg excursion (including the shape of the $\delta^{13}C_{carb}$ curve as a function of stratigraphic position, as well as the pre-excursion, peak-excursion and post-excursion $\delta^{13}C_{carb}$ values and the degree of scatter) have hampered detailed correlation between sections and obscured a fundamental understanding of the environmental and/or ecological changes that caused the Guttenberg excursion (Patzkowsky *et al.*, 1997; Ludvigson *et al.*, 2004; Panchuck *et al.*, 2005; Young *et al.*, 2005; Panchuck *et al.*, 2006; Young *et al.*, 2008; Bergström *et al.*, 2010a).

In North America, stratigraphic correlations have been facilitated by the co-occurrence of the Guttenberg excursion and the two widely traceable K-bentonites, the Deicke and Millbrig (Kolata *et al.,* 1986; Kolata *et al.,* 1987; Kolata *et al.,* 1996; Kolata *et al.,* 1998; Kolata *et al.*, 2001). These bentonites act as time markers used to test chemostratigraphic and sequence stratigraphic models, providing a framework in which to investigate temporal and spatial variation in sedimentation rates (Leslie & Bergström, 1997), erosion (Railsback *et al.*, 2003), facies migration and sequence development (Holland & Patzkowsky, 1998), as well as geochemical and isotopic heterogeneities in carbonates and their palaeoceanographic sources

(Panchuk *et al.,* 2006; Fanton & Holmden, 2007). Ordovician strata are replete with bentonites (e.g., Kolata *et al*. 1996) and care must be taken in cross-continental correlation of K-bentonites, as apatite phenocryst geochemistry (Sell & Sampson, 2011) and radiometric ages (e.g., Huff, 2008) of Laurentian and Baltoscandian K-bentonites suggest that some previous bentonite-based correlations may not be correct.

The goals of this work are to: (i) document cm-scale variability in $\delta^{13}C_{carb}$ and $\delta^{18}O_{carb}$ and use petrographic and trace geochemical indicators of diagenesis better to understand the processes by which isotopic signals can be altered as they relate to depositional setting; (ii) develop an objective sample screening procedure to be used in bulk carbonate analysis for identifying least-altered data; (iii) use $\delta^{13}C_{carb}$ chemostratigraphy to correlate between two localities in Missouri, USA and re-evaluate existing stratigraphic relationships; and (iv) use this interpretative framework to compare the stratigraphic expression of the Guttenberg excursion in Missouri with existing records from across the continent to test hypotheses on the existence of large scale (10^3 to 10^4 km) spatial gradients in $\delta^{13}C_{carb}$ (i.e., "aquafacies" of Holmden *et al*., 1998) at this time.

2.2 Geologic Setting

Strata investigated in the present study occur within the Mohawkian Series of North America, which is roughly equivalent to the uppermost Sandbian to lower Katian Global Series (Figure 1;lBergström *et al.,* 2009b). Sections begin in the uppermost Turinian and end in the lower to middle Chatfieldian (North American Stages) based on correlations using globally extensive K-bentonites and biostratigraphy (Thompson, 1991; Leslie, 2000; Bergström *et al.,* 2009b; Bergström *et al.,* 2010a,b). During this time, Missouri was located in sub-equatorial

latitudes 15 to 30°S (Scotese & McKerrow, 1990 where sedimentation occurred in a warm, shallow sea (Figure 2A). The Mohawkian contains a major change in sediment deposition across Missouri (Thompson, 1991), other portions of the upper Mississippi Valley (Kolata *et al.,* 1998), and the mid-South (Holland & Patzkowsky, 1998). In Missouri, the geographic thickness patterns of stratigraphic units become roughly inverted by early Chatfieldian time (Kolata *et al.,* 1998) as the carbonate depocentre shifted north towards Iowa. The uplift of the Ozark Dome (modern day St. Francois Mountains) may have partially controlled sedimentation patterns and is thought to have intermittently interrupted regional carbonate sedimentation during the Early to Middle Ordovician, although sedimentation became more continuous during the Late Ordovician highstand (McCracken, 1966; Thompson, 1991). Further, the rhyolites and granites of the Ozark dome may have been an important siliciclastic source for the present study sections (Figure 2B). Although Mohawkian-aged strata in Missouri have been studied for over 100 years (e.g., Ulrich, 1904; Kay, 1935; Templeton & Willman, 1963; Kolata *et al.*, 1986), there is a dearth of literature that directly focuses on their deposition, sequence stratigraphy, and chemostratigraphy, especially when compared to the time-equivalent Trenton-Black River succession of the eastern United States (e.g., Brett *et al.*, 2004; Mitchell *et al.,* 2004; McLaughlin & Brett, 2007).

Chronostratigraphic relationships of selected Upper Ordovician sections across the North American Craton are shown in Figure 1 and were constructed using K-bentonite stratigraphy, biostratigraphy, and $\delta^{13}C_{carb}$ stratigraphy. The studied interval ranges from the upper Plattin Group through the lower Kimmswick Limestone. The Plattin Group (Platteville equivalent outside of Missouri, Figure 1) is thickest in nearby southwestern Illinois where it reaches over 200 m (Kolata *et al.,* 2001). The Plattin is ~140 m thick in southeastern Missouri near Cape Girardeau and thins northwestward, where 300 km northwest it is 14 m thick (Martin *et al.,*

1961). The Plattin is uppermost Turinian and is equivalent to the upper Black River succession of New York, based on K-bentonite stratigraphy of the Deicke K-bentonite dated to 454.5 ± 0.5

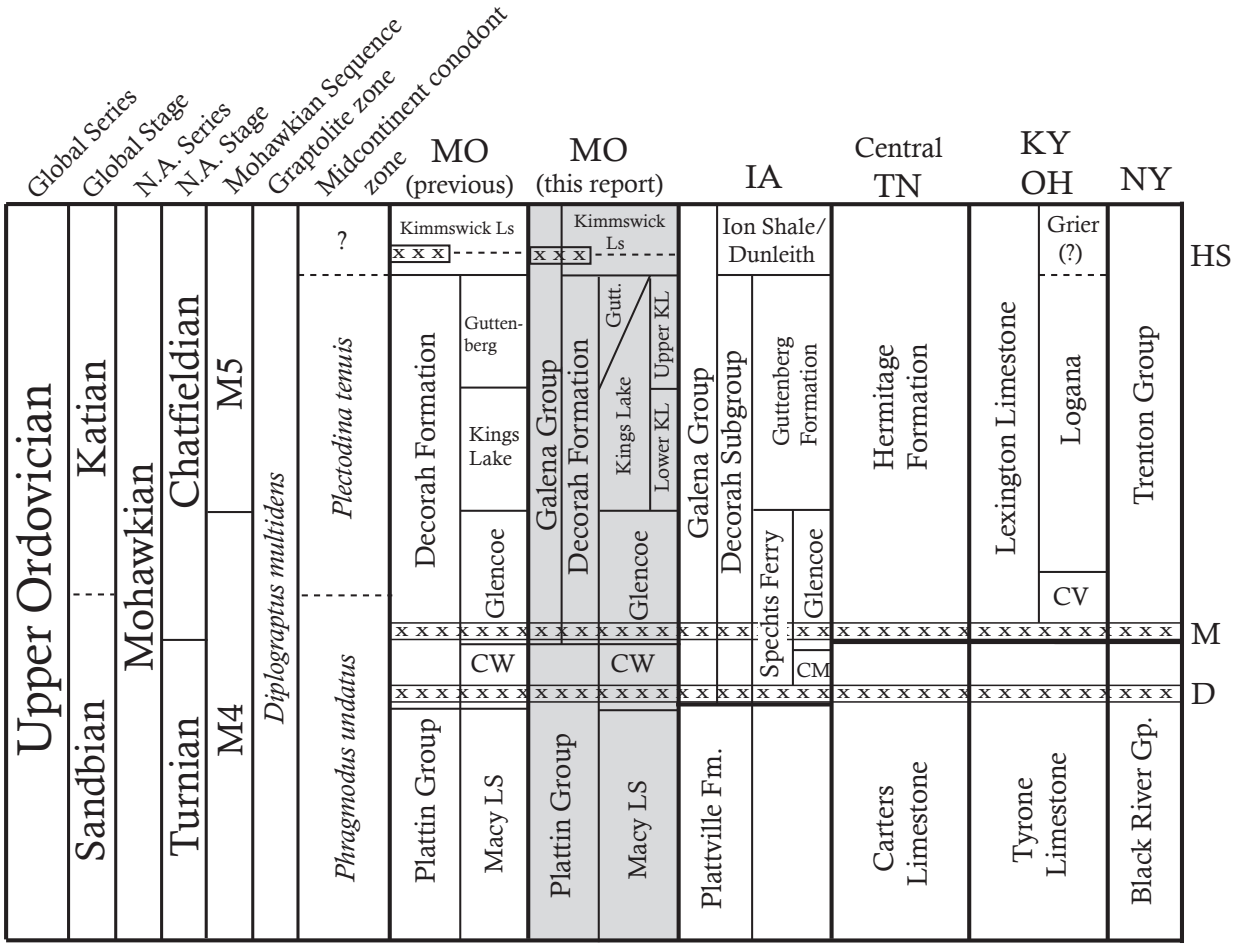

Figure 1. Proposed chronostratigraphic relationships of select locations within the United States. Series and stages taken from Bergström *et al.* (2009b). M4 and M5 refer to Mohawkian sequences (Holland & Patzkowsky, 1997; Holland & Patzkowsky, 1998). Biozones taken from Leslie (2000). Information for "Missouri (previous)" taken from Thompson (1991). "Missouri (this report)" constructed from new data and placement of the Castlewood Limestone into the Plattin group according to Kolata *et al.* (1998). "Upper KL" and "Lower KL" correspond to new divisions of the Kings Lake Limestone used in this work for central-southern Missouri. IA stratigraphy adapted from Ludvigson *et al.* (2004). Kentucky and Ohio information taken from Leslie (2000) and McLaughlin & Brett (2007). New York information adapted from Leslie (2000) and Mitchell *et al.* (2004). Horizontal bars with "X" correspond to K-bentonites. CM = Carimona, CV = Curdsville, CW = Castlewood, D = Deicke K-bentonite, Fm = Formation, Gp = Group, HS = House Springs K-bentonite, KW = Kimmswick Limestone, Ls = Limestone, M = Millbrig K-bentonite. Where correlations are ambiguous dashed lines and questions marks are used.

Ma (Tucker, 1992), and conodont biostratigraphy (Leslie, 2000; Brett *et al.,* 2004). The Plattin Group is interpreted to represent a major transgressive cycle as flooding spread north and west from the Sebree Trough, a bathymetric low that runs NE to SW along the northwestern Kentucky border (Witzke & Kolata, 1988). Plattin Group strata are dominated by thin-bedded, somewhat nodular mudstones characterized by fine-grained, heavily bioturbated, high-purity (>95% carbonate) limestones with partially dolomitized burrows (Thompson, 1991).

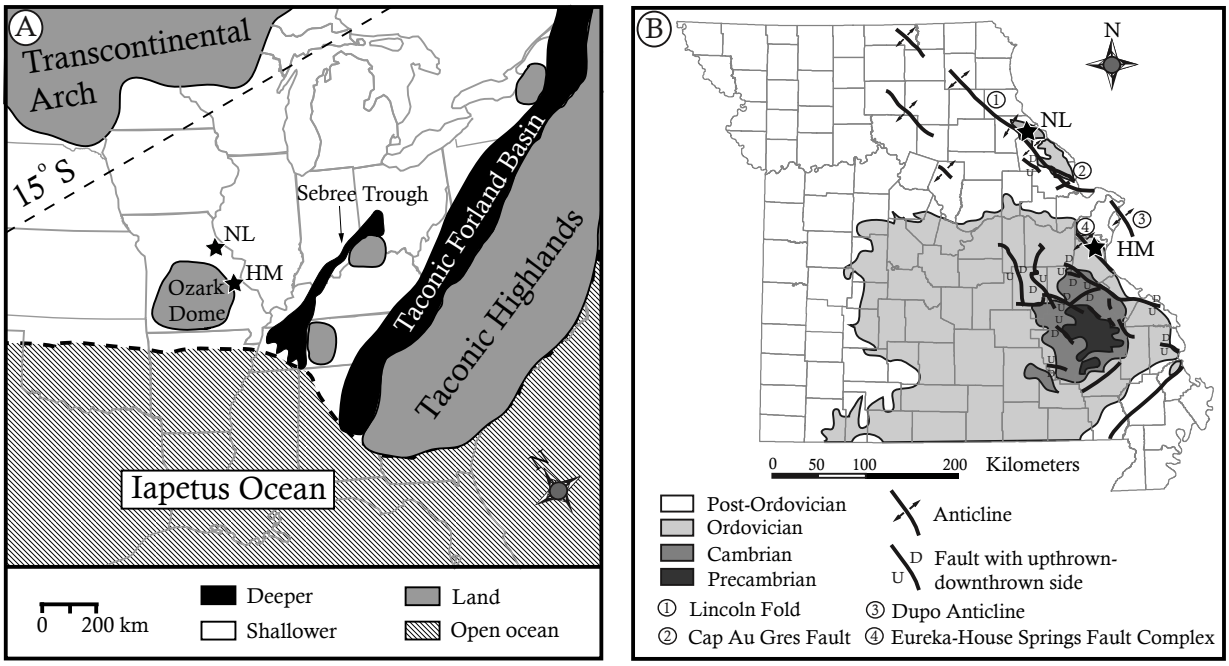

Figure 2. (A) Palaeogeographic map showing general depositional environment and important geologic structures (adapted from Scotese & McKerrow, 1990; Holland & Patzkowsky, 1998, Kolata *et al*., 2001; Simo *et al.*, 2003). Stars represent sample locations HM = Highway MM and NL = New London. (B) Map of Missouri showing sample locations, generalized surface stratigraphy (under the Pleistocene alluvium), and major structural features of eastern Missouri. Surface strata adapted from Missouri Department of Natural Resources (2009). Structural features adapted from McCracken (1966). Strata are sedimentary except Precambrian igneous rocks.

The overlying Galena Group is thickest in the northwest and pinches out approaching the Sebree Trough, where Plattin Group deposits are thickest; this represents an apparent

restructuring of sediment deposition patterns from Plattin time (Witzke & Kolata, 1988). In Missouri, Galena Group strata comprise the Decorah Formation (composed of the Glencoe Shale, Kings Lake Limestone, and Guttenberg Limestone) and the overlying Kimmswick Limestone. The Glencoe Shale contains dark, thinly bedded, fissile, carbonate-poor shales intercalated with planar, thin, sometimes discontinuous brachiopod-bryozoan calcarenites and calcirudites (Thompson, 1991; Kolata *et al.,* 1998), as well as the Millbrig K-bentonite, which is dated to 453.1 ± 1.3 Ma (Tucker & McKerrow, 1995) and defines the Turinian-Chatfieldian boundary (Ludvigson *et al*., 2004). The overlying Kings Lake Limestone is composed mostly of blue-grey carbonate mudstones and storm-bed packstones, both with thin blue shale partings. Kings Lake facies have been interpreted as transitional between the Glencoe Shale and the overlying Guttenberg Limestone in northeastern Missouri (Kolata *et al.,* 1986). In central and southern Missouri, the Kings Lake Limestone is unconformably overlain by the Kimmswick Limestone, while it is conformable with the overlying Guttenberg Limestone in northernmost Missouri. The Guttenberg Limestone is only found north of St. Louis, Missouri and like the underlying Kings Lake Limestone, is composed of mudstones with frequent carbonate storm beds. In Missouri, the brown mud and shale partings of the Guttenberg distinguish the unit from the underlying blue-grey mud and shale partings of the Kings Lake Limestone. The contact between the Guttenberg and the overlying Kimmswick Limestone is a minor unconformity in northern Missouri and rip-up lithoclasts from the Guttenberg Limestone and Kings Lake Limestone are found up to 20 cm into the lowermost Kimmswick Limestone (Kolata *et al.,* 1998).

The Kimmswick Limestone is a well-cemented, medium-grained to fine-grained crinoid-brachiopod-bryozoan grainstone (Thompson, 1991; Kolata *et al.,* 1998). Strata are thick to

massively bedded with evidence for crossbedding rare or absent in upper portions (Thompson, 1991). The Kimmswick is a very pure limestone (>98% carbonate) that contains abundant cm-diameter burrows that weather to a 'Swiss-cheese' texture similar to the Plattin Limestone. It is exposed at the surface in northern Missouri and erosionally truncated and overlain by Mid–Late Paleozoic sandstones south of St. Louis.

2.3 Study Locations

Two locations in eastern Missouri were chosen for high-resolution chemostratigraphic study (Figure 2). The first site is located 8 kilometres south of New London, Missouri along the eastern frontage road (East Side Drive) off of Highway 61, which is located a few hundred metres north of Spencer Creek (Lat: 39.522415°N, Long: 91.344629°W). The New London section is the same as Location 53 in Kolata *et al.* (1986). The sampled interval begins with 7.5 metres of the upper Plattin Limestone and continues through the Decorah Formation and extends 8 metres into the Kimmswick Limestone (Figure 3). The second site, Highway MM, is a fresh road-cut exposure found along Missouri State Highway MM near Barnhart, Missouri (Lat: 38.394101°N, Long: 90.543364°W) approximately 15 kilometres west of Location 63 of Kolata *et al.* (1986). This study is the first published geologic record for this location that the authors are aware of. The Highway MM section begins in the uppermost 10 to 15 m of the Plattin Limestone and continues through the Decorah Formation and into the first 5 m of the Kimmswick Limestone (Figure 4).

3. METHODS

3.1 Sampling and petrology methods

Field sampling in both locations was completed over a lateral distance of ~300 m along a single outcrop face. Individual beds (Highway MM: n = 80; New London: n = 69) were sampled at regular intervals where possible and some beds were collected in replicate (Tables 1 and 2). No large faults, fractures, folds, joints, or igneous features were observed at either location. Stratigraphic columns were constructed using a combination of the Dunham nomenclature and Wentworth-Udden grain-size terminology (Flügel, 2009). Stratigraphic units were identified in the field using the criteria in Thompson (1991). Deicke, Millbrig, and House Springs K-bentonites were identified in the field based on stratigraphic position (Kolata *et al.,* 1986), thickness, colour, clay content, degree of lithification, bedding geometry, and zircon abundance. In addition, several minor bentonites (HMMA, HMKL-1, NLKL-1, and NLM-2) were identified and named for the location/formation. Two of these bentonites (HMKL-1 and NLKL-1) were tentatively correlated in this study and may be equivalent to the Elkport K-bentonite of the upper Mississippi Valley (Kolata *et al.*, 1986); however, no definitive correlation of these minor bentonites to equivalents outside of the study area is made.

Forty-seven thin sections from 45 individual beds were analysed under transmitted and reflected light microscopy on a Leica petrographic microscope (model DM-2500P; Leica Microsystems GmbH, Wetzlar, Germany) with a maximum magnification of 500x. Photographs were taken with a Leica (model DFC 295) microscope-mounted camera.

3.2 Geochemical methods

3.2.1 Stable Carbon and Oxygen Isotope Analysis of Carbonate

Carbonate samples were drilled from polished rock slabs cut perpendicular to the bedding plane using a Woodtek Drill (model 109370; Woodworkers Supply Inc., Casper, Wyoming, USA) fitted with 1 to 2 mm carbide drill bit tips. Powdered samples were placed in vials, flushed with He gas, and converted to CO_2 through reaction with anhydrous phosphoric acid (Epstein & Mayeda, 1953). Acidified samples were heated for 1 to 23 hours at 70°C on a Gas Bench II (Thermo Fisher Scientific, Waltham, MA, USA). Evolved CO_2 was analysed on a Thermo Fischer Delta V Plus Isotope Ratio Mass Spectrometer at Washington University. Values are reported in permil (‰) relative to the Vienna Pee Dee belemnite (VPDB) standard. All runs contained internal standards as well as international standards NBS-18, NBS-19 and LSVEC. For a single run, one standard deviation (1σ) averaged 0.04‰ for $\delta^{13}C_{carb}$ and $\delta^{18}O_{carb}$ for all standards, while average reproducibility (1σ) for $\delta^{13}C_{carb}$ of replicate samples for a single run was 0.07‰. Reproducibility (1σ) across all sampling days for $\delta^{13}C_{carb}$ was 0.09‰ for NBS-18, 0.10‰ for NBS-19, and 0.25‰ for LSVEC and for $\delta^{18}O_{carb}$ was 0.12‰ for NBS-18 and NBS-19 and 0.13‰ for LSVEC.

Samples were dominantly micrite and skeletal grainstones with no large altered phases or features (e.g., spar, marl, stylolites, dolomitized burrows, etc.), although selected diagenetic textures were analysed to test for isotopic alteration and trace element abundance patterns as a function of distance from the altered texture. The desired sampling resolution in these sections precluded relying on a brachiopod-based approach (Veizer *et al.,* 1997; Veizer *et al.,* 1999; Brand, 2004). In total, more than 700 samples (with over 100 duplicates) were drilled with multiple parallel transects to identify lateral intra-sample variability and pinpoint the mixing of

isotopically distinct components. More than 450 samples were screened to construct bed-averaged isotope values for 66 beds from Highway MM and 69 beds from New London. Bed-averaged values were obtained by taking an unweighted average of individual microdrilled samples identified as 'least-altered' based on textural and petrographic analyses (*see below*).

3.2.2 Carbonate content (%carb), total organic carbon content (TOC), $\delta^{13}C_{org}$

Carbonate content (wt. %carb) was determined using a gravimetric method from the dissolution of 2to 5 g of bulk material. Hand samples were cut in ~2 cm vertical intervals to document vertical variability across a single bed and diagenetic textures were avoided. Total organic carbon content (TOC) and $\delta^{13}C_{org}$ were measured on aliquots of rinsed and dried residues of acid digestion by combustion to CO_2 on an ECS 4010 Elemental Analyzer (Costech Analytical Technologies Inc., Valencia, California, USA) and measured on a Thermo Fischer Delta V Plus Isotope Ratio Mass Spectrometer at Washington University. Values are reported in permil (‰) relative to the Vienna Pee Dee belemnite (VPDB) standard. TOC was determined by comparing the area of the evolved CO_2 peak to standards run at varied masses, and corrected for the carbonate content of the sample. A total of 151 samples were analysed for $\delta^{13}C_{org}$. Average standard deviations (1σ) for $\delta^{13}C_{org}$ standards USGS 24 (graphite), IAEA CH-6 (sucrose), and IAEA CH-3 (cellulose) were 0.11‰, 0.14‰, and 0.13‰, respectively.

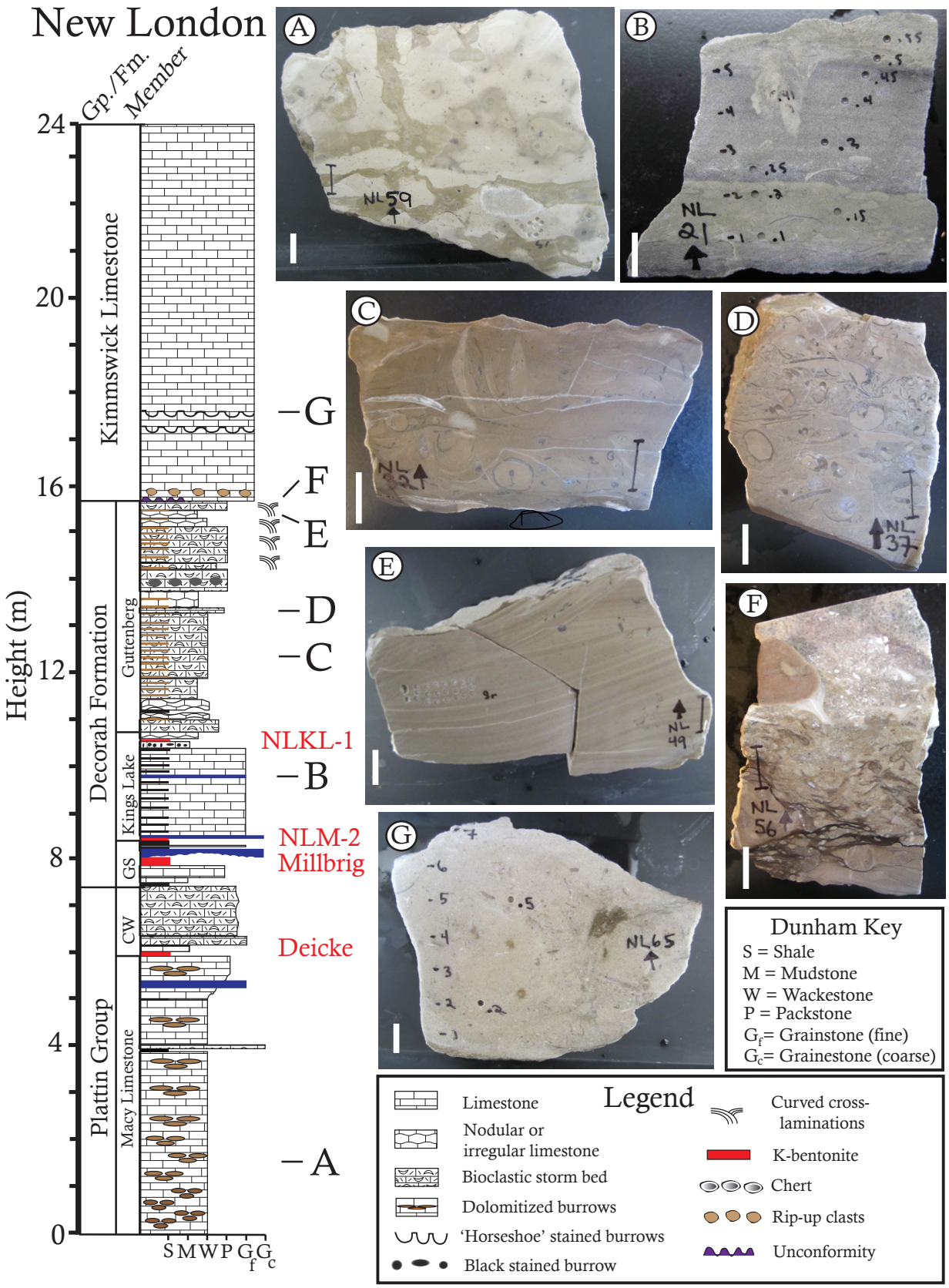
New London
Gp./Fm.
Member
Height (m)
24
20
16
12
8
4
0
Kimmswick Limestone
Decorah Formation
Guttenberg
Kings Lake
GS
CW
Plattin Group
Macy Limestone
S M W P G$_f$ G$_c$
G
F
E
D
C
NLKL-1
B
NLM-2
Millbrig
Deicke
A
A
B
C
D
E
F
G
Dunham Key
S = Shale
M = Mudstone
W = Wackestone
P = Packstone
G$_f$= Grainstone (fine)
G$_c$= Grainestone (coarse)
Legend
Limestone
Nodular or irregular limestone
Bioclastic storm bed
Dolomitized burrows
'Horseshoe' stained burrows
Black stained burrow
Curved cross-laminations
K-bentonite
Chert
Rip-up clasts
Unconformity

Figure 3. Lithology and selected facies for New London. See Figure 1 for biozone, sequence, and stratigraphic designations. Scale bars (white) are 1 cm. Pen markings used for carbonate sampling. Samples are as follows: (A) NL59, lower Plattin wackestone, (B) NL21, burrowed calcarenite with dolomitic zones (green), (C) NL32, muddy tempestite wackestone, (D) NL37, muddy tempestite packstone, (E) NL49, cross-laminated mudstone, (F) NL56, lowermost Kimmswick with Guttenberg rip-up clasts, (G) NL65, clean Kimmswick grainstone with burrowing (brown).

3.3.3 Elemental abundance

Samples were prepared for inductively coupled plasma optical emission spectrometry (ICP-OES) on an Optima 7300DV ICP-OES (PerkinElmer Inc., Waltham, Massachusetts, USA) at Washington University. Approximately 1.0 mg of carbonate powder was dissolved in 10% (Optima grade) acetic acid or with 5% HNO_3 (Optima grade) in 15 mL Falcon centrifuge tubes. Samples were placed on a shaker table and left to dissolve overnight (~12 hours). Samples were filtered through a 0.2 mm nylon filter prior to analysis. Standards were run at 1, 10, 20, 50, 100, and 500 ppb concentrations for Mn and Sr, while Ca and Mg were run using 1, 10, 50, and 100 ppm standards. Costech multi-element standards were used in combination with single element standards with no first-order spectral interferences. Standards for Ca, Mg, Mn, and Sr had an average reproducibility (1σ) of <1% across concentrations. The spectral lines used were Ca = 317.933 nm, Mg = 279.077 nm, Mn = 257.61 nm, and Sr = 407.771 nm.

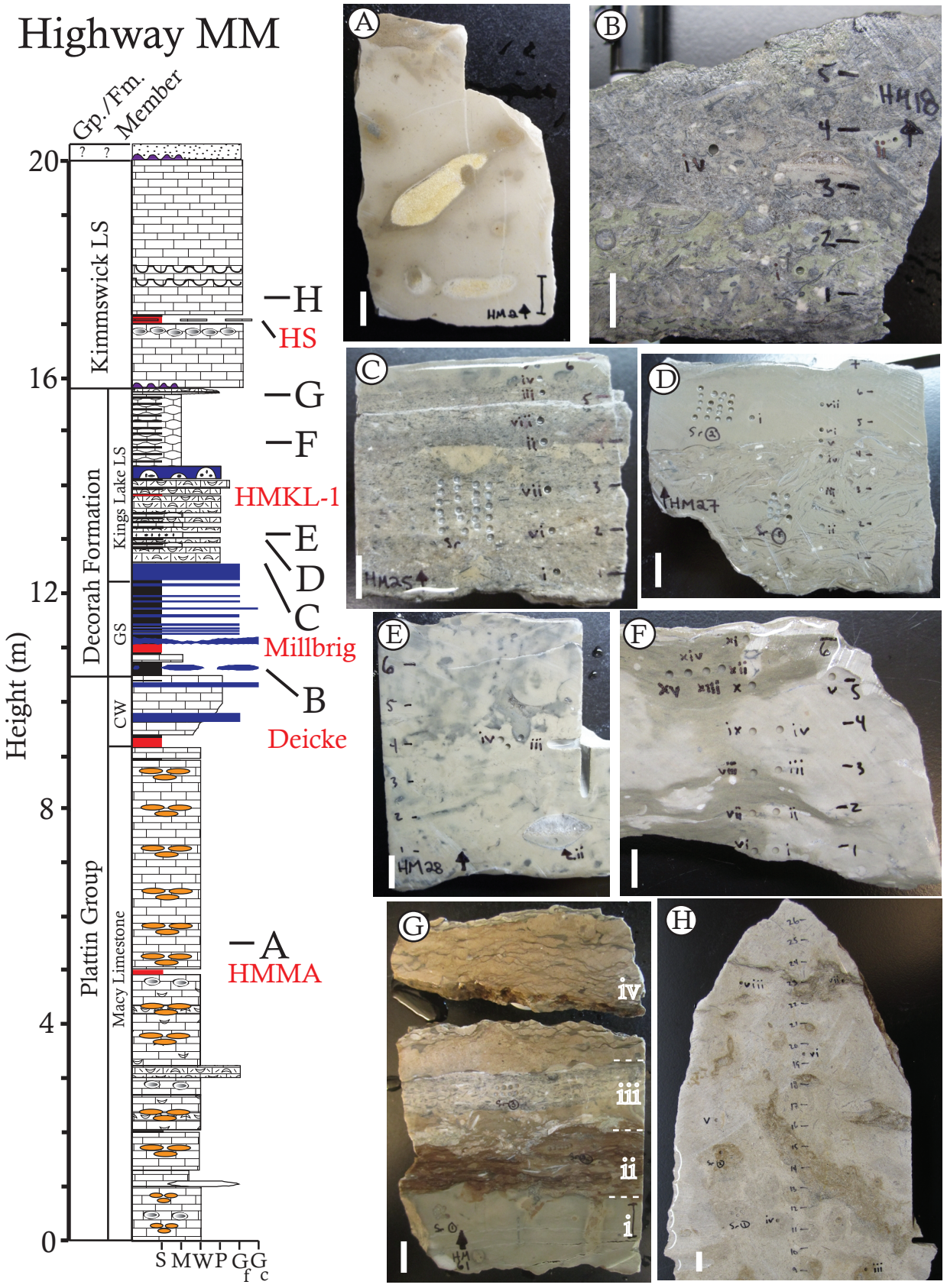
Highway MM
Gp./Fm.
Member
Height (m)
20
16
12
8
4
0
Kimmswick LS
Decorah Formation
Kings Lake LS
GS
CW
Plattin Group
Macy Limestone
H
HS
G
F
HMKL-1
E
D
C
Millbrig
B
Deicke
A
HMMA
S M W P G G
f c
A
B
C
D
E
F
G
H
HM18
HM25
HM27
HM28
HM61
iv
iii
ii
i

Figure 4. Lithology and selected facies for Highway MM. See Figure 1 for biozone, sequence, and stratigraphic designations. See Figure 3 for legend. Scale bars (white) are 1 cm. Pen markings used for carbonate sampling. Samples are as follows: (A) HM2, upper Plattin mudstone-wackestone with yellow dolomitized burrows, (B) HM18, coarse-grained calcarenite with dolomitic green clay, (C) HM25, fine-grained calcarenite, (D) HM27, tempestite packstone, (E) HM28, mudstone with black stained burrows, (F) HM55, wackestone showing dolomitic 'wispy brushtrokes', (G) HM61, zone i (0-3 cm) mudstone capped by hardground, zone ii (3-5 cm) is argillaceous and dolomitized, zone iii (5-8 cm) is a tempestite lens, and zone iv (8-14 cm) is stylonodular mudstone, (H) HM42, burrowed lower Kimmswick grainstone.

4. PETROGRAPHIC, SEDIMENTOLOGIC RESULTS & INTERPRETATIONS

4.1 Plattin Limestone

4.1.1 Observations

The upper Plattin Limestone consists of the Macy and Castlewood Members. The Macy Member is composed of thin-bedded to medium-bedded, heavily burrowed mudstones and wackestones with occasional grainstone lenses (Figs 3A, 4A, and 4B). When weathered, differential cementation of burrows and surrounding sediment imparts a 'Swiss cheese-like' appearance to the rock. The overlying Castlewood Limestone is heavily bioturbated, thick to massively bedded with occasional stylolites. Burrows in the Plattin are large (~2 cm diameter), pastel-yellow (Figure 4A) or brown-grey (Figs 3A and 4A) in hand sample. Burrows are filled with euhedral dolomite crystals 20 to 100 μm in diameter set in a fine-grained calcite matrix (Figure 5A). Dolomite abundance is positively correlated to bioturbation intensity, which decreases stratigraphically up within the Plattin Group. Thin section analysis shows dolomite abundance decreasing to <1% (by area) a few mm away from burrows. In general, bioclastic lenses and matrix materials were predominantly calcite. Plattin strata occasionally contain identifiable bryozoa, echinoderm fragments, and trilobites set in a calcite micrite matrix. Fossil texture preservation was poorer relative to the Decorah Formation and average whole fossil size smaller in the Plattin Limestone relative to other units in this study.

4.1.2 Interpretation

The Plattin Limestone is interpreted to represent a sub-tidal environment with stable sea-level conditions that terminated with the upward shoaling Castlewood Member. The small grain size and high burrow abundance is interpreted to represent deposition in oxygenated, intermittently calm conditions, while the absence of evaporites and obvious subaerial exposure features are in agreement with a consistently submerged subtidal environment.

4.2 Glencoe Shale

4.2.1 Observations

The Glencoe Shale is composed of dark green to grey, thinly bedded, fissile shales and deep blue to purple calcarenites and calcirudites (Figs 4B and 5B) that sometimes pinch out over decimetres to metres. Occasional bioclastic beds were present (Figure 5C). Sedimentological structures (e.g., cross-bedding, grading) and burrows were uncommon. Scouring created cm-scale relief in some beds. Dolomite is absent or in trace amounts throughout most of the matrix, but is found in yellow, red, and green diagenetic textures associated with bedding planes and burrow fill. Thin section analyses showed clasts to be supported in a granular cement fabric with higher total cement content found in finer-grained grainstones. The Glencoe Shale was nearly twice as thick at Highway MM compared to New London with a larger amount of shale found at Highway MM. The boundary between the Glencoe Shale and overlying Kings Lake Limestone is more abrupt at Highway MM and marked by a significant reentrant, while the lithologic transition is more gradational at New London.

4.2.2 Interpretation

The Glencoe Shale formed in a shallow sub-tidal environment (Thompson, 1991). The presence of shales and calcareous tempestites suggests calm-water conditions punctuated by high-energy storm events that brought in allochthonous bioclasts.

4.3 Kings Lake Limestone

4.3.1 Observations

The Kings Lake Limestone differs lithologically between sections. The entirety of the Kings Lake at New London and the interval from the base of the Kings Lake to just above HMKL-1 at Highway MM is made of blue-grey wackestones and grainstones (Figs 3B, 4C, 4D, and 4E) with abundant thin shale partings. Above HMKL-1 the Kings Lake Limestone is more mud rich (Figure 4). Fossils are abundant in hand sample and thin section throughout the entire Kings Lake and include trilobites, brachiopods, ostrocods, and bryozoa (Figs 4D and 5D), while rare crinoid stalks were found in shale partings. At New London, the Kings Lake contact with the overlying Guttenberg Limestone occurs just above a bentonite horizon (NLKL-1).

The contact between the Kings Lake and Kimmswick Limestones at Highway MM has relief up to 7 cm with possible evidence for karstification in the uppermost 30 cm of the Kings Lake. A potential hardground was identified ~15 cm below the Kimmswick contact (Figure 4G). In both locations, the Kings Lake contains little dolomite (<3%), except in the 'wispy brushstroke' textures, which are only found at Highway MM (Figure 4F) and which vary in dolomite concentration up to ~40%.

4.3.2 Interpretation

The Kings Lake Limestone was deposited during transgression in a sub-tidal, shallow sea, likely distal to a siliciclastic sediment source. At Highway MM, the Kings Lake represents a wider range of depositional environments than at New London, as evidenced by the lithologic differences above and below HMKL-1. Hereafter, the zones above and below HMKL-1 are referred to as the Lower and Upper Kings Lake, respectively. The transition to higher mud content and increased fossil preservation in the Upper Kings Lake (Highway MM) is interpreted to represent deposition in the deepest and most distal water facies at this location, similar to conditions ascribed to the Guttenberg Limestone at New London. The Lower Kings Lake at Highway MM is lithologically correlative with all of the Kings Lake at New London, while the Upper Kings Lake is lithologically equivalent with the Guttenberg Limestone at New London (*see below*).

4.4 Guttenberg Limestone

4.4.1 Observations

The Guttenberg Limestone is only found at New London and is lithologically similar to the Upper Kings Lake Limestone at Highway MM. This is seen in the mudstones and wackestone-packstone tempestites of the Upper Kings Lake (Highway MM) and Guttenberg (New London) (Figure 3C, D, and E), except that Guttenberg Limestone mud and shale fractions are brown (rather than blue), which is correlated with higher TOC content. Macrofossils and microfossils are abundant (Figure 3C and D), while spar and dolomite abundances are low. Burrowing textures are common, but textures are less obvious in hand sample relative to other units in this study. Low-angle cross-laminations were observed in the upper 1 to 2 m with lighter

laminations corresponding to coarser grain sizes, decreased organic content, and increased cement abundance (Figure 3E). The Guttenberg Limestone is unconformably overlain by the Kimmswick Limestone with a few centimetres of erosional relief present at the contact.

4.4.2 Interpretation

Similar to the Kings Lake Limestone, the Guttenberg Limestone formed in a shallow epeiric sea distal to siliclastic sediment sources. Lithologic similarities between the Guttenberg at New London and the Upper Kings Lake at Highway MM argue for similar depositional and environmental characteristics. This also suggests that the Upper Kings Lake and Guttenberg may be partially time-equivalent. There is no evidence to support erosion of the Guttenberg Limestone south of St. Louis as previously reported (Thompson, 1991; Kolata *et al.,* 1998).

4.5 Kimmswick Limestone

4.5.1 Observations

The Kimmswick Limestone is a heavily burrowed, fine- to coarse-grained limestone and appears somewhat saccharine in outcrop. The dominant mineral is calcite with up to 1 to 3% disseminated dolomite in a granular mosaic cement fabric (*sensu* Flügel, 2009). Grains are dominantly bioclastic. Burrows contain variable dolomite concentrations with darker, better-defined burrows bearing the highest dolomite concentrations (up to ~40% dolomite) (Figure 4H). The lowermost ~20 cm of the Kimmswick contains large (up to 10 cm) rip-up clasts from the underlying Guttenberg (at New London) (Figure 3F) and Upper Kings Lake (at Highway MM) strata.

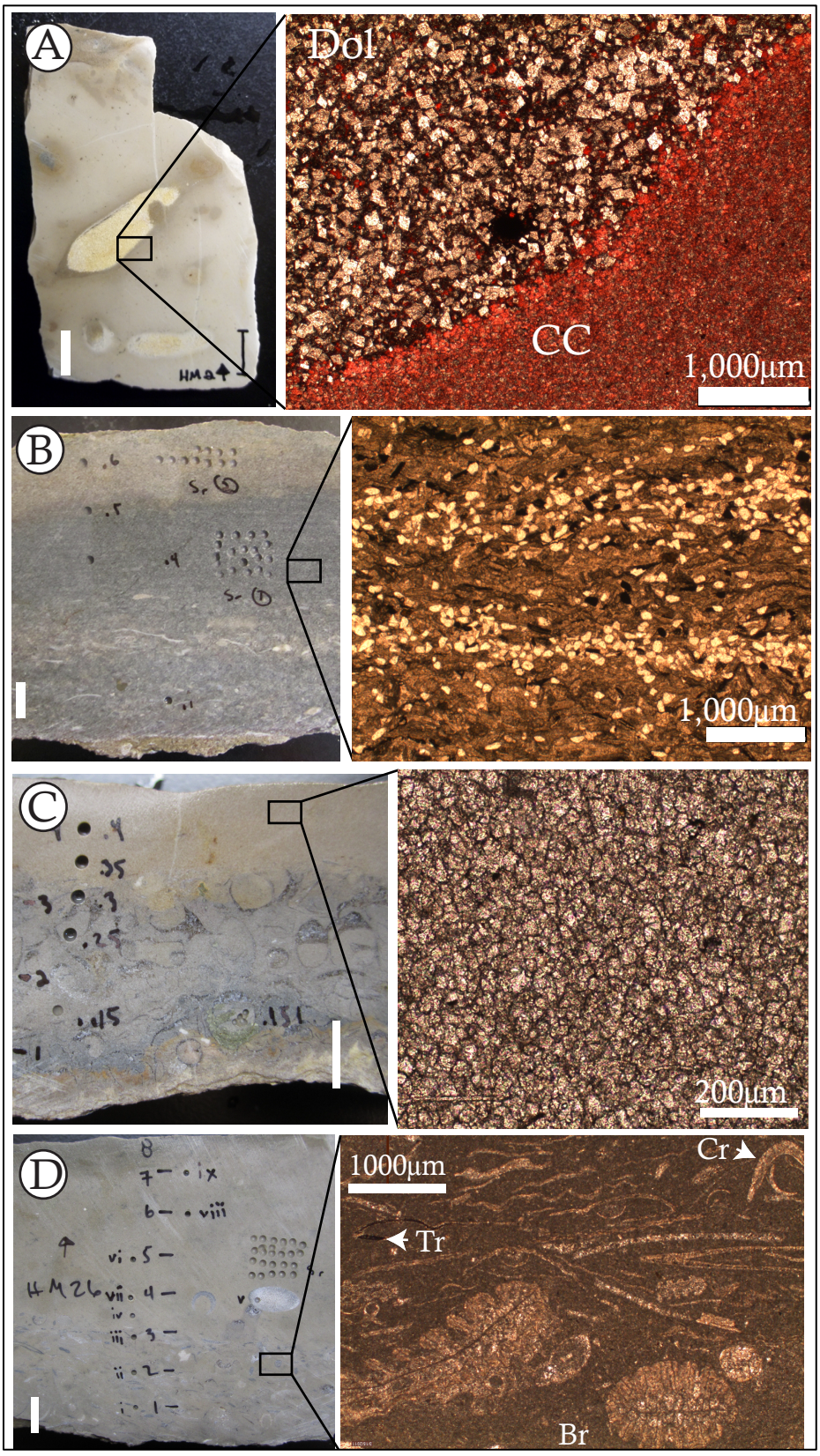
A
Dol
CC
1,000µm
B
1,000µm
C
200µm
D
1000µm
Cr
Tr
Br

Figure 5. Thin section photomicrographs and their corresponding hand sample location. Scale bars in hand samples (white) are 1 cm. (A) Stained thin section of HM2 in plane polarized light shows muddy and dolomitized burrows. Calcite (CC) is red and dolomite (Dol) is white. Darker spots in hand sample are dolomitized similar to yellow burrows. (B) Fine-grained calcarenite NL19 in plane polarized light. (C) NL14 under plane-polarized light showing carbonate silt or mud aggregates that possibly formed by vadose zone alteration. (D) HM26 with plane-polarized light shows whole bioclast-bearing storm bed. Tr = trilobite (partially pyritized), Cr = crinoid arm, and Br = bryozoan.

Porosity is highest in the upper portions of the Kimmswick where pores are lined by a chalky yellow dolomitic material. While Kimmswick burrow structures are similar to those of the Plattin Limestone, the burrow walls are not as well defined and overall mud content is much lower (Figs 3G and 4H). Cross-bedding was not observed in this study, but has been reported stratigraphically farther up the Kimmswick from a section near Barnhart, Missouri (Thompson, 1991).

4.5.2 Interpretation

The Kimmswick Limestone marked a return to a higher energy environment impacted by wave-tide action, consistent with the presence of fragmented bioclasts, and mud-poor composition. The nature of the contact (including rip-up clasts) with the underlying Guttenberg Limestone (New London) and Kings Lake Limestone (Highway MM) is also consistent with a transition to a higher energy environment with the onset of Kimmswick deposition. The stratigraphically thick, monotonous grainstones of the Kimmswick Limestone suggest constant environmental conditions during deposition.

5. GEOCHEMICAL RESULTS

5.1 Stratigraphic trends

Overall, $\delta^{13}C_{carb}$ and $\delta^{18}O_{carb}$ values range from -2‰ to 3‰ and -8‰ to -4‰, respectively, with similar profiles in both sections (Figure 6; Table S1 (New London); Table S2 (Highway MM). The Guttenberg excursion dominates the $\delta^{13}C_{carb}$ profile, rising from a baseline of $\delta^{13}C_{carb}$ near 0‰ in the base of the Kings Lake Limestone to a peak of 3‰ in the middle Kings Lake Limestone (Highway MM) and Guttenberg Limestone (New London), before returning to 0‰ in the Kimmswick Limestone (Fig 6). In addition, there is a small (1 to 2‰) negative excursion in $\delta^{13}C_{carb}$ found across the Deicke K-bentonite. $\delta^{18}O_{carb}$ averages -5.5‰ and -5‰ for New London and Highway MM, respectively, with lower values in the Glencoe Shale (Highway MM only), Kings Lake Limestone (New London only), and Kimmswick Limestone. A rise in $\delta^{18}O_{carb}$ accompanies the rising limb of the $\delta^{13}C_{carb}$ Guttenberg excursion at both localities, while a less-pronounced fall in $\delta^{18}O_{carb}$ is paired with the falling limb of the Guttenberg excursion only at Highway MM.

Superimposed on these first-order trends is permil-level scatter associated with different textures and mineralogy. Spar, single large clasts, and cement-rich and microclast-rich zones typically had lower $\delta^{13}C_{carb}$ and $\delta^{18}O_{carb}$, while dolomite-rich regions had variable $\delta^{13}C_{carb}$ and $\delta^{18}O_{carb}$, depending upon formation and texture. For example, yellow dolomitic burrow fill in the Plattin Limestone had $\delta^{13}C_{carb}$ values similar to the calcitic matrix and elevated in $\delta^{18}O_{carb}$ by 0.2-0.9‰, while the smoky grey dolomite-rich zone in the same formation had $\delta^{13}C_{carb}$ values and $\delta^{18}O_{carb}$ up to 4‰ and 0.4‰ higher, respectively. Geochemical analysis ([Ca]/[Mg] ratios and [Sr] values) and thin section observations support the link between observed isotopic

variability and dolomitization and/or secondary cementation. Samples with significant dolomite (>5%) were omitted from stratigraphic correlation.

Isotopic variability can occur in data across multiple spatial scales from the individual hand sample to the formation level. Secondary carbonates of meteoric origin often contain lower $\delta^{13}C_{carb}$ and $\delta^{18}O_{carb}$ values than primary material (e.g., Allen & Mathews, 1982; Veizer *et al.,* 1997; Veizier *et al.,* 1999; Brand, 2004) and high-temperature calcite has a lower $\delta^{18}O_{carb}$ signature owing to the strongly temperature-dependent fractionation of oxygen isotopes during calcite precipitation (Epstein & Mayeda, 1953). To test for the influence of secondary phases of meteoric origin, $\delta^{13}C_{carb}$ vs. $\delta^{18}O_{carb}$ cross-plots were constructed (Figure 7). Data were divided into the three main stratigraphic units: the Plattin, Decorah, and Kimmswick. No consistent formation-scale covariance patterns were observed between sections.

$\delta^{13}C_{org}$ values ranged from -33‰ to -24‰ (Figure 6). $\delta^{13}C_{org}$ is most negative beneath the Deicke K-bentonite and peaks in the Guttenberg (New London) (Figure 6A) and Kings Lake Formations (Highway MM) (Figure 6B). From the initial baseline values in the Plattin Limestone, $\delta^{13}C_{org}$ increases twice, once each across the Deicke and Millbrig K-bentonites, above which it steadily rises up to the contact with the Kimmswick Limestone. $\delta^{13}C_{org}$ rapidly returns to pre-excursion values (-30 ‰) in the basal Kimmswick. The isotopic offset between carbonate carbon and organic carbon, $\Delta^{13}C$ (= $\delta^{13}C_{carb} - \delta^{13}C_{org}$), shows no systematic relationship between sections except in the interval from the HMKL-1/NLKL-1 bentonite to the Kimmswick contact, where $\Delta^{13}C$ steadily decreases from 30‰ to 29‰ (Figure 6).

TOC is less than 0.2% in most of the Plattin Limestone, Glencoe Shale, and Kimmswick Limestone. Highest TOC values are found in the Decorah Formation (0.6% at Highway MM, 2.5% at New London). In contrast, carbonate content was highest in the Plattin Limestone and

Kimmswick Limestone and lowest in the Decorah Formation. Two intervals of decreased carbonate content are observed: one near the Millbrig K-bentonite and the other, a few metres above the HMKL-1/NLKL-1 bentonite (Figure 6).

Strontium concentrations ([Sr]) were consistent and averaged ~300 ppm in the Plattin Limestone. [Sr] also averaged ~300 ppm in the Glencoe Shale, increased to around 1,000 ppm in the Lower Kings Lake Limestone (Highway MM only) and Guttenberg Limestone (New London only), and consistently averaged ~200 ppm in the Kimmswick Limestone (Tables 1,2). Formational averages were similar between sections. Microdrilling results show dolomite-rich and recrystallized zones had decreased [Sr].

In summary, geochemical characteristics show little variation throughout the Plattin (with the exception of the Castlewood Limestone) and Kimmswick Limestones (Figure 6). These units are characterized by low TOC, [Sr], $\delta^{13}C_{carb}$, $\delta^{13}C_{org}$, $\delta^{18}O_{carb}$, and high carbonate purity. This homogeneous geochemical profile is paralleled by the observed lithologic homogeneity in these units. Geochemical patterns show clear signals of increasing $\delta^{13}C_{carb}$, TOC, [Sr], and decreasing %carb in the Decorah Formation. Within the Decorah the Upper Kings Lake Limestone at Highway MM has geochemical trends similar to those seen in the Guttenberg Limestone of New London (Figure 6), but with lower TOC. The geochemical similarities between the Upper Kings Lake Limestone (Highway MM) and Guttenberg Limestone (New London) are consistent with the lithologic similarities for the same strata.

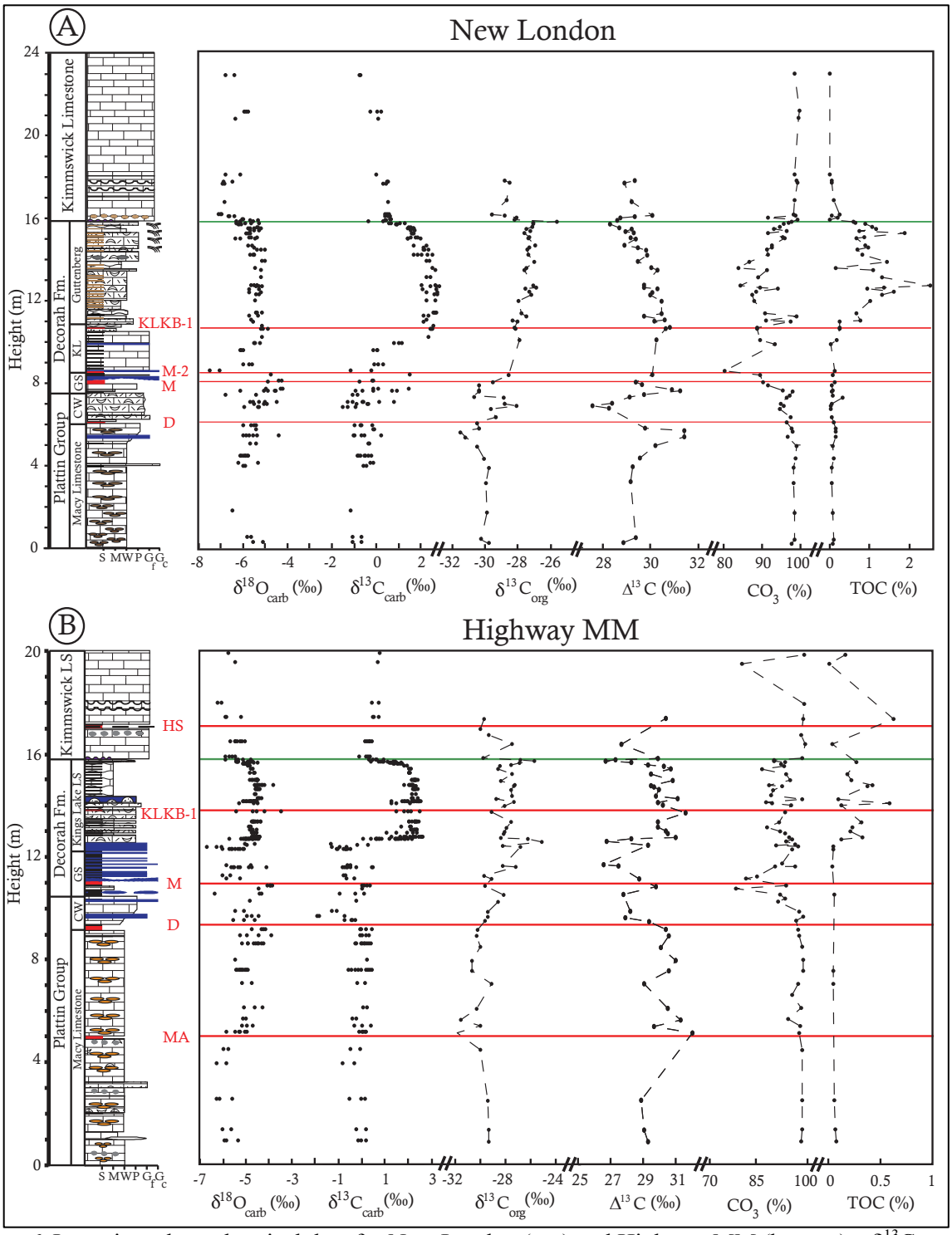

Figure 6. Isotopic and geochemical data for New London (top) and Highway MM (bottom). $\delta^{13}C_{carb}$ and $\delta^{18}O_{carb}$ are microdrilled samples. All other values are bed-averaged (Tables 1 and 2). Isotopic data are reported in ‰ relative to VPDB.

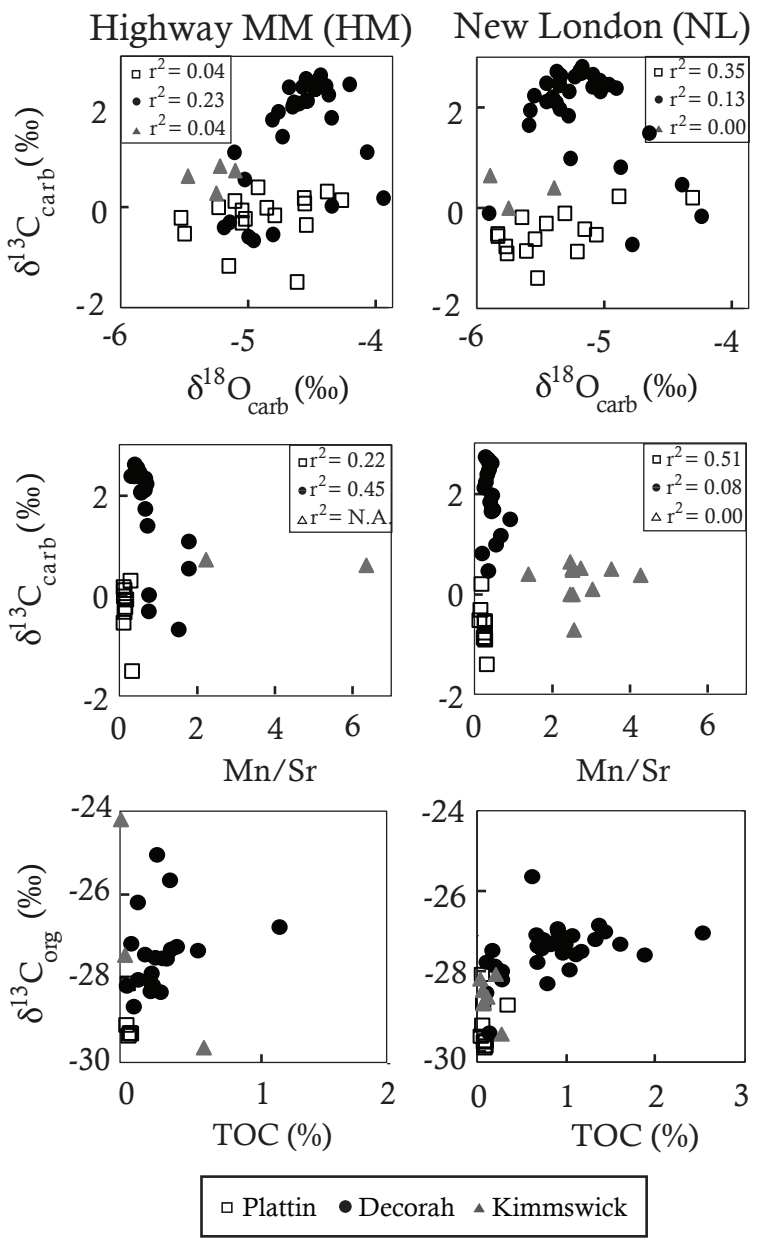

Figure 7. Geochemical cross-plot results for New London (left) and Highway MM (right). Values are isotope-texture screened and $\delta^{18}O_{carb}$ filtered (see *Methods*). r^2 corresponds to linear least-squares fit; see Tables 1 and 2 for values. $\delta^{13}C_{carb}$, $\delta^{13}C_{org}$, and $\delta^{18}O_{carb}$ values are reported in ‰ relative to VPDB.

5.2 Intra-bed $\delta^{13}C_{carb}$ and $\delta^{18}O_{carb}$ variability

Centimetre-scale drilling transects were completed to assess small-scale $\delta^{13}C_{carb}$ and $\delta^{18}O_{carb}$ variability within individual samples in order to better constrain primary signatures used for correlation and carbon cycle reconstruction. These results revealed significant isotopic heterogeneity within single beds (Figure 8) and many samples showed vertical increases in $\delta^{13}C_{carb}$ and $\delta^{18}O_{carb}$ over just a few cm (Figure 8A and B), while isotopic scatter in other samples was restricted to bedding planes (Figure 8C). Excluding heavily dolomitized zones and other obviously altered textures, the magnitude of change within individual beds in $\delta^{13}C_{carb}$ was up to 2.0‰, while the change in $\delta^{18}O_{carb}$ was up to 3.0‰. This isotopic variability was sometimes related to lithological transitions. For example, in Plattin sample NL4 (Figure 8A), a fine-grained calcarenite that grades upward to a mudstone, $\delta^{13}C_{carb}$ was 1‰ higher and $\delta^{18}O_{carb}$ was 1.6‰ higher in the mudstone portion. These data fell along a mixing line ($r^2 = 0.99$, $n = 6$) and correlate with cement content and grain size.

Drilling transects across differing textures (Figure 9) allowed the identification of component mixing where dolomite, cement, and clasts influenced bulk isotope signatures. Coupled petrographic and isotopic analyses showed the highest $\delta^{13}C_{carb}$ and $\delta^{18}O_{carb}$ samples to be muds and dolomite-rich zones while cements and recrystallized materials had the lightest $\delta^{13}C_{carb}$ and $\delta^{18}O_{carb}$ (e.g., Figure 8A). A linear $\delta^{13}C_{carb}$-$\delta^{18}O_{carb}$ trend is then an isotope mixing line where points on the line represent gradational changes in the relative proportions of two components. This logic was the basis for constructing an "isotope-texture screen" to select the 'least-altered' $\delta^{13}C_{carb}$ and $\delta^{18}O_{carb}$ values from populations within single samples.

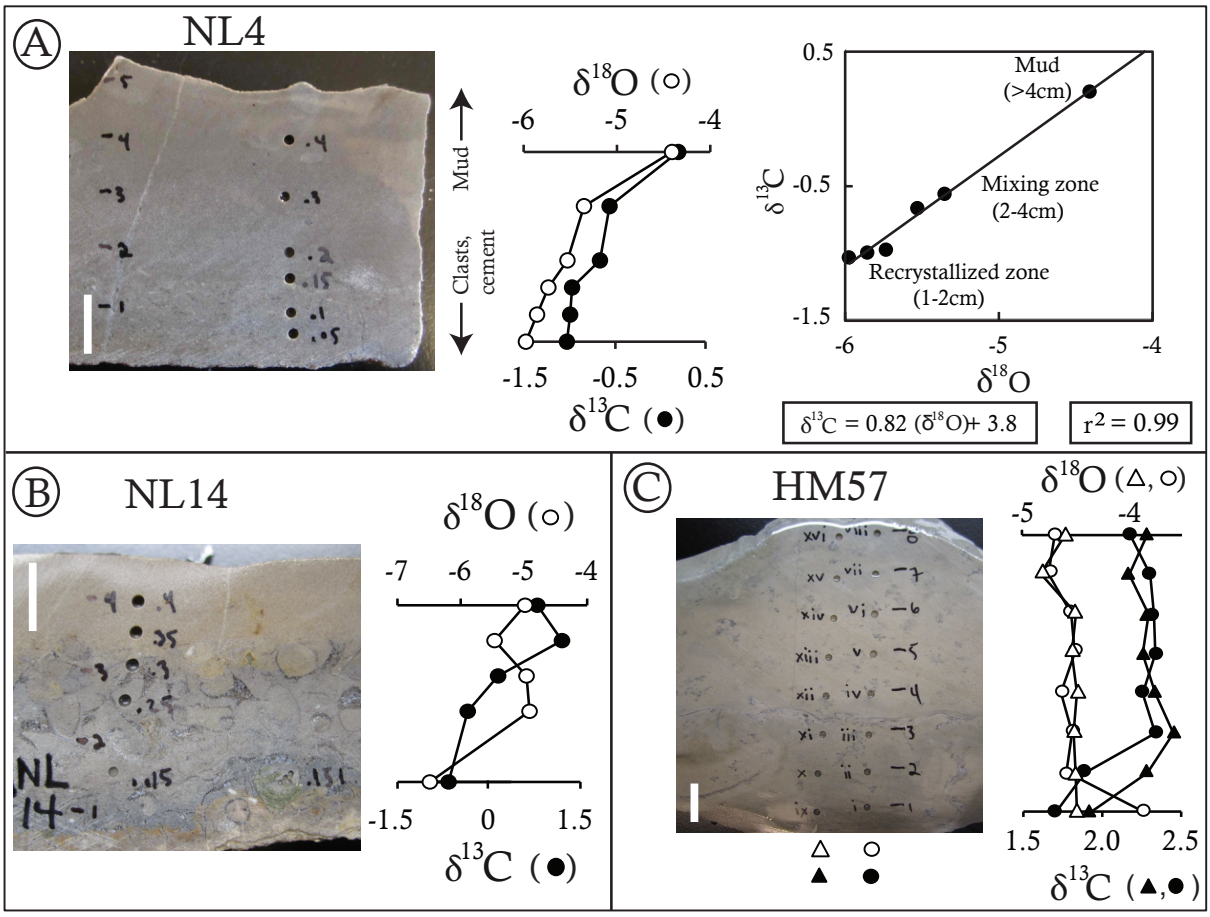

Figure 8. Vertical and lateral trends in $\delta^{13}C_{carb}$ (black symbols) and $\delta^{18}O_{carb}$ (white symbols) in hand samples. Multiple transects are split by symbol type (left = triangles, right = circles). All values are reported in ‰ relative to VPDB. Scale bar (white) is 1 cm. (A) Calcarenite grading upwards to mudstone NL4. Linear regression of NL4 showing correlation in $\delta^{13}C_{carb}$ and $\delta^{18}O_{carb}$. Strong correlation results from linear mixing of a coarser, cement-rich component in base of rock with an isotopically heavier mud component near the top. Sample contains <1% dolomite. (B) Wackestone-Packstone NL14. Vertical enrichment primarily results from increasing fractions of isotopically heavy mud, but contains more than two isotopically distinct components. (C) Mudstone HM57. Lower $\delta^{13}C_{carb}$ and higher $\delta^{18}O_{car}$ at bottom result from mixing with 'wispy brushstroke' texture, which contains abundant dolomite and affects the bulk isotope signals in the lower 2 cm.

In some cases, plots showed changes in $\delta^{13}C_{carb}$ while $\delta^{18}O_{carb}$ was invariant. For example, brown Guttenberg mudstones-packstones had higher $\delta^{13}C_{carb}$ in darker brown micrite and lower $\delta^{13}C_{carb}$ in light brown micrite while $\delta^{18}O_{carb}$ was constant. Petrographic analyses revealed a larger average crystal size, a likely diagenetic feature, in lighter shades of micrite that corresponded with lower $\delta^{13}C_{carb}$, therefore the higher $\delta^{13}C_{carb}$ values from darker zones were

taken as more representative of primary $\delta^{13}C_{carb}$. When no petrographic or geochemical evidence could indicate which textures/phases were most primary, an average of all values was taken.

5.3 $\delta^{18}O_{carb}$ filter

While the 'isotope-texture screen' is useful in identifying the 'least-altered' values within a single sample, it does not necessarily help in deciding whether those values are themselves well-suited for chemostratigraphic correlation. To address this problem, samples can be filtered using their $\delta^{18}O_{carb}$ value. $\delta^{18}O_{carb}$ filtering is done by excluding samples with $\delta^{18}O_{carb}$ values below a certain threshold where the threshold is defined as some value below the mean $\delta^{18}O_{carb}$ value for samples that passed the 'isotope-texture' screen for a given formation. The $\delta^{18}O_{carb}$ cutoff value was arbitrarily picked as one standard deviation (1σ) lighter than the formational average. The $\delta^{18}O_{carb}$ cutoff values for each formation can be found in Table S3.

Hereafter, correlations and environmental reconstructions use only $\delta^{13}C_{carb}$ data that passed isotope-texture screening *and* $\delta^{18}O_{carb}$ filtering. A decision tree (Figure 10) shows the process used to construct these 'least-altered' $\delta^{13}C_{carb}$ values. The full list of samples along with information as to whether they pass or fail the isotope-texture screening and $\delta^{18}O_{carb}$ filter can be found in Tables 1 and 2.

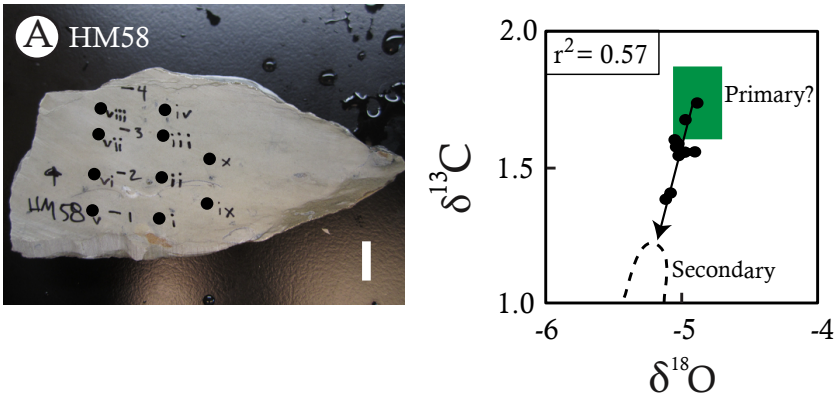

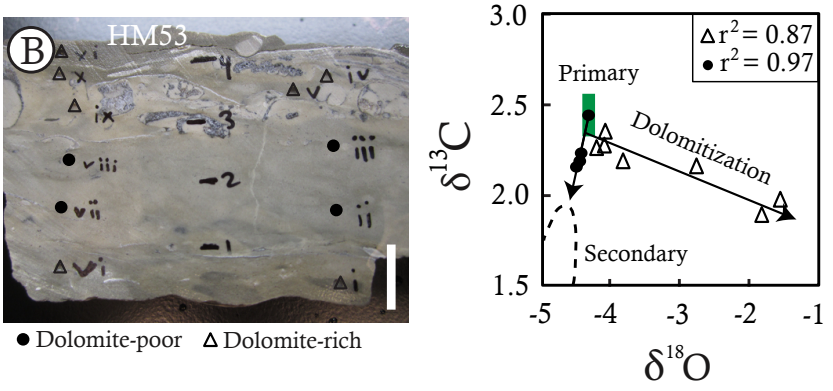

● Dolomite-poor △ Dolomite-rich

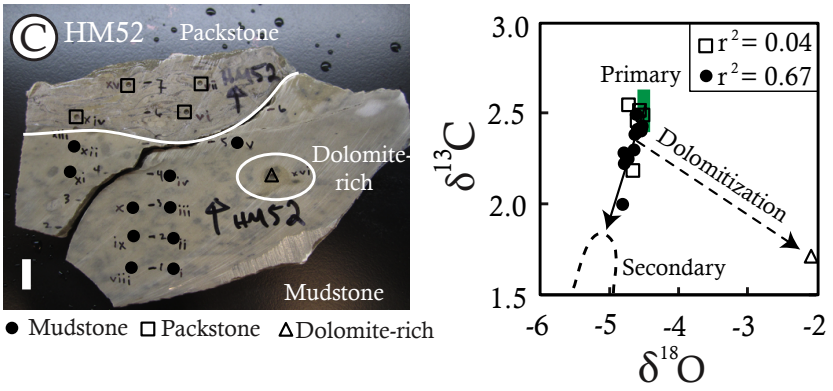

● Mudstone □ Packstone △ Dolomite-rich

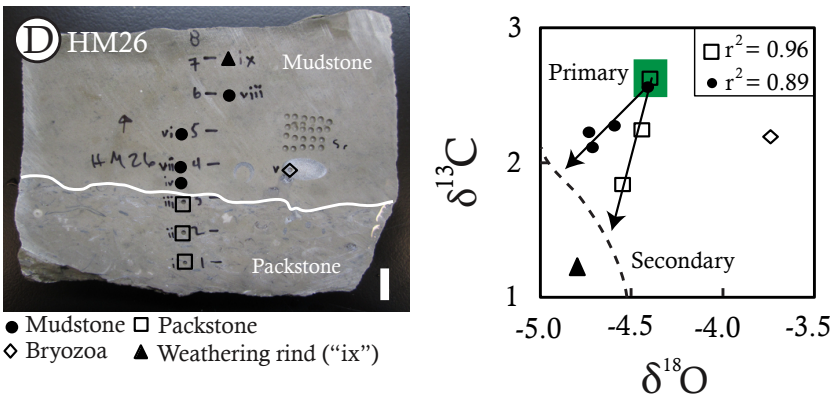

● Mudstone □ Packstone
◇ Bryozoa ▲ Weathering rind ("ix")

Figure 9. Plots of $\delta^{13}C_{carb}$ vs. $\delta^{18}O_{carb}$ for single hand samples. All values are reported in ‰ relative to VPDB. Scale bar (white) is 1 cm. Filled green rectangles show 2σ error ($\delta^{13}C_{carb}$ = 0.18‰, $\delta^{18}O_{carb}$ = 0.26‰) and represent inferred 'primary' values. 'Dolomitization' refers to the trend for increasing amounts of dolomite in microdrilled samples; 'secondary' refers exclusively to non-primary calcite. (A) Mudstone HM58 showing typical two-component mixing line. (B) Wackestone HM53 showing three components. (C) Mudstone-packstone HM52 showing similar trends to HM53. (D) Mudstone-Packstone HM26 showing different mixing line slopes. Convergence upon a single value is consistent with both lithologies in the sample having common primary $\delta^{13}C_{carb}$ and $\delta^{18}O_{carb}$ values with differing diagenetic histories associated with the different Dunham classification.

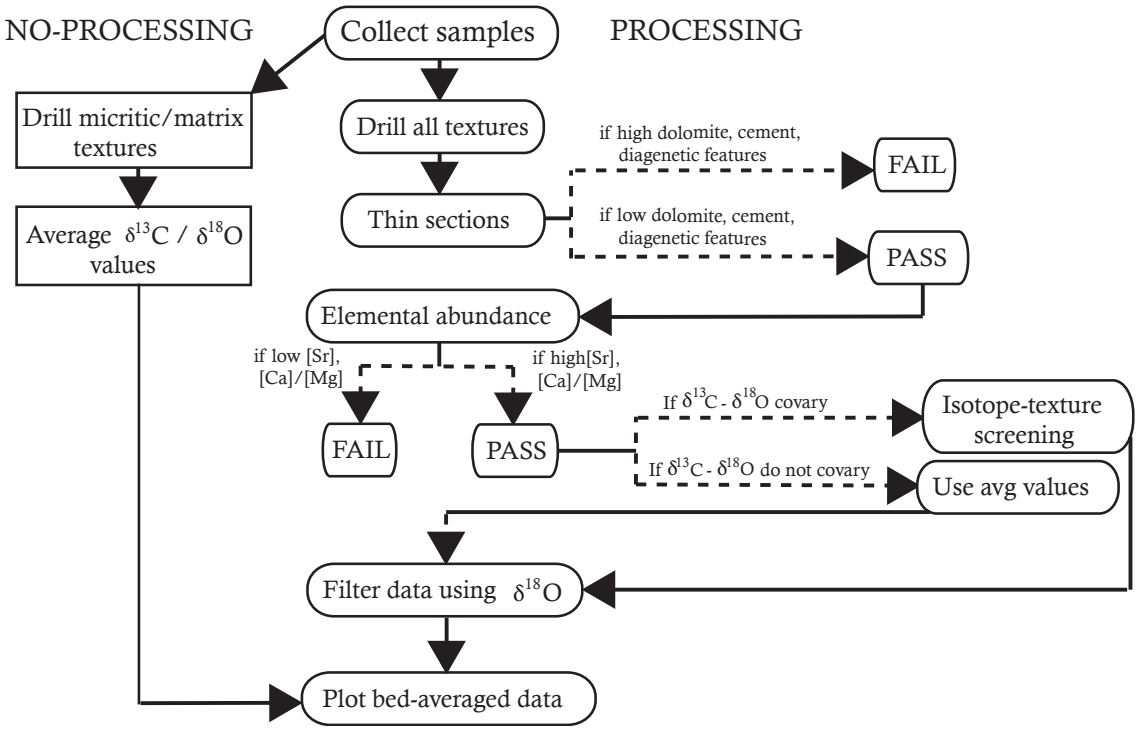

Figure 10. Decision tree for isotope-texture screening and $\delta^{18}O_{carb}$ filtering.

6. DISCUSSION

6.1 Intra-sample geochemical variability

Variations in bulk $\delta^{13}C_{carb}$ values within and between individual samples can result from analysing mixtures of two or more isotopically distinct components (i.e., mud, cement, and clasts). This was elegantly demonstrated by Swart (2008) who showed that Cenozoic periplatform and ramp $\delta^{13}C_{carb}$ values were decoupled from open ocean signal due to mixing of

isotopically distinct aragonite from the shallow platform with pelagic calcite materials. As shown in Figs 8 and 9, varying mixtures of mud, clasts, cements, and dolomite explain much of the isotopic variability within individual hand samples. The largest range in $\delta^{13}C_{carb}$ values within an individual sample was greater than 2.0‰ (equal to ~80% of the magnitude of the Guttenberg excursion), highlighting the importance of both sample screening and high-resolution data for stratigraphic correlation and palaeoenvironmental or palaeoceanographic reconstructions. From these results, it is apparent that $\delta^{13}C_{carb}$ and $\delta^{18}O_{carb}$ scatter within a single sample is often unrelated to a primary marine (i.e., water column) environmental signal and, instead, reflects the mixing of diagenetic components and primary materials. This framework provides an objective criterion for the selection of the 'least-altered' $\delta^{13}C_{carb}$ values.

Because secondary carbonates often contain lower $\delta^{13}C_{carb}$ and $\delta^{18}O_{carb}$, the heaviest $\delta^{13}C_{carb}$ values are usually considered more primary (Figure 9A). For this work, accepting only the heaviest $\delta^{13}C_{carb}$ would lead to incorporation of substantial diagenetic artifacts because dolomite-rich samples occasionally had $\delta^{13}C_{carb}$ signatures and frequently had $\delta^{18}O_{carb}$ signatures heavier than the reconstructed 'least-altered' values. When dolomite was present, plots with two linear mixing lines provided an objective argument for choosing most-primary $\delta^{13}C_{carb}$ and $\delta^{18}O_{carb}$ values (e.g., Figure 9B and C).

Not all of the samples characterized fell along a linear mixing line. This may be the result of multi-component mixing (e.g., Figure 9B, C, and D), natural environmental variation, or cryptic diagenetic alteration; samples that showed poor covariation across $\delta^{13}C_{carb}$ and $\delta^{18}O_{carb}$ over a range in excess of analytical precision are believed to result from one of these causes. For example, Figure 9D shows two intersecting mixing lines for the mudstone and packstone portions of sample HM26. The intersection of these two lines is interpreted to represent primary

$\delta^{13}C_{carb}$ and $\delta^{18}O_{carb}$ signatures for all components, while the different downward trajectories represent the inclusion of different secondary cements possibly relating to different diagenetic histories. Such scatter prevented development of a well-constrained dolomite-rich $\delta^{13}C_{carb}$ and $\delta^{18}O_{carb}$ signature and is thought to result either from multiple generations of dolomite and/or calcite cement that precipitated under different conditions or from variable amounts of calcite/dolomite within the dolomitized zone. In such cases, 'least-altered' samples were selected based on qualitative trends in the $\delta^{13}C_{carb}$-$\delta^{18}O_{carb}$ sample population.

Centimetre-scale isotope transects revealed that *the majority* of samples had isotopic offsets arising from variable amounts of secondary material. Only 2 of 11 samples (18%) were identified as 'least altered' in Figure 9A, demonstrating that *most* samples carried a significant secondary signal (i.e., offset from 'primary' by more than twice instrumental precision). The impact of secondary alteration on $\delta^{13}C$ and $\delta^{18}O$ may be further tested on the micron-scale using secondary ion mass spectrometry (SIMS) or similar instruments to allow for grain-specific isotope analysis. In sum, confident identification of 'least-altered' components requires a combination of petrographic, elemental abundance, and isotopic analyses, particularly when the magnitude of intrabed $\delta^{13}C_{carb}$ variability is similar to that of the stratigraphic signal being investigated.

6.2 $\delta^{18}O_{carb}$ filter

A $\delta^{18}O_{carb}$ filter was applied to all samples that passed the above isotope-texture screening. This filter was designed to exclude samples subjected to pervasive resetting of $\delta^{18}O_{carb}$ such as would occur during meteoric diagenesis. The $\delta^{18}O_{carb}$ isotope filter provides an objective criterion for formation-scale sample discrimination in isotopically heterogeneous rocks,

provided careful petrographic and chemical characterization has been done. Because $\delta^{18}O_{carb}$ is easier to reset than $\delta^{13}C_{carb}$ during diagenesis (Lohmann, 1988), a $\delta^{18}O_{carb}$ filter provides a conservative method for isolating 'least-altered' $\delta^{13}C_{carb}$ data. Without $\delta^{18}O_{carb}$ filtering, some $\delta^{13}C_{carb}$ data sets may be artificially noisy and the resulting chemostratigraphic correlations and environmental reconstructions may be misleading or inaccurate.

While careful screening and filtering can aid in arriving at a 'least-altered' $\delta^{13}C_{carb}$ profile a small number of samples that displayed clear textural evidence of post-depositional alteration would have passed both the isotope-texture screening and the $\delta^{18}O_{carb}$ filter. This demonstrates that the isotope-texture and $\delta^{18}O_{carb}$ filters remain imperfect screens for identifying alteration and that petrographic and trace element abundance data should be considered. Some beds yielded $\delta^{13}C_{carb}$ values different than those from beds above and below representing a break in a stratigraphically consistent $\delta^{13}C_{carb}$ pattern. If these aberrant $\delta^{13}C_{carb}$ values were primary, they would represent a complex and rapidly changing global carbon cycle (Kump & Arthur, 1999), but it is mechanistically simpler to invoke alteration by diagenetic fluids. While no samples in this work were discarded based on stratigraphic continuity of $\delta^{13}C_{carb}$ alone this may be sufficient evidence to omit samples in other studies. If done, care should be taken to avoid a model-driven interpretation of data that excludes real negative excursions in $\delta^{13}C_{carb}$.

6.3 $\delta^{13}C$ chemostratigraphic correlations and relative sedimentation rates

Figure 11 shows the proposed chemostratigraphic relationships between Localities Highway MM and New London using $\delta^{13}C_{carb}$ data that passed both the isotope-texture screen and $\delta^{18}O_{carb}$ filter. The Guttenberg excursion is a conspicuous feature of the $\delta^{13}C_{carb}$ profile at both sections, where it is preserved as an ~2.5‰ positive excursion, a magnitude similar to those

previously reported from other Laurentian sections (Bergström *et al.*, 2010a). The continuity of the $\delta^{13}C_{carb}$ signal throughout the Guttenberg excursion at Highway MM suggests that the Guttenberg Limestone was never deposited at Highway MM and that any erosion was less substantial than previously thought (Kolata *et al.,* 1986; Kolata *et al.,* 1987, Thompson, 1991) as the Guttenberg Limestone is the member that contains the Guttenberg excursion in northern Missouri. A comparison of $\delta^{13}C_{carb}$ profiles shows that the difference in thickness of the Kings Lake Limestone between New London and Highway MM and the absence of the Guttenberg Limestone at Highway MM can be best explained if the Upper Kings Lake Limestone (Highway MM) is a synchronous southern facies equivalent of the Guttenberg Limestone (New London). Figure 12A shows the Guttenberg excursion curve for Missouri sections normalized for excursion duration. The similarity in morphologies between Highway MM and New London during the falling stage of the Guttenberg excursion shows that sedimentation at Highway MM was as continuous as that at New London, but slower. This provides further evidence against erosion of the Guttenberg time-equivalent strata at Highway MM as erosion would produce a different normalized excursion morphology. These data are in strong agreement with lithological and geochemical observations.

Comparison of relative sedimentation rate (RSR) between localities can be used to understand spatial differences in deposition rates. The RSR is a unitless ratio of lithological thickness of a given $\delta^{13}C_{carb}$ interval from one section to another (here the ratio of stratigraphic thickness in New London strata relative to that in Highway MM strata). In the present case, the intervals are defined by a combination of K-bentonites and features in the $\delta^{13}C_{carb}$ profiles (Figure 11). In this manner, the isotopes reveal the partitioning of time between units and show the geographic relationship in relative sedimentation rates.

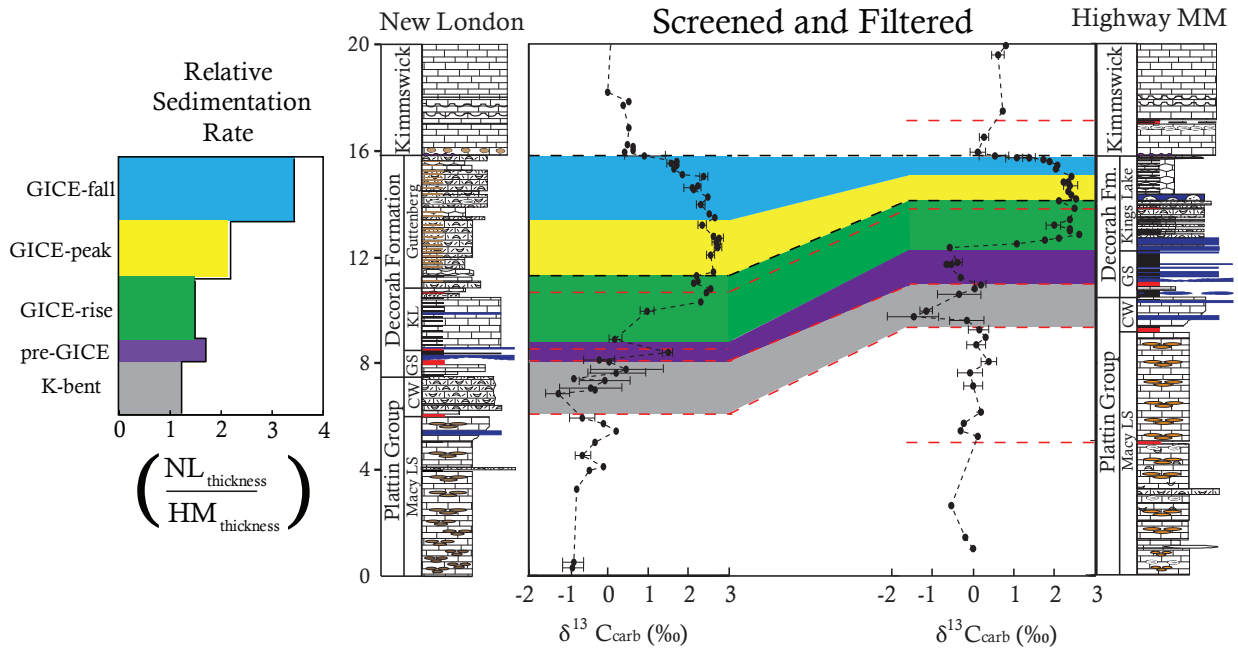

Figure 11. $\delta^{13}C_{carb}$ correlations with screened and filtered data across the Guttenberg isotopic carbon excursion (GICE). Height is in metres. Colours correspond to chonostratigraphic intervals. "K-bent" chronozone is bounded by K-bentonites and independent of $\delta^{13}C_{carb}$. The remaining intervals are defined by $\delta^{13}C_{carb}$ chemostratigraphy. Bar graph shows relative sedimentation rate (RSR) of New London relative to Highway MM. Error bars represent standard deviation (1σ) of bed-averaged values.

The RSR is near unity during the "K-bent" chronozone and through the onset of the Guttenberg excursion, arguing for a similar sedimentation rates at Highway MM and New London. The RSR increases above the HMKL-1/NLKL-1 bentonite near peak Guttenberg excursion $\delta^{13}C$ values, as net sedimentation rates at New London outpaced those at Highway MM. A possible hardground ~15 cm below the Kimmswick contact at Highway MM suggests that sedimentation was very condensed at this locality, but as Figure 12A shows, not so condensed as to significantly change the normalized excursion morphology at Highway MM. Lack of evidence for subaerial exposure is consistent with a continuously submerged environment at Highway MM and that the high RSR resulted, at least in part, from declining sediment production rates and/or a decrease in the creation of new accommodation space at this location. The shift in RSR is roughly coincident with the start of the Taconic Orogeny (Rodgers,

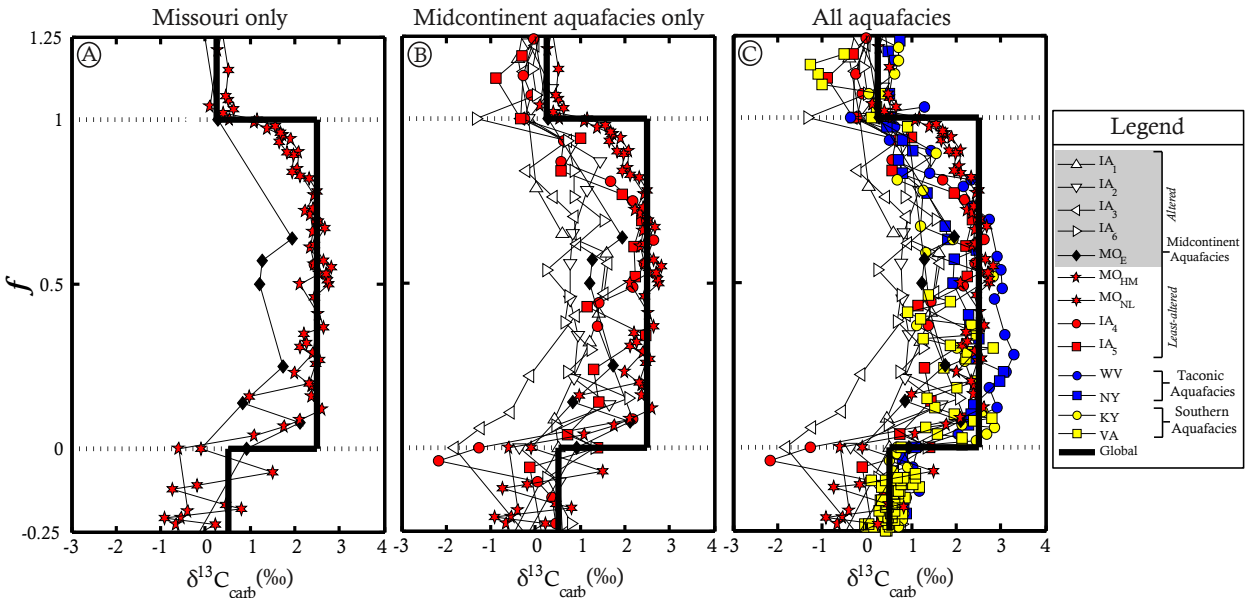

Figure 12. Plot of normalized Guttenberg $\delta^{13}C_{carb}$ excursions in Laurentian sections where the duration of the excursion is normalized from 0 to 1, with 0 defined as the beginning of the excursion and 1 as the end. Generalized global $\delta^{13}C_{carb}$ values (heavy solid line) for the pre-, peak-, and post-Guttenberg excursion taken from Bergström *et al*. (2009b). Instrumental error (1 standard deviation) is less than symbol size. (A) Normalized excursions for Missouri (MO) sections. Eureka (MO_E, black diamonds) from Ludvigson *et al.* (2000), Highway MM (MO_{HM}, red pentagrams) and New London (MO_{NL}, red hexagrams) from this report. (B) Normalized excursions "Midcontinent aquafacies". Iowa (IA) subscripts refer to sample localities of Ludvigson *et al.* (2004). Note the general agreement in pre- Guttenberg, peak- Guttenberg, and post-Guttenberg excursion values and lower degrees of scatter in least-altered sections compared to altered sections. (C) Normalized excursions for all aquafacies with aquafacies designations taken from Young *et al.* (2005). Data for Virginia (VA), West Virginia (WV), and Kentucky (KY) from Young *et al.* (2005). New York (NY) data is unpublished.

1971), and the differential subsidence may be the result of a far-field tectonic forcing on the inner craton (*see* discussion in Holland & Patzkowsky, 1998) or changing regional tectonics related to the Ozark Dome. Future development of robust correlations in the overlying Kimmswick Limestone could test whether these sedimentation patterns continue in younger strata.

6.4 $\delta^{13}C_{org}$

Sedimentary organic carbon is filtered through a complex network of biological processing during carbon fixation, heterotrophic reworking, and microbial respiration. As such, the $\delta^{13}C_{org}$ signal reflects not only variations in $\delta^{13}C$ from the parent dissolved inorganic carbon (DIC) source, but also changing ecological and environmental (e.g., facies-dependent) factors. Therefore, fractionation can be influenced strongly by local signals and resulting interpretations of $\delta^{13}C_{org}$ data are less straightforward than $\delta^{13}C_{carb}$ (Hayes *et al.*, 1999). The Guttenberg excursion is weakly expressed in $\delta^{13}C_{org}$, where the signal is either superimposed over varying biological fractionation or variable organic sourcing, as evidenced by the difference in stratigraphic expression in $\delta^{13}C_{org}$ relative to $\delta^{13}C_{carb}$ (Figure 6). The magnitude of the Guttenberg excursion in $\delta^{13}C_{org}$ is ~2‰, while the $\delta^{13}C_{carb}$ excursion is ~2.5‰ at both locations. Other reported Guttenberg excursion $\delta^{13}C_{org}$ excursions were found to have magnitudes of ~1‰ from West Virginia (Young *et al.,* 2008), ~3‰ from Pennsylvania (Patzkowsky *et al.,* 1997), and ~8‰ from Iowa (Pancost *et al.,* 1999). In this latter case, compound-specific analysis of TOC components was used to correct for organic matter source mixing; the resulting reconstructed, source-independent magnitude of the Guttenberg excursion was ~3.5‰ (Pancost *et al.,* 1999). The $\delta^{13}C_{org}$ is particularly variable in the zone above and below the Millbrig at Highway MM and New London making exact correlations difficult and the absence of the Millbrig in the Iowa core makes comparison speculative. Higher order trends in $\delta^{13}C_{org}$ are apparent at Highway MM, which may result from source mixing (Pancost *et al.,* 1999), unidentified diagenesis, a complex local signal, and/or decoupling of the $\delta^{13}C_{org}$ and $\delta^{13}C_{carb}$ system.

During catagenesis (i.e., thermal cracking), TOC decreases as organic matter is converted to simple hydrocarbons (e.g., methane). These resulting hydrocarbons are often depleted in ^{13}C,

leaving the residual TOC enriched in ^{13}C. Similar trends can be obtained by biological remineralization of organic matter by microbial respiration during or after deposition. As such, cross-plots of $\delta^{13}C_{org}$ vs. TOC can provide insight into processes that alter $\delta^{13}C_{org}$. A pattern of increasing $\delta^{13}C_{org}$ as TOC decreases can thus be indicative of alteration in the $\delta^{13}C_{org}$ signal (e.g., Dehler *et al.,* 2005) or mixture of isotopically distinct components (e.g., Johnston *et al*., 2012). Instead, a trend toward low $\delta^{13}C_{org}$ with low TOC (this is particularly noticeable at New London) is observed; however, because the low TOC and ^{13}C-depleted samples come from strata below and above the Guttenberg excursion (Plattin and Kimmswick Limestones, respectively), while the high TOC, ^{13}C-enriched samples come from strata containing the Guttenberg excursion, this pattern most likely reflects primary environmental variability rather than alteration or contamination.

Nearly all autochthonous marine organic carbon is originally derived from the marine inorganic carbon reservoir by way of photosynthesis. Assuming a constant fractionation factor during photosynthesis, $\delta^{13}C_{org}$ should be consistently offset from $\delta^{13}C_{carb}$ by a fixed amount. This means that $\delta^{13}C_{carb}$ and $\delta^{13}C_{org}$ should move in parallel. The isotopic offset between coeval carbonate and organic carbon, $\Delta^{13}C$ (= $\delta^{13}C_{carb}$ - $\delta^{13}C_{org}$), can be plotted to visually show if either carbon profile deviates from parallel behavior. The $\Delta^{13}C$ profiles (Figure 6) are similar between sections only from the HMKL-1/NLKL-1 bentonites on the rising limb of the Guttenberg excursion to the excursion termination. $\Delta^{13}C$ curves from Highway MM and New London have a similar morphology to the $\Delta^{13}C$ curves from Iowa (IA) Iowa and Pennsylvnaia (PA)(Patzkowsky *et al.,* 1997) in that all curves immediately decline following peak-Guttenberg excursion values. This is evidence of a spatially coherent $\Delta^{13}C$ signal (on at least the continental-scale) with varying degrees of local overprinting. The authors agree with Pancost *et*

al. (1999), who argued that $\delta^{13}C_{org}$ correlations during this interval will be complicated by source mixing and prefer to use (screened and filtered) $\delta^{13}C_{carb}$, rather than $\delta^{13}C_{org}$ for continental and global correlations. Excluding the Decorah Formation, the lack of strong agreement in $\Delta^{13}C$ between sections suggests that existing paired $\delta^{13}C_{carb}$ and $\delta^{13}C_{org}$ data are insufficient to answer questions of global biogeochemical C cycling patterns across the whole study interval. More data, reflecting regionally reproducible trends, will be needed to extract additional meaning and evaluate possible causes of $\Delta^{13}C$ variation.

6.5 Correlation summary

The Guttenberg excursion is a clearly identifiable chemostratigraphic feature in both sections presented here regardless of the degree of sample screening and filtering. Correlations with unprocessed data have higher scatter (Figure 6) and as such, the unprocessed signal has less potential to make the confident high-resolution correlations needed to test geochemically based hypotheses. For example, a compilation of all data from this work (i.e., including those that did not pass the screening or filtering) would result in a Guttenberg excursion morphology that is relatively depleted in ^{13}C and more similar to that of the $\delta^{13}C_{carb}$ profile from Eureka, Missouri, a location ~13 km from Highway MM (Ludvigson *et al.,* 1996). It is possible that differences between the 'least-altered' data and the adjacent $\delta^{13}C_{carb}$ profile from Eureka could arise from local water column gradients; however, based on both the scatter in the unscreened data and the similarity between the two 'least-altered' $\delta^{13}C_{carb}$ profiles, it seems mechanistically more plausible that the lower $\delta^{13}C$ values and stratigraphic variability of the Eureka section (Ludvigson *et al.*, 1996) may in part arise from sample selection, insufficient sampling density, and/or diagenetic overprinting rather than the preservation of a primary $\delta^{13}C_{carb}$ signature.

Detailed analysis of isotopic variability – in the context of petrographic and geochemical indicators for alteration – is necessary to ascertain the origin of these disparities. High-resolution correlations using processed data (Figure 11) show that carefully screened bulk $\delta^{13}C_{carb}$ data can be used to correlate sections that at first glance seem to have significant local overprints, a problem that has hindered high-resolution correlations across Late Ordovician Laurentia (e.g., Ludvigson *et al.,* 2004; Young *et al.,* 2005; Bergström *et al.,* 2010a; Bergström *et al.,* 2010b; Coates *et al.,* 2010). While it may not be required for lower-order correlations, detailed sample screening can greatly increase knowledge of the sources of $\delta^{13}C_{carb}$ variability and fine-tune the understanding of basin-scale sedimentary and geochemical processes.

6.6 Depositional facies, sea level, $\delta^{13}C$ and $\delta^{18}O$

Facies likely exhibited both direct and indirect controls on $\delta^{13}C_{carb}$ and $\delta^{18}O_{carb}$ values at the bed scale and formation scale. Single beds (i.e., hand samples) showed differing isotope values related to burrow abundance and grain size. For example, samples from the peritidal Plattin Limestone contained high amounts of calcitic mud with relatively invariant $\delta^{13}C_{carb}$ and $\delta^{18}O_{carb}$ values, while burrows were isotopically more variable. The burrows likely functioned as conduits for post-depositional fluids and represent an indirect control of facies on isotope values. Samples from more hydrologically energetic facies, such as the Kimmswick Limestone, contained exhumed clasts from underlying formations, a direct control on bulk isotope values. Grainstones also are more porous than mudstones, facilitating inclusion of primary cements (direct control) and later recrystallization (indirect control). The more energetic facies limit the amount of carbonate mud, requiring sampling of the clast-cement mixtures that are associated with lower $\delta^{13}C_{carb}$ and $\delta^{18}O_{carb}$ values. In this context grainstone facies are more susceptible to

alteration (and an apparent isotopic offset) than muddier lithologies from less energetic facies. This seems to be the most likely cause for the low $\delta^{18}O_{carb}$ values in the grainstones of the Glencoe Shale and Kimmswick Limestone relative to the Decorah Formation and Plattin Limestone.

Facies controls on isotope values at the formation scale include the biological pump (Freeman, 2001) and "aquafacies" model (*sensu* Holmden *et al.*, 1998) and are the result of sea-level, microbial activity, and connectivity with the open ocean. As a result of the biological pump, DIC in shallow waters will become relatively enriched in ^{13}C as ^{12}C-rich organic carbon is formed and subsequently exported to the deep ocean (where part of it may be oxidized back to DIC). In contrast, the aquafacies model invokes local oxidation of organic matter to generate shallow waters of the cratonic interior that are hydrologically restricted and depleted in ^{13}C relative to the open ocean. These models can be compared with $\delta^{13}C_{carb}$ values observed for Localities Highway MM and New London. The highest $\delta^{13}C_{carb}$ values were observed in the Kings Lake and Guttenberg Formations, both of which are thought to represent the deepest and lowest energy facies. This result is opposite of what the biological pump model predicts and suggests that the biological pump is not controlling the stratigraphic variation in $\delta^{13}C_{carb}$ values in this interval in the Missouri area. The peak Guttenberg excursion values observed here match those in other Laurentian localities and do not match predicted $\delta^{13}C_{carb}$ for the Missouri region based on aquafacies-induced gradients in $\delta^{13}C_{DIC}$ (Young *et al.*, 2005). This suggests that the aquafacies model is not appropriate for this interval at these locations.

Isotope gradients can also result from more localized phenomena. Previous work on a slope-to-platform top transect of Carboniferous carbonates from Northwest Spain (Immenhauser *et al.*, 2003) revealed a $\delta^{13}C_{carb}$ gradient with heaviest values occurring in the deepest facies.

Immenhauser *et al.* (2003) explain the heavier $\delta^{13}C_{carb}$ values as resulting from the increased proportion of ^{13}C-enriched ocean water mixed in during high-amplitude transgression and varying early diagenetic histories. A proportionally lower amount of ^{13}C-enriched waters is mixed with the 'aged' platform top water in offshore areas resulting in a relatively lower $\delta^{13}C_{carb}$ profile in the more shoreward facies. This mixing model is also not appropriate for the Guttenberg excursion for several reasons. First, this excursion is confidently correlated over multiple basins on the Laurentian craton and believed to be a global event, which is not the case for the middle Atokan $\delta^{13}C_{carb}$ shift (Immenhauser *et al.*, 2003). This suggests that the mechanism responsible for the Guttenberg excursion would have to apply to the entire craton, if not the globe, and therefore includes numerous different facies and at a spatial scale where it is unrealistic to expect riverine waters to significantly impact $\delta^{13}C_{carb}$. Second, if the Guttenberg excursion represents the simple mixing of ocean water with ^{13}C-depleted, chemically-evolved epeiric platform water then the open ocean baseline must have been ~+3‰. (The absence of any abyssal Ordovician-aged seafloor precludes establishing an independent open ocean baseline.) If so, then the entire suite of existing records for this geologic period do not preserve an open ocean signal (e.g., Bergström *et al*., 2009b). Finally, while sea level is thought to have risen throughout the Late Ordovician (Munnecke *et al.*, 2010), there is no corresponding, continuous increase in $\delta^{13}C_{carb}$ of epeiric carbonates associated with this increase in ocean connectivity. Therefore, it does not appear that a transgression that increased ocean connectivity everywhere was the responsible for the Guttenberg excursion.

Another model explaining the relationship between sea level and $\delta^{13}C_{carb}$ has been proposed by Fanton & Holmden (2007), whereby sea level rise was accompanied by an increased flux of nutrient-rich open ocean water to the inner craton. This led to locally increased

primary productivity and organic carbon burial, which in turn increased $\delta^{13}C_{DIC}$. However, the agreement in $\delta^{13}C_{carb}$ values during the Guttenberg excursion across the Laurentian palaeocontinent argues that the origin of the higher $\delta^{13}C_{carb}$ values is the result of *global* processes (e.g., global organic carbon burial) rather than local or regional processes (e.g., runoff contributions from nearby highlands, microbial oxidation of organic matter).

6.7 Regional & global implications

Correlations from screened and filtered data give insight into the geochemical nature of ancient epeiric seas by discriminating against secondary signals. The correlations between New London and Highway MM are consistent with the Guttenberg excursion being an isochronous excursion that occurred in an isotopically well-mixed ocean. The magnitude of the Guttenberg excursion reported here (2.5‰) is comparable to those reported for the Guttenberg excursion from Iowa (2‰, Pancost *et al.*, 1999; 1.5-3‰, Ludvigson *et al.,* 2004), Pennsylvania (3‰, Patzkowsky *et al.,* 1997), Kentucky (2.0‰, Coates *et al.*, 2010), Virginia (2‰, Young *et al.,* 2005), West Virginia (2‰, Young *et al.,* 2005), and Tennessee (2.0-2.5‰, Bergström *et al.*, 2010a) (Figure 12). The pre-excursion, peak-excursion, and post-excursion values reported here also very closely match those reported for the "generalized $\delta^{13}C_{carb}$ curve" of Bergström *et al.* (2009b) (Figure 12). Compilation of these data can be used to understand geographic gradients and stratigraphic variability in $\delta^{13}C_{carb}$ records and their possible syndepositional and diagenetic causes.

Despite the general agreement in the aforementioned Guttenberg excursion $\delta^{13}C$ records, a detailed examination of some reports reveals local and regional variations in the stratigraphic expression of the Guttenberg excursion. For a single location in eastern Iowa, Ludvigson *et al.*

(1996) argued that primary micritic $\delta^{13}C_{carb}$ might be decoupled from coeval brachiopod $\delta^{13}C_{carb}$ signatures as a result of water column stratification. Comparisons of bulk carbonate $\delta^{13}C_{carb}$ data with coeval brachiopods from St. Louis County, Missouri (Shields *et al.,* 2003) show no systematic difference between the two material types, although the stratigraphic resolution of the brachiopods is low and the scatter in $\delta^{13}C_{carb}$ is relatively high in the Castlewood Limestone and Glencoe Shale equivalents, where the brachiopods were sampled. The present authors find no evidence for the stratification of the inner cratonic sea in the Missouri region.

Laterally restricted aquafacies with unique water column isotopic signatures have been proposed as an explanation for regional patterns in $\delta^{13}C_{carb}$ during the Guttenberg excursion (e.g., Young *et al.*, 2005). The data set of Ludvigson *et al.* (2004) shows apparent spatial variability in Guttenberg excursion $\delta^{13}C_{carb}$ curves in 6 cores from Iowa. Localities 4 and 5 of Ludvigson *et al.*(2004) have a $\delta^{13}C_{carb}$ profile very similar to that of New London while Locality 1 (located <50 km away from Localities 4 and 5) shows a different morphology; cores farther away have even more divergent profiles (Figure 12B). It is possible that these cores reflect different water column processes on the regional scale. Yet, the presence of Guttenberg excursion curves in Iowa that have the same pre-excursion, peak-excursion, and post-excursion values as the Missouri sections presented in this work (Figure 12B) and from more distal locations (e.g., West Virginia) (Figure 12C) suggests an alternative explanation, namely: *local syndepositional and post-depositional alteration is superimposed over a signal representing precipitation from an isotopically homogenous epeiric sea*. A prevalent mechanism by which such local variation could result is the metabolic oxidation of organic matter by microbes, which has been proposed as a contributing factor producing lower $\delta^{13}C_{carb}$ values in the pore waters and modern sediments of the Bahama Banks and Florida (Patterson & Walter, 1994). This results in scattered and lower

average $\delta^{13}C_{carb}$ values on the local scale. The present authors find this explanation more consistent with the data from this report than stratigraphically coherent gradients in $\delta^{13}C_{DIC}$ in the ancient ocean, which should not produce the observed $\delta^{13}C_{carb}$ trends characterized by high scatter and low $\delta^{13}C_{carb}$ values. The Iowa cores with $\delta^{13}C_{carb}$ profiles similar to the two new Missouri sections (despite the ~1,000 km distance between the Iowa and Missouri sections) may be the most representative of open marine values, whereas the stratigraphically variable $\delta^{13}C_{carb}$ profiles in adjacent cores (despite their proximity to each other) would result from diagenetic alteration or a local water-column signal that is unrelated to any large-scale 'ocean-to-inner craton' gradient. Importantly, the sections with low stratigraphic scatter in $\delta^{13}C_{carb}$ all meet the 'generalized' peak-Guttenberg excursion value (~2.5‰) of Bergstrom *et al.* (2009b), while sections with higher scatter do not meet the peak value. The $\delta^{13}C_{carb}$ scatter is preferentially toward lower $\delta^{13}C_{carb}$ values. This differs from true 'noise' (i.e., random scatter around a mean value), which should also have values that are *heavier* than the mean $\delta^{13}C_{carb}$, which is not observed (Figure 12B and C). In this view, the midcontinent Guttenberg excursion curve (corresponding to "midcontinent aquafacies") of Young *et al.* (2005) was constructed using sections that may have been impacted by diagenetic overprinting and does not reflect a primary craton-scale $\delta^{13}C_{carb}$ gradient. This interpretation suggests that more locations may have undergone more substantial diagenetic alteration than previously assumed.

This work does not argue that large-scale isotopic gradients could not exist in another time period or location, or for isotopic systems other than carbon (e.g., neodymium). This work does argue that for the specific case of midcontinent records of the Guttenberg excursion no long-range spatial gradient in $\delta^{13}C_{carb}$ is required to explain the observed trends. Instead, the existing Guttenberg excursion records are more parsimoniously interpreted as reflecting

differential alteration of a spatially *homogenous* primary $\delta^{13}C_{carb}$ signal, rather than faithful preservation of what is essentially a spatially *heterogenous* $\delta^{13}C_{carb}$ primary signal. Figure 12B separates the midcontinent aquafacies into two categories, those thought to track the global $\delta^{13}C_{carb}$ record and those that do not, the former being suitable for chemostratigraphic correlation and reconstructions of ocean chemistry. Missouri sections Highway MM and New London (Midcontinent aquafacies) have the same basic Guttenberg excursion values as the more hydrologically connected Taconic and Southern aquafacies sections. Correlation with Iowa sections suggests that any pre-existing regional $\delta^{13}C_{carb}$ gradient (Panchuck *et al.*, 2006) was abolished in the Missouri-Iowa region during Guttenberg excursion-time coincident with the craton-wide Mohawkian transgression (e.g., Kolata *et al.,* 1998; Kolata *et al*., 2001).

It is clear that studies used to reconstruct spatial or temporal variability in ocean chemistry or carbon cycling need to be conducted at a high sampling resolution and data need to be placed in a rigorous depositional context and evaluated based on petrographic and geochemical indicators of alteration whenever possible. Because the understanding of oceanic connectivity and the biogeochemical C-cycle hinge on $\delta^{13}C_{carb}$ chemostratigraphic correlations, differing treatment of data sets can profoundly change the understanding of the Earth System.

7. CONCLUSIONS

This work supplies techniques for assessing diagenetic alteration of $\delta^{13}C_{carb}$ and $\delta^{18}O_{carb}$ over a large range of spatial scales and contributes to the general understanding of C-isotope homogeneity and hydrologic connectivity in ancient epeiric seas. Results from this work demonstrate that the variable Guttenberg carbon isotope excursion profiles can be explained in terms of local diagenetic alteration and are not consistent

with the previously proposed "aquafacies" model, which invoked an isotopically heterogeneous epeiric sea that formed as a result of a stable long-term and long-range ocean-to-craton $\delta^{13}C_{DIC}$ gradient. Specifically:

1. Significant isotopic heterogeneity (up to 2‰ in $\delta^{13}C_{carb}$ and 3‰ in $\delta^{18}O_{carb}$) within single hand samples can be superimposed over the Guttenberg carbon isotope excursion. These variations typically result from the admixture of multiple isotopically distinct components of primary and secondary origin, rather than from dynamic carbon cycling or spatially heterogeneous reservoirs. Screening of $\delta^{13}C_{carb}$ data using petrographic, geochemical, and isotopic methods explains apparent differences in $\delta^{13}C_{carb}$ profiles between sections and the resulting correlations have higher stratigraphic resolving power than unprocessed data.

2. Normalized $\delta^{13}C_{carb}$ excursion profiles can help identify alteration at the outcrop scale by comparing $\delta^{13}C_{carb}$ morphologies from within a single basin. Normalized $\delta^{13}C_{carb}$ curves for the Guttenberg excursion show that ^{13}C-enriched locations have regionally reproducible $\delta^{13}C_{carb}$ profiles and low $\delta^{13}C_{carb}$ scatter. In contrast, sections that are relatively depleted in ^{13}C are associated with poor regional reproducibility of $\delta^{13}C_{carb}$ trends and high $\delta^{13}C_{carb}$ scatter, patterns consistent with local diagenetic alteration.

3. The strong agreement in absolute values of $\delta^{13}C_{carb}$ before, at the peak of, and after the Guttenberg excursion in sections identified as 'least-altered' support an isotopically homogenous carbon reservoir.

4. Paired $\delta^{13}C_{carb}$ and $\delta^{13}C_{org}$ data yield $\Delta^{13}C$ profiles that are similar during the peak and falling stage of the Guttenberg excursion; the regional reproducibility of this trend suggests preservation of a primary $\Delta^{13}C$ signature in this interval with possible global implications.

Chemostratigraphic correlations between Localities Highway MM and New London give insight into the temporal and spatial relationships of Upper Ordovician strata in central and northern Missouri and relate them to other strata of similar age.

1. High-resolution $\delta^{13}C_{carb}$ records show that the Upper Kings Lake and Guttenberg Limestones in Missouri, previously thought to be successive, are largely coeval. The stratigraphically smooth $\delta^{13}C_{carb}$ profiles support a less substantial erosional history in eastern Missouri during post-Kings Lake, pre-Kimmswick time than has been previously reported.
2. Lithologic and chemostratigraphic evidence suggests that a thickening of the Guttenberg excursion interval in northern Missouri largely resulted from an increased relative sedimentation rate in northern Missouri during the last half of the Guttenberg excursion.

8. ACKNOWLEDGEMENTS

The authors wish to thank R. Folkerts for her indispensable assistance in the field; D. Kolata for guidance in the field and for discussions of the regional stratigraphy; D. McCay for help preparing and analysing samples; S. Young, R. Criss, F. Moynier, and J. Catalano for discussions; P. Skemer for use of laboratory equipment; and B. Mahan for assistance with

microscopy and photography. The manuscript was greatly improved by insightful comments from L. Kump and an anonymous reviewer as well as A. Immenhauser and T. Frank. Support was provided in part by funding from the Agouron Institute, the ACS Petroleum Research Fund (Grant No. 51357-DNI2), and a Hanse-wissenschaftskolleg Fellowship awarded to D.A.F. In addition, isotope analyses and travel were partly funded by a DOSECC graduate research grant and a GSA graduate research grant awarded to J.G.M.

9. REFERENCES

Allan, J.R., Matthews, R.K. (1982) Isotope signatures associated with early meteoric diagenesis. *Sedimentology*, v. **29**, 797-817.

Bergström, S.M., Huff, W.D., Saltzman, M.R., Kolata, D.R., Leslie, S.A. (2004) The greatest volcanic ash falls in the Phanerozoic: Trans-Atlantic relations of the Ordovician Millbrig and Kinnekulle K-bentonites. *The Sedimentary Record*, v. **2**, 4-8.

Bergström, S.M., Xu, C., Schmitz, B., Young, S., Jia-Yu, R., Saltzman, M.R. (2009a) First documentation of the Ordovician Guttenberg $\delta^{13}C$ excursion (Guttenberg excursion) in Asia: chemostratigraphy of the Pagoda and Yanwashan formations in southeastern China. *Geol. Mag.*, v. **146**, 1-11.

Bergström, S.M., Chen, X., Gutiérrez-Marco, J.C., Dronov, A., (2009b) The new chronostratigraphic classification of the Ordovician System and its relations to major regional series and stages and to δ13C chemostratigraphy. *Lethaia*, v. **42**, 97-107.

Bergström, S.M., Schmitz, B., Saltzman, M.R., Huff, W.D., (2010a) The Upper Ordovician Guttenberg δ13C excursion (Guttenberg excursion) in North America and Baltoscandia: Occurrence, chronostratigraphic significance, and paleoenvironmental relationships. In: *Geol. Soc. Am. Spec. Pap.*, **466** (Ed S.C. Finney, Berry, W.B.N.), pp. 36-67.

Bergström, S.M., Young, S., Schmitz, B. (2010b) Katian (Upper Ordovician) $\delta^{13}C$ chemostratigraphy and sequence stratigraphy in the United States and Baltoscandia: A regional comparison. *Palaeogeography, Palaeoclimatology, Palaeoecology*, v. **296**, 217-234.

Bergstrom, S.M., Agematsu, S., Schmitz, B. (2010c) Global Upper Ordovician correlation by means of $\delta^{13}C$ chemostratigraphy: implications of the discovery of the Guttenberg $\delta^{13}C$ excursion (Guttenberg excursion) in Malaysia. *Geol. Mag.*, v. **147**, 641-651.

Brand, U. (2004) Carbon, oxygen and strontium isotopes in Paleozoic carbonate components: an evaluation of original seawater-chemistry proxies. *Chem. Geol.*, v. **204**, 23-44.

Brand, U., Tazawa, J., Sano, H., Azmy, K., Lee, X. (2009). "Is mid-late Paleozoic ocean-water chemistry coupled with epeiric seawater isotope records?" *Geology,* v. **37**: 823-826.

Brett, C.E., McLaughlin, P.I., Cornell, S.R. and Baird, G.C. (2004) Comparative sequence stratigraphy of two classic Upper Ordovician successions, Trenton Shelf (New York-Ontario) and Lexington Platform (Kentucky-Ohio): implications for eustasy and local tectonism in eastern Laurentia. *Palaeogeogr. Palaeoclimatol. Palaeoecol.*, v. **210**, 295-329.

Coates, J.W., Ettensohn, F.R., Rowe, H.D. (2010) Correlations across a facies mosaic within the Lexington Limestone of central Kentucky, USA, using whole-rock stable isotope compositions. In: *Geol. Soc. Am. Spec. Pap.*, **466** (Ed S.C. Finney, Berry, W.B.N.), pp. 177-193.

Dehler, C.M., Elrick, M., Bloch, J.D., Crossey, L.J., Karlstrom, K.E., Des Marais, D.J. (2005) High-resolution delta C-13 stratigraphy of the Chuar Group (ca. 770-742 Ma), Grand Canyon: Implications for mid-Neoproterozoic climate change. *Geol. Soc. Am. Bull.,* v. **117**, 32-45.

Epstein, S., Mayeda, T.K. (1953) Variations of O^{18} content of waters from natural sources. *Geochim. Cosmochim. Acta*, v. **4**, 213-224.

Fanton, K.C., Holmden, C. (2007) Sea-level forcing of carbon isotope excursions in epeiric seas: implications for chemostratigraphy. *Can. J. Earth Sci.*, v. **44**, 807-818.

Freeman, K.H. (2001) Isotope Biogeochemistry of Marine Organic Carbon. In: *Reviews in Mineralogy & Geochemistry 43: Stable Isotope Geochemistry* (Ed J.W. Valley, Cole D.R.), v. **43**, 579-605. Mineralogical Society of America and Geochemical Society.

Flügel, E. (2009) *Microfacies of Carbonate Rocks: Analysis, Interpretation and Application*. Springer Verlag, Berlin, 984 pp.

Hayes, J.M., Strauss, H., Kaufman, A.J. (1999) The abundance of ^{13}C in marine organic matter and isotopic fractionation in the global biogeochemical cycle of carbon during the past 800 Ma. *Chem. Geol.*, v. **161**, 103-125.

Holland, S.M., Patzkowsky, M.E. (1997) Distal orogenic effects on peripheral bulge sedimentation: Middle and Upper Ordovician of the Nashville Dome. *J. Sed. Res.*, v. **67**, 250-263.

Holland, S.M., Patzkowsky, M.E. (1998) Sequence stratigraphy and relative sea-level history of the Middle and Upper Ordovician of the Nashville Dome, Tennessee. *J. Sed. Res.*, **6v. 8**, 684-699.

Holmden, C., Creaser, R.A., Muehlenbachs, K., Leslie, S.A. and Bergstrom, S.M. (1998) Isotopic evidence for geochemical decoupling between ancient epeiric seas and bordering oceans: Implications for secular curves. *Geology*, v. **26**, 567-570.

Huff, W.D. (2008) Ordovician K-bentonites: Issues in interpreting and correlating ancient tephras. *Quatern. Int.*, v. **178**, 276-287.

Immenhauser, A., Kenter, J.A.M., Ganssen, G., Bahamonde, J.R., Vliet, A.V., Saher, M.H. (2002) Origin and significance of isotope shifts in Pennsylvanian carbonates (Asturias, NW Spain). *Journal of Sedimentary Research*, v. **72**, 82-94.

Immenhauser, A., Della Porta, G., Kenter, J.A.M., Bahamonde, J.R. (2003) An alternative model for positive shifts in shallow-marine carbonate $\delta^{13}C$ and $\delta^{18}O$. *Sedimentology*, v. **50**, 953-959

Immenhauser, A., Holmden, C., Patterson, W. (2008) Interpreting the carbon-isotope record of ancient shallow epeiric seas: Lessons from the recent. In: *Dynamics of Epeiric Seas* (Ed B.R. Pratt, Holmden, C.), *Geological Association of Canada Special Paper*, v. **48**, 137-174.

Joachimski, M.M. (1994) Subaerial exposure and deposition of shallowing upward sequences: evidence from stable isotopes of Purbeckian peritidal carbonates (basal Cretaceous), Swiss and French Jura Mountains. *Sedimentology*, 41, 805-824.Johnston, D.T., Macdonald, F.A., Gill, B.C., Hoffman, P.F., Schrag, D.P. (2012) Uncovering the Neoproterozoic carbon cycle. *Nature*, **4v. 83**, 320-324.

Jones, D.S., Fike, D.A., Finnegan, S., Fischer, W.W., Schrag, D.P., McCay, D. (2011) Terminal Ordovician carbon isotope stratiraphy and glacioeustatic sea-level change across Anticost Island (Québec, Canada). *Geol. Soc. Am. Bull.,* v. **123**, 1645-1664.

Kay, G.M. (1935) Ordovician System of the upper Mississippi Valley. In: *Kansas Geological Society 9th regional field conference, Upper Mississippi River Valley*, pp. 281-295. Kansas Geological Society.

Kaljo, D., Martma, T., Saadre, T. (2007) Post-Hunnebergian Ordovician carbon isotope trend in Baltoscandia, its environmental implications and some similarities with that of Nevada. *Palaeogeogr. Palaeoclimatol. Palaeoecol.*, v. **245**, 138-155.

Knoll, A.H., Hayes, J.M., Kaufman, A.J., Swett, K., Lambert, I.B. (1986) Secular variation in carbon isotope ratios from Upper Proterozoic Successions of Svalbard and East Greenland. *Nature*, v. **321**, 832-838.

Kolata, D.R., Frost, J.K., Huff, W.D. (1986) K-bentonites of the Ordovician Decorah Subgroup, upper Mississippi Valley: Correlation by chemical fingerprinting. *Illinois State Geological Survey Circular*, v. **537**, 30 pp.

Kolata, D.R., Frost, J.K., Huff, W.D. (1987) Chemical correlation of K-bentonite bed in the Middle Ordovician Decorah Subgroup, upper Mississippi Valley. *Geology*, 15, 208-211.

Kolata, D.R., Huff, W.D., Bergström, S.M. (1996) Ordovician K-bentonites of eastern North America. *Geol. Soc. Am. Spec. Pap.*, v. **313**, pp. 84.

Kolata, D.R., Huff, W.D., Bergström, S.M. (1998) Nature and regional significance of unconformities associated with the Middle Ordovician Hagan K-bentonite complex in the North American midcontinent. *Geol. Soc. Am. Bull*, v. **110**, 723-739.

Kolata, D.R., Huff, W.D., Bergström, S.M. (2001) The Ordovician Sebree Trough: An oceanic passage to the Midcontinent United States. *Geol. Soc. Am. Bull*, v. **113**, 1067-1078.

Kump, L., R., Arthur, M.A. (1999) Interpreting carbon-isotope excursions: carbonates and organic matter. *Chem. Geol.*, v. **161**, 181-198.

Leslie, S.A., Bergström, S.M. (1997) Use of K-bentonite beds as time-planes for high-resolution lithofacies analysis and assessment of net rock accumulation rate: An example from the upper Middle Ordovician of eastern North America. In *Paleozoic Sequence Stratigraphy, Biostratigraphy, and Biogeography: Studies in Honor of J. Granville ("Jess") Johnson* (Ed G. Klapper, Murphy, M.A., and J.A. Talent), *Geol. Soc. Am. Spec. Pap., v.* ***321***, 11-21.

Leslie, S.A. (2000) Mohawkian (Upper Ordovician) conodonts of eastern North America and Baltoscandia. *J. Paleontol.*, v. **74**, 1122-1147.

Lohmann, K.C. (1988) Geochemical patterns of meteoric diagenetic systems and their application to studies of paleokarst. In: *Paleokarst* (Ed N.P. James, Choquette, P.W.), pp. 416. Springer-Verlag, New York City.

Ludvigson, G.A., Jacobson, S.R., Witzke, B.J., Gonzàlez, L.A. (1996) Carbonate component chemostratigraphy and depositional history of the Ordovician Decorah Formation, Upper Mississippi Valley. In *Paleozoic sequence stratigraphy; views from the North American Craton* (Ed B.J. Witzke, Ludvigson, G.A., and J. Day), *Geological Society of America Special Paper*, v. **306**, 67-86.

Ludvigson, G.A., Witzke, B.J., Schneider, C.L., Smith, E.A., Emerson, N.R., Carpenter, S.J., González, L.A. (2000) A profile of the mid-Caradoc (Ordovician) carbon isotope excursion at the McGregor Quarry, Clayton County, Iowa. *Geological Society of Iowa Guidebook*, 70, 25-31.

Ludvigson, G.A., Witzke, B.J., Gonzàlez, L.A., Carpenter, S.J., Schneider, C.L., Hasiuk, F. (2004) Late Ordovician (Turinian-Chatfieldian) carbon isotope excursions and their stratigraphic and paleoceanographic significance. *Palaeogeogr. Palaeoclimatol. Palaeoecol.*, v. **210**, 187-214.

Martin, J.A., Knight, R.D., Hayes, W.C. (1961) Ordovician System. In: *The stratigraphic succession in Missouri* (Ed. J.W. Koenig), Missouri Geological Survey and Water Resources, v. **40**, 32-35.

Martma, T. (2005) Ordovician carbon isotopes. In. Põldvere, A. (Ed.), *Estonian Geological Sections, Kerguta (564) Drill Core: Geol. Surv. Estonia Bull.*, v. **7**, 25-30.

McCracken, M.H. (1966) Major structural features of Missouri [Map]. Missouri Department of Natural Resources: Division of Geology and Land Survey, Rolla. http://www.dnr.mo.gov/geology/adm/publications/map-MajorStrucFeatures.pdf

McLaughlin, P.I., Brett, C.E. (2007) Signatures of sea-level rise on the carbonate margin of a Late Ordovician foreland basin: A case study from the Cincinnati Arch, USA. *Palaios*,v. **22**, 245-267.

Missouri Department of Natural Resources (2009) Generalized Geology Map of Missouri [Map]. Missouri Department of Natural Resources: Division of Geology and Land Survey, Rolla. www.dnr.mo.gov/geology.

Mitchell, C.E., Adhya, S., Bergström, S.M., Joy, M.P., Delano, J.W. (2004) Discovery of the Ordovician Millbrig K-bentonite Bed in the Trenton Group of New York State: implications for regional correlation and sequence stratigraphy in eastern North America. *Palaeogeogr. Palaeoclimatol. Palaeoecol.*, v. **210**, 331-346.

Munnecke, A., Calner, M., Harper, D.A.T. and Servais, T. (2010) Ordovician and Silurian sea-water chemistry, sea level, and climate: A synopsis. *Palaeogeography Palaeoclimatology Palaeoecology*, **2v. 96**, 389-413.

Pancost, R.D., Freeman, K.H. and Patzkowsky, M.E. (1999) Organic-matter source variation and the expression of a late Middle Ordovician carbon isotope excursion. *Geology*, v. **27**, 1015-1018.

Panchuk, K.M., Holmden, C. and Kump, L.R. (2005) Sensitivity of the epeiric sea carbon isotope record to local-scale carbon cycle processes: Tales from the Mohawkian Sea. *Palaeogeogr. Palaeoclimatol. Palaeoecol.*, v. **228**, 320-337.

Panchuk, K.M., Holmden, C.E. and Leslie, S.A. (2006) Local controls on carbon cycling in the Ordovician midcontinent region of North America, with implications for carbon isotope secular curves. *J. Sed. Res.*, v. **76**, 200-211.

Patterson, W.P., Walter, L.M. (1994) Depletion of ^{13}C in seawater ΣCO_2 on modern carbonate platforms: Significance for the carbon isotopic record of carbonates. *Geology*, v. **22**, 885-888

Patzkowsky, M.E., Slupik, L.M., Arthur, M.A., Pancost, R.D., Freeman, K.H., (1997) Late Middle Ordovician environmental change and extinction: Harbinger of the Late Ordovician or continuation of Cambrian patterns? *Geology*, v. **25**, 911-914.

Railsback, L.B., Holland, S.M., Hunter, D.M., Jordan, E.M., Díaz, J.R., Crowe, D.E. (2003) Controls on geochemical expression of subaerial exposure in Ordovician limestones from the Nashville Dome, Tennessee, U.S.A. *J. Sed. Res.*, v. **73**, 790-805.

Rodgers, J. (1971) The Taconic Orogeny. *Geol. Soc. Am. Bull.*,v. **82**, 1141-1178.

Scotese, C.R., McKerrow, W.S. (Eds.) (1990) Revised world maps and introduction. In *Paleozoic paleogeography and biogeography*, *Geological Society of London Memoir*, v. **12**, 1-21.

Sell, B.K., Samson, S.D. (2011) Apatite phenocryst compositions demonstrate a miscorrelation between the Millbrig and Kinnekulle K-bentonites of North America and Scandinavia. *Geology*, v. **39**, 303-306.

Shields, G.A., Carden, G.A.F., Veizer, J., Meidla, T., Rong, J.Y. and Li, R.Y. (2003) Sr, C, and O isotope geochemistry of Ordovician brachiopods: A major isotopic event around the Middle-Late Ordovician transition. *Geochim. Cosmochim. Acta*, v. **67**, 2005-2025.

Simo, J.A., Emerson, N.R., Byers, C.W. and Ludvigson, G.A. (2003) Anatomy of an embayment in an Ordovician epeiric sea, Upper Mississippi Valley, USA. *Geology*, v. **31**, 545-548.

Swart, P.K. (2008) Global synchronous changes in the carbon isotopic composition of carbonate sediment unrelated to changes in the global carbon cycle. *Proc. Natl Acad. Sci. USA*, v. **105**, 13741-13745.

Templeton, J.S., Willman, H.B. (1963) Champlainian Series (Middle Ordovician) in Illinois. *Illinois State Geological Survey Bulletin*, v. **89**, 260 p.

Thompson, T.L. (1991) Paleozoic Successions in Missouri Part II: Ordovician System. *Missouri Geological Survey Report of Investigations*, v. **70**, 110-213.

Tucker, R.D. (1992) U-Pb dating of plinian-eruption ashfalls by the isotope dilution method: a reliable and precise tool for time-scale calibration and biostratigraphic correlation. *Geol. Soc. Am. Meeting*, v. **24**, A198.

Tucker, R.D., McKerrow, W.S. (1995) Early Paleozoic chronology: a review in light of new U-Pb zircon ages from Newfoundland and Britain. *Can. J. Earth Sci.*, v. **32**, 368-379.

Ulrch, E.O. (1904) The quarrying industry of Missouri (Ed E.R. Buckley, Buehler, H.A.), 2, pp. 109-111. Missouri Bureau of Geology and Mines.

Veizer, J., Bruckschen, P., Pawellek, F., Diener, A., Podlaha, O.G., Carden, G.A.F., Jasper, T., Korte, C., Strauss, H., Azmy, K. and Ala, D. (1997) Oxygen isotope evolution of Phanerozoic seawater. *Palaeogeogr. Palaeoclimatol. Palaeoecol.*, v. **132**, 159-172.

Veizer, J., Ala, D., Azmy, K., Bruckschen, P., Buhl, D., Bruhn, F., Carden, G.A.F., Diener, A., Ebneth, S., Godderis, Y., Jasper, T., Korte, C., Pawellek, F., Podlaha, O.G., Strauss, H. (1999) $^{87}Sr/^{86}Sr$, $\delta^{13}C$ and $\delta^{18}O$ evolution of Phanerozoic seawater. *Chem. Geol.*, v. **161**, 59-88.

Witzke, B.J., Kolata, D.R. (1988) Changing structural and depositional patterns, Ordovician Champlainian and Cincinnatian Series of Iowa-Illinois. *Iowa Department of Natural Resources Guidebook*, **8**, 55-77.

Young, S.A., Saltzman, M.R., Bergström, S.M. (2005) Upper Ordovician (Mohawkian) carbon isotope ($\delta^{13}C$) stratigraphy in eastern and central North America: Regional expression of a perturbation of the global carbon cycle. *Palaeogeogr. Palaeoclimatol. Palaeoecol.*, v. **222**, 53-76.

Young, S.A., Saltzman, M.R., Bergstrom, S.M., Leslie, S.A. and Xu, C. (2008) Paired $\delta^{13}C_{carb}$ and $\delta^{13}C_{org}$ records of Upper Ordovician (Sandbian-Katian) carbonates in North America and China: Implications for paleoceanographic change. *Palaeogeogr. Palaeoclimatol. Palaeoecol.*, v. **270**, 166-178.

10. SUPPLEMENTAL TABLES

Sample ID	Height (m)	$\delta^{13}C_{carb}$ (‰)	α	$\delta^{18}O_{carb}$ (‰)	α	Screen	$\delta^{18}O_{carb}$ filter	$\delta^{13}C_{org}$ (‰)	$\Delta^{13}C$ (‰)	Sr (ppm)	Mn/Sr	$\%CO_3$	TOC (%)	Unit
NL57	0.24	-0.88	0.27	-5.31	0.31	2/2	2/2	-29.7	28.85	271	0.22	97.9	0.09	P:MA
NL58	0.47	-0.87	0.26	-5.71	0.13	2/2	2/2	-30.2	29.37	207	0.26	98.6	0.10	P:MA
NL59	1.78					1/1	0/1	-29.9		213	0.37	98.6	0.08	P:MA
NL60	3.18	-0.78	0.04	-5.87	0.04	1/1	1/1	-29.9	29.13	262	0.25	98.2	0.07	P:MA
NL61	3.93	-0.53	0.09	-5.94	0.06	1/1	1/1	-29.8	29.24	395	0.11	98.2	0.06	P:MA
NL1	4.09	-0.20	0.09	-5.75	0.62	4/4	1/4							P:MA
NL2	4.45	-0.57	0.22	-5.94	0.13	8/8	8/8	-30.1	29.50	280	0.25	98.9	0.12	P:MA
NL3	5.00	-0.32	0.02	-5.56	0.20	2/2	2/2	-30.5	30.15	411	0.14	99.1	0.09	P:MA
NL4	5.42	0.20	0.00	-4.41	0.00	1/6	1/1	-31.2	31.39	377	0.17	96.7	0.16	P:MA
NL5	5.70	-0.12	0.02	-5.41	0.00	2/2	2/2	-31.5	31.37			98.1	0.16	P:MA
NL6	5.89	-0.63	0.31	-5.64	0.25	4/4	4/4	-30.4	29.72			97.8	0.15	P:MA
NL7	6.14					FAIL	N.A.	-30.5				96.5	0.11	P:MA
NL8	6.35					FAIL	N.A.	-29.3		381	0.27	97.5	0.05	P:CW
NL9	6.80	-1.42	0.17	-5.63	0.46	3/3	3/3	-29.6	28.21	264	0.30	94.8	0.03	P:CW
NL10	6.93	-0.55	0.29	-5.16	0.29	1/3	1/1	-28.1	27.54	268	0.26	95.7	0.04	P:CW
NL11	7.03	-0.43	0.77	-5.25	0.45	6/6	6/6	-28.8	28.37			94.9	0.06	P:CW
NL12	7.27	0.23	0.53	-4.99	0.00	3/3	3/3	-28.8	29.07			96.4	0.33	P:CW
NL13	7.41	-0.92	0.11	-5.86	0.80	2/2	1/2	-30.6	29.71	409	0.26	97.4	0.09	P:CW
NL14	7.60	0.81	0.14	-4.97	0.14	5/5	4/5	-30.4	31.19	586	0.18	98.0	0.06	D:GS
NL15	7.70	0.46	0.89	-4.49	0.40	3/3	3/3	-30.4	30.84	382	0.34	95.4	0.08	D:GS
NL16	8.02	-0.74	0.02	-4.88	0.05	1/1	1/1	-30.4	29.61			91.6	0.07	D:GS
NL17	8.09	-0.18	0.04	-4.34	0.08	4/4	4/4	-29.5	29.37			90.2	0.13	D:GS
NL70	8.22					FAIL	N.A.							D:GS
NL18	8.37	1.50	0.12	-4.75	0.06	1/1	1/1	-28.5	30.04	487	0.91	89.4	0.09	D:GS
NL19	8.61					1/3	0/1			323	0.74	80.3	0.13	D:KL
NL71	8.86	-0.11	0.05	-6.00	0.06	3/3	2/3							D:KL
NL20	9.22					FAIL	N.A.	-27.8	28.51	187	2.09	84.8	0.10	D:KL
NL72	9.60					5/5	0/5							D:KL
NL21	9.93	0.99	0.01	-5.37	0.16	3/3	3/3			429	0.54	93.3	0.04	D:KL
NL22	10.24	2.33	0.09	-5.13	0.06	1/6	1/1	-27.9	30.21			89.5	0.19	D:KL
NL23	10.63	2.47	0.04	-5.07	0.16	3/3	3/3	-28.1	30.59			88.7	0.25	D:KL
NL24	10.74	2.55	0.02	-5.14	0.05	1/3	1/1	-28.2	30.77			88.7	0.27	D:G
NL25	10.98	2.13	0.04	-5.55	0.07	1/1	1/1	-28.0	30.13	986	0.24	97.5	0.27	D:G
NL26	11.05	2.25	0.00	-5.65	0.00	1/1	1/1	-28.3	30.56	852	0.28	91.2	0.78	D:G
NL27	11.28	2.22	0.15	-5.51	0.29	2/2	2/2	-27.5	29.69			99.0		D:G
NL28	11.41	2.63	0.05	-5.33	0.12	4/6	4/4	-27.8	30.41	601	0.43	90.7	0.67	D:G
NL29	12.01	2.45	0.29	-5.45	0.02	1/4	1/1	-28.0	30.42			88.1	1.03	D:G
NL30	12.30	2.75	0.00	-5.29	0.00	1/3	1/1	-27.2	29.96	912	0.27	87.5	1.32	D:G
NL31	12.39	2.73	0.19	-5.47	0.38	2/3	2/2	-27.3	30.06			88.6	1.60	D:G
NL32	12.54	2.70	0.00	-5.28	0.00	1/2	1/1	-27.5	30.25	783	0.34	94.2	0.95	D:G
NL33	12.67	2.83	0.00	-5.27	0.12	2/3	2/2	-26.9	29.69			89.5	1.36	D:G
NL34	12.76	2.65	0.01	-5.44	0.10	1/5	1/1	-27.0	29.70			84.4	2.52	D:G
NL35	13.14	2.43	0.00	-5.19	0.00	2/2	2/1					88.9	1.32	D:G
NL36	13.46	2.67	0.00	-5.19	0.00	1/3	1/1	-27.6	30.26	791	0.34	91.4	1.10	D:G
NL37	13.59	2.52	0.02	-5.45	0.04	1/3	1/1	-27.5	30.00			83.9	0.16	D:G
NL38	13.92	2.40	0.03	-5.01	0.03	2/2	2/2	-27.0	29.42	755	0.32	86.7	1.43	D:G
NL39	14.23	2.50	0.03	-5.55	0.06	1/5	1/1	-27.3	29.84	748	0.36	91.7	0.82	D:G
NL40	14.49	2.33	0.00	-5.38	0.00	1/5	1/1	-27.4	29.78			91.4	0.71	D:G
NL41	14.58	2.11	0.21	-5.48	0.08	1/1	1/1	-27.3	29.44			92.5	0.98	D:G
NL42	14.67	1.95	0.39	-5.68	0.13	1/2	1/1	-26.9	28.89			92.7	0.89	D:G
NL43	15.02	1.98	0.11	-5.45	0.06	1/3	1/1	-27.4	29.36	606	0.44	96.0	0.67	D:G
NL44	15.09	1.84	0.04	-5.38	0.02	1/3	1/1	-27.3	29.14	667	0.39	95.5	0.87	D:G
NL45	15.25	1.66	0.00	-5.69	0.00	1/3	1/1	-27.6	29.25	636	0.43	91.5	1.87	D:G
NL46	15.40	1.70	0.00	-5.48	0.27	2/3	2/2	-27.2	28.92	613	0.45	96.5	0.74	D:G
NL47	15.50	1.68	0.00	-5.62	0.19	5/5	5/5	-27.5	29.19	606	0.47	93.2	1.16	D:G

NL48	15.58	1.55	0.00	-5.36	0.03	1/3	1/1	-27.1	28.66			94.7	1.06	D:G
NL49	15.73					3/3	0/3	-27.0		447	0.75	95.7	0.90	D:G
NL50	15.75	1.17	0.16	-5.78	0.19	3/3	2/3	-27.1	28.26	480	0.66	96.9	0.66	D:G
NL51	15.77					2/3	0/2	-25.6				97.9	0.61	D:G
NL52	15.90	0.39	0.03	-5.49	0.24	1/3	1/1	-28.2	28.59	321	1.38	99.3	0.02	KW
NL53	15.96	0.64	0.02	-6.00	0.04	2/2	2/2	-28.1	28.72	187	2.45	91.6	0.20	KW
NL54	16.13	0.51	0.12	-6.54	0.14	1/3	1/1	-28.8	29.31	177	2.51	98.9	0.06	KW
NL55	16.21	0.47	0.00	-7.00	0.09	2/2	1/2	-29.6	30.05	181	2.51	98.2	0.26	KW
NL62	16.81	0.51	0.05	-6.83	0.07	1/1	1/1	-28.7	29.17	174	2.73	98.5	0.10	KW
NL64	17.70	0.37	0.08	-6.85	0.07	2/2	2/2	-28.5	28.86	121	4.27	99.4	0.05	KW
NL65	17.80	0.50	0.02	-6.67	0.27	2/2	2/2	-28.8	29.32	145	3.52	99.2	0.06	KW
NL66	18.15	-0.01	0.01	-6.46	0.47	2/2	2/2			207	2.45	98.5	0.01	KW
NL67	20.85	0.09	0.08	-6.36	0.05	1/1	1/1			121	3.03	99.7		KW
NL68	21.18	-0.01	0.25	-5.85	0.10	1/3	1/1			196	2.52	99.9		KW
NL69	23.01	-0.73	0.04	-6.59	0.29	2/2	2/2			172	2.55	98.7	0.02	KW

Table S1. Geochemical data for location New London. Values are bed average. $\delta^{13}C_{carb}$. $\delta^{13}C_{org}$, and $\delta^{18}O_{carb}$ reported relative to VPDB. σ: one standard deviation for total number of samples (n) in a given bed. "Texture screen" refers to number of samples that passed the isotope-texture screen out of total number of samples. "FAIL" corresponds to beds that had only secondary textures present. "$\delta^{18}O_{carb}$ filter" refers to the number of samples that passed the $\delta^{18}O_{carb}$ filter out of total number of samples that passed the isotope-texture screen. Unit abbreviations are CW = Castlewood, D = Decorah Formation, G = Guttenberg Limestone, GS = Glencoe Shale, KL = Kings Lake Limestone, KW = Kimmswick Limestone, MA = Macy Member, P = Plattin Group.

Sample ID	Height (m)	$\delta^{13}C_{carb}$ (‰)	α	$\delta^{18}O_{carb}$ (‰)	α	Texture screen	$\delta^{18}O_{carb}$ filter	n	$\delta^{13}C_{org}$ (‰)	$\Delta^{13}C$ (‰)	Sr (ppm)	Mn/Sr	$\%CO_3$	TOC (%)	Unit
HM62	0.92	0.00	0.07	-5.33	0.08	3/3	1/3	1	-29.3	29.3	276	0.11	98.5	0.08	P:MA
HM63	1.38	-0.21	0.03	-5.63	0.05	2/2	1/2	1	-29.3	29.1	220	0.14	98.9	0.07	P:MA
HM64	2.54	-0.53	0.02	-5.60	0.02	3/3	1/3	1	-29.4	28.9	262	0.10	99.0	0.06	P:MA
HM65	3.94					2/2	0/2				220	0.15			P:MA
HM66	4.48					2/2	0/2		-30.0		251	0.13	98.9	0.10	P:MA
HM1	5.17	0.12	0.07	-5.20	0.21	6/6	5/6	5	-31.8	32.0	392	0.12	98.1		P:MA
HM2	5.40	-0.31	0.02	-5.15	0.04	1/3	1/1	1	-30.0	29.7	312	0.12	98.4		P:MA
HM3	5.67	-0.23	0.06	-5.12	0.05	1/2	1/1	1	-31.5	31.3			94.5		P:MA
HM4	6.09	0.18	0.09	-4.66	0.40	3/3	3/3	3	-30.3	30.5	405	0.10	98.5		P:MA
HM5	6.59					0/3	N.A.						96.0		P:MA
HM6	7.07	-0.01	0.24	-4.95	0.32	2/6	2/2	2	-29.1	29.1			97.8	0.05	P:MA
HM7	7.58	-0.07	0.31	-5.15	0.15	9/9	9/9	9	-30.7	30.6	362	0.17	99.1	0.05	P:MA
HM8	7.98	0.39	0.20	-5.02	0.60	2/2	2/2	2	-30.6	31.0			99.2		P:MA
HM9	8.60	0.07	0.24	-4.66	0.32	8/9	8/8	8	-30.0	30.1			98.9		P:MA
HM10	8.93	0.31	0.04	-4.48	0.04	1/3	1/1	1	-30.3	30.6	305	0.28	97.9		P:MA
HM11	9.16	0.14	0.24	-4.37	0.27	4/4	4/4	4	-30.2	30.4			97.8		P:MA
HM12	9.52	-0.16	0.42	-4.89	0.49	7/7	7/7	7	-29.6	29.4			97.1		P:CW
HM13	9.67	-1.49	0.65	-4.72	0.24	3/3	3/3	3	-29.4	27.9	308	0.32	99.3		P:CW
HM14	9.87	-1.17	0.16	-5.25	0.27	2/2	2/2	2	-29.4	28.2			97.9		P:CW
HM15	10.26					FAIL	N.A.		-28.6				91.6		P:CW
HM16	10.28					FAIL	N.A.				389	0.37	93.7		P:CW
HM17	10.55	-0.36	0.54	-4.64	0.50	4/4	3/4	3	-28.1	27.8			92.2	0.06	P:CW
HM18	10.73	0.02	0.05	-4.44	0.03	1/1	1/1	1			348	0.75	78.8		D:GS
HM19/70	10.85	0.18	0.14	-4.04	0.17	5/5	5/5	5	-29.6	29.8			94.0		D:GS
HM20	11.13	-0.30	0.06	-5.24	0.02	2/2	1/2	1	-29.1	28.8	448	0.75	81.7		D:GS
HM21	11.24					2/2	0/2		-29.7		442	0.96	85.1		D:GS
HM71	11.55					2/2	0/2								D:GS
HM73/22	11.57	-0.66	0.08	-5.06	0.40	4/4	2/4	2	-28.2	27.5	359	1.52	96.3	0.05	D:GS
HM78	11.64	-0.54	0.14	-4.90	0.36	3/3	3/3	3	-27.2	26.6			90.6	0.08	D:GS
HM23	11.71	-0.40	0.14	-5.29	0.04	2/2	2/2	2					92.8		D:GS
HM72	12.28					FAIL	N.A.								D:GS
HM50	12.35	-0.59	0.02	-5.10	0.04	1/9	1/1	1					96.0	0.05	D:GS
HM24	12.42					1/3	0/1	2	-26.8		461	1.43	97.6	0.05	D:KL
HM74	12.48	1.09	0.03	-4.17	0.01	1/4	1/1	1	-28.2	29.3			91.1	0.25	D:KL
HM75	12.48					FAIL	N.A.						96.8	0.08	D:KL
HM77	12.58	1.78	0.03	-4.45	0.03	1/1	1/1	1	-25.1	26.8			94.1	0.28	D:KL
HM25/60	12.67	2.11	0.09	-4.63	0.11	3/23	3/3	3	-26.2	28.3	664	0.65	96.0	0.13	D:KL
HM26/76	12.76	2.62	0.00	-4.53	0.19	2/13	2/2	2	-28.3	31.0	843	0.39	94.6	0.31	D:KL
HM27	12.90	2.39	0.06	-4.67	0.01	1/5	1/1	1	-28.1	30.5	1036	0.30	93.7		D:KL
HM51	13.01	2.39	0.03	-4.78	0.01	1/8	1/1	1	-28.0	30.4	721	0.38	92.3	0.22	D:KL
HM28	13.14	2.00	0.18	-4.75	0.11	4/4	4/4	4	-27.9	29.9			88.3	0.24	D:KL
HM29	13.34	2.41	0.05	-4.49	0.11	3/13	3/3	3	-27.5	29.9	769	0.38	91.9	0.32	D:KL
HM30	13.75	2.53	0.05	-4.55	0.04	1/3	1/1	1	-29.1	31.6			93.7		D:KL
HM31	14.04	2.11	0.06	-4.65	0.03	1/3	1/1	1	-28.0	30.2			95.7	0.13	D:KL
HM32/52	14.15	2.55	0.09	-4.65	0.19	1/21	1/1	1	-27.3	29.9	657	0.46	88.9	0.59	D:KL
HM53	14.24	2.44	0.02	-4.30	0.03	1/7	1/1	1	-28.7	31.1			99.0	0.10	D:KL
HM33	14.41	2.35	0.03	-4.57	0.03	1/4	1/1	1	-27.5	29.8	582	0.66	89.4		D:KL
HM54	14.59	2.41	0.17	-4.50	0.09	1/9	1/1	1	-27.5	30.0			89.9	0.35	D:KL
HM55	14.74	2.35	0.03	-4.58	0.03	1/11	1/1	1	-27.3	29.7	636	0.61	92.7	0.38	D:KL
HM56	14.78	2.24	0.03	-4.47	0.03	1/6	1/1	1	-27.3	29.5	582	0.69	88.9	0.43	D:KL
HM57	14.97	2.45	0.04	-4.52	0.04	1/13	1/1	1	-28.3	30.8	686	0.52	95.4	0.23	D:KL
HM34	15.24	2.06	0.03	-4.70	0.10	3/3	3/3	3	-27.4	29.5	662	0.55	94.1	0.19	D:KL
HM35	15.40	2.09	0.01	-4.74	0.02	2/2	2/2	2	-28.6	30.7	711	0.55	86.7		D:KL
HM36	15.52	1.90	0.00	-4.86	0.01	2/2	2/2	2	-28.4	30.3			93.4		D:KL
HM58	15.58	1.74	0.04	-4.91	0.06	1/10	1/1	1	-27.5	29.3	676	0.66	92.6	0.27	D:KL

HM61/79/80-1	15.64	1.40	0.16	-4.83	0.18	8/8	8/8	8	-26.9	28.3	553	0.72	93.8		D:KL
HM61/79/80-3	15.69	1.09	0.27	-5.21	0.27	6/6	6/6	6	-25.7	26.7	259	1.78	90.5	0.38	D:KL
HM61/79/80-4	15.74	0.55	0.34	-5.13	0.24	6/6	4/6	4	-26.8	27.3	259	1.78	90.4	1.20	D:KL
HM38	15.86	0.12	0.19	-5.59	0.12	4/4	3/4	3	-29.8	29.9			98.9		KW
HM39	16.46	0.28	0.11	-5.35	0.20	7/7	7/7	7	-27.5	27.7			99.8	0.04	KW
HM40	16.81					FAIL	N.A.		-29.3				98.6		KW
HM41	16.96					FAIL	N.A.		-30.0						KW
HM42	17.40	0.73	0.05	-5.20	0.05	3/3	1/3	1	-29.7	30.4	202	2.23	99.3	0.63	KW
HM67	17.96					2/2	0/3				220	2.53	99.5		KW
HM68	19.54	0.62	0.14	-5.57	0.16	3/3	3/3	3	-24.2	24.8	202	6.36	80.5	0.01	KW
HM69	19.91	0.82	0.04	-5.32	0.38	3/3	3/3	3					99.5	0.17	KW

Table S2. Geochemical data for location Highway MM. See Table S1 for column header definitions and stratigraphic abbreviations.

Location	Unit	Avg $\delta^{18}O_{carb}$	1σ	$\delta^{18}O_{carb}$ Cutoff
Highway MM	Plattin	-5.1‰	0.6‰	-5.7‰
Highway MM	Decorah	-4.9‰	0.5‰	-5.4‰
Highway MM	Kimmswick	-5.5‰	0.3‰	-5.8‰
New London	Plattin	-5.6‰	0.5‰	-6.1‰
New London	Decorah	-5.4‰	0.5‰	-5.9‰
New London	Kimmswick	-6.5‰	0.5‰	-7.0‰

Table S3. $\delta^{18}O_{carb}$ filter table. "Average $\delta^{18}O_{carb}$" refers to formational average $\delta^{18}O_{carb}$ of beds that passed isotope-texture screening. σ: one standard deviation of formation-averaged values; "$\delta^{18}O_{carb}$ cutoff" is set to be 1σ below the formation-averaged $\delta^{18}O_{carb}$ values; samples with $\delta^{18}O_{carb}$ values below this cutoff were omitted from chemostratigraphic correlations.

Chapter 3

Applying C-isotope Stratigraphy using Well Cuttings for High-Resolution Chemostratigraphic Correlation of the Subsurface

J. Garrecht Metzger[1], David A. Fike[1] and L. B. Smith[2]

[1]Department of Earth and Planetary Sciences, Washington University, 1 Brookings Dr., St. Louis, MO 63130 USA; (gmetzger@levee.wustl.edu; dfike@levee.wustl.edu)
[2]Smith Stratigraphic LLC, 397 State St., Albany, NY 122120; (smithstrat@gmail.com)

 Manuscript received December 20, 2012; provisional acceptance March 26, 2013; revised manuscript received August 01, 2013; final acceptance April 01, 2014.

Metzger, J. G., Fike, D.A., Smith, L.B., 2014, Applying C-isotope Stratigraphy using Well Cuttings for High-Resolution Chemostratigraphic Correlation of the Subsurface *in* Smith, L. B., ed., AAPG Bulletin Special Volume in Honor of Fred Read, Volume **98**, AAPG, p. 1551-1576. DOI: 10.1306/04011412231.

1. ABSTRACT

Basin-scale correlations in the subsurface generally rely on lithostratigraphic information synthesized from wire-line logs and, in some cases, well cuttings and cores. However, lithostratigraphic boundaries are often diachronous and, as such, the correlations based upon them may not provide reliable timelines. In this paper, we use $\delta^{13}C_{carb}$ data from well cuttings and a core to generate chronostratigraphic logs of Late Ordovician-aged strata spanning the Black River Group, Trenton Group, and Utica Shale across the subsurface of New York State. While particular $\delta^{13}C_{carb}$ values may be impacted by (primary) variability in local dissolved inorganic carbon reservoirs and/or (secondary) diagenetic alteration, it is possible to identify

spatially and stratigraphically coherent patterns in $\delta^{13}C_{carb}$, which can be used to effectively correlate time-equivalent strata on a basin-wide (or even global) scale, including across lithologies (e.g., between limestone and calcareous shale). The present study emphasizes the use of well cuttings, as these are commonly collected during drilling and can provide the maximum lateral resolution for subsurface correlation. Parallel geochemical (percent carbonate and total organic carbon) and isotopic ($\delta^{18}O_{carb}$ and $\delta^{13}C_{org}$) data are used to understand the origin of stratigraphic and spatial variability in the $\delta^{13}C_{carb}$ signal and to identify diagenetic alteration. Stratigraphically coherent $\delta^{13}C_{carb}$ trends across New York were used to identify six isotopically distinct packages of time-equivalent strata within these formations. Pairing chemostratigraphic and lithostratigraphic data improves our ability to document the diachronous nature of lithologic contacts, including the base of the Utica Shale, which is progressively younger moving west through New York.

2. INTRODUCTION

Several chronostratigraphic tools that can be combined with lithostratigraphy to allow for the temporal correlation of strata. Radiometric dating of detrital minerals in ash beds (e.g., U/Pb or Ar/Ar), provide a means for absolute time determination in sedimentary strata (Bowring et al., 1993; Goldman et al., 1994; Berkley and Baird, 2002; Maloof et al., 2005; Ramezani et al., 2007). These approaches, however, are often difficult to apply in the subsurface because ash beds are infrequently deposited, limited subsurface volcanic materials may be available for sampling, and the resulting age resolution may be too coarse for fine-scale correlations. When ash beds are not present, radiometric ages of organic-rich strata can be obtained using Re-Os isotopes; however, this approach is unlikely to provide sufficient resolution (< 1 Myr) for fine-

scale correlations (e.g., Selby & Creaser, 2005; Selby et al., 2009) and the potential impact of diagenesis on the resulting Re-Os ages remains poorly understood. Biostratigraphy is a powerful tool for chronostratigraphic correlation of strata on a local, regional, and global scale (Goldman et al., 1994; Brett, 1995; Patzkowsky, 1995; Kirchner and Brett, 2008). While biostratigraphy can often be productively applied in the subsurface (Gartner et al., 1983; Gradstein et al., 1988; Gradstein et al., 1992; Armentrout 1996; Witrock et al., 2003) there can be challenges arising from the limited sample availability from cores and destruction of larger biostratigraphically relevant fossils during generation of cuttings fragments. These challenges are most pronounced in the Paleozoic before the rise of abundant planktonic microfossils (e.g., foraminifera, coccolithophores) that are so useful for Mesozoic and Cenozoic biostratigraphy (*see* Witrock et al., 2003).

Isotope chemostratigraphy has the potential to generate high-resolution chronostratigraphic correlations. The stable isotope composition of marine carbonates ($\delta^{13}C_{carb} = [(^{13}C/^{12}C_{sample})/(^{13}C/^{12}C_{standard}) - 1] * 10^3$ in units of per mil (‰) relative to the V-PDB standard) records the coeval carbon isotopic composition of ambient dissolved inorganic carbon (DIC) in the ocean. Changes in $\delta^{13}C_{DIC}$ are thought to primarily derive from changes in the global burial flux of organic carbon, which is enriched in ^{12}C, the lighter stable isotope of carbon, relative to the local DIC pool, and can occur at timescales greater than 10^3 years (Mitchell et al., 1996; Hayes et al., 1999; Kump and Arthur, 1999; Saltzman, 2003). Increased burial of organic matter with low $\delta^{13}C$ values, results in a concomitant increase in $\delta^{13}C$ of the marine DIC reservoir from which it is derived. Because $\delta^{13}C_{DIC}$ is well mixed in the surface ocean on the thousand-year time scale, coeval carbonates from around the globe preserve similar $\delta^{13}C_{carb}$ signatures, which enables high-resolution correlation of strata across vast distances. However, the preservation of

a global $\delta^{13}C_{carb}$ signature can be overprinted either by (primary) environmental variability in the local $\delta^{13}C_{DIC}$ composition (Gruber et al., 1999) or by (secondary) diagenetic alteration (Patterson and Walter, 1994); chemostratigraphic data need to be screened to assess these impacts and reconstruct representative $\delta^{13}C_{carb}$ records. The resulting time-varying $\delta^{13}C_{carb}$ patterns preserved in marine carbonates have been used extensively to correlate both outcrop and subsurface sections from around the globe (Knoll et al., 1986; Burns and Matter, 1993; Hayes et al., 1999; Veizer et al., 1999; Pancost et al., 1999; Saltzman et al., 2000; Herrle et al., 2004; Tsikos et al., 2004; Fike et al., 2006; Hesselbo et al., 2007; Young et al., 2008; Maloof et al., 2010; Jones et al., 2011; Sabatino et al., 2013). Yet, the majority of existing chemostratigraphic work has focused on generating a time-series record of particular paleoenvironmental conditions (e.g., ocean redox) or global (basin-to-basin) stratigraphic correlation; such studies do not often have a sampling density sufficient to generate high-resolution chronostratigraphic tie points within individual basins. Furthermore, with limited sampling locations within a basin, it is difficult to assess local variability in $\delta^{13}C_{carb}$ (e.g., arising from spatial gradients in ocean chemistry or subsequent diagenetic alteration) that may be superimposed on the primary temporal signal of interest (Patterson and Walter, 1994; Immenhauser et al., 2003; Swart and Eberli, 2005; Swart, 2008). Diagenetic alteration typically results from precipitation of carbonate cements in porewaters, wherein bacterial processes have altered the local $\delta^{13}C_{DIC}$ composition (e.g., through respiration, Coleman and Raiswell, 1981; or methanogenesis; Hein et al. 2006) or via later-stage recrystallization of carbonates under the influence of meteoric or basinal fluids in which ambient $\delta^{13}C_{DIC}$ has been similarly impacted by oxidation of organic matter (Allan and Mathews, 1982; Joachimski, 1994; Swart & Kennedy 2012).

Here, by combining chemo- and lithostratigraphic data from multiple subsurface boreholes, we demonstrate the potential of $\delta^{13}C_{carb}$–based approaches for high-resolution, intrabasinal correlations, assessment of diagenetic alteration, and the identification of diachronous lithostratigraphic contacts. The resulting $\delta^{13}C_{carb}$ chemostratigraphy can be used to reconstruct how sedimentation and facies varied across a basin as a function of space and time.

The purpose of this study is fivefold: (1) to collect $\delta^{13}C_{carb}$ data from a series of core and cuttings samples from multiple subsurface wells; (2) to assess respective impacts of cuttings sampling resolution (vertical) and well density (lateral) on the ability to resolve $\delta^{13}C_{carb}$ signals in a single well and across a region; (3) to evaluate diagenetic alteration of $\delta^{13}C_{carb}$ in cuttings samples; (4) to produce chemostratigraphic logs suitable for correlation through the Late Ordovician-aged subsurface strata of New York State, USA (Figure 1); and (5) to identify stratigraphic intervals with distinctive $\delta^{13}C_{carb}$ character that can be used for basin-wide correlation. By focusing on ubiquitous cuttings samples, we hope to encourage the broad application of these techniques for the correlation of source rock and reservoir strata in basins of varying age from around the world.

3. GEOLOGIC CONTEXT

The study interval ranges from the Beekmantown Group, which straddles the Cambro-Ordovician boundary, through the Late Ordovician Black River Group, Trenton Group, and Utica Shale (Figure 2). The lowermost unit of the study is the Beekmantown Group, composed of the Upper Cambrian Galway Formation and Little Falls Dolomite and the more limestone-rich Lower Ordovician Tribes Hill Formation (Smith, 2006). The Beekmantown Group is at least partially equivalent with the Knox Group of the southern United States (e.g., Tennessee; Patchen

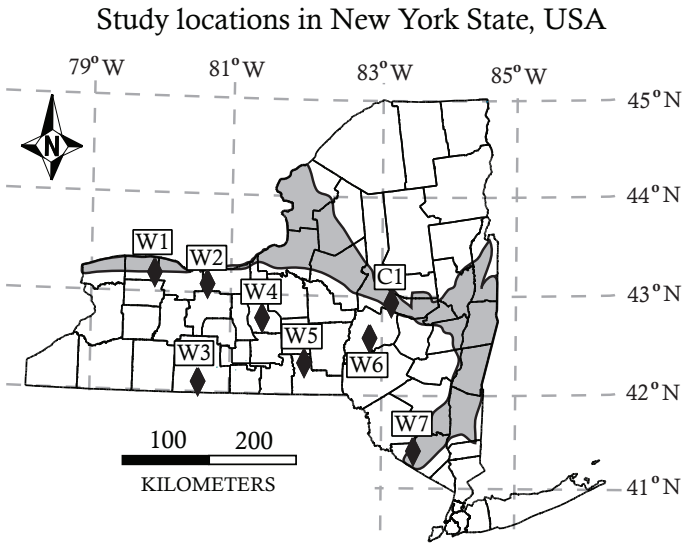

Figure 1. Outcrop map of Late Ordovician sedimentary rocks (gray) and study locations (black diamonds). Map modified from Dicken et al. (2008). For study location information see Table 1.

Well ID	Type	API#	Operator	County	Well Name	Lat. (°)	Long. (°)	$\delta^{13}C_{carb}$ ref.
W1	Cuttings	31-073-09540	Consolidated Gas Supply Corp.	Orleans	Maxon Roger 1	43.1885	-78.0376	Smith, 2006; this work
W2	Cuttings	31-117-04754	William J. Duscherer	Wayne	Smith Frank 1	43.0824	-77.2696	Smith, 2006; this work
W3	Cuttings	31-101-03924	Dominion Transmission Inc.	Steuben	Olin 1	42.0631	-77.4303	This work
W4	Cuttings	31-011-23158	Hensoil Inc.	Cayuga	Carter 1	42.7843	-76.5421	This work
W5	Cuttings	31-007-05087	Fenix and Scisson Inc.	Broome	Richards 1	42.3235	-75.9474	This work
W6	Cuttings	31-077-10834	Amoco Production Company	Otsego	Hoose 1	42.9291	-74.7438	This work
W7	Cuttings	31-071-01001	Croms-Well Inc.	Orange	Fee High Barney 1	41.4246	-74.4539	This work
C1	Core	NA	National Lead Company	Montgomery	NA	42.9291	-74.7438	This work

Table 1. Well and core information. API = American Petroleum Institute.

et al., 2006). Beekmantown strata are truncated by the Knox Unconformity, a major unconformity that spans most of Lower Ordovician and all of Middle Ordovician time in the New York area (Patchen et al. 2006).

Overlying the Knox Unconformity, the Late Ordovician Black River Group consists of clean to argillaceous, burrowed limestones, variably dolomitized, that were deposited in a regionally extensive peritidal to subtidal ramp (Keith 1989; Patchen et al., 2006). The Black

River Group lithology is uniform over large distances extending as far west as Missouri (Thompson, 1991). The Black River Group is overlain unconformably by the Trenton Group (Mitchell et al., 2004), although in places Trenton Group strata are found directly above the Knox Unconformity.

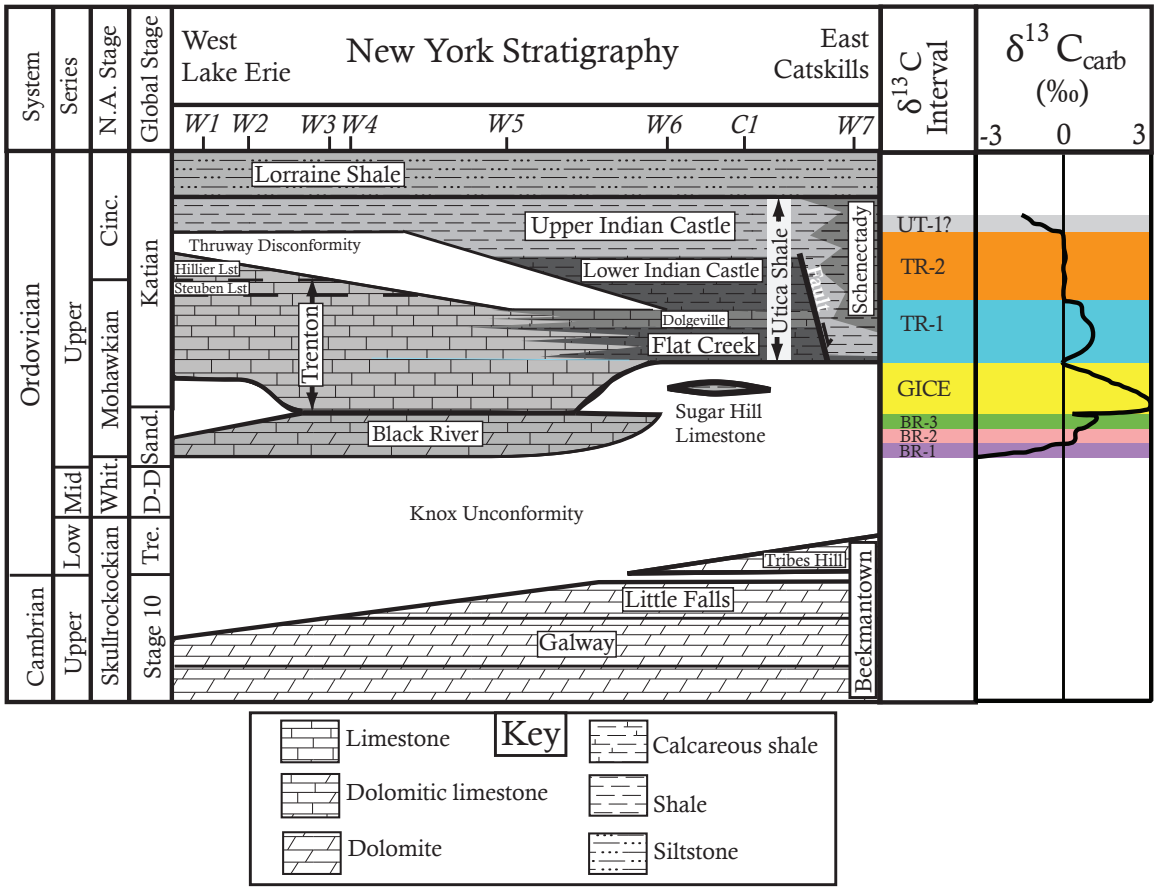

Figure 2. Chronostratigraphic relationships of Late Ordovician formations in New York (left), generalized $\delta^{13}C_{carb}$ intervals and $\delta^{13}C_{carb}$ chemostratigraphic profiles (right, see discussion in text). Stage abbreviations are Whit = Whiterockian, Cinc = Cininnatian, Sand = Sandbian, D-D = Darriwilian to Dapingian, Tre = Tremadocian. New $\delta^{13}C_{carb}$ intervals (BR = Black River Group, TR = Trenton Group, UT = Utica Shale) are named for lowest formation they are found in. GICE = Guttenberg isotopic carbon excursion (see text). "?" next to UT-1 suggests interval is not suitable for correlation (see Discussion). $\delta^{13}C_{carb}$ reference curve with intervals taken from data in this work. Values are in permil (‰) relative to V-PDB. Study locations (W1-W7, C1) are shown in their approximate position along the west to east transect.

The Trenton Group is primarily composed of limestone and argillaceous limestone and was deposited in a subtidal environment in central and western New York with deeper basinal sections deposited in the east (Brett and Baird, 2002).

Lithologies are varied, ranging from muddy, light gray and brown, mostly pure carbonates to dark, organic-rich calcareous shales. Rocks are most often muddy, but do contain shelly lag beds, arenites, and other coarser-grained materials (e.g., Brett and Baird, 2002). In the western and central parts of New York, the Trenton Group is capped by the Thruway Disconformity (Baird and Brett, 2002; Brett and Baird, 2002), which cuts down into progressively older strata to the south and east. Where present, the Thruway Disconformity is overlain by the Utica Shale; where the disconformity is absent in southeastern New York, the Trenton grades upward into the Utica Shale.

In eastern New York, the dark gray to black facies of Mohawkian and Cincinnatian (Upper Ordovician North American Stages) strata are referred to here as the Utica Shale, which comprises the Flat Creek and Indian Castle Shale members (after Brett and Baird, 2002). The Utica Shale is composed of variably calcareous shales with infrequent micritic beds, with colors ranging from gray to black. Deposition of the Trenton Group and Utica Shale is concurrent with the last stage of the Taconic Orogeny (van Staal and Barr, 2012). Here, organic-rich strata were deposited in a zone between the shallow marine carbonates of the Trenton to the west and deep-water turbidite facies found in eastern New York (Smith, 2010). The Lorraine Shale overlies the Utica Shale and has upward increasing sand and silt content.

Despite much study, it remains uncertain how to best correlate the Trenton Group of western New York with the Utica Shale of the eastern part of the state (Figure 2) and multiple different correlations have been proposed (*see* Brett and Baird, 2002 for an in-depth discussion

of correlation history). Outcrop-based correlations using lithostratigraphic, biostratigraphic, and K-bentonite data suggest that the Trenton Group-Utica Shale contact is time-transgressive with a younger Utica Shale base in the west (Brett and Baird, 2002). Specifically, the calcareous and organic-rich Flat Creek, Dolgeville and Lower Indian Castle Formations are thought to be time-equivalent to the Trenton Group, while the Upper Indian Castle Shale (Utica Shale) is younger than the Trenton Group in New York State. Additional work, particularly in the subsurface, is needed to further clarify geographic and temporal relationships of the Trenton Group-Utica Shale interval.

4. METHODS

Geophysical wireline logs and geological sample logs were obtained from the Empire State Oil and Gas Information system (http://esogis.nysm.nysed.gov/). A list of all wells and cores used in this study can be found in Table 1. Hereafter, wells are referred to by a 5-digit numerical identifier; the full API 10-digit identifier and well location can be found in Table 1. Lithologies for statigraphic columns were obtained from geologic sampling logs for each well and were described by a geologist soon after the well was completed. Gamma ray values for core C1 were obtained using a CoreLab Instruments Spectral Gamma Logger Model SGL-300 at the Ohio Department of Natural Resources Division of Geological Survey. Calibration was run each day with API standards 0 and 200 (API units).

Cuttings samples were collected from the New York State Geologic Survey and catalogued at Washington University. A representative subsample of each cuttings sample was collected for analyses. Cuttings were collected into stratigraphic intervals of ~0.5-9 m at the borehole and therefore represent a lithologic average over that interval. To help assess the

impact of lithologic mixing in analysis of cuttings samples, several individual carbonate chips were taken from selected intervals in well W7. When picking individual chips those with macroscopic pyrite, recrystallized material, or macroscopic spar were excluded. Individual chips were powdered for chip-specific analysis, alongside aggregated subsamples (~0.5g, representing ~10% total cuttings mass) and bulk-homogenized powder. For other samples, cuttings were homogenized by powdering 0.5-10 g of samples. Core samples were micro-drilled to collect powders for isotopic and geochemical analysis.

Weight percent carbonate minerals (%carb) was determined by gravimetric analyses following the dissolution of 0.1-0.5 g of powder with 6M HCl at Washington University. Complete dissolution of carbonate fraction was obtained by addition of excess acid and agitation on a shaker table for >12 hours. TOC was measured at Washington University by combustion of homogenized acid-insoluble residues on a Costech ECS 4010 Elemental Analyzer, whereby the emitted CO_2 was quantified and calibrated against standards of known TOC compositions. Additional TOC for well W7 was measured at the New York State Museum on a UIC Coulometrics CM 5130 Acidification module.

Stable isotope analyses were conducted at Washington University. Carbon isotopes are reported as $\delta^{13}C = ({}^{13}C/{}^{12}C_{sample}/{}^{13}C/{}^{12}C_{standard} - 1) * 10^3$ in units of per mil (‰) relative to the V-PDB standard. Oxygen isotopes are reported as $\delta^{18}O = ({}^{18}O/{}^{16}O_{sample}/{}^{18}O/{}^{16}O_{standard} - 1) * 10^3$ in units of per mil (‰) relative to the V-PDB standard. Carbonates ($\delta^{13}C_{carb}$ and $\delta^{18}O_{carb}$) were analyzed on a Gas Bench II attached to a ThermoFischer Delta V Plus isotope ratio mass spectrometer. A test set of samples were roasted at 380°C for ~12 hours to liberate volatile organic compounds and revealed no systematic offset for $\delta^{13}C_{carb}$ and a minor (< ~0.3‰) effect on $\delta^{18}O_{carb}$ in roasted and unroasted samples. The effect on $\delta^{18}O_{carb}$ was too small relative to the

magnitude of $\delta^{18}O_{carb}$ to impact our interpretations. Therefore, the remaining samples were not roasted prior to $\delta^{13}C_{carb}$ and $\delta^{18}O_{carb}$ analysis. Additional carbonate analyses were done at the University of Albany using a GV Instruments Optima mass spectrometer for well W1 and portions of W2. Calibration of $\delta^{13}C_{carb}$ and $\delta^{18}O_{carb}$ was done by comparison to International Atomic Energy Association standards NBS-19 and NBS-18, National Institute of Standards and Technology standard LSVEC, and in-house standards. Long-term running reproducibility (1σ = 1 standard deviation) for multiple day replicates for $\delta^{13}C_{carb}$ and $\delta^{18}O_{carb}$ was 0.09‰ and 0.12‰, respectively

Cuttings samples for organic carbon analyses were washed prior to processing to reduce contamination from organic carbon in the drilling fluid. Organic carbon isotopes ($\delta^{13}C_{org}$) were measured from the acid-insoluble organic matter (see TOC and %carbonate [$\%_{carb}$] methods discussed previously) and were analyzed by combustion to CO_2 on a Costech ECS 4010 Elemental Analyzer attached to a Delta V Plus mass spectrometer. $\delta^{13}C_{org}$ was calibrated against international standards from the United States Geological Survey, USGS 24 (graphite), and International Atomic Energy Association standards IAEA CH-6 (sucrose) and IAEA CH-3 (cellulose). During this study, typical precision (1σ) for $\delta^{13}C_{carb}$ and $\delta^{18}O_{carb}$ replicates of NBS-19 for a single run was 0.04‰. Typical multi-day reproducibility (1σ) for $\delta^{13}C_{org}$ standards was 0.13‰.

5. RESULTS

5.1 Stratigraphic Trends

$\delta^{13}C_{carb}$ and $\delta^{18}O_{carb}$ data are presented alongside gamma ray logs in Figure 3. Clear stratigraphic $\delta^{13}C_{carb}$ trends are apparent in the sections. A rise in $\delta^{13}C_{carb}$ is observed from ~-3

to 1‰ above the Knox unconformity to the top of the Black River Group. A conspicuous interval where $\delta^{13}C_{carb}$ changes from 0‰ to 3‰ and returns to 0‰ is observed in the four westernmost wells above the top of the Black River Group. This interval thickens towards the center of the transect. Above this interval, $\delta^{13}C_{carb}$ values average around 1‰ in all wells, thickening towards the eastern and western edges of the transect. Above the 1‰ interval, $\delta^{13}C_{carb}$ values average ~0‰ in all but the two central wells, W3 and W5. $\delta^{13}C_{carb}$ values fall below 1‰ where the gamma ray values are highest in the uppermost parts of the wells.

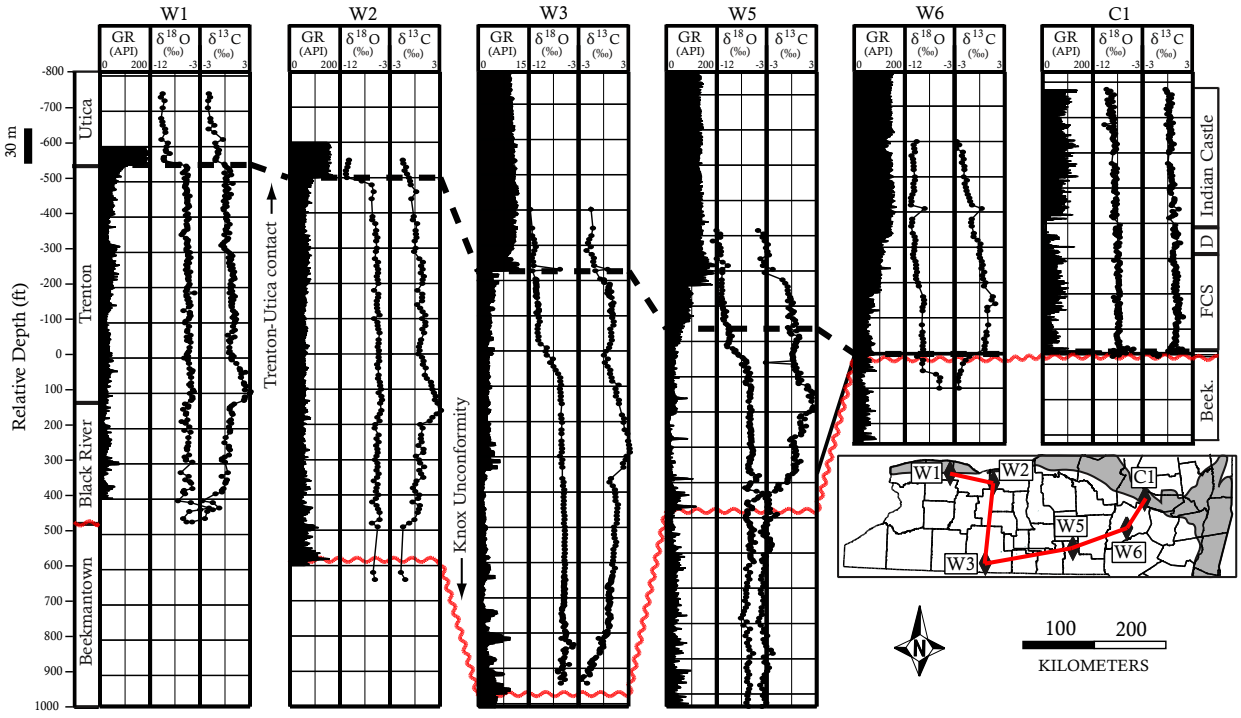

Figure 3. $\delta^{13}C_{carb}$, $\delta^{18}O_{carb}$, and gamma ray log data for select wells. Isotope values are in permil (‰) relative to V-PDB. D = Dolgeville, FCS = Flat Creek Shale. Formations unmarked below FCS in core C1 are Sugar River Limestone and Black River Group (see text). Map shows transect through these wells with Trenton-Utica outcrop belt shown in gray. Where gamma ray logs are truncated, data were not available.

$\delta^{18}O_{carb}$ values vary between -2 and -13‰. Highest values are found in the Beekmantown Group. Lowest $\delta^{18}O_{carb}$ values are found in the Utica Shale and upper Trenton

Group. Variation in $\delta^{18}O_{carb}$ is lowest in the Black River Group and lower to mid Trenton Group.

Gamma ray values are intermediate and variable in the Beekmantown Group. Upsection, gamma ray readings are lowest in the Black River, intermediate in the Trenton Group, and highest in the Utica Shale. The gamma ray values increase gradually from the Trenton Group to Utica Shale in the easternmost wells. Conversely, in the three westernmost wells, the gamma ray values sharply increase at the Trenton-Utica contact.

Figures 4-6 show lithologic and geochemical trends of locations W5, W6, and C1. The Beekmantown Group is dolomitized and locally sandy with high %carbonate and low total organic carbon (TOC). The Black River Group (where present) has a high %carbonate and very low TOC and can be variably dolomitized in the lower portions near the contact with the Beekmantown Group (Smith, 2006). The overlying Trenton Group carbonates are argillaceous with increasing clay content upsection. The Utica Shale is dominated by dark, carbonate strata with dark shale interbeds in the eastern locations (W6, C1) and is more correctly described as a marl in much of the section due to its relatively high carbonate content. The Utica Shale is the western sections (W1-4) is exclusively a carbonate-poor black shale.

Percent carbonate slowly declines through the Utica Shale in the easternmost locations W6 (Figure 4) and C1 (Figure 6) and the Trenton Group in W5 (Figure 5). The %carbonate is higher in the Utica Shale of eastern locations W6 and C1. Total organic carbon (TOC) averages ~2% the Utica Shale of eastern locations W6 (Figure 4) and C1 (Figure 6), while it is more varied in W5 (Figure 5). In this well, TOC ~0% Black River and lower Trenton strata, ~0.75% in the upper Trenton, and ~1.5% in the Utica.

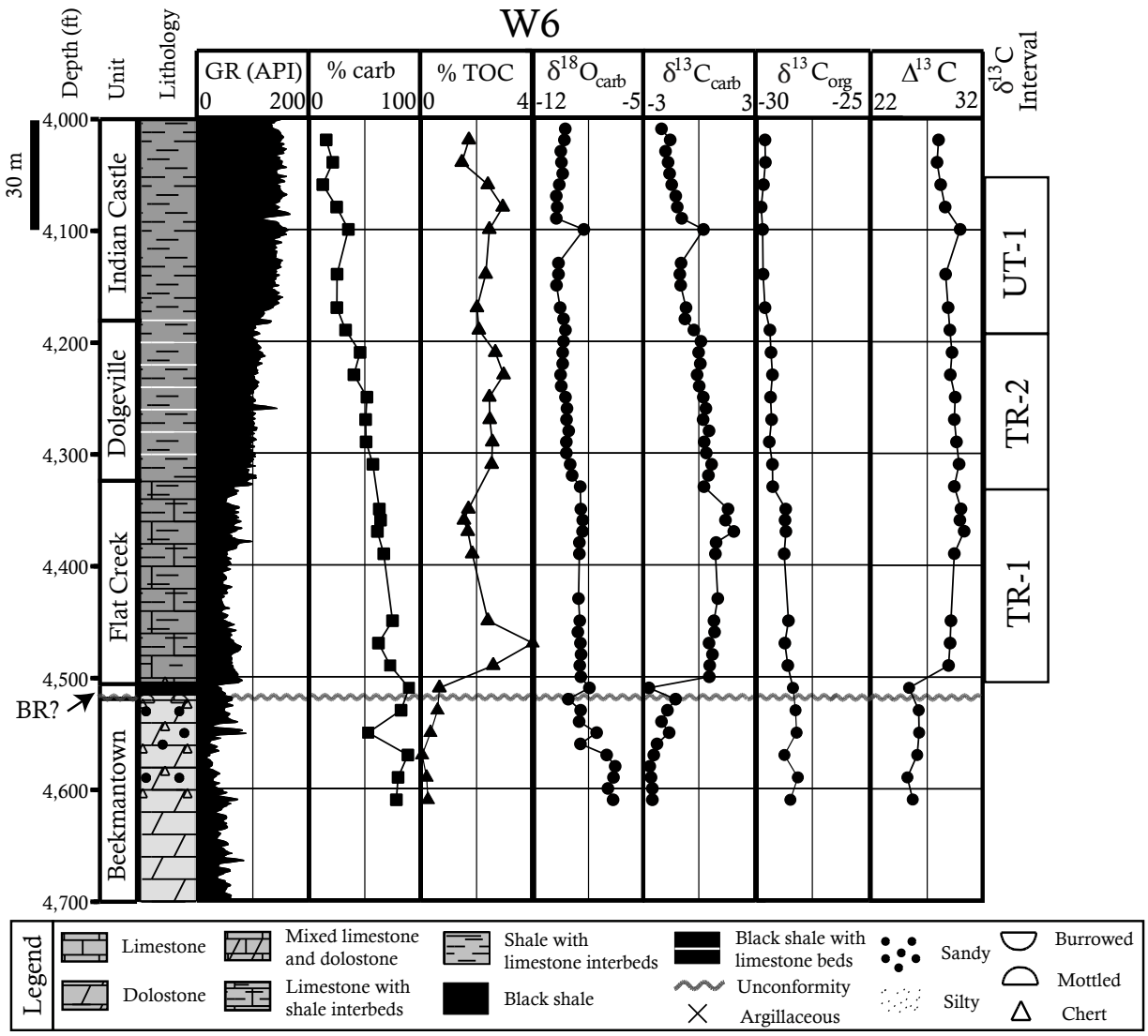

Figure 4. Geologic, geophysical, and geochemical results for well W6. %carb and %TOC are given as mass percent. Isotope values are in permil (‰) relative to V-PDB. Symbol size is > 1σ long-term average analytical error. Knox Unconformity marked by thick wavy line. Flat Creek, Dolgeville, and Indian Castle are all part of the Utica Shale Group (see text). BR = Black River. Lithological color corresponds to general shade of rocks.

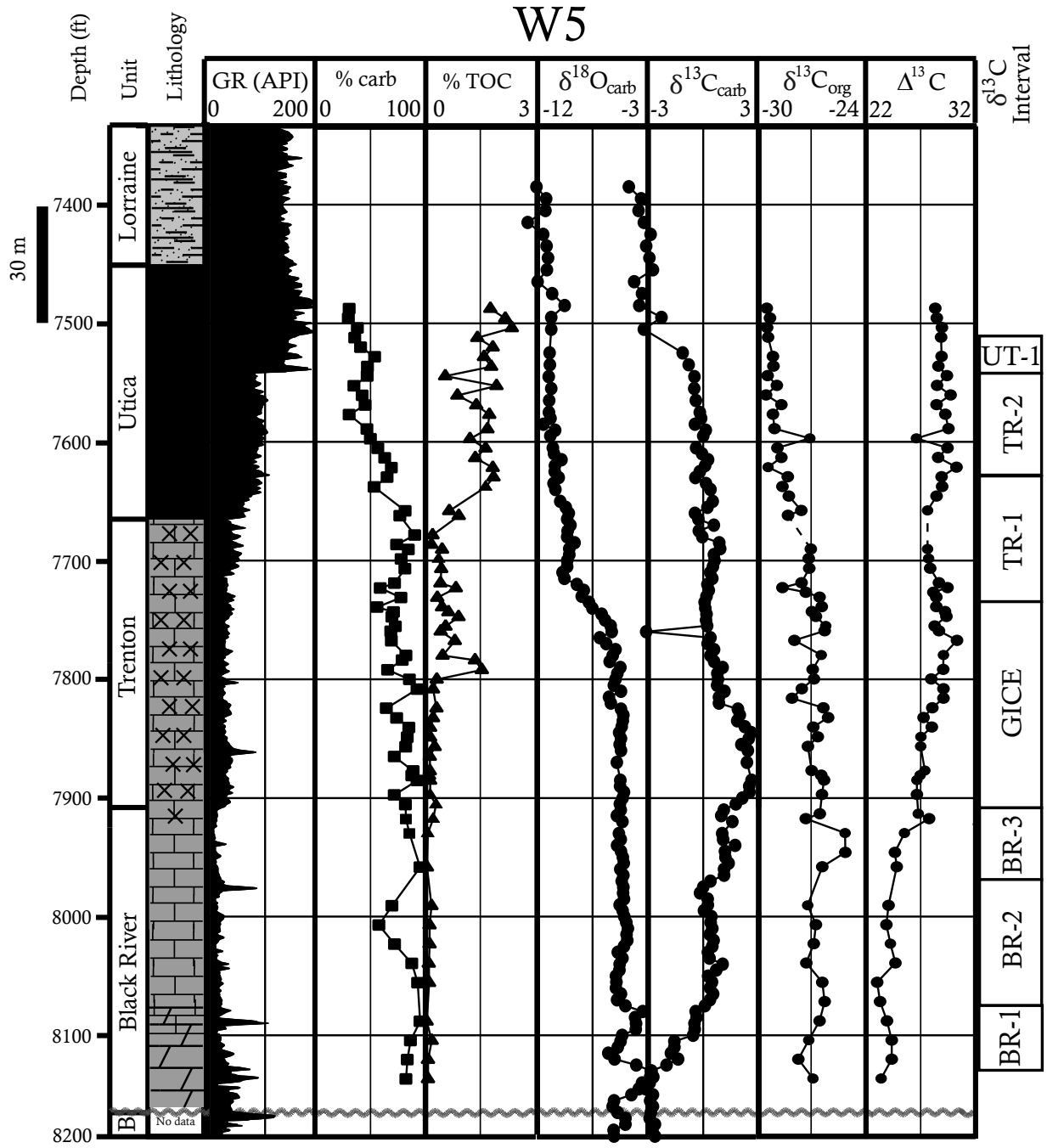

Figure 5. Geologic, geophysical, and geochemical results for well W5. %carb and %TOC are given as mass percent. Isotope values are in permil (‰) relative to V-PDB. Symbol size is > 1σ long-term average analytical error. One outlier ($\delta^{13}C_{org}$ = -22.68‰, $\Delta^{13}C$ = 22.83‰) at depth 7765 ft. was removed for clarity. Knox Unconformity marked by thick wavy line. See Figure 4 for lithology and symbol legend.

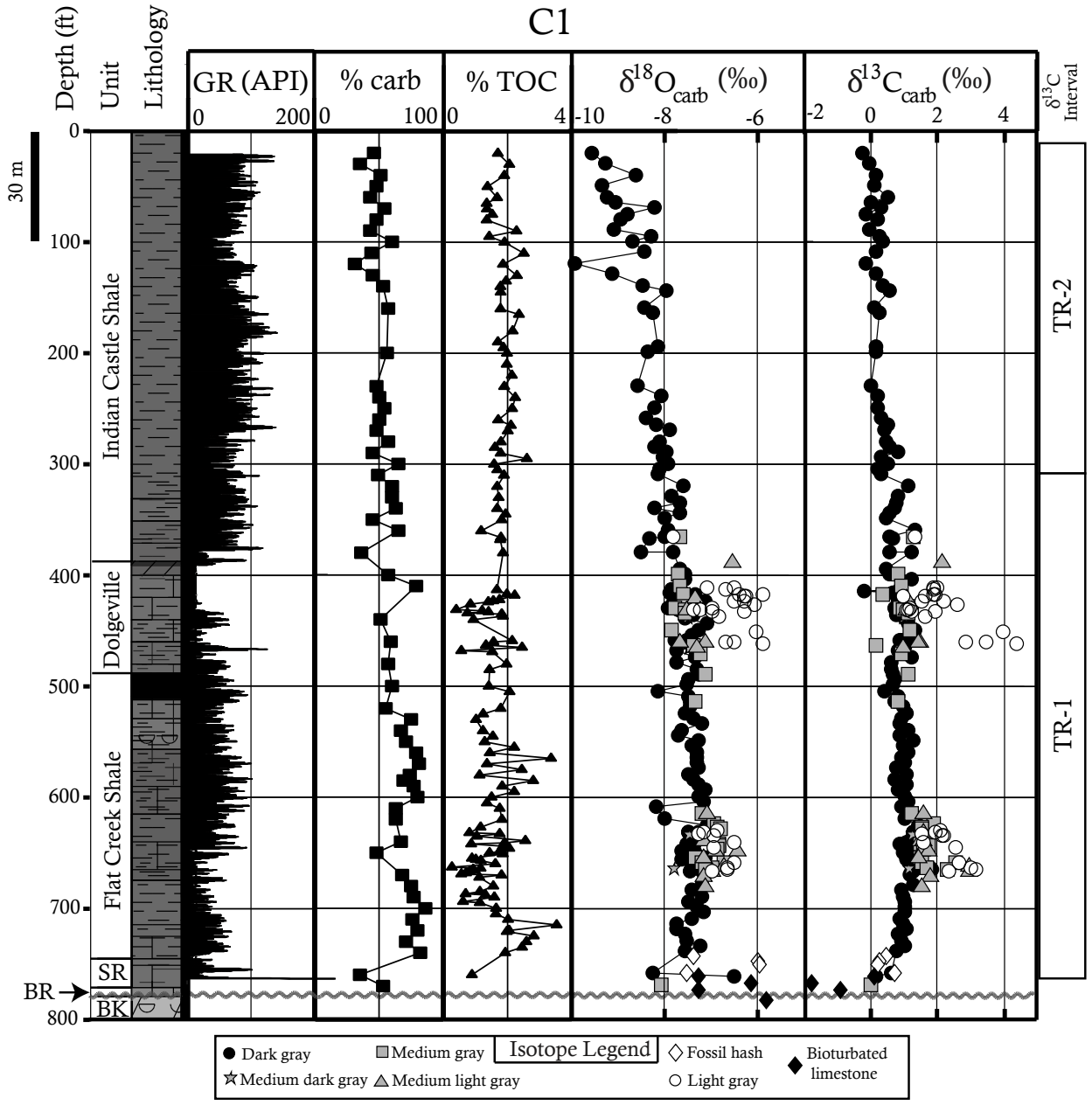

Figure 6. Geologic and geochemical results for core C1. Isotope values are in permil (‰) relative to V-PDB. Symbol size is > 1σ long-term average analytical error. Isotope legend refers to $\delta^{13}C_{carb}$ and $\delta^{18}O_{carb}$ logs, where colors refer to color-specific sampling of lithologies (see text). Knox Unconformity marked by thick wavy line. BK = Beekmantown Group, BR = Black River Group, SR = Sugar River Limestone. See Figure 4 for lithology and symbol legend.

In general, $\delta^{13}C_{org}$ is relatively constant in the highest %carbonate strata where post-Black River Group gamma ray values are lowest in (Figures 4 and 5). $\delta^{13}C_{org}$ averages ~-27‰ in

W5 and declines to ~-30 in the Utica Shale. $\delta^{13}C_{org}$ averages -28.5‰ in W6 (Figure 4) and declines to ~-30‰ in the Indian Castle Member of the Utica Shale. $\Delta^{13}C$ (= $\delta^{13}C_{carb} - \delta^{13}C_{org}$) averages 28.5‰ in W6 and very closely matches the pattern of $\delta^{13}C_{carb}$ because $\delta^{13}C_{org}$ has little variability. In W5, $\Delta^{13}C$ increases from ~23‰ to 30‰ from the Black River Group to the upper Trenton Group values then vary 29‰ upsection. The large-scale changes in $\Delta^{13}C$ are not dominantly controlled by $\delta^{13}C_{carb}$ or $\delta^{13}C_{org}$, but rather a combination of changing values in both.

5.1.1 Location C1

Location C1, the most northeastern study section and only core, is dominated by dark calcareous shales and shaley carbonates. The strata above the Knox Unconformity are all part of the Utica Shale except for a very thin (tentative) Black River Group and Sugar River Limestone (Trenton Group) in the ~10m of section immediately above the unconformity (Figure 6). Some lithologies contained lighter and darker beds (e.g., the Flat Creek Shale). The lighter beds were dominantly fine-grained with occasional coarse sand-sized grains composed of fossil debris. Lighter beds sometimes displayed a diffuse contact with surrounding beds. Evidence of cm-scale scouring was present in the Utica Shale members.

Additional samples were taken at cm-scale resolution in select intervals to investigate possible lithology-dependent variability in the $\delta^{13}C_{carb}$ signal. Samples were split into five different categories based upon a qualitative assessment of their color. In general, the 2 darkest shades are stratigraphically coherent (i.e., have little scatter) in their isotopic trends. In contrast, the two lightest, most carbonate-rich layers displayed high degrees of scatter in both $\delta^{18}O_{carb}$ and $\delta^{13}C_{carb}$, where the $\delta^{13}C_{carb}$ scatter is skewed toward heavier values relative to the overlying and underlying strata

5.1.2 Stratigraphic Summary

We focus on the stratigraphic trends observed in the strata of the Black River Group, Trenton Group and Utica Shale. Gamma ray logs show similar patterns across formation boundaries with the Utica Shale having highest gamma ray emission. Percent carbonate is highest in the Beekmantown and Black River Groups and decreases upsection. Trends in %carb and gamma ray values are roughly opposite one another. The inverse relationship between %carb and gamma ray logs suggests that the gamma ray signatures predominantly track potassium-rich siliciclastic input (e.g., from detrital clay minerals), rather than organic carbon. TOC is highest in Trenton Group and Utica Shale. $\delta^{18}O_{carb}$ is generally highest in the formations with highest %carb (i.e, Beekmantown Group to Trenton Group). $\delta^{18}O_{carb}$ is not stratigraphically consistent between sections from the middle Trenton upwards and is most variable in dolomitized zones (as described in the cuttings geologic sampling logs) and zones with low %carb. Consistent patterns in $\delta^{13}C_{carb}$ are apparent across multiple wells. These include (stratigraphically ascending): 1) a rise from -3‰ to 0‰ in the Black River, 2) a stable interval of 0.5‰ in the Black River, 3) a rise from ~1‰ to ~1.5‰ in the Black River, 4) a peak at 3‰ in the Trenton, 5) a stable interval of 1‰ in the Trenton and Utica, 6) a stable interval of 0‰ in the Trenton and Utica, 7) and a drop to -1.5‰ in the Utica. This drop in $\delta^{13}C_{carb}$ below 0‰ is coincident with a decline in %carb as well as a parallel decrease in $\delta^{13}C_{org}$.

5.2 Impact of Lithologic Mixing on $\delta^{13}C_{carb}$ in Cuttings

A series of tests were conducted on select cuttings samples from well W7 to evaluate the impact of lithologic mixing in analysis of cuttings samples. Three stratigraphic intervals were

investigated in well W7 (Figure 7), each containing a different background $\delta^{13}C_{carb}$ trend (declining, increasing, or constant) with decreasing depth as defined by data from bulk-homogenized cuttings. For each sample investigated, several carbonate chips ('single chips') were individually analyzed for $\delta^{13}C_{carb}$ and $\delta^{18}O_{carb}$, as well as a powder representing ~0.5g ('subsample'). These were compared with the $\delta^{13}C_{carb}$ and $\delta^{18}O_{carb}$ data from the homogenized bulk sample ('bulk'). A comparison of these results is shown in Figure 7, with the intervals comprising the distinct $\delta^{13}C_{carb}$ trends represented in Figure 7B-D. Single chip data are characterized by increased variability in $\delta^{13}C_{carb}$ and $\delta^{18}O_{carb}$ when compared with bulk samples or the subsamples. Single chip $\delta^{13}C_{carb}$ scatter increases when the baseline bulk $\delta^{13}C_{carb}$ signal is increasing or decreasing. Single chip $\delta^{13}C_{carb}$ scatter is low when the bulk $\delta^{13}C_{carb}$ signal is not changing. While single chips reasonably track the bulk $\delta^{13}C_{carb}$ signal (albeit with increased variability), the ~0.5 g subsample more closely tracks the $\delta^{13}C_{carb}$ signal of the bulk signal.

5.3 Impact of Sampling Resolution

A comparison of $\delta^{13}C_{carb}$ profiles sampled at different resolutions through the same interval is shown in Figure 8. The variable vertical sampling resolution between locations results in differing stratigraphic morphologies of the same $\delta^{13}C_{carb}$ signal, where a lower sampling resolution results in a smoother isotopic record. The interval of elevated $\delta^{13}C_{carb}$ (gray) is ~30ft at the New London outcrop in Missouri (see Metzger & Fike, 2013 for discussion of locality), while the same interval is >300ft in New York well W4. The sampling resolution in well W4 is 30ft; a similar sampling resolution in New London would reduce the entire interval of elevated $\delta^{13}C_{carb}$ values to a single data point.

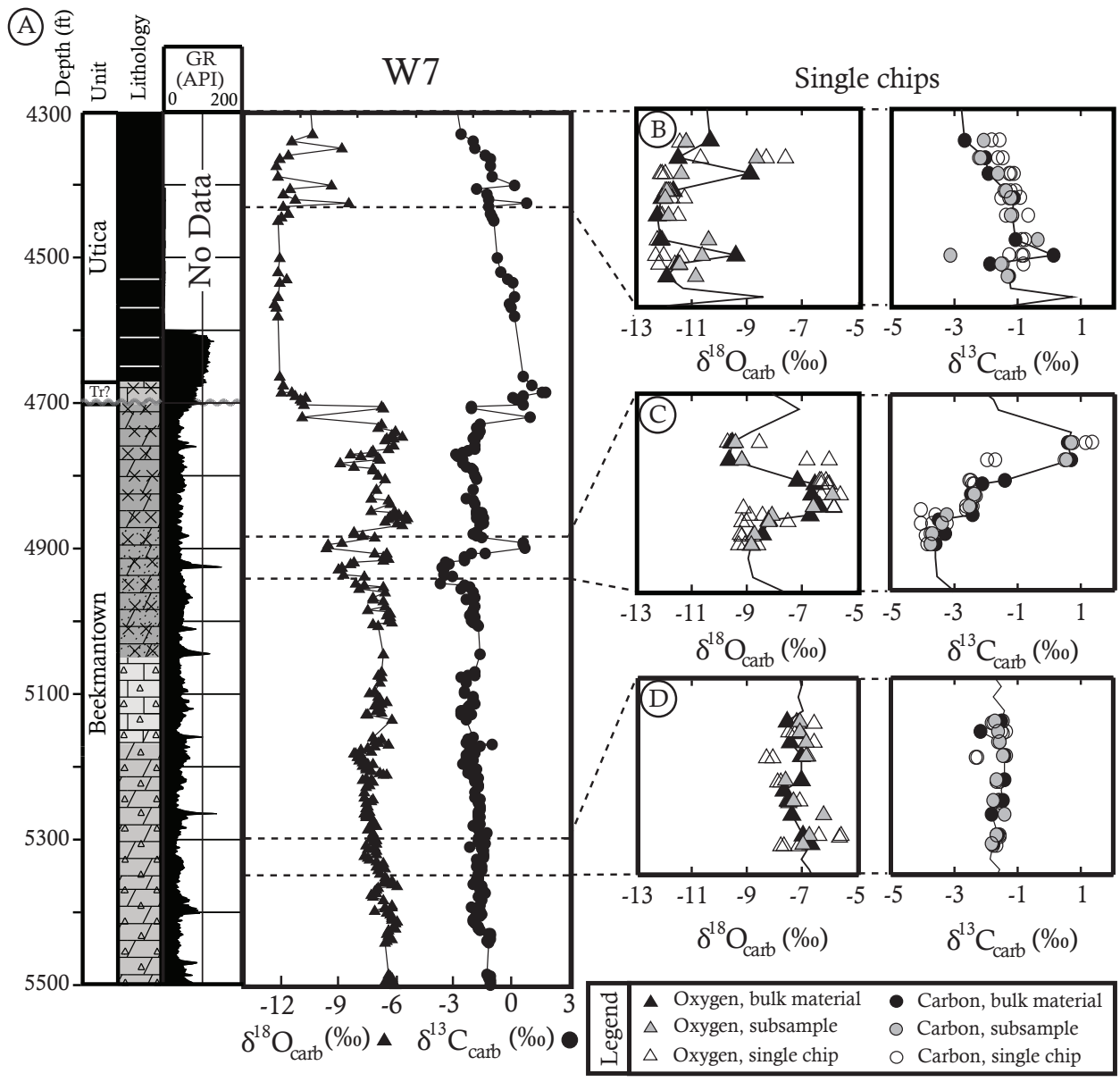

Figure 7. Comparison of isotopic results of bulk material (filled symbols), multi-chip subsamples (gray symbols), and single chips (empty symbols) for well W7. Three intervals from the entire well (A) were chosen for their distinct $\delta^{13}C_{carb}$ patterns; upwards declining (B), upwards increasing (C), and constant (D). Isotope values are reported in permil (‰) relative to V-PDB. In subplots B, C, and D, bulk material values are shown only when single chips were analyzed at the same depth. Bulk material values are connected by a solid line. Up to three single chips were analyzed for a given depth. Symbol size is > 1σ long-term average analytical error. One outlier ($\delta^{13}C_{carb}$ = 5.13‰, $\delta^{18}O_{carb}$ = -6.69‰) from bulk carbonate at depth 4540 ft. was removed for clarity.

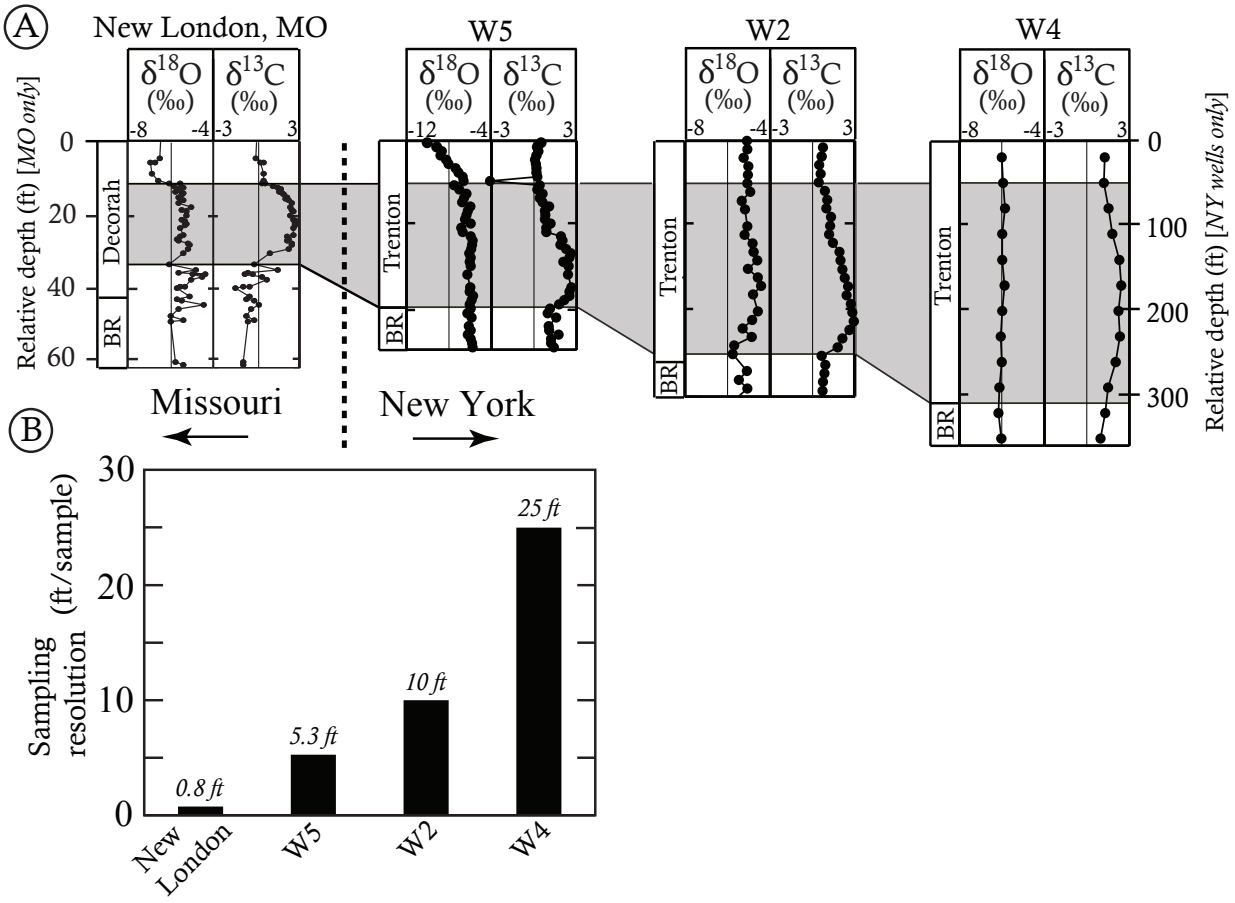

Figure 8. Comparison of sampling resolution for wells and outcrop during the Guttenberg excursion interval (shaded). (A) Correlations between age-equivalent outcrop in Missouri, USA (Chapter 2) and New York wells presented here. Sampling resolution is coarser moving to the right, associated with decreasing resolution of the GICE interval. Missouri outcrop y-axis (left) is exaggerated relative to the three subsurface sections. (B) Bar graph of sampling resolution for the different locations showing number of feet per sample. High values correspond to low sampling resolution

6. DISCUSSION

$\delta^{13}C_{carb}$ can be used to chronologically correlate strata because the $\delta^{13}C_{DIC}$ value synchronously changes across any well-mixed portion of the ocean. Stratigraphically meaningful correlations require preservation of the original $\delta^{13}C_{carb}$ signal and various post-depositional processes may alter $\delta^{13}C_{carb}$ values. Sampling methods (e.g., vertical sampling resolution and sample selection) are an additional control on the resolution and accuracy of $\delta^{13}C_{carb}$ logs. Here, we identify 7 intervals with distinctive $\delta^{13}C_{carb}$ signatures that can be used

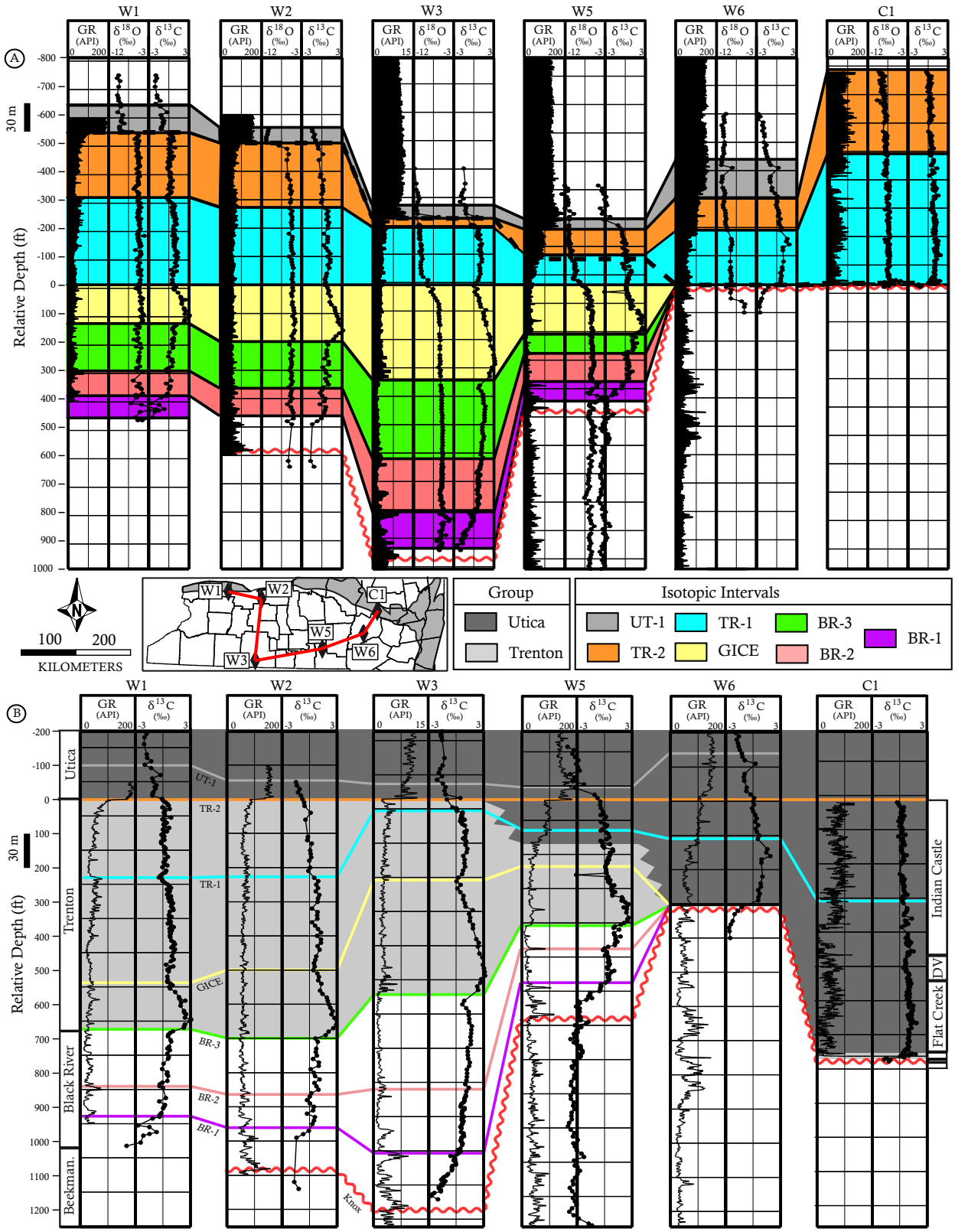
A
W1
W2
W3
W5
W6
C1
GR (API)
δ18O (‰)
δ13C (‰)
30 m
Relative Depth (ft)
N
100 200
KILOMETERS
Group
Utica
Trenton
Isotopic Intervals
UT-1
TR-1
BR-3
BR-1
TR-2
GICE
BR-2
B
Utica
Trenton
Black River
Beekman.
Knox
Indian Castle
DV
Flat Creek

Figure 9. Proposed correlations of the New York subsurface based on $\delta^{13}C_{carb}$. Red line (map) shows sampling transect for both (A) and (B). GM = gamma ray (in API units). (Note that API range is 0-200 API units for all locations except for W3 where range was 0-15 API units due to a different gain setting during analysis. The 0-15 API unit range in this well is roughly equivalent to the 0-200 units in other wells.) $\delta^{13}C = \delta^{13}C_{carb}$ given in ‰ relative to VPDB, $\delta^{18}O = \delta^{18}O_{carb}$ given in permil (‰) relative to VPDB, BK = Beekmantown Group, BR = Black River Group, SR = Sugar River Limestone. (A) Isotopic intervals (colored zones) show shift in the sediment depocenter from western and central New York from $\delta^{13}C_{carb}$ to eastern New York following the GICE. Isotopic intervals are defined and discussed in text (see *Correlations*). Generalized $\delta^{13}C_{carb}$ curve for New York region and chronostratigraphic relationships are found in Figure 1. The basal contact of the Utica Shale is marked by a thick dashed red line. Wells are hung on base of $\delta^{13}C_{carb}$ interval TR-1. (B) Sampling transect showing time-equivalent nature of lower Utica (dark gray) and upper Trenton (light gray) facies. Wells hung on top of $\delta^{13}C_{carb}$ interval TR-2.

for correlation. We then examine evidence of alteration of the original $\delta^{13}C_{carb}$ signal and the impact of sampling resolution on the morphology of $\delta^{13}C_{carb}$ logs.

Seven discrete $\delta^{13}C_{carb}$ intervals, bounded by correlation points in the carbon isotope logs, have been identified within the stratigraphic interval examined (Figure 9): three in the Black River Group (BR-1, BR-2 and BR-3) and four in Trenton Group and Utica Shale (GICE, TR-1, TR-2, and UT-1). These are defined as follows:

- BR-1: an interval of increasing $\delta^{13}C_{carb}$ from -3‰ to 0‰ in the Black River Group.
- BR-2: a stable interval of ~ +0.5‰ in $\delta^{13}C_{carb}$ in the Black River Group above BR-1.
- BR-3: an interval starting at ~1‰ in $\delta^{13}C_{carb}$ and increasing to ~1.5% in the Black River Group above BR-2.
- GICE: a positive excursion in $\delta^{13}C_{carb}$, increasing from ~0.5‰ to 3‰ before decreasing back to ~0‰. Known as the Guttenberg isotopic carbon excursion (GICE), this positive $\delta^{13}C_{carb}$ excursion has been identified in much of central and eastern Laurentia (e.g., Ludvigson et al, 2004; Young et al., 2005; Bergström et al., 2010; Chapter 2) as well as Sweden (Bergström *et al.,* 2004), China (Young *et al.,* 2005; Bergström *et al.,* 2009), and Malaysia (Bergström *et al.,* 2010). In this study it begins near the base of the Trenton Group.

- TR-1: a stable interval of +1‰ in $\delta^{13}C_{carb}$ in the Trenton Group (western-central NY) and Utica Shale (eastern NY) that postdates the Guttenberg excursion.

  TR-2: a stable interval of ~ 0‰ in $\delta^{13}C_{carb}$ above TR-1.

- UT-1: an interval of decreasing $\delta^{13}C_{carb}$ from ~ 0 to -1.5‰.

Figure 2 shows a $\delta^{13}C_{carb}$ reference curve (divided into seven $\delta^{13}C_{carb}$ intervals) for the New York region and its relationship to formation boundaries across the state.

6.1 Evaluating Diagenetic Alteration

Diagenetic (post-depositional) processes can alter original $\delta^{13}C_{carb}$ values in marine carbonates (Allan and Matthews, 1982; Patterson and Walker, 1994; Melim et al. 2004; Chapter 2), giving rise to apparent spatial heterogeneities in $\delta^{13}C_{carb}$ values and limiting the ability to use $\delta^{13}C_{carb}$ for correlations. There are several recognized mechanisms by which diagenesis can alter $\delta^{13}C_{carb}$. The most common is oxidation of organic matter ($\delta^{13}C_{org}$ ~ -30‰), which results in a decrease in $\delta^{13}C_{DIC}$ of pore fluids and subsequently a decrease in $\delta^{13}C_{carb}$ of any strata that re-equilibrate with such porefluids. This can happen either as meteoric diagenesis, where soil carbon is the source (e.g., Knauth & Kennedy, 2009; Swart and Kennedy, 2012), or during burial diagenesis (e.g., Derry, 2010), where oxidation results from thermal breakdown of migrating hydrocarbons or *in situ* organic matter.

6.1.1 Covariation in $\delta^{13}C_{carb}$, $\delta^{18}O_{carb}$, and %carb

Geochemical cross-plots can provide context for identifying possible post-depositional alteration. An examination of covariation between geochemical parameters and $\delta^{13}C_{carb}$ can constrain possible diagenetic pathways. Often, covariation in $\delta^{13}C_{carb}$ and $\delta^{18}O_{carb}$ are examined.

This is because changes in $\delta^{18}O_{carb}$ are largely or entirely independent of changes in $\delta^{13}C_{carb}$ prior to alteration and therefore covariation between these two parameters is not expected. However, in meteoric fluids both $\delta^{13}C$ and $\delta^{18}O$ are low (e.g., Bathurst, 1975; Allan and Matthews, 1982; Lohmann, 1988) and covarying $\delta^{13}C_{carb}$ and $\delta^{18}O_{carb}$ can indicate isotopic alteration by meteoric diagenesis (we note that while covariation can indicate diagnetic alteration, the absence of covariation cannot be taken as evidence of primary $\delta^{13}C_{carb}$ values being retained). For example, covariation in $\delta^{13}C_{carb}$ and $\delta^{18}O_{carb}$ is observed in formations that have undergone visibile karstification (e.g., Lohmann, 1988). When considering diagenetic alteration of $\delta^{13}C_{carb}$ two important points must be considered: 1) most diagenetic mechanisms decrease $\delta^{13}C_{carb}$; and 2) $\delta^{18}O_{carb}$ is easier to reset than $\delta^{13}C_{carb}$ during diagenesis because of the relative abundance of O relative to C in any diagenetic fluid (e.g., Banner and Hanson, 1990). This offset in oxygen and carbon concentrations in diagenetic fluids allows quantitative description of the volume of diagenetic fluid required to change the rock's $\delta^{13}C_{carb}$ and $\delta^{18}O_{carb}$ values. This is normally described in terms of fluid to rock ratios (fluid:rock). Most relevant here is the molar ratio of the cumulative flux of porefluids migrating through a sample to the volume of carbonate material within the sample. Under low fluid:rock, the $\delta^{18}O_{carb}$ is vulnerable to change, while the $\delta^{13}C_{carb}$ is less susceptible due to the lower carbon content of the fluids (Banner and Hanson, 1990). For a given flux of diagenetic fluids, siliciclastic-dominated strata with low percent carbonate will have their $\delta^{13}C_{carb}$ and $\delta^{18}O_{carb}$ signatures more easily altered compared to the same volume of carbonate-rich strata. However, the low porosity/permeability of fine-grained siliciclastics (e.g., shales) results in decreased fluid flux, thereby increasing preservation potential of a primary isotopic signature in lower %carb strata. Bulk rock $\delta^{13}C_{carb}$ signatures can also be altered by the addition of pore-filling secondary cement, which adds secondary material to void spaces, rather

than sequential equilibration of the bulk rock itself with the diagenetic fluid. These factors must be considered when interpreting $\delta^{13}C_{carb}$ records in fine-grained lithologies with low carbonate contents.

Most of the formations in this study do not show strong covariation in $\delta^{13}C_{carb}$ and $\delta^{18}O_{carb}$ (Figure 10) and therefore we find no formation-scale evidence of meteoric diagenesis. However, in Trenton Group strata, $\delta^{13}C_{carb}$ and $\delta^{18}O_{carb}$ show moderate to strong correlation in all wells ($r^2 = 0.33$ to 0.65). Understanding the origin of the covariation in the Trenton Group requires closer examination and we will look at well W3 as an example. There are three $\delta^{13}C_{carb}$ intervals present in the Trenton Group: the GICE, TR-1, and TR-2. These intervals are all characterized by minimal stratigraphic variability (i.e., scatter) and relatively high values of $\delta^{13}C_{carb}$, both inconsistent with the variably decreasing $\delta^{13}C_{carb}$ expected from alteration by diagenetic fluids with low $\delta^{13}C$ values. Examining $\delta^{18}O_{carb}$ values in these three intervals we see a general trend toward decreased $\delta^{18}O$ values. This trend, however, is not consistent from well to well. Thus, while the uppermost GICE, TR-1 and TR-2 show consistent $\delta^{13}C_{carb}$ signatures between sections, they are characterized by variable $\delta^{18}O_{carb}$ profiles. The low and spatially variable $\delta^{18}O_{carb}$ values and spatially reproducible $\delta^{13}C_{carb}$ profiles supports diagenetic alteration to $\delta^{18}O_{carb}$, but not $\delta^{13}C_{carb}$ (Figure 9). This is consistent with *low* water:rock (because $\delta^{18}O_{carb}$ is more easily reset) suggesting that the low scatter $\delta^{13}C_{carb}$ did not result from homogenization during diagenesis. The simultaneous decrease in both $\delta^{13}C_{carb}$ and $\delta^{18}O_{carb}$ in the uppermost GICE is merely coincidental because the GICE shows the same decline in other wells (wells W2 and W1) with no change in $\delta^{18}O_{carb}$ (Figure 9). It is the combination of variably altered $\delta^{18}O_{carb}$ values against a changing primary $\delta^{13}C_{carb}$ trend, rather than diagenetic alteration of $\delta^{13}C_{carb}$ itself, that produces a moderate degree of covariance in each of the three isotopic intervals in

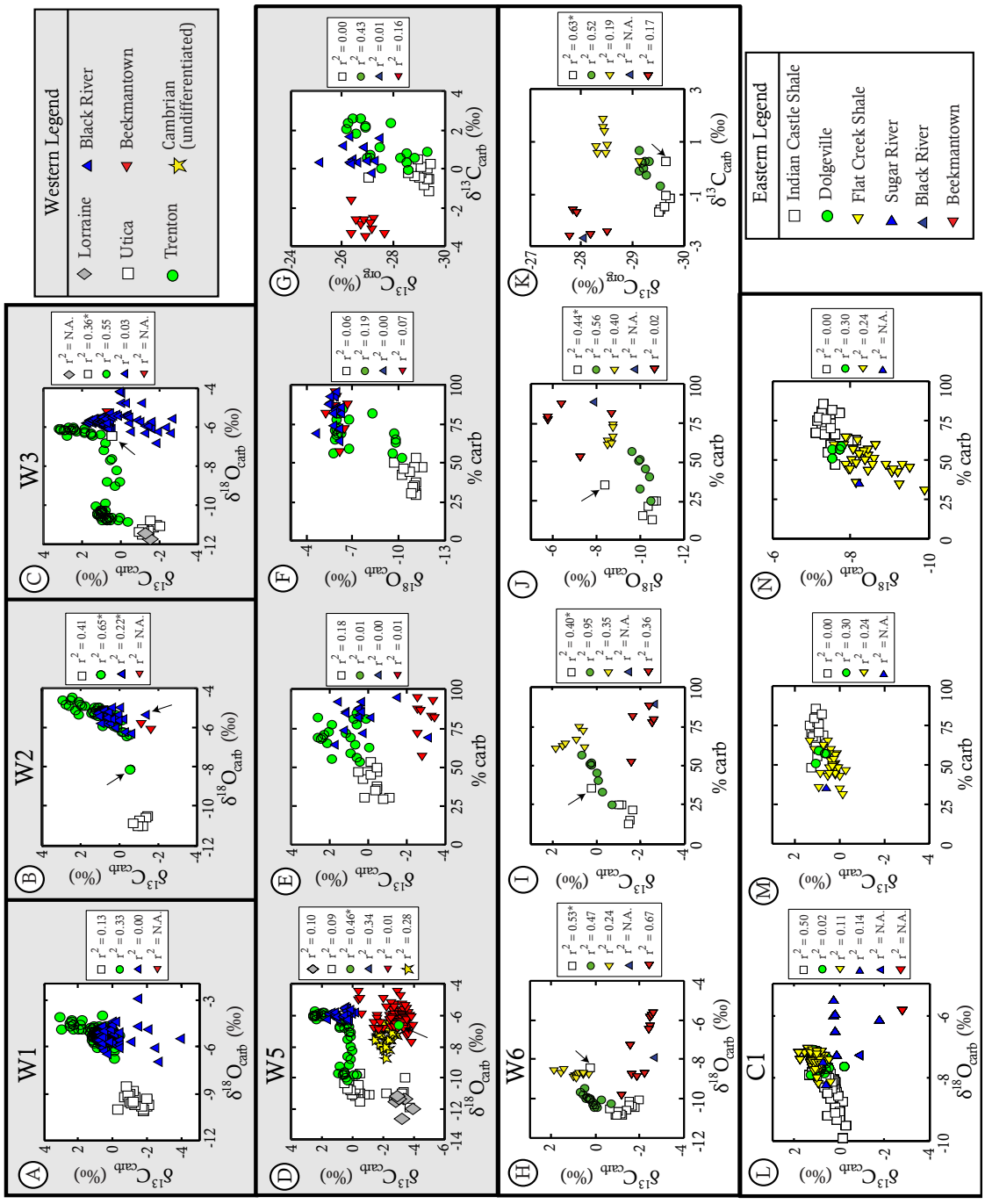

Figure 10. Geochemical cross-plots of well W1 (A), W2 (B), W3 (C), W5 (D-G), W6 (H-K), and core C1 (L-N). Western sections have gray background. Eastern sections have white background. * indicates outliers omitted from r^2 calculation. These outliers are shown by arrows. For all isotope values, symbols are larger than 1σ long-term average analytical error. No r^2 is given for data sets with n<3.

Trenton Group strata (e.g., Figure 10, well W5: $r^2 = 0.55$). Further evidence of a low water:rock

can be seen in TR-1 of wells W1, W2, and W3 (Figure 9), where $\delta^{13}C_{carb}$ is consistent while $\delta^{18}O_{carb}$ shows great disparity between wells.

Another interval of possible isotopic alteration is UT-1. The $\delta^{13}C_{carb}$ interval UT-1 shows an upward decrease in $\delta^{13}C_{carb}$ from 0‰ to -1.5‰, a parallel decrease in %carb, and constant, but low $\delta^{18}O_{carb}$ (Figures 4,5). Because $\delta^{18}O_{carb}$ can be reset under low water:rock (in this case "rock" is equivalent to carbonate content), then UT-1 can be plausibly the result of 1) meteoric diagenesis under a fixed flux of fluid where strata with lower %carb have lower $\delta^{13}C_{carb}$ or, 2) differential fluid:rock ratios across the strata with a fixed %carb where $\delta^{13}C_{carb}$ is lower in strata where fluid flux was higher. If $\delta^{13}C_{carb}$ interval UT-1 is diagenetic in origin, then this unit may not represent coeval strata, but instead capture a regionally extensive diagenetic event or episode, information which may be useful for other purposes (e.g, reservoir development) beyond chronostratigraphic correlation.

6.1.2 $\delta^{13}C_{org}$ & $\Delta^{13}C$

Another isotopic parameter, $\delta^{13}C_{org}$, can be used to identify potential alteration of $\delta^{13}C_{carb}$. This is because organic matter is derived from the local dissolved inorganic carbon (DIC) reservoir and is isotopically offset from DIC as a result of biological carbon fixation (e.g., Hayes et al., 1999). The offset is relatively constant when the conditions controlling the source (e.g., growth rate, $[CO_2]_{aq}$, Popp et al., 1997) and preservation (e.g., thermal maturity, Des Marais, 1997) of organic matter are stable, so any variation in $\delta^{13}C_{DIC}$ (i.e., what is eventually recorded in $\delta^{13}C_{carb}$) should appear as a parallel variation in $\delta^{13}C_{org}$. This, in turn, leads to a constant $\Delta^{13}C$ (= $\delta^{13}C_{carb} - \delta^{13}C_{org}$; e.g., Kump and Arthur, 1999). Variations in $\delta^{13}C$ can provide constraints on possible processes that change $\delta^{13}C_{carb}$ or $\delta^{13}C_{org}$ signatures. For example, in the middle of the

GICE interval of well W5 (Figure 6), $\Delta^{13}C$ increases for ~90ft upsection before returning to a relatively stable value of 29‰. This results from a larger decrease in $\delta^{13}C_{org}$ than $\delta^{13}C_{carb}$. Meteoric diagenesis should not affect $\delta^{13}C_{org}$ and the stable and high $\delta^{18}O_{carb}$ values in this interval provide further evidence that meteoric diagenesis is unlikely the source of the change in $\Delta^{13}C$. Rather, a short-term change in organic carbon source or composition (with a different isotopic fractionation from DIC and therefore a different $\delta^{13}C_{org}$ value) could explain the pattern and this explanation has been proposed for strata of similar age in Iowa (Pancost et al. 1999) and elsewhere (Pancost et al. 2013).

6.1.3 Stratigraphic Reproducibility

Consistent $\delta^{13}C_{carb}$ patterns across multiple locations in a region are deemed stratigraphically reproducible. The lack of regional stratigraphic reproducibility can reveal local (diagenetic or primary) overprints on the $\delta^{13}C_{carb}$ signals. A primary oceanic $\delta^{13}C_{carb}$ signal will be consistent over a large area, whereas the isotopic composition of diagenetic fluids (or a local deviation in $\delta^{13}C_{DIC}$) are *inherently variable* over large distances. To have stratigraphically reproducible diagenetic $\delta^{13}C_{carb}$ patterns means all locations must have been modified in such a way that the combination of (1) the degree of diagenesis and (2) the isotopic signature of the diagenetic fluid(s) resulted in the same alteration of the $\delta^{13}C_{carb}$ signal. The large local range in O and C isotope signatures of diagenetic fluids and the differing lithological properties of the rocks in different areas will tend to produce scatter in $\delta^{13}C_{carb}$ and $\delta^{18}O_{carb}$ of altered rocks. The inverse, low scatter (particularly in $\delta^{13}C_{carb}$) is consistent with a primary oceanic signal, which should produce a smoothly changing isotopic record through time. Intervals BR-2, BR-3, GICE, TR-1, and TR-2, show very consistent, smoothly changing $\delta^{13}C_{carb}$ patterns between sections,

strong evidence for a primary signal. Some $\delta^{13}C_{carb}$ intervals show minor discrepancies between wells (TR-1 of W2, BR-1 of W1), but the overall trends are clear enough to distinguish between $\delta^{13}C_{carb}$ intervals.

All but one of the $\delta^{13}C_{carb}$ intervals in this work are characterized by stable, high $\delta^{13}C_{carb}$ values or during *positive* rather than *negative* trends. The single negative interval, UT-1, does not carry a stratigraphically reproducible morphology, is found in strata with low carbonate abundance and low $\delta^{18}O_{carb}$ suggesting this interval is the product of alteration. However, the stable $\Delta^{13}C$ values in UT-1 suggest alteration is minimal. There are stratigraphic arguments arguing against UT-1 being a correct chronostratigraphic correlation. The base of the Utica Shale is younger in the west (Ruedemann, 1925; Kay, 1937), because of this we would predict that the isotopes would not align. At this time, the primary nature of this interval is unlikely.

Absence of covariation in geochemical parameters and stratigraphic reproducibility cannot prove alteration *did not occur*; they merely provide no evidence for alteration. Conversely, covariation and lack of stratigraphic reproducibility can show areas where alteration most likely *did occur* (e.g. UT-1), an important distinction. Minor differences in $\delta^{13}C_{carb}$ for a given isotope interval do exist between wells (e.g., small negative shifts in TR-1 of W2) and may be the result of primary or secondary overprints to the $\delta^{13}C_{carb}$ trend, but the larger $\delta^{13}C_{carb}$ patterns (at the scale of 10s-100s of feet) in each interval are sufficient to distinguish them from the other $\delta^{13}C_{carb}$ intervals.

6.1.4 Relationship between color and isotopes in core C1

Centimeter-scale sampling of light and dark layers (Figures 6,11) in core C1 reveals significant color-specific covariation between $\delta^{13}C_{carb}$ and $\delta^{18}O_{carb}$. Stratigraphically, the

intervals TR-1 and TR-2 are clearly defined in the darkest layers of core C1, while interbedded lighter layers showed high isotopic scatter as well as $\delta^{13}C_{carb}$ values higher than observed in other wells (Figure 6). While data from the dark layers cluster together in a $\delta^{13}C_{carb}$ vs. $\delta^{18}O_{carb}$ cross-plot (Figure 11), the lighter layers are arranged along a line that intersects the centroid of the samples from the darker layers, a pattern consistent with a linear mixture of two isotopically distinct components: a dark primary carbonate phase and a lighter-colored diagenetic carbonate component. Therefore $\delta^{13}C_{carb}$values obtained from the lighter layers are not representative of global (or even basin-wide) $\delta^{13}C_{carb}$ and should not be used for chemostratigraphic correlation.

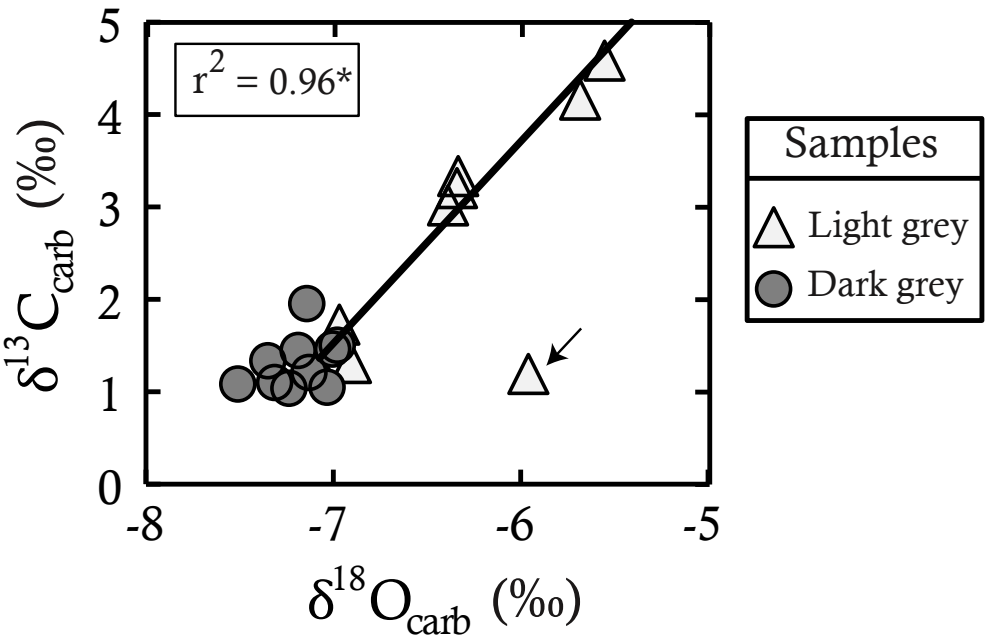

Figure 11. Isotopic cross-plots for light (concretionary) and dark samples from core C1. r^2 refers to linear least-squares fit. * = one outlier (arrow) omitted from regression calculation.

One possible source for the higher $\delta^{13}C_{carb}$ values observed in the lighter component is precipitation in fluids that were impacted by microbial methanogenesis. Because methane carries a low $\delta^{13}C$ value relative to the surrounding dissolved inorganic carbon (DIC) reservoir

(e.g., Conrad, 2005), methane production leads to an increase in local $\delta^{13}C_{DIC}$ if the methane is not re-oxidized and returned to the DIC reservoir. Methanogensis has been argued to be the source of high $\delta^{13}C_{carb}$ values in septarian concretions of the Devonian-aged Marcellus Shale of central New York (Siegel et al. 1987). Some of the lighter beds in core C1 are fossil-poor micrite in thin section, display diffuse contacts with darker beds and appear concretionary in outcrop (G.C. Baird, 2013, *personal communication*) suggesting that some of the lighter bands may be concretionary or impacted by *in situ* carbonate precipitation during lithification and/or diagenesis. Widespread, abundant concretions have been observed in the Kope Formation of Kentucky and Ohio (Brett et al., 2008), which is partially contemporaneous with the Utica Shale of New York. The high degree of scatter, lack of regionally reproducible $\delta^{13}C_{carb}$ values or vertical trends, and petrographic characteristics of some of the lighter-colored layers is consistent with a significant secondary overprint of isotope values and suggests these materials should be avoided when correlating.

The higher $\delta^{13}C_{carb}$ values in the lighter carbonate layers may explain the origin of the heavier than expected $\delta^{13}C_{carb}$ values in depths 5,350-5,370ft of well W6 (Figure 4) as the lighter colored layers correlate lithologically to the higher than expected $\delta^{13}C_{carb}$ values in W6. While cuttings samples were screened for obvious alteration (e.g. macroscopic spar or pyrite), they were not screened by color, so it is possible that these three samples contain the lighter material with higher $\delta^{13}C_{carb}$ values as seen in core C1. Alternatively, the higher $\delta^{13}C_{carb}$ values in W6 could be explained by a local $\delta^{13}C_{DIC}$ signal. Grain specific $\delta^{13}C_{carb}$ analyses and an increased well density could test this hypothesis.

6.2 Evaluation of Lithologic Mixing on $\delta^{13}C_{carb}$ in Cuttings

Results from the single chip test in well W7 indicate moderate degrees of isotopic heterogeneity on a scale smaller than the cuttings sampling resolution (i.e., within a single cuttings sampling interval). Variability in $\delta^{13}C_{carb}$ of single chips is higher when the baseline $\delta^{13}C_{carb}$ values of bulk cuttings is changing. This variability is interpreted to result from the mixture of stratigraphically varying components within the cuttings sample. The $\delta^{13}C_{carb}$ values of multiple individual chips approximate the subsample $\delta^{13}C_{carb}$ values (~0.5g) which in turn approximate the bulk $\delta^{13}C_{carb}$ values of the bulk material (except in cases of strongly varying background $\delta^{13}C_{carb}$ and/or $\delta^{18}O_{carb}$ signals). The range of values in $\delta^{13}C_{carb}$ suggests that only a small number of chips (coarse sand and larger) need to be powdered to satisfactorily approximate the total sample values.

In general, the magnitude of $\delta^{18}O_{carb}$ variability was higher than that of the stratigraphically equivalent $\delta^{13}C_{carb}$. This is consistent with the theoretical prediction that $\delta^{18}O_{carb}$ is easier to reset during diagenesis (e.g., Banner and Hanson, 1990). Small-scale variation in porosity and permeability can result in variable $\delta^{18}O_{carb}$ over the stratigraphic interval that a single cuttings sample represents (e.g., 10 ft). Those materials with higher permeability will have more fluids pass through them and therefore are more susceptible to alteration of the original $\delta^{18}O_{carb}$ signal (for a fixed carbonate content). When picking material in a given sample, micritic components seem to have the best potential to record a primary oceanic $\delta^{13}C_{carb}$ signal (e.g., Metzger & Fike, 2013).

6.3 Evaluation of Sampling Resolution

In chemostratigraphic studies, the geographic resolution is set by the lateral well spacing, while the temporal resolution is set by the stratigraphic (vertical) sampling resolution. A high stratigraphic sampling density most closely reproduces the evolving marine $\delta^{13}C_{carb}$ record. Cuttings typically average lithology over depths of ~1-10m, while core and outcrop studies only average over the width of the drill bit used for sampling (a few mm). For this reason, at a given sampling resolution, chemostratigraphic profiles from cuttings will be smoother than the equivalent profiles obtained from cores or outcrops. As seen in Figure 8, low sampling resolution in well W4 dampens the magnitude of isotopic variations and can give the appearance of lateral isotopic variability between localities where there is none. Low sampling resolution also obscures the stratigraphic position of distinct isotopic tie points (e.g., the low sampling resolution in well W4 is not appropriate for detailed chemostratigraphic correlation). Similar effects of averaging are present in other geochemical records, such as TOC and %carb. This stratigraphic averaging is important for calibrating isotopic data against other borehole data such as wireline logs (e.g., gamma ray), which more accurately track true depth. When choosing wells for a study, especially across a large range of sedimentation rates, the sampling resolution must be sufficient to identify, resolve, and correlate geochemical features of interest.

6.3.1 Summary

Covariation in isotopic and geochemical parameters can supply one method for evaluating diagenetic alteration. Pairing of $\delta^{13}C_{carb}$ with $\delta^{13}C_{org}$ can be used to test for meteoric diagenesis during negative $\delta^{13}C_{carb}$ excursions; however, this method is limited by the natural variability in organic carbon sources and should be used in tandem with other screening

procedures. Stratigraphic reproducibility of $\delta^{13}C_{carb}$ trends in closely spaced wells can discriminate between basin-wide and local $\delta^{13}C_{carb}$ signals. This combined approach helped in identifying the diagenetic origin of both high $\delta^{13}C_{carb}$ (e.g., core C1) and low $\delta^{13}C_{carb}$ values (e.g., TR-1 in well W2, Figure 9). Low degrees of scatter and stratigraphic reproducibility of $\delta^{13}C_{carb}$ intervals BR-2, BR-3, GICE, TR-1, and TR-2 strongly suggest these intervals represent a primary basin-wide or global $\delta^{13}C_{DIC}$ signal. Analysis within this report suggests that the vast majority of the rocks within the interval BR-1 retain the original $\delta^{13}C_{carb}$ signal, but are variably impacted by local diagenetic processes. It is unlikely that $\delta^{13}C_{carb}$ values in UT-1 track a primary oceanic signal.

6.4 Geologic Implications

Correlations using $\delta^{13}C_{carb}$ intervals reveal stratigraphic relationships not apparent using gamma ray logs and geologic sampling logs. For example, the Black River Group can be confidently subdivided into 3 chronstratigraphic units based on $\delta^{13}C_{carb}$ logs. These chronostratigraphic divisions are very similar to divisions that would be made using gamma ray logs (except for the uppermost part of the Black River Group in W3, where isotopic data suggest variable erosion of the upper Black River strata) and suggest that the environmental change was synchronous across the basin. Conversely, $\delta^{13}C_{carb}$ interval TR-1 shows the diachronous nature of environmental change across the basin as the shaley facies form in the eastern portion of the basin first. Further, $\delta^{13}C_{carb}$ intervals BR-1, BR-2, and BR-3 show that differences in thickness of the Black River Group between sections result mainly from differences in the thickness of the upper portion of the Black River (i.e., BR-3). The fact that BR-3 is proportionally much thicker in the well W3 may result from non-deposition or erosion of the uppermost Black

River strata in the regions of the flanking wells. In this interpretation, the top of interval BR-3 in wells W1 and W2 are truncated and would correlate with the middle of interval BR-3 in well W3. This correlation is supported by the fact that the highest $\delta^{13}C_{carb}$ values in BR-3 are found in the upper part of this interval in well W3 and not seen in BR-3 from adjacent wells with a thinner BR-3 interval. An unconformity between the Black River and overlying Trenton groups is known in outcrop strata north of the western wells near Lake Erie (Mitchell et al., 2004) and the unconformity may extend down to our study area, manifested as variable truncation of the uppermost BR-3 interval.

The $\delta^{13}C_{carb}$ interval above BR-3 is the GICE. This interval appears to be fully preserved in the western 3 wells examined here (W1, W2, and W3) and mostly present in W5. This is evidenced by the gradual thickening and thinning of the GICE and the preservation of both the rise and fall in $\delta^{13}C_{carb}$ values across the basin. In eastern New York, either nondeposition occured during GICE-time or erosion subsequently removed GICE strata. This is shown in Figure 9A where $\delta^{13}C_{carb}$ intervals BR-2, BR-3, and the GICE pinch out between wells W5 and W6. TR-1 sediment accumulation in the eastern wells began immediately following the GICE interval, as evidenced by the thick rising limb of interval TR-1 prior to the 1‰ plateau. If more time were missing, the rise in $\delta^{13}C_{carb}$ would not be captured and would instead appear as a step-change in $\delta^{13}C_{carb}$. This places tight chronostratigraphic boundaries on the events and factors that controlled sedimentation across the basin. Assuming that sedimentation was restricted in eastern New York due to insufficient accommodation space, then new accommodation space was created just after the end of the GICE. The increase in accommodation space likely arose from extensional faulting where eastern New York was rapidly thrust downward following the GICE

interval. The tectonic activity shifted the basin depocenter from southwestern New York (near well W3) in pre-GICE time to eastern New York (near core C1) in post-GICE time.

Coupled lithostratigraphy and chemostratigraphy can be used to reconstruct basin dynamics. Figure 9 shows the relative position of the base of the Utica Shale contact (lithostratigraphic contact; red wavy line in Figure 9) and top of TR-1 (chemostratigraphic contact; top of blue zone in Figure 9). These lines cross as followed from east to west across New York State. This relationship demonstrates the time-transgressive nature of the Utica Shale contact, where the basal Utica Shale is progressively younger westward across New York. This is in general agreement with interpretations of Brett and Baird (2002) who used lithostratigraphic, biostratigraphic, and K-bentonite data to construct their chronostratigraphic correlations of outcrops in central and eastern New York.

Figure 9B shows two sets of correlations arising from lithostratigraphic (light and dark gray shaded backgrounds) and chemostratigraphic methods (colored lines). A detailed chronostratigrpahic understanding of the diachronous nature of the lithologic change is made possible using the $\delta^{13}C_{carb}$ data and produces a different depositional history than may otherwise be constructed for the Trenton-Utica sequence using gamma ray logs and geologic sample logs alone. Correlations based upon shifts in gamma ray logs and lithologic transitions from limestones to shales would suggest more missing strata in eastern New York than the correlations based upon $\delta^{13}C_{carb}$ data. While the time-transgressive nature of the Trenton-Utica contact has been identified in previous studies (see Baird and Brett, 2002; Brett and Baird, 2002), these studies were done using outcrops with abundant fossils, event beds, and K-bentonites, materials which are rare or unavailable in the subsurface. This agreement suggests $\delta^{13}C$ chemostratigraphy is a fruitful way to link together subsurface regions and their correlative

outcrop belts within a unified chronostratigraphic framework. This study demonstrates the power of $\delta^{13}C_{carb}$ stratigraphy for understanding chronostratigraphic relationships in the subsurface, especially across different depositional facies and lithologies (Figure 9B) where biostratigraphy may not be practical or feasible.

7. CONCLUSIONS

The ubiquity of well cuttings and the ability to rapidly analyze large numbers of samples for $\delta^{13}C_{carb}$, $\delta^{18}O_{carb}$, and $\delta^{13}C_{org}$ have created an opportunity to scale-up chemostratigraphic studies from a few outcrops and cores to a *network* of wells to obtain the spatial density needed to assemble a high-resolution, basin-wide correlative framework in the subsurface. The sampling of wells in a high spatial density that results in large data sets can be used to resolve small (‰-level) changes in $\delta^{13}C_{carb}$ that may otherwise be ascribed to "noise" when considering single sections alone. Multiple $\delta^{13}C_{carb}$ intervals can be found within a single formation or lithology demonstrating the potential high-resolution correlative power of $\delta^{13}C_{carb}$ chemostratigraphy from large data sets. We believe this study demonstrates that $\delta^{13}C_{carb}$ can provide robust chronostratigrpahic correlations across thick stratigraphic packages and over large lateral distances with small sample volumes and limited labor investments. $\delta^{13}C_{carb}$ chemostratigraphic may be particularly useful in basins where environmental segregation of species during deposition limits the utility of biostratigraphy, such as the Permian Kuff Formation of Saudi Arabia (Dasgupta et al., 2001), the Jurassic Arab Cycles of Saudi Arabia (Al-sharhan and Whittle, 1995), and the Silurian of the Michigan Basin (Mesolella et al., 1974). Several points must be kept in mind for a cuttings-based chemostratigraphic study:

1) Wells for cuttings-based studies must be chosen carefully based on their maximum vertical sampling resolution and the number of available wells in a given area needed to create the desired spatial resolution. Wells with coarse sampling intervals can limit the stratigraphic resolutions possible, as well as shift the isotopic values and stratigraphic position of local isotopic minima and maxima.

2) Isotopic analysis of single chips show that only a small fraction (e.g., < 0.5g) of a standard cuttings sample must be homogenized to obtain representative isotopic values.

3) The resulting data must be screened for diagenetic alteration that could otherwise skew resulting chemostratigraphic correlations. In particular, parallel $\delta^{13}C_{carb}$ and $\delta^{13}C_{org}$ trends are strong evidence for a primary $\delta^{13}C$ signal in both phases. Similarly, covariation in $\delta^{13}C_{carb}$, $\delta^{18}O_{carb}$, TOC, and carbonate abundance can be indicators for diagenetic alteration

4) Diagenetic alteration of a single location cannot be fully assessed without comparison of isotopic trends (here $\delta^{13}C_{carb}$, $\delta^{13}C_{org}$, and $\delta^{18}O_{carb}$) from multiple sections within a basin because traditional techniques for assessing diagenetic alteration (e.g., covariation in $\delta^{13}C_{carb,}$ $\delta^{18}O_{carb}$) can also result from primary environmental signals. Testing for reproducible $\delta^{13}C_{carb}$ patterns from closely spaced wells ("stratigraphic reproducibility") is a rigorous technique for assessing diagenetic alteration at the basin scale.

Chemostratigraphic study of Late Ordovician strata of New York has revealed that:

1) Consistent with results using biostratigraphic, lithostratigraphic, and event bed stratigraphic methods from outcrops in central New York State, the Trenton Group-Utica Shale contact is time-transgressive in subsurface regions south and west of the outcrop belt with the basal Utica Shale being progressively younger moving west across New York. This can be seen in the

$\delta^{13}C_{carb}$ composite presented herein for the New York region of the Upper Ordovician Mohawkian and Cinncinnatian Series.

2) The locus of sedimentation shifted from southwestern New York (during the deposition of the Black River Group to middle Trenton Group) to eastern New York during deposition of the Utica Shale as a result of local tectonic forces likely related to the Taconic orogeny.

8. ACKNOWLEDGEMENTS

We would like to thank Alexa Stolorow and James Leone for assistance with Petra and guidance in the field, Brian Slater and Kathleen Bonk for their help with core sampling, Dwight McCay and Claire Beaudoin their help in the lab. J.G.M. would like to thank Dr. Robert Criss and Richard Nyahay for thought provoking discussions and Martin Pratt for computational assistance. Digitized logs were processed using IHS Petra © (v. 3.6.2). This manuscript was greatly improved from reviews by N. Harris, G. Baird, R. Koepnick, and F. McDonald. Funding was provided by the Agouron Institute and a grant from the ACS Petroleum Research Fund (#51357-DN12) awarded to D.A.F. and support from the Hanse-wissenschaftskolleg to D.A.F. and J.G.M. in the form of a Hanse Fellowship and a Twin Fellowship, respectively.

9. REFERENCES

Allan, J. R., Matthews, R.K., 1982, Isotope signatures associated with early meteoric diagenesis: Sedimentology, v. 29, p. 797-817.

Alsharhan, A. S., Whittle, G.L., 1995, Carbonate-evaporite sequences of the Late Jurassic, southern and southwestern Arabian Gulf: AAPG Bulletin, v. 79, p. 1608-1630.

Armentrout, J. M., 1996, High resolution sequence biostratigraphy: examples from the Gulf of Mexico Plio-Pleistocene, *in* J. A. Howell, Aitken, J.F., ed., Geological Society of London

Special Publication No. 104: High Resolution Sequence Stratigraphy: Innovations and Applications: London, The Geological Society, p. 65-86.

Baird, G. C., Brett, C.E., 2002, Indian Castle Shale: late synorogenic siliclastic succession in an evolving Middle to Late Ordovician foreland basin, eastern New York State: Physics and Chemistry of the Earth, v. 27, p. 203-230.

Banner, J. L., Hanson, G.N., 1990, Calculation of simultaneous isotopic and trace element variations during water-rock interaction with applications to carbonate diagenesis: Geochimica et Cosmochimica Acta, v. 54, p. 3123-3137.

Bathurst, R. G. C., 1975, Carbonate sediments and their diagenesis: Developments in Sedimentology, v. 12: Amsterdam, Elsevier, 658 p.

Bergström, S. M., Huff, W.D., Saltzman, M.R., Kolata, D.R., Leslie, S.A., 2004, The greatest volcanic ash falls in the Phanerozoic: Trans-Atlantic relations of the Ordovician Millbrig and Kinnekulle K-bentonites: The Sedimentary Record, v. 2, p. 4-8.

Bergström, S. M., Xu, C., Schmitz, B., Young, S., Jia-Yu, R., Saltzman, M.R., 2009, First documentation of the Ordovician Guttenberg $\delta^{13}C$ excursion (GICE) in Asia: chemostratigraphy of the Pagoda and Yanwashan formations in southeastern China: Geological Magazine, v. 146, p. 1-11.

Bergstrom, S. M., Agematsu, S., Schmitz, B., 2010, Global Upper Ordovician correlation by means of $\delta^{13}C$ chemostratigraphy: implications of the discovery of the Guttenberg $\delta^{13}C$ excursion (GICE) in Malaysia: Geological Magazine, v. 147, p. 641-651.

Berkley, J. L., Baird, G.C., 2002, Calcareous K-bentonite deposits in the Utica Shale and Trenton Group (Middle Ordovician), of the Mohawk Valley, New York State: Physics and Chemistry of the Earth, v. 27, p. 265-278.

Bowring, S. A., Grotzinger, J.P., Isachsen, C.E., Knoll, A.H., Pelechaty, S.M., Kolosov, P., 1993, Calibrating rates of Early Cambrian evolution: Science, v. 261, p. 1293-1298.

Brett, C. E., 1995, Sequence stratigraphy, biostratigraphy, and taphonomy in shallow marine environments: Palaios, v. 10, p. 597-616.

Brett, C. E., Baird, G.C., 2002, Revised stratigraphy of the Trenton Group in its type area, central New York State: sedimentology and tectonics of a Middle Ordovician shelf-to-basin succession: Physics and Chemistry of the Earth, v. 27, p. 231-263.

Brett. C.E., K., B.T., Tsujita, C.J., Dattilo, B.F., 2008, Depositional dynamics recorded in mixed siliciclastic-carbonate marine successions: Insights from the Upper Ordovician Kope Formation of Ohio and Kentucky, U.S.A., *in* B. R. Pratt, Holmden, C., ed., Dynamics of Epeiric Seas, Geological Association of Canada, Special Paper 48, p. 73-102.

Burns, S. J., Matter, A., 1993, Carbon isotopic record of the latest Proterozoic from Oman: Eclogae Geologicae Helvetiae, v. 86, p. 595-607.

Coleman, M. L., Raiswell, R., 1980, Carbon, oxygen, and sulphur isotope variations in concretions from the Upper Lias of N.E. England: Geochimica et Cosmochimica Acta, v. 45, p. 329-340.

Conrad, R., 2005, Quantification of methanogenic pathways using stable carbon isotopic signatures: a review and a proposal: Organic Geochemistry, v. 36, p. 739-752.

Dasgupta, S. N., Hong, M.R., Al-Jallal, I.A., 2001, Reservoir charecterization of Permian Khuff-C carbonate in the supergiant Ghawar Field of Saudi Arabia: The Leading Edge, v. 20, p. 706-717.

Derry, L. A., 2010, On the significance of $\boldsymbol{\delta}^{13}C$ correlations in ancient sediments: Earth and Planetary Science Letters, v. 296, p. 497-501.

Marais, D., 1997, Isotopic evolution of the biogeochemical carbon cycle during the Proterozoic Eon: Organic Geochemistry, v. 27, p. 185-193.

Dicken, C. L., Nicholson, S.W., Horton, J.D., Kinney, S.A., Gunther, G., Foose, M.P., Mueller, J.A.L., 2008 (revision), Preliminary integrated geologic map databases for the United States: Delware, Maryland, New York, Pennsylvania, and Virginia, United States Geological Survey, http://pubs.usgs.gov/of/2005/1325/, accessed October 24th, 2012.

Fike. D.A., G., J.P., Pratt, L.M., Summons, R.E., 2006, Oxidation of the Ediacaran Ocean: Nature, v. 444.

Gartner, S., Chen, M.P., Stanton, R.J., 1983, Late Neogene Nannofossil biostratigraphy and paleoceanography of the northeastern Gulf of Mexico and adjacent areas: Marine Micropaleontology, v. 8, p. 17-50.

Goldman, D., Mitchell, C.E., Bergström, S.M., Delano, J.W., and Tice, S., 1994, K-bentonites and graptolite biostratigraphy in the Middle Ordovician of New York State and Quebec: A new chronostratigraphic model: Palaios, v. 9, p. 124-143.

Gradstein, F. M., Kaminski, M.A., Berggren, W.A., 1988, Cenozoic foraminiferal biostratigraphy of the central North Sea: Abh. Geol. Bundensanst (Austria), v. 41, p. 97-108.

Gradstein, F. M., Kristiansen, I.L., Loemo, L., Kaminski, M.A., 2003, Cenozoic foraminiferal and dinoflagellate cyst biostratigraphy of the central North Sea: Micropaleontology, v. 38, p. 107-137.

Gruber, N., Keeling, C.D., Bacastow, R.B., Guenther, P.R., Lueker, T.J., Wahlen, M., Meijer, H.A.J., Mook, W.G., Stocker, T.F., 1999, Spatiotemporal patterns of carbon-13 in the global surface oceans and the oceanic Suess effect: Global Biogeochemical Cycles, v. 13, p. 307-335.

Hayes, J. M., Strauss, H., Kaufman, A.J., 1999, The abundance of ^{13}C in marine organic matter and isotopic fractionation in the global biogeochemical cycle of carbon during the past 800 Ma: Chemical Geology, v. 161, p. 103-125.

Hein, J. R., Normark, W.R., McIntyre, B.R., Lorenson, T.D., Powell II, C.L., 2006, Methanogenic calcite, ^{13}C-depleted bivavle shells, and gas hydrate from a mud volcano offshore southern California: Geology, v. 34, p. 109-112.

Herrle, J.O., Kößler, Friedrich, O., Erlenkeuser, H., Hemleben, C., 2004, High-resolution carbon isotope records of the Aptian to Lower Albian from SE France and The Mazagan Plateau (DSDP Site 545): a stratigraphic tool for paleoceanographic and paleobiologic reconstruction: Earth and Planetary Science Letters, v. 218, p. 149-161.

Hesselbo, S.P., Jenkyns, H.C., Duarte, L.V., Oliveira, L.C.V., 2007, Carbon-isotope record of the early Jurassic (Toarcian) Oceanic Anoxic Event from fossil wood and marine carbonate (Lusitanian Basin, Portugal): Earth and Planetary Science Letters, v. 253, p. 455-470.

Immenhauser, A., Della Porta, G., Kenter, J.A.M., Bahamonde, J.R., 2003, An alternative model for positive shifts in shallow-marine carbonate $\delta^{13}C$ and $\delta^{18}O$: Sedimentology, v. 50, p. 953-959.

Jones, D. S., Fike, D.A., Finnegan, S., Fischer, W.W., Schrag, D.P., McCay, D., 2011, Terminal Ordovician carbon isotope stratiraphy and glacioeustatic sea-level change across Anticost Island (Québec, Canada): GSA Bulletin, v. 123, p. 1645-1664.

Joachimski, M. M., 1994, Subaerial exposure and deposition of shallowing upward sequences: evidence from stable isotopes of Purbeckian peritidal carbonates (basal Cretaceous), Swiss and French Jura Mountains: Sedimentology, v. 41, p. 805-824.

Keith, B. D., 1989, Regional facies of Upper Ordovician Series of eastern North America, *in* B. D. Keith, ed., The Trenton Group (Upper Ordovician Series) of eastern North America, v. 29, American Association of Petroleum Geologists, p. 1-16.

Kay, G. M., 1937, Stratigraphy of the Trenton Group: Geological Society of America Bulletin, v. 48, p. 233-302.

Kirchner, B. T., and Brett, C.E., 2008, Subsurface correlation and paleogeography of a mixed siliclastic-carbonate unit using distinctive faunal horizons: toward a new methodology: Palaios, v. 23, p. 174-184.

Kirschbaum, M. A., Schenk, C.J., Cook, Ryder, R.T., Charpentier, R.R., Klett, T.R., Gaswirth, S.B., Tennyson, M.E., Whidden, K.J., 2012, Assessment of Undiscovered Oil and Gas Resources of the Ordovician Utica Shale of the Appalachian Basin Province, 2012, U.S. Geological Survey, 6 pgs.

Knauth, L. P., Kennedy, M.J., 2009, The late Precambrian greening of the Earth: Nature, v. 460, p. 728-732.

Knoll, A. H., Hayes, J.M., Kaufman, A.J., Swett, K., Lambert, I.B., 1986, Secular variation in carbon isotope ratios from Upper Proterozoic Successions of Svalbard and East Greenland: Nature, v. 321, p. 832-838.

Kump, L., R., Arthur, M.A., 1999, Interpreting carbon-isotope excursions: carbonates and organic matter: Chemical Geology, v. 161, p. 181-198.

Lehmann, D. B., C.E., Cole, R., Baird, G., 1995, Distal sedimentation in a peripheral foreland basin: Ordovician black shales and associated flysch of the western Taconic foreland, New York State and Ontario: Geological Society of America Bulletin, v. 107, p. 708-724.

Lohmann, K. C., 1988, Geochemical patterns of meteoric diagenetic systems and their application to studies of paleokarst, *in* N. P. James, Choquette, P.W., ed., Paleokarst: New York City, Springer-Verlag, p. 416.

Ludvigson, G. A., Witzke, B.J., Gonzàlez, L.A., Carpenter, S.J., Schneider, C.L., Hasiuk, F., 2004, Late Ordovician (Turnian-Chatfieldian) carbon isotope excursions and their

stratigraphic and paleoceanographic significance: Palaeogeography, Palaeoclimatology, Palaeoecology, v. 210, p. 187-214.

Maloof, A. C., Schrag, D.P., Crowley, J.L., and Bowring, S.A., 2005, An expanded record of Early Cambrian carbon cycling from the Anti-Atlas Margin, Morocco: Canadian Journal of Earth Science, v. 42, p. 2195-2216.

Maloof, A. C., Ramezani, J., Bowring, S.A., Fike, D.A., Porter, S.M., Mazouad, M., 2010, Constraints on early Cambrian carbon cycling from the duration of the Nemakit-Daldynian—Tommotian boundary $\delta^{13}C$ shift, Morocco: Geology, v. 38, p. 623-626.

Melim, L. A., Swart, P.K., Eberli, G.P., 2004, Mixing-zone diagenesis in the subsurface of Florida and the Bahamas: Journal of Sedimentary Research, v. 74, p. 904-913.

Mesolella, K. J., Robinson, J.D., McCormic, L.M., Ormiston, A.R., 1974, Cyclic deposition of Silurian carbonates and evaporites in Michigan Basin: American Association of Petroleum Geologists Bulletin, v. 58, p. 34-62.

Metzger, J.G., and Fike, D.A., 2013, Techniques for assessing spatial heterogeneity of carbonate $\delta^{13}C$: Implications for craton-wide isotope gradients: Sedimentology, DOI: 10.1111/sed.12033.

Mitchell, C. E., Adhya, S., Bergström, S.M., Joy, M.P., Delano, J.W., 2004, Discovery of the Ordovician Millbrig K-bentonite Bed in the Trenton Group of New York State: implications for regional correlation and sequence stratigraphy in eastern North America: Palaeogeography Palaeoclimatology Palaeoecology, v. 210, p. 331-346.

Mitchell, S. F., Paul, C.R.C., Gale, A.S., 1996, Carbon isotopes and sequence stratigraphy, *in* J. A. Howell, Aitken, J.F., ed., Geological Society Special Publication No. 104: High Resolution Sequence Stratigraphy: Innovations and Applications: London, The Geological Society.

Pancost, R. D., K. H. Freeman, and M. E. Patzkowsky, 1999, Organic-matter source variation and the expression of a late Middle Ordovician carbon isotope excursion: Geology, v. 27, p. 1015-1018.

Patchen, D. G., Hickman, J.B., Harris, D.C., Drahovzal, J.A., Lake, P.D., Smith, L.B., Nyahay, R., Schulze, R., Riley, R.A., Baranoski, M.T., Wickstrom, L.H., Laughrey, C.D., Kostelnick, J., Harper, J.A., Avary, K.L., Bocan, J., Hohn, M.E., and McDowell, R., 2006, A geologic play book for Trenton Limestone-Black River Limestone Appalachian

Basin exploration: Morgantown, West Virginia, U.S. Department of Energy Report, accessible at <http://www.wvgs.wvnet.edu/www/tbr/project_reports.asp>, West Virginia Geological Survey, 601 p.

Patterson, W. P., Walter, L.M., 1994, Depletion of ^{13}C in seawater ΣCO_2 on modern carbonate platforms: Significance for the carbon isotopic record of carbonates: Geology, v. 22, p. 885-888.

Patzkowsky, M. E., 1995, Gradient analysis of Middle Ordovician brachiopod biofacies: biostratigraphic, biogeographic, and macroevolutionary implications: Palaios, v. 10, p. 154-179.

Popp, B. N., Parekh, P., Tilbrook, B., Bidigare, R.R., Laws, E.A., 1997, Organic carbon $\delta^{13}C$ variations in sedimentary rocks as chemostratigraphic and paleoenvironmental tools: Palaeogeography Palaeoclimatology Palaeoecology, v. 132, p. 119-132.

Ramezani, J., Schmitz, M.D., Davydov, V.I., Bowring, S.A., Snyder, W.S., and Northrup, C.J., 2007, High-precision U-Pb zircon age constraints on the Carboniferous-Permian boundary in the southern Urals stratotype: Earth and Planetary Science Letters, v. 256, p. 244-257.

Rodgers, J., 1971, The Taconic Orogeny: Geological Society of America Bulletin, v. 82, p. 1141-1178.

Ruedemann, R., 1925, The Utica and Lorraine Formations of New York, Part I: Stratigraphy, New York State Museum Bulletin No. 258, p. 176.

Sabatino, N., Vlahović, Jenkyns, H.C., Scopelliti, G., Neri, R., Prtoljan, B., Velić, I., 2013, Carbon-isotope record and palaeoenvironmental changes during the early Toarcian oceanic anoxic event in shallow-marine carbonates of the Adriatic Carbonate Platform in Croatia: Geological Magazine, v. 150, p. 1085-1102.

Saltzman, M. R., 2003, Organic carbon burial and phosphogenesis in the Antler foreland basin: An out-of-phase relationship during the Lower Mississippian: Journal of Sedimentary Research, v. 73, p. 844-855.

Saltzman, M. R., Ripperdan, R.L., Brasier, M.D., Lohmann, K.C., Robison, R.A., Chang, W.T., Peng, S.C., Ergaliev, E.K., and Runnegar, B., 2000, A global carbon isotope excursion (SPICE) during the Late Cambrian: relation to trilobite extinctions, organic-matter burial and sea level: Palaeogeography Palaeoclimatology Palaeoecology, v. 162, p. 211-223.

Selby, D., Creaser, R.A., 2005, Direct Radiometric Dating of Hydrocarbon Deposits Using Rhenium-Osmium Isotopes: Science, v. 308, p. 1293-1295.

Selby, D., Mutterlose. J., Condon, D.J., 2009, U-Pb and Re-Os geochronology of the Aptian/Albian and Cenomanian/Turonian stage boundaries: Implications for timescale calibration, osmium isotope seawater composition and Re-Os systematics in organic-rich sediments: Chemical Geology, v. 265, p. 394-409.

Siegel, D. I., Chamberlain, S.C., Dossert, W.P., 1987, The isotopic and chemical evolution of mineralization in septarian concretions: Evidence for episodic paleohydrogeologic methanogensis: Geological Society of America Bulletin, v. 99, p. 385-394.

Smith, L. B., 2006, Origin and reservoir characteristics of Upper Ordovician Trenton-Black River hydrothermal dolomite reservoirs in New York: American Association of Petroleum Geologists Bulletin, v. 90, p. 1691-1718.

Smith, L.B., 2010, Impact of Syndepositional Faulting on the Distribution of Organic-Rich Utica Shale, New York State (abstract) *in:* AAPG Eastern Section Program with abstracts, p. 49.

Swart, P. K., Eberli, G., 2005, The nature of the $\delta^{13}C$ of periplatform sediments: Implications for stratigraphy and the global carbon cycle: Sedimentary Geology, v. 175, p. 115-129.

Swart, P. K., 2008, Global synchronous changes in the carbon isotopic composition of carbonate sediments unrelated to changes in the global carbon cycle: Proceedings of the National Academy of Sciences, v. 105, p. 13741-13745.

Swart, P. K., Kennedy, M.J., 2012, Does the global stratigraphic reproducibility of $\delta^{13}C$ in Neoproterozoic carbonates require a marine origin? A Pliocene-Pleistocene comparison: Geology, v. 40, p. 87-90.

Thompson, T. L., 1991, Paleozoic Successions in Missouri Part 2: Ordovician System: Missouri Geological Survey Report of Investigations, v. 70 part 2: Rolla, Missouri Department of Natural Resources, Division of Geology and Land Survey, 282 p.

Tsikos, H., Jenkyns, H.C., Walsworth-Bell, B., Petrizzo, M.R., Forster, A., Kolonic, S., Erba, E., Premoli Silva, I., Baas, M., Wagner, T., Sinninghe Damste, J.S., 2004, Carbon-isotope stratigraphy recorded by the Cenomanian-Turonian Oceanic Anoxic Event: correlation

and implications based on three key localities: Journal of the Geological Society of London, v. 161, p. 711-719.

van Staal, C. R., Barr, S.M., 2012, Lithospheric architecture and tectonic evolution of the Canadian Appalachians and associated Atlantic Margin, *in* J. A. Percival, Cook. F.A., Clowes, R.M.,, ed., Tectonic Styles in Canada: the LITHOPROBE Perspective, v. Special Paper 49, Geological Association of Canada, p. 41-97.

Veizer, J., Ala, D., Azmy, K., Bruckschen, P., Buhl, D., Bruhn, F., Carden, G.A.F., Diener, A., Ebneth, S., Godderis, Y., Jasper, T., Korte, C., Pawellek, F., Podlaha, O.G., Strauss, H., 1999, $^{87}Sr/^{86}Sr$, $\delta^{13}C$ and $\delta^{18}O$ evolution of Phanerozoic seawater: Chemical Geology, v. 161, p. 59-88.

Witrock, R. B., Nixon, L.D., Post, P.J., Ross, K.M., 2003, Biostratigraphic chart of the Gulf of Mexico offshore region, Jurassic to Quaternary, New Orleans, U.S. Department of the Interior, Bureay of Ocean Energy Management, Regulation, and Enforcement.

Young, S. A., Saltzman, M.R., Bergström, S.M., 2005, Upper Ordovician (Mohawkian) carbon isotope ($\delta^{13}C$) stratigraphy in eastern and central North America: Regional expression of a perturbation of the global carbon cycle: Palaeogeography, Palaeoclimatology, Palaeoecology, v. 222, p. 53-76.

Young, S. A., M. R. Saltzman, S. M. Bergstrom, S. A. Leslie, and C. Xu, 2008, Paired $\delta^{13}C_{carb}$ and $\delta^{13}C_{org}$ records of Upper Ordovician (Sandbian-Katian) carbonates in North America and China: Implications for paleoceanographic change: Palaeogeography Palaeoclimatology Palaeoecology, v. 270, p. 166-178.

Chapter 4

Tectonic and Climatic Controls on Sea Level Change

J. Garrecht Metzger[1], L. B. Smith[2], Jahan Ramezani[3], Samuel Bowring[3], and David A. Fike[1]

[1]Department of Earth and Planetary Sciences, Washington University in Saint Louis
[2]Smith Stratigraphic LLC, 397 State St., Albany, NY 122120
[3]Department of Earth, Atmospheric, and Planetary Sciences, Massachusetts Institute of Technology

1. ABSTRACT

The Ordovician Period marks the first transition from Greenhouse to Icehouse conditions in the Phanerozoic. This glaciation was previously thought to be confined to the terminal stage of the Ordovician, the Hirnantian, but is now believed to start in the penultimate stage, the Katian. The onset of the glaciation is not well understood and may extend back to the Sandbian-Katian boundary ~10 Myr prior to the Hirnantial glacial maximum. Different studies have offered arguments for early Katian glaciation based on temperature and ice volume proxies, the initiation of upwelling zones in Laurentia, contraction of carbonate platforms to more equatorial latitudes, widespread erosional unconformities, and shifts from "tropical-type" to "temperate-type" carbonates. Here we present stratigraphic data from the subsurface of the eastern United States spanning the late Sandbian to early Katian Stages. Spatial patterns in sediment accumulation are consistent with long-term averages for the Ordovician except near the Sandbian-Katian boundary where the locus of sedimentation locus shifts basinward briefly before moving onto the platform. The sedimentation pattern is assumed to be controlled by changes in sea level. The interpreted changes in sea level are consistent with sea level curves

from other regions of Laurentia, Gondwana, and a eustatic curve. The regression-transgression cycle occurs entirely within the duration of the Guttenberg isotopic carbon excursion (GICE), a globally correlated +3‰ event. U-Pb ages from K-bentonites (altered volcanic ash beds) that bracket this excursion in Missouri are used to constrain the depositional cycle to ~400 kyr. The brief duration of the cycle suggests it is not due to long-term sedimentation patterns associated with downwarping or extensional faulting in Laurentia. Rather, it is consistent with a eustatic sea level change driven by glaciation. The stratigraphic trends outlined here along with multiple lines of evidence from previous studies are consistent with an early Katian glacial cycle.

2. INTRODUCTION

2.1 Background

The Ordovician Period (444-485 Ma) was a time of extremely high relative sea level, which peaked near the Sandbian-Katian boundary ~453.4 Ma (Haq & Shutter, 2008). Beneath the surface of the water some of the largest carbonate platforms of the Phanerozoic were formed (Kiessling, 2003). The vast, shallow oceans served as incubators for marine invertebrates, helping drive the greatest biological radiation of metazoa (animals) in Earth history (Webby et al, 2004). The diversification came to a halt at the end of the Ordovician when climatic shift brought about the first major glaciation in nearly 140 Myr and the first since the evolution of calcifying animals. Approximately 85% of marine species disappeared from the face of the Earth in what would be the first of five major mass extinctions of the Phanerozoic, the Hirnantian Extinction (Sepkoski, 1996; Sheehan, 2001). The temporal association of the extinction and the glaciation has been interpreted as a causal link between climate change and extinction as ocean temperatures dropped and habitats shrank (Finnegan et al. 2012a).

Glaciation and global cooling may also have had profound impacts on the carbon cycle (Finnegan et al., 2012b), ocean circulation (Hermann et al., 2004; Pope & Steffan, 2003), and weathering (Page et al., 2007; Kump et al., 1999). Because of this, emphasis has been placed on understanding the timing and extent of glaciation (e.g., Frakes et al., 1992; Loi et al., 2010; Finnegan et al., 2011; Holmden et al., 2013; Melchin et al., 2013). The glacial episode known in the Hirnantian Epoch is now viewed as the "peak" glacial episode as various lines of evidence are converging to suggest low temperatures and initiation of glaciation in the preceding Katian (Pope & Read, 1998; Hamoumi, 1999; Pope & Steffan, 2003; Saltzman & Young, 2005; Young et al., 2005; Haq & Shutter, 2008; Page et al., 2007; Trotter et al., 2008; Finnegan et al., 2011; Rosenau et al., 2012; Elrick et al, 2013; Melchin et al., 2013); however, Katian cooling and glaciation does not go unchallenged (Brenchley et al., 1994; Ettensohn, 2010; Quinton & MacLeod, 2014).

The most direct test for glaciation is the presence of glaciogenic deposits such as diamictites, drop stones, tunnel valleys, and glacial pavements. Unfortunately, the chronological constraints on unambiguous glaciogenic deposits remain poor (e.g., Frakes et al., 1992) and we are aware of only one study that shows tentative glacial deposits prior to the Hirnantian (Dennis et al., 2007). Early and Middle Katian glaciogenic deposits may not be recorded in the rock record as the glaciers are thought to have resided in the interior of Gondwana far removed from sedimentary basins (Loi et al., 2010). Therefore, while some stratigraphic, sedimentological, geochemical, and paleontological data may be consistent with glaciation, they do not necessarily demonstrate the presence of terrestrial ice. Here, we detail the existing stratigraphic and sea level interpretations for the Sandbian and Katian Stages of Laurentia and discuss how new data presented here further supports an onset of glaciation in the Katian.

We employ two main methods of correlation in this study. Geophysical correlations using gamma ray logs allow correlation based on rock composition. This is done using logs acquired in the subsurface (all cuttings locations and some cores) or direct scanning of selected cores. In the interval discussed in this chapter, the gamma ray signal is almost entirely a function of K-bearing mineral abundance, specifically K-aluminosilicate clays (unpublished data). Strata high in carbonate produce low gamma ray values while shale- and silt- dominated strata produce high values. K-bentonites show prominent spikes in gamma ray values and are used as time planes. The second method employed for correlation is based on $\delta^{13}C_{carb}$ values. $\delta^{13}C_{carb}$ is a time-varying signal that can be used for chronostratigraphic correlations in relative time (Chapters 2,3). This method is especially useful for correlation in intervals with few unique gamma ray or lithological signals. Detailed explanation of $\delta^{13}C_{carb}$ methods can be found in Chapters 2 and 3.

2.2 Evidence for Ordovician Glaciation

The Late Ordovician glaciation was a high-latitude event that took place near the paleo south pole on the Gondwanan paleocontinent (Brenchley, 2004). In an early summary work, Frakes et al. (1992) argued that glaciation began during the Katian or earlier (Figure 1) citing glaciogenic deposits, contraction patterns in carbonate deposition from 45° to 30° latitude (interpreted as cooling), and ecological shifts recorded in the fossil record to more cold-favoring species. The ages of the glaciogenic deposits have since been revised so that nearly all of them fall within the Hirnantian or Lower Silurian (Loi et al., 2010). Other support for glaciation in the Katian comes from a combination of indirect evidence. Conodont apatite oxygen isotopes ($\delta^{18}O_{PO4}$) show an inflection at the Sandbian-Katian boundary interpreted as a shift toward cooler

temperatures and/or increased ice volume (Trotter et al., 2008). However, more recent work on conodont paleothermometry in the Katian is contradictory. Quinton & MacLeod (2014) found no evidence for Katian cooling, while Elrick et al. (2013) interpreted $\delta^{18}O_{PO4}$ oscillations in mixed shale-limestone facies as cyclic changes in sea water temperature and/or ice volume. The estimated sea level oscillations (<60 m) calculated from Laurentian conodonts (assuming changes in $\delta^{18}O_{PO4}$ are derived in part from changes in global terrestrial ice volume) are consistent with sea level change estimates based on stratigraphic interpretations from Gondwana (25-75 m), the paleocontinent at the south pole that would have hosted the glaciers (Loi et al., 2010). Clumped isotope (Δ_{47}) data from carbonates are consistent with the presence of terrestrial ice as far back as the early Katian (Eiler, 2007; Finnegan et al., 2011), but are too sparse in this interval for firm conclusions.

In Laurentia there is a significant lithological shift across the Sandbian-Katian boundary. A transition in carbonate composition and texture from the Black River to Trenton Groups is interpreted to represent a shift from tropical-type carbonates (*sensu* Lees, 1975) to temperate-type carbonates (Holland & Patzkowsky, 1997; Pope & Read, 1998; Kolata et al., 2001; Pope & Steffan, 2003; Ettensohn, 2010) based on associations of faunal and compositional characteristics of modern carbonates (e.g., Lees, 1975; Nelson, 1988; Jones & Desrochers, 1992). The cause of the carbonate transition is thought to be from upwelling of cooler water (Kolata et al., 1998; Kolata et al., 2001; Pope & Steffan, 2003) or, in the absence of upwelling, a drop in seawater temperature. A dramatic increase in the abundance of phosphorite and chert deposits in Laurentia has been interpreted as the birth of an upwelling zone (Pope & Steffan, 2003), which results from increased ocean circulation and the growth of downwelling zones on the edges of glaciated continents (Schlesinger, 1996). Upwelling may also be driven by

tectonism where changes in basin topography in epeiric seas facilitates the upward movement of cool, deep ocean water (Ettensohn, 2010). The deposition of black shales found in the lower Katian is also hypothesized to represent a drop in the vigorousness of ocean circulation possibly from deglaciation (Page et al., 2007; Melchin et al., 2013). The development of less oxygen-rich facies, such as black shales, could also arise form tectonic activity, where sills and mountain ranges formed during orogenies inhibit circulation atop the craton (Lehmann et al., 1995; Ettensohn, 2010).

Other indicators of glaciogenic sea level change may be found in stratigraphic surfaces. A craton-scale unconformity separates the Black River and Trenton Groups and has been interpreted as a significant drop in relative sea level (Kolata et al., 1998). This Laurentian sea level lowstand is roughly contemporaneous with a Gondwanan lowstand (Loi et al., 2010), but age-calibration for Gondwanan locations is currently inadequate to establish firm conclusions. The coincident occurrence of significant lithological, paleontological, and geochemical change unambiguously shows that major environmental shifts are occurring, but the exact cause of this change is inconclusive and remains contested.

2.3 Study Region Geology

In general, the major structural features of the Taconic Foreland Basin that influenced sedimentation patterns, such as basin orientation, are associated with reactivated basement faults, crustal topography, and downwarping during the Taconic Orogeny (Lehmann et al., 1995; Ettensohn, 2010). The orogeny was largely a compressional event with the collision of island arcs in the eastern edge of Laurentia (van Staal & Baar, 2012; Macdonald et al., 2014), but extensional faulting was also present in New York resulting from lithospheric flexture distal to

the collision zone (Lehman et al., 1994). During the majority of the study interval, the accumulation of sediments was most rapid in the foreland basin sections where sediment loading

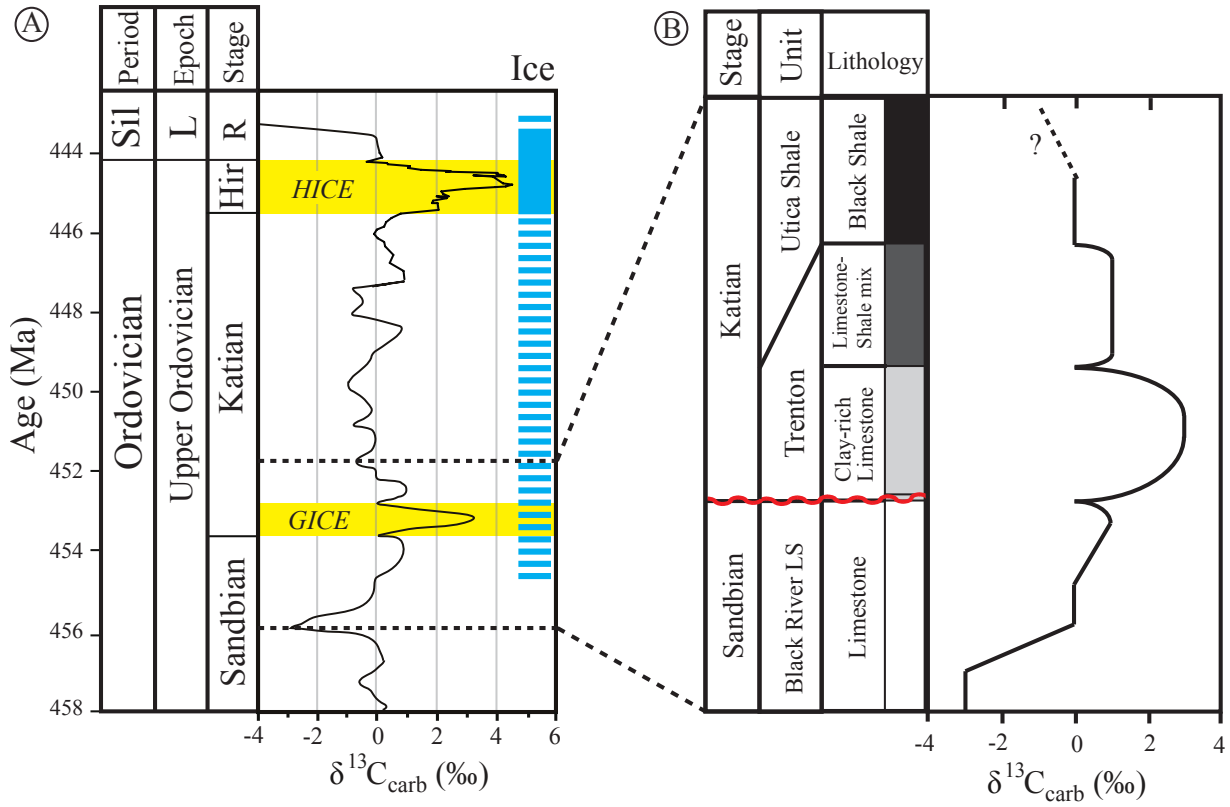

Figure 1. A) Chronostratigraphic relationships between $\delta^{13}C_{carb}$ and terrestrial ice in the Ordovician. $\delta^{13}C_{carb}$ and timescale modified from Bergström et al., (2009) to include revised upper Sandbian-lower Katian $\delta^{13}C_{carb}$ and U-Pb age data (Chapter 3). Guttenberg excursion (GICE) and Hirnantian isotope excursion (HICE) highlighted in yellow. Ice represents confirmed glaciogenic deposits (solid) and tentative (dashed) glacial presence (based on Frakes et al., 1992; Salzmann & Young, 2005; Loi et al., 2010; Finnegan et al., 2011). Research interval for this work bracketed by dashed lines and shown in (B). Sil = Silurian, L = Lower, R = Rhuddanian. B) Selected interval for this study showing relationship between stratigraphic units, generalized lithology, and $\delta^{13}C_{carb}$ for foreland basin deposits in Laurentia.

drove the highest subsidence rates (Figure 2). Most areas, with the exception of the most rapidly subsiding portions of the foreland basin, show a prominent unconformity (the "Knox" unconformity) that separates the Lower Ordovician with the Middle and Upper Ordovician (depending on location) and is tectonic in origin (Ettensohn, 1994). Above the Knox Unconformity, the lowermost unit in the study, the Black River Group, is nearly a kilometer

thick in eastern West Virginia (Patchen et al., 2006) and a few hundred meters thick in the interior platforms. The overlying unit is the Trenton Group carbonates. The Trenton Group is ~100 m in much of the study region. The transition to darker, more argillaceous Trenton strata above the Black River began earlier in the more basinal sections (Lehmann et al., 1995). Following deposition of the argillaceous Trenton Group carbonates, the Utica Shale completes the transition to fully silicilastic strata (Figure 1) and is thought to represent a decrease in oxygen availability (e.g., Baird & Brett, 2002). The onset of Utica Shale deposition is known to be diachronous, where the base of the unit is younger to the west (i.e, landward; Ettensohn, 1994; Baird & Brett, 2002; Brett & Baird, 2002; Chapter 3). Siliciclastic deposition dominated eastern Laurentia for the rest of the Ordovician (Swezey, 2008).

K-bentonites are frequently deposited in the Late Ordovician (Kolata et al., 1996). These ash beds often contain zircons, which can be radiometrically dated using the U-Pb decay series. These zircons are thought to crystallize shortly before eruption so that their calculated U-Pb age is equivalent to their age of deposition. This allows bentonites to be used as indicators of absolute age. Because $\delta^{13}C_{carb}$ can be used as a relative chronostratigraphic tool, the coupling of K-bentonite beds with strong $\delta^{13}C_{carb}$ signals allows K-bentonite ages to be confidently extrapolated to areas outside of where they were collected or deposited. Quantitative sedimentation rates can be then calculated in areas without radiometric ages. The concentration of zircons in K-bentonites is sufficiently low that it requires a large sample size to obtain sufficient quality zircons also, bentonites are difficult to identify in cores that have not undergone surface weathering. This precludes the use of cuttings and most cores for this age dating method, which leaves outcrops as the only viable option. Eastern Missouri is an ideal study region because it contains both the entirety of the GICE as well as bentonites before,

during, and after the excursion. Two sections are described in detail in Chapter 2 and were chosen for K-bentonite sampling. The reader is referred to this work for detailed geological and geochemical discussion.

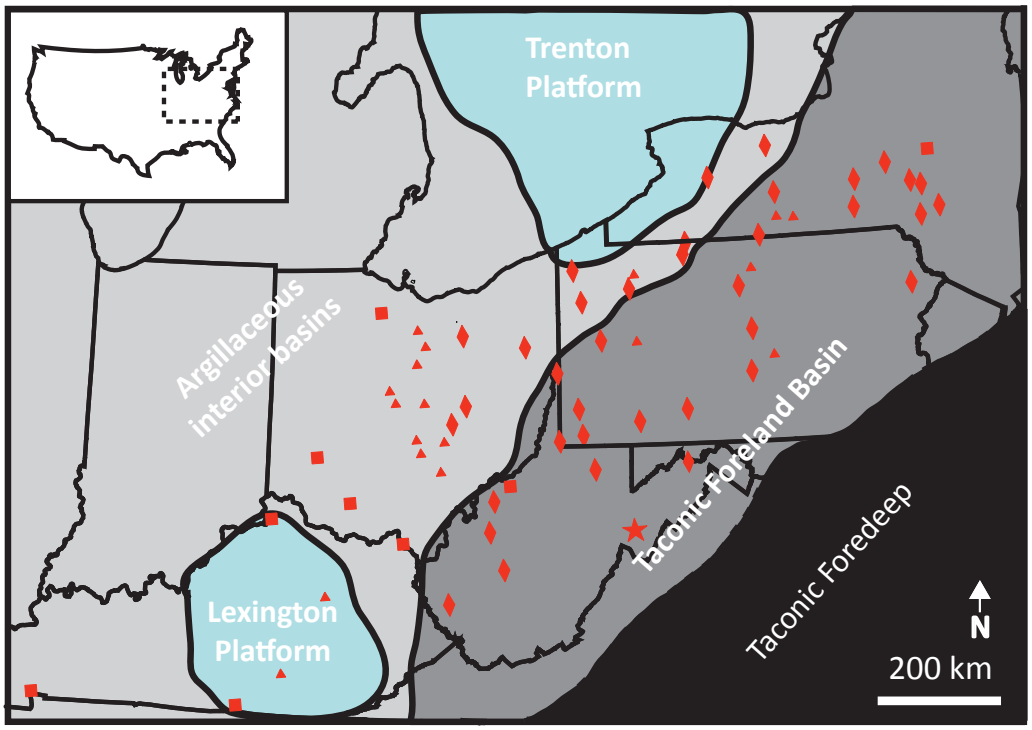

Figure 2. Generalized facies of study region during latest Sandbian to early Katian time (after Keith, 1986; Patchen et al., 2006). Study locations are cores (squares), cuttings for geophysical and $\delta^{13}C_{carb}$ correlation (diamonds), cuttings for geophysical correlation (triangles), and outcrop (star) used for $\delta^{13}C_{carb}$ correlation. Grey scale represents general depth and color of samples. Platform regions have highest carbonate content.

3. METHODS

3.1 Stratigraphic Methods

Most geophysical well logs, cuttings samples, and cores were obtained from publicly available wells and cores at the New York, Pennsylvania, Ohio, and West Virginia state geologic surveys. Cuttings and core were were donated from Range Resources and EQT while Smithstrat LLC donated data. Three cores were scanned for gamma ray analyses at the Ohio State

Geological Survey using a CoreLab Instruments Spectral Gamma Logger (Model SGL-300). Cross sections and isopachs were made using Petra™. $\delta^{13}C_{carb}$ correlations were based upon the $\delta^{13}C_{carb}$ timeline in Chapter 3. Cross sections only include wells with robust $\delta^{13}C_{carb}$ correlations. For isopach maps constructed using $\delta^{13}C_{carb}$, wells with noisy, insufficient, or absent $\delta^{13}C_{carb}$ records were only correlated when $\delta^{13}C_{carb}$ and lithologic signals were tightly coupled in nearby locations, which resulted in the exclusion of some locations. Such lithologic tie points include K-bentonites, which can be easily traced across closely spaced wells.

3.2 Sample collection

The average cuttings sample interval was 10 ft. (0.91 m) and the range was from 1-20 ft. Approximately 2 g of material was collected for each cutting sample, but this varied depending on availability. When necessary, cuttings were washed to remove remnants of drilling mud. A representative fraction of the cuttings was then selected for powdering. Obvious diagenetic material and large fossils were removed by hand (e.g., spar, oxidized pyrite, brachiopod fragments) when possible. Some cuttings were too fine-grained to filter manually and the relative abundance of materials (e.g., color, spar, oxidized Fe) was qualitatively assessed and noted. Cuttings were crushed using a carbide or ceramic mortar and pestle. Each core was drilled every 5 ft. (1.5 m) when possible and different textures and materials (e.g., fossil, matrix, clasts, spar) were occasionally sampled to identify diagenetic alteration. Cores were drilled using a carbide drill bit ~0.5-2 mm in diameter and ~10-100 mg of sample was collected.

K-bentonites were identified in the field based on lithologic features and stratigraphic position. Bentonites were unlithified, off-white clays that would stain a deep orange when coated with oxidized iron. Bentonites were collected across single, continuous beds. Fresh

material was exposed manually by scraping away bentonite coated by oxidized iron (Figure 3). 1-10 L were collected for zircon isolation using fresh gloves for each sample to avoid any cross contamination.

Figure 3. Millbrig K-bentonite at location Highway MM (see Chapter 2 for map). Oxidized iron (likely from pyrite) bounds the upper and lower portions of the bed. Lack of staining indicates minimal exposure to oxidizing fluids. Green shale bounding bentonite is Glencoe Shale (Chapter 2, Figures 1,4). Hammer head is 18 cm.

3.3 Carbon and oxygen isotope methods

Carbonate carbon ($\delta^{13}C_{carb}$) and carbonate oxygen ($\delta^{18}O_{carb}$) analyses were analyzed on a Gas Bench II attached to a Delta V Plus or a MAT 252 isotope ratio mass spectrometer at Washington University in Saint Louis. Data were corrected by comparison to international isotope standards NBS-18, NBS-19, and LSVEC and/or in-house standards calibrated to the international standards. Most samples were run on the Delta V Plus where long-term

reproducibility (1σ = 1 standard deviation) for multi-day replicates was 0.09‰ and 0.12‰ for $\delta^{13}C_{carb}$ and $\delta^{18}O_{carb}$, respectively. Long-term reproducibility for multi-day replicates on the MAT 252 was 0.11‰ and 0.26‰ for $\delta^{13}C_{carb}$ and $\delta^{18}O_{carb}$, respectively.

3.4 Zircon methods

Bentonites were processed for zircon isolation at the Bowring Isotope Geochronology Lab at the Massachusetts Institute of Technology. Separation of clays from denser material was done by suspending clay particles in a beaker and washing them over the top by continually cycling fresh water. Solids were dried under a heat lamp for 1 hour. Heavy-mineral concentrates were obtained using heavy-liquid separation. Zircons were isolated manually under a light microscope. Preference was given to prismatic zircons with elongated glass inclusions (Figure 4). Zircons were chemically annealed using the method of Mattinson (2005) to preferentially dissolve high-U zones that are the most vulnerable to radiation damage and Pb-loss, which would result in dischordant ages. Annealing was done in a 900°C furnace for 60 hours. Zircons were loaded into FEP Teflon® capsules and leached in 29M HF in high-pressure Parr® vessels at 210°C for 12 hours leaving the samples partially dissolved. Zircons are then transferred to Sallivex® FEP beakers and successively exposed to 4N HNO_3 and 6N HCl on a hot plate inside of an ultrasonic bath. Samples were rinsed with ultra-pure deionized water between acid rinses. Clean zircons were loaded intro microcapsules and mixed with a ^{205}Pb-^{233}U-^{235}U spike (EARTHTIME ET535) and completely dissolved in 29M HF at 210°C for 48 hours.

Pb and U were separated using ion-exchange chromatography modified from Krogh (1973). For each sample, U and Pb isolates were loaded together with a silica gel-H_3PO_4

solution onto a single degassed Re filament. U and Pb isotope abundances were measured on a VG Sector 54 multi-collector thermal ionization mass spectrometer. Pb measurements were made using a peak-hopping mode by ion counting with a Daly photomultiplier detector. U isotopes were measured as U-oxide ions on three Faraday detectors in static mode. Pb/U ratios were corrected for initial Th/U ratios in magma. Data reduction and error propagation were done using Tripoli and U-Pb_Redux applications as part of EARTHTIME (Bowring et al., 2008; McLean et al., 2008). Mean weighted $^{206}Pb/^{238}U$ ages are taken from coherent clusters of the youngest ages obtained.

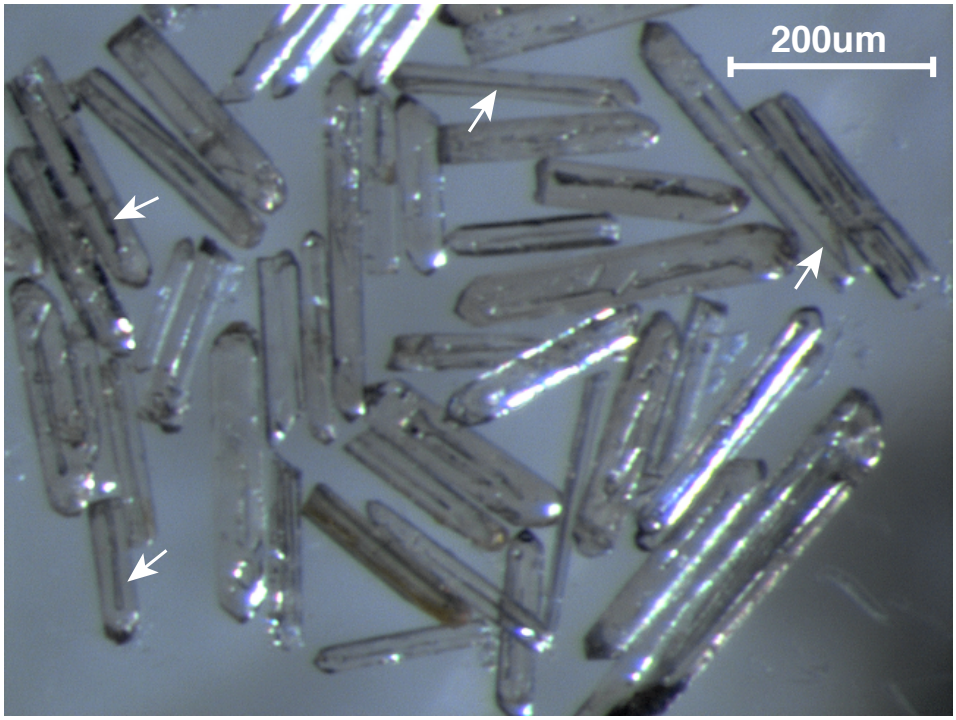

Figure 4. Zircons (pre-annealing) under reflected light [70x mag.]. Sample shown is Deicke K-bentonite from New London. Prominent examples of glass inclusions are shown with arrows.

4. RESULTS

4.1 $\delta^{13}C_{carb}$ stratigraphy

4,697 unique samples were analyzed for $\delta^{13}C_{carb}$ and $\delta^{18}O_{carb}$ from 53 locations (see Appendix for data tables). These data were combined with data from Chapter 3 and from unpublished data (*personal communication*, T. Smith) for a total data set of ~7,000 $\delta^{13}C_{carb}$ and $\delta^{18}O_{carb}$ values. Isopach maps were constructed for $\delta^{13}C_{carb}$ time slices using the least squares method in Petra™ (Figure 5). This visualizes sediment thickness through time based on $\delta^{13}C_{carb}$ intervals (Chapter 3). Sediment accumulation during deposition of the Black River and lower Trenton Group was greatest in the most basinal part of West Virginia. The locus of sedimentation shifts northeast to Pennsylvania during the deposition of the upper Trenton (Figure 5E) and continues to migrate northeast into New York. Another area of prominent sedimentation appears in the Ohio-West Virginia border region (Figure 5F). The sedimentation locus then shifts to eastern New York overlaying areas of known extensional faulting (Figure 5G). Sedimentation then moves landward into the argillaceous basins of Ohio and onto the Trenton Platform at the close of the Trenton-Utica transition (Figure 5H).

A cross-section through West Virginia and southeastern Pennsylvania reveals shifts in sedimentation locus on a finer scale (Figure 6). Sedimentation is relatively even through deposition of the Black River Group and shifts basinward during the lower-mid GICE. Sedimentation then becomes highest in the most landward sections at the end of the GICE and subsequent TR-1 interval. Location M244 suggests sedimentation moved basinward again during TR-2, but this trend is not reproduced in the other basinward sections and may be the result of local diagenetic alteration (see Chapter 3).

4.2 Zircon geochronology

Zircon ages were obtained for 7 different K-bentonite beds at two locations in Missouri, USA (Table 1). Internal analytical uncertainty averaged 0.13 Ma. Deicke and Millbrig ages are within 2σ uncertainty between sections. The Deicke and Millbrig are also indistinguishable from one another at each location. M-2, a bed just above the Millbrig at New London is also indistinguishable from the Millbrig. At Highway MM, the KLKB-1 and House Springs K-bentonites are calculated be 0.24 and 0.49 Ma years younger than the Millbrig, respectively. The Millbrig K-bentonite is found stratigraphically just below the Guttenberg $\delta^{13}C_{carb}$ excursion, the KLKB-1 K-bentonite is located near the peak, and the House Springs K-bentonite is found just above (Figure 7). Sedimentation rates were calculated for each section (Figure 8).

Figure 5. Isopachs (in feet) of $\delta^{13}C_{carb}$ intervals. Generalized $\delta^{13}C_{carb}$ reference curve is plotted alongside generalized lithological changes for Taconic Foreland Basin. Each $\delta^{13}C_{carb}$ interval is represented by a capital letter where the GICE is found in D-F. * = measured ages while other ages are extrapolated based on calculated sedimentation rate.

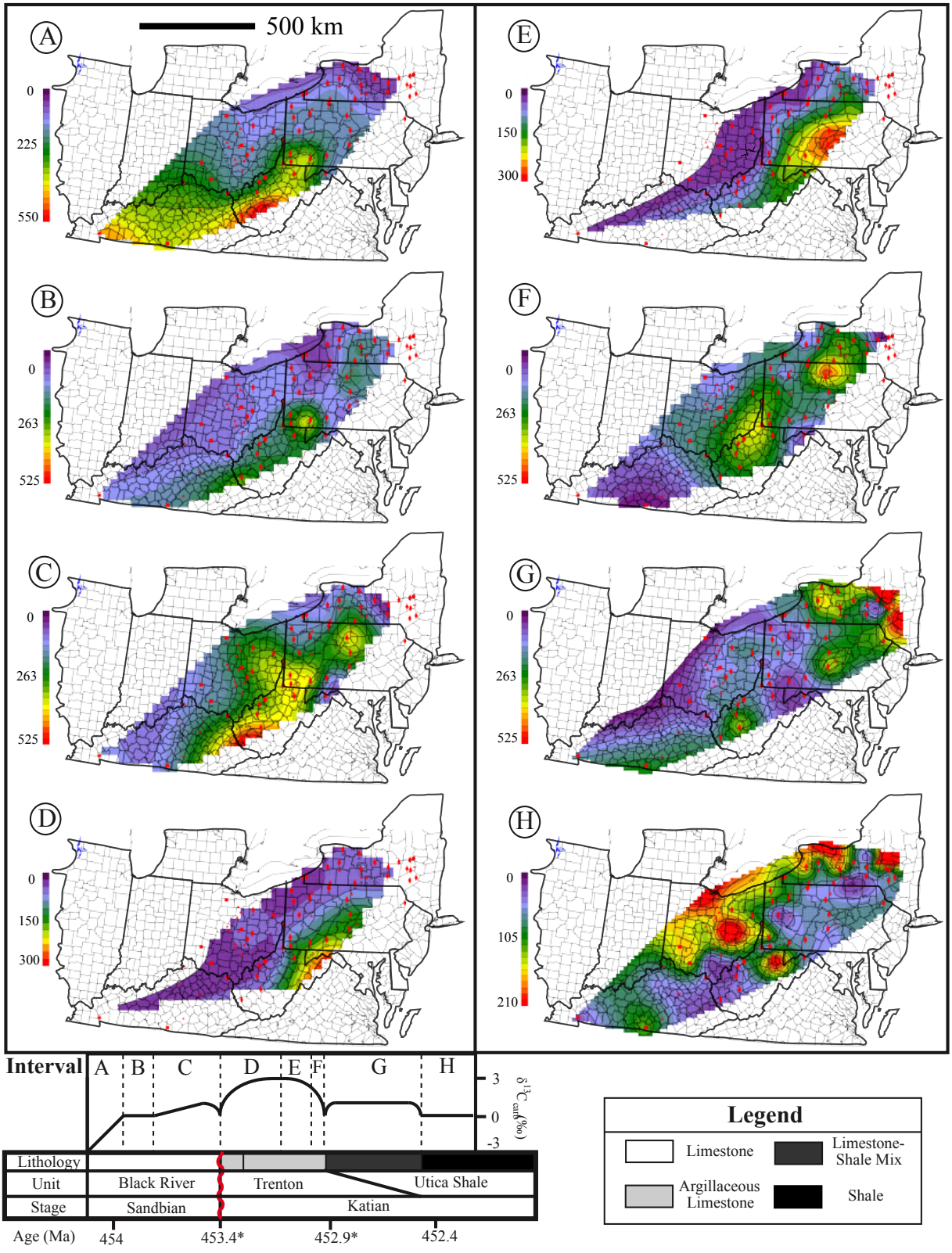
A
500 km
0
225
550
B
0
263
525
C
0
263
525
D
0
150
300
E
0
150
300
F
0
263
525
G
0
263
525
H
0
105
210
Interval
A
B
C
D
E
F
G
H
3
0
-3
$\delta^{13}C_{carb}$ (‰)
Lithology
Unit
Stage
Black River
Trenton
Utica Shale
Sandbian
Katian
Age (Ma)
454
453.4*
452.9*
452.4
Legend
Limestone
Limestone-Shale Mix
Argillaceous Limestone
Shale

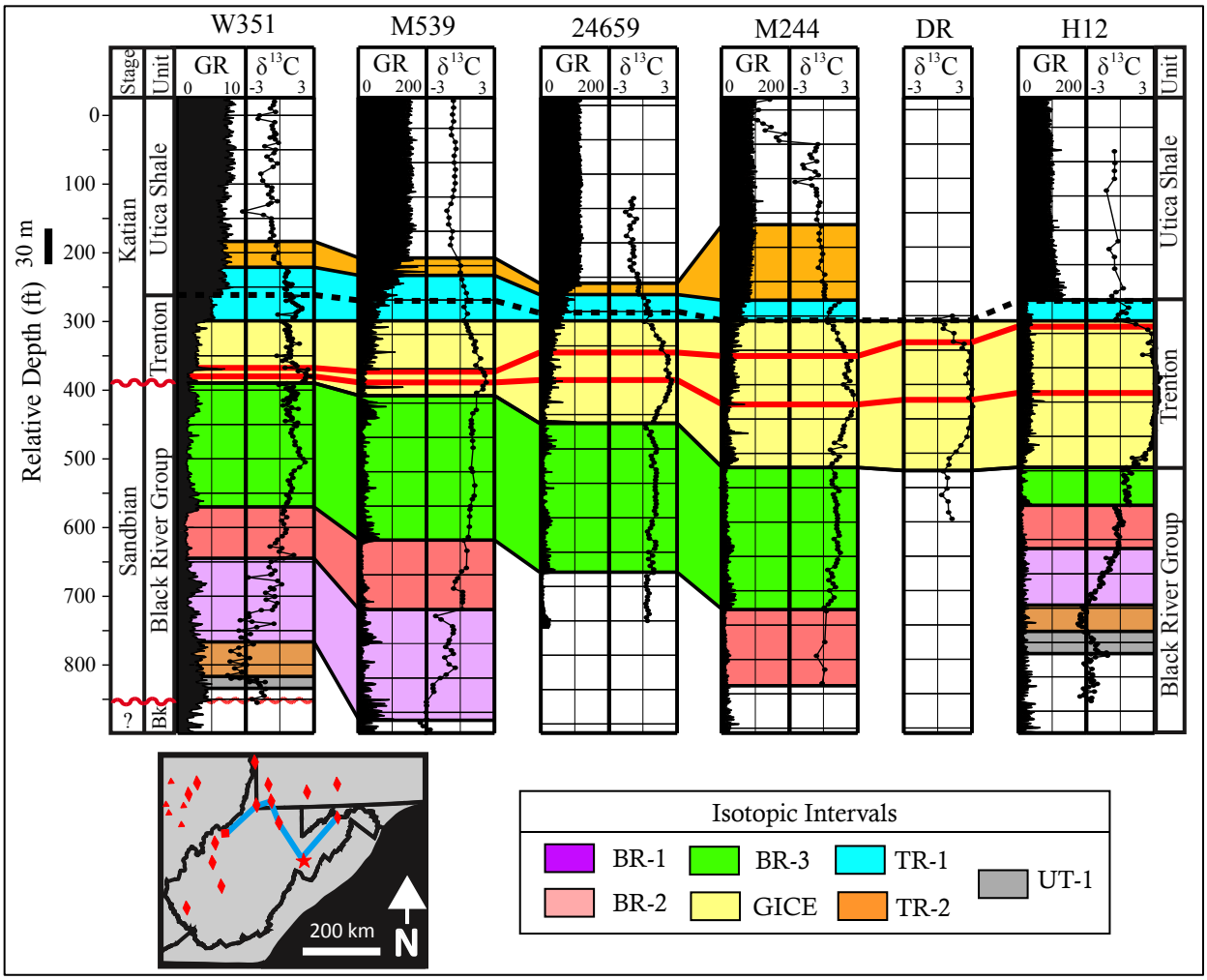

Figure 6. Landward (left) – basinward (right) transect across West Virginia and southwestern Pennsylvania. Colored zones represent $\delta^{13}C_{carb}$ intervals from Chapter 3. W351 is a composite of solid rock core and well cuttings sampling (see Appendix). M593, 24659, M244, and H12 are cuttings. DR is "Dolly Ridge" outcrop section of Young et al., (2005). GR = gamma ray data in API units. $\delta^{13}C_{carb}$ in units of ‰ relative to Vinnna Peedee Belemnite (V-PDB). $\delta^{13}C$ data can be found in Appendix. Bk = Beekmantown and is Lower to Middle Ordovician in age.

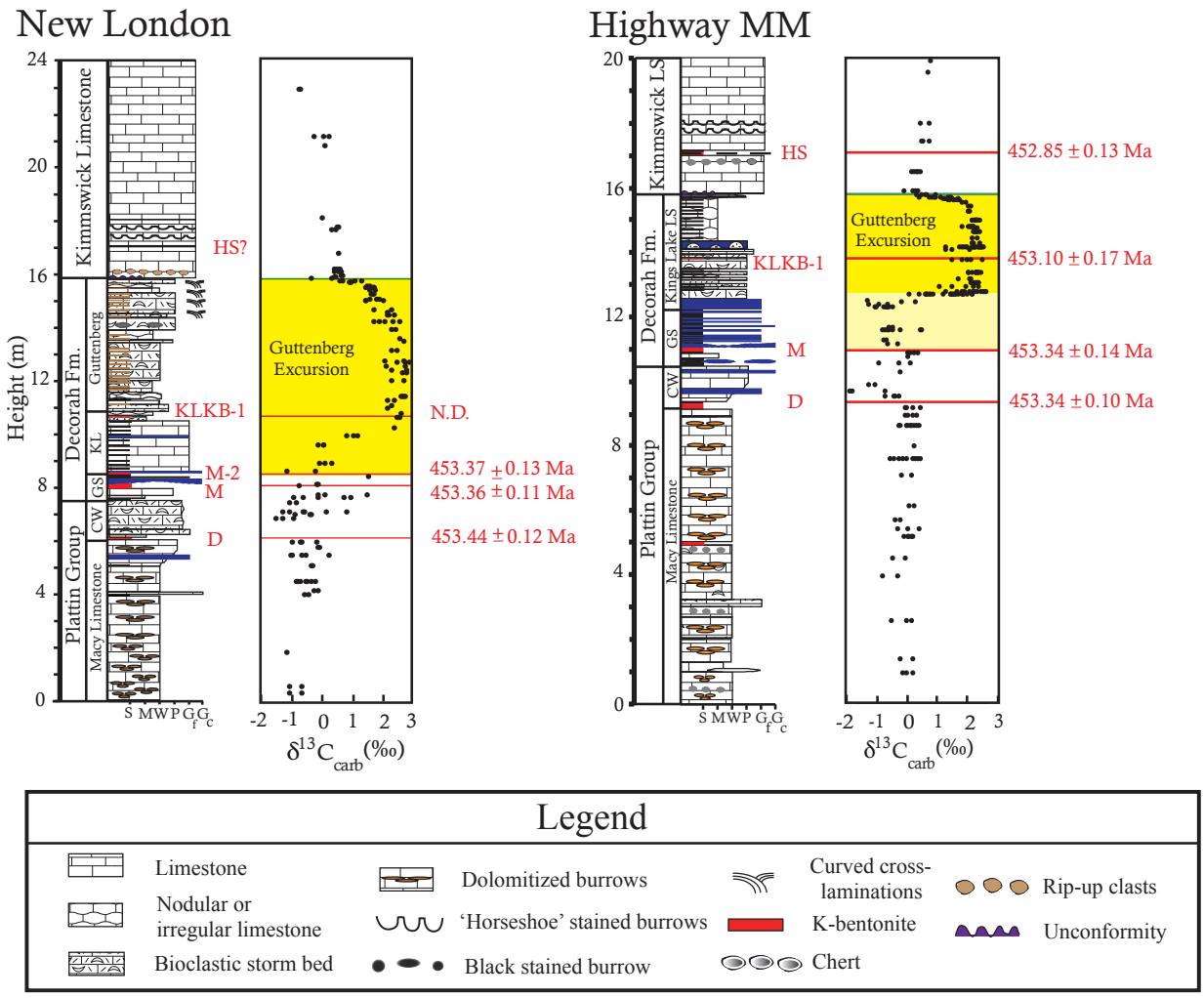

Figure 7. Missouri sections sampled for K-bentonites and their calculated mean ages with X internal uncertainty (2σ, Table 1). KLKB-1 and House Springs K-bentonites at New London are thought to correlate with beds of same name at Highway MM based on stratigraphic position. At New London, both represent thin (≤ 1 cm) shale beds. An insufficient number of zircons for analysis were obtained for KLKB-1 at New London, possibly indicating it represents a different bentonite (or a non-bentonitic horizon) than KLKB-1 at Highway MM. Not enough material from the House Springs K-bentonite at New London was able to be collected for zircon isolation. The Guttenberg excursion at Highway MM may actually begin at the Millbig K-bentonite and is shown in light yellow (see Section 5.1).

Sample	Section	$^{206}Pb/^{238}U$ Date (Ma)	error (2σ)			MSWD	*n*
			X	Y	Z		
M-2	New London	453.37	0.13	0.23	0.54	0.68	5
Millbrig	New London	453.36	0.11	0.22	0.53	1.4	7
Deicke	New London	453.44	0.12	0.22	0.53	0.55	6
House Springs	Highway MM	452.85	0.13	0.23	0.54	0.31	5
KLKB-1	Highway MM	453.10	0.17	0.26	0.55	0.70	5
Millbrig	Highway MM	453.34	0.14	0.24	0.54	0.49	4
Deicke	Highway MM	453.34	0.10	0.22	0.53	0.19	6

Table 1. Age results for K-bentonites. HM = Highway M, NL = New London. X = internal (analytical) uncertainty in the absence of all external or systematic errors; Y = incorporates the U-Pb tracer calibration error; Z—includes X and Y, as well as the uranium decay constant errors. MSWD = mean square of weighted deviates. *n* = number of zircon analyses included in the calculated date. Comparison with U-Pb dates obtained using different tracers or different isotopic chronometers (e.g., ^{40}Ar-^{39}Ar) requires Z error. Internal comparison for this study requires only X error.

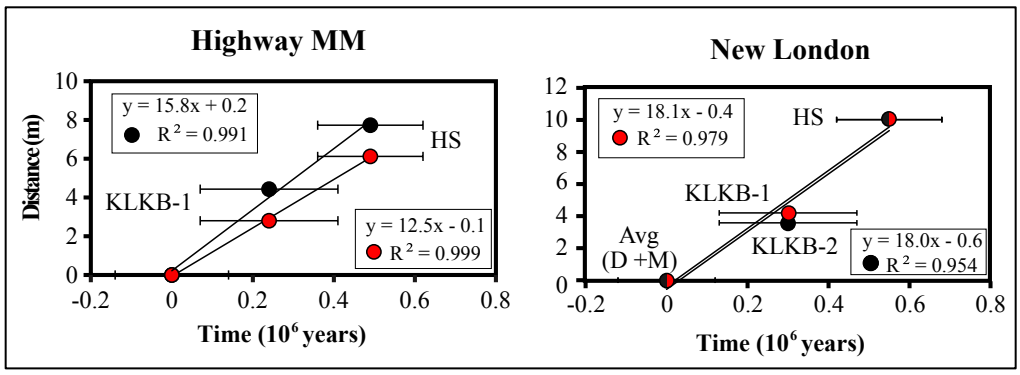

Figure 8. K-bentonite bed heights plotted versus time. Height is given as distance above reference bentonite. Sedimentation rate given in boxes for different combinations of bentonites. Error bars represent 2σ internal analytical uncertainty (X-type). D = Deicke, HS = "House Springs", M = Millbrig. Reference bentonite for Highway MM is Deicke (black) or Millbrig. Using either the Deicke or the Millbrig as the reference bed results in ~26% difference in slope at Highway MM and a ~5% difference at New London. House Springs bentonite age at New London is taken from Highway MM because the House Springs bentonite was too small to be sampled for zircons. KLKB-1 at New London may not correlate with KLKB-1 at Highway MM so the sedimentation rate was calculated using an alternative correlation (KLKB-2). Using the mean height of the Deicke and Millbrig (beds with identical ages) and either KLKB-1 or KLKB-2 results in a <2 % difference in slope.

5. DISCUSSION

5.1 K-bentonite Ages

The high-resolution ages obtained from zircons sampled in Missouri are within external uncertainty (Z-type) of existing published values for the Deicke & Millbrig (Tucker et al., 1990;

Sell et al., 2013); however, the age obtained for the Deicke is ~1 Myr younger than previously calculated (Tucker et al., 1990). This may be due to changes in instrumentation, lab techniques, and international standard calibration. The Millbrig K-bentonite is most closely associated with the lower bound of the GICE. We discuss the following ages in the context of an internally consistent data set of bentonite ages rather than extrapolate to all purported Deicke and Millbrig beds across Laurentia (Kolata et al., 1987; Sell et al., 2013). The duration of the GICE is calculated to be ~370-450 kyr using sedimentation rates for Highway MM and New London, respectively. At Highway MM, the GICE duration was calculated assuming the top of the Millbrig is the base of the GICE. At Highway MM, the base of the GICE is in heavily altered rocks in which the initial $\delta^{13}C_{carb}$ rise is believed to be obscured by diagenesis. For the purposes of this manuscript, an intermediate value of 400 kyr was chosen as the duration of the GICE. The most important distinction is that the different sedimentation rates all still produce an excursion that is hundreds of thousands of years in duration. This duration can be used to help constrain the mechanisms driving changes in sedimentation during the study interval.

5.2 Correlations and sea level

The $\delta^{13}C_{carb}$ intervals of Chapter 3 that were established in the foreland basin strata of New York State were readily identifiable across the southerly portions of the foreland basin (Figure 6), as expected for widespread and relatively continuous deposition across the foreland basin. In the interior sections, some intervals were condensed or absent, namely the lower portions of the GICE (Figure 5). This is consistent with previous subsurface correlations using geophysical data that suggest the lower portion of the Trenton Group in Ohio is missing (Kolata et al., 1998). The shallow-to-deep transect across West Virginia (Figure 6) shows a prominent

shift in sedimentation locus during the GICE. The lowermost portions of the excursion are thickest in the deeper sections and increasingly condensed in the shallower sections. The uppermost limb of the GICE shows the reverse trend and is thickest in shallower sections. This oscillation is a departure from the background trends in sedimentation, both at the scale of the Black River $\delta^{13}C_{carb}$ intervals and at the scale of whole formations (Patchen et al., 2006), which show consistently thicker deposits in the more basinal sections. If this pattern of shifting sedimentation locus during the GICE is related to sea level then sections in the interior carbonate platform should only preserve the top portion of the GICE, if any all. This pattern is observed in multiple regions in Kentucky where only the top part of the GICE is preserved (Figure 5; Coates et al., 2010). This is also observed in Ohio (Figure 5).

Sediment accumulation rate is related to sea level because sea level can change accommodation space, which is the vertical distance that sediment can accumulate without being suspended and carried away by waves or currents. Accommodation space decreases when sea level falls, during uplift, or when sedimentation is faster than subsidence. Accommodation space increases when sea level rises or subsidence outpaces sediment supply. Subsidence is often the main control on accommodation space over long time scales ($\geq 10^6$ yrs) or within active tectonic areas, such as zones of extensional block faulting (Coe et al., 2005). Eustatic sea level change can become the dominant control on accommodation space at shorter time scales. Assuming sediment deposition is a function of sea level, then shifts in the locus of sedimentation can be used to infer changes in sea level.

A descriptive model was constructed to illustrate how the region of sediment accumulation would change over time with shifting sea level (Figure 9). The model begins with fairly even sediment accumulation rates across the basin, consistent with long-term trends

(Patchen et al., 2006). During the GICE, the shift in sedimentation locus can be interpreted as an initial fall and then subsequent rise in sea level. Sedimentation during the intervals following the GICE largely continues the pattern associated with sea level rise. This is manifest in the isopach map as a shift in depositional locus from the foreland basin to the platform (Figure 5). The change in sea level during $\delta^{13}C_{carb}$ interval TR-1 is somewhat ambiguous, but trends during the intervals just before the GICE and after TR-2, are much less so. A sea level curve can then be generated for the foreland basin sections (Figure 10), broadly consistent with other Taconic Foreland Basin sea level curves (Patzkowsky et al., 1997) and some (Haq & Shutter, 2008), but not all eustatic reconstructions (Munnecke et al., 2010). The regression-transgression pattern observed in the GICE is consistent with that proposed in the Tennessee carbonate platform regions (Holland & Patzkowsky, 1998). Our sea level curve is also consistent with that proposed for parts of Gondwana (Loi et al., 2010), but not Baltica (Munnecke et al., 2010). Correlations at this temporal resolution across continents are difficult, as radiogenic ages for K-bentonites have not produced sufficiently similar or precise ages for supposedly equivalent eruptions (Min et al., 2001; Sell et al., 2013).

Figure 9. Descriptive depositional model showing relationship between relative rate of sediment accumulation (black bars) over time in a simplified low-angle basin. (A) is youngest interval and model time corresponds to highlighted portion of the $\delta^{13}C_{carb}$ curve. A) TR-1 up to TR-2, B) falling limb of GICE, C) base of GICE up falling limb, D) $\delta^{13}C_{carb}$ intervals are BR-1 to 3. FWB = fair-weather wave base, SWB = storm wave base.

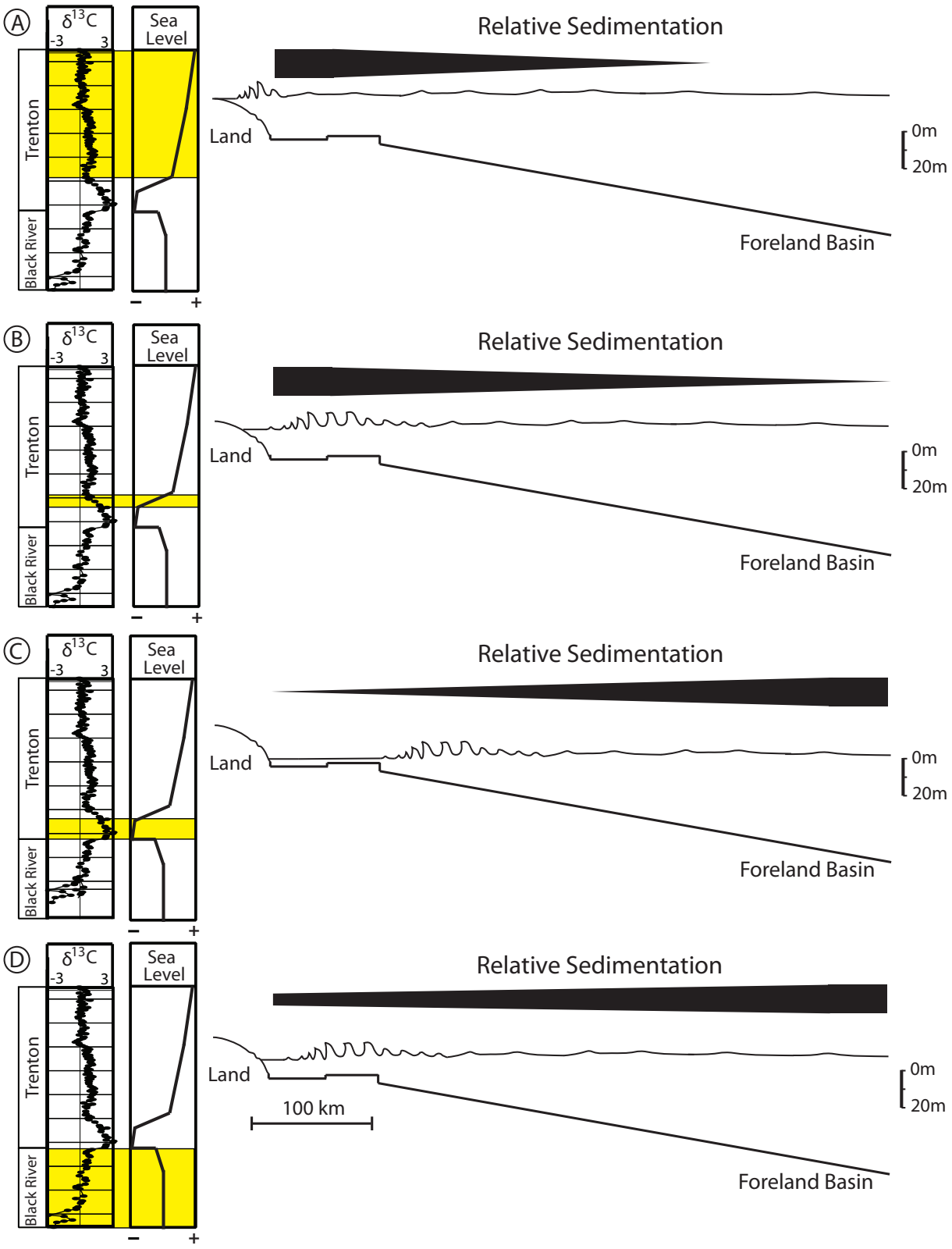
A
δ13C
-3
3
Sea Level
Trenton
Black River
−
+
Relative Sedimentation
Land
0m
20m
Foreland Basin
B
δ13C
-3
3
Sea Level
Trenton
Black River
−
+
Relative Sedimentation
Land
0m
20m
Foreland Basin
C
δ13C
-3
3
Sea Level
Trenton
Black River
−
+
Relative Sedimentation
Land
0m
20m
Foreland Basin
D
δ13C
-3
3
Sea Level
Trenton
Black River
−
+
Relative Sedimentation
Land
100 km
0m
20m
Foreland Basin

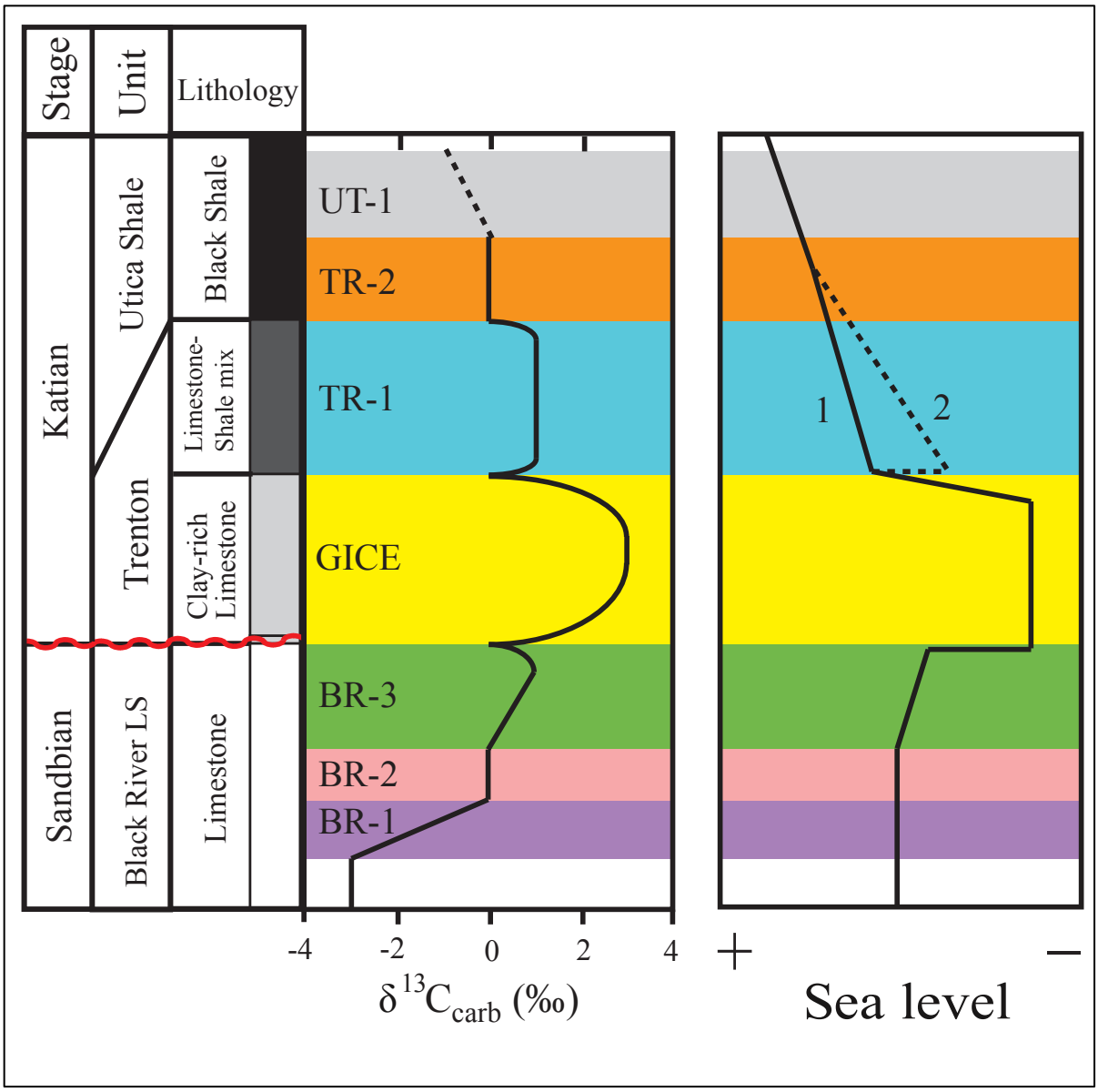

Figure 10. Proposed generalized sea level curve for the Taconic Foreland Basin based on $\delta^{13}C_{carb}$ and lithological correlations. $\delta^{13}C_{carb}$ intervals from Chapter 3. In general, the GICE represents an initial regression and subsequent transgression. Transgression continues through the Utica Shale, but is less clear in $\delta^{13}C_{carb}$ interval TR-1 (Figure 5F-G). For sea level curve, (1) is drawn for southerly parts of foreland basin (Figure 6), and (2) is drawn for northern parts (Figure 5G). Spatial differences in deposition in TR-1 in different parts of the foreland basin may reflect local differences sedimentation supply and/or subsidence rate that overprint the eustatic rise.

5.3 Driver of sea level change

The prominent bi-directional shift in sedimentation locus during the GICE can be constrained to take place within ~400 kyr. If the cycle is caused by changing sea level, then we must propose a mechanism that can both lower and raise sea level in less than half of a million years. Processes in the solid Earth (such as mantle convection) that drive craton-scale subsidence operate on time scale of 10^6-10^9 years (Conrad, 2013). Ettensohn (1994) argues that the major controls on basin development and sedimentation in Laurentia are tectonogenic and that these processes may be cyclic on the scale of ~5 Myr. The GICE sea level shift (~400 kyr cycle) is too brief to be caused by tectonic processes such as downwarping and foreland bulge migration (Ettensohn, 1994) . Even if migration of a foreland bulge was rapid, the predicted trends in sedimentation are different than those observed in Figure 6. However, tectonic activity is clearly expressed in some areas. Extensional faulting immediately following the GICE in New York (Figure 5G) results in a dramatic shift in deposition rates over short distances, in agreement with field-based studies in the same region (Baird & Brett, 2002). This pattern is not consistent with the trend observed in Figure (6) in the southerly parts of the foreland basin. If the gradient in sediment accumulation rate along the transect was due to a similar gradient in subsidence, then the faulted blocks would need to be infilled within a few hundred thousand years. We cannot exclude this as a possible mechanism, but the large distance (hundreds of kilometers), short duration, and similarity in sea level curves from other regions (Patzkowsky et al., 1997; Holland & Patzkowsky, 1998; Saltzman & Young, 2005) suggest a short-lived, long-distance period of differential subsidence is not likely the driving mechanism for the observed sedimentation patterns. The progradational-retrogradational cycle coincident with the GICE also appears to be

anomalous within the older Late Ordovician sediment accumulation patterns, which show stable long-term patterns through the Sandbian (Patchen et al., 2006).

Glaciation is known to drive short-lived (10^3-10^5 yr) sea level changes (Conrad, 2013). The duration of the sea level cycle is ~400 kyr, consistent with the period of Earth's orbital eccentricity (413 kyr). Orbitally forced glacial cycles are thought to drive the Pleistocene glaciations (Imbrie et al., 1993), but the periodicity of glacial cycles does not always correlate with a prominent Milankovitch cycle frequency and may depend in part on ocean circulation patterns or indirect responses to orbital forcing (Imbrie et al., 1993). No attempt is made here to analytically assess Milankovitch-like orbital forcing as this is beyond the scope of this study. Others have asserted that meter-scale cycles in siliciclastic strata represent 400 kyr cycles in the Katian (Loi et al., 2010). These workers constructed a backstripping model with astronomically calibrated sediment cycles that agrees with the long-term eustatic sea level curve proposed for the Katian (Haq & Shutter, 2008) and the curve proposed here. Whether or not the backstripping model is an accurate representation of true sea level change is debatable, but the convergence of similar sea level curves from vastly different regions using different methods suggests that the general trend of falling and subsequent rising sea level during the early Katian is real.

Numerous arguments using different approaches have been put forth invoking seawater cooling and/or glaciation near the Sandbian-Katian boundary (e.g., Frakes et al., 1992; Pope & Read, 1998; Pope & Steffan, 2003; Saltzmann & Young, 2005; Young et al., 2005; Trotter et al., 2008). The dramatic increase in the deposition of phosphorites and cherts at this time is thought to derived from upwelling of cooler, nutrient-rich ocean water, a phenomenon that is interpreted as representing increased vigor of ocean circulation during glacial periods. Alternatively, upwelling waters could stem from a deepening of a cratonic trough to a depth sufficient to

become connected with cool, open ocean waters (Ettensohn, 2010). However, others have argued that sustained, long-distance upwelling is unrealistic (Page et al., 2007). Therefore, while phosphorite and chert deposition is consistent with recent upwelling during glaciation and thought to be coincident with the GICE, no clear mechanism is agreed upon that can bring cool, nutrient-rich water over such a large area and long period of time.

In a review of Ordovician and Silurian black shales, Melchin et al., (2013) argue that the prominent glacial episodes of the Late Ordovician and Early Silurian are followed by extensive black shale deposition. This includes black shale deposition in the early Silurian following the terminal Ordovician (Hirnantion) glaciation. The deposition of black shales has been interpreted to represent a decline in ocean circulation and an advance of oxygen-poor water into the cratonic seas during warming and deglaciation (e.g., Page et al., 2007). Deposition of the Utica Shale is diachronous across Laurentia with the base of the unit being progressively younger towards the continental interior. Deposition likely started around the Sandbian-Katian boundary (base of the GICE) in the most basinal areas and become widespread across much of eastern North America following the GICE (Patchen et al., 2006). This pattern in black shale deposition seems to be in general agreement with patterns summarized by Melchin et al. (2013), but black shales could form in other ways. Ettensohn (2010) argues that the closing phase of the Taconic Orogeny could have resulted in restricted and isolated basins due to sill formation and basin closure during uplift. Black shales are also known to occur in eastern North America during two other major orogenic phases in the Paleozoic (Ettensohn, 1994). The sedimentological shift from carbonate to black shales and changing sea level proposed here are broadly consistent with the deglacial black shale theory reviewed by Melchin et al., (2013). This does not exclude a tectonic (or other) origin for black shales, but it does show a similar relationship between sea level

change and black shale deposition for the early Katian and the Hirnantian, a confirmed glacial interval.

Temperature and sea level proxies are somewhat contradictory during the Katian. Trotter et al. (2008) noticed a long-term increase in $\delta^{18}O_{PO4}$ interpreted as declining seawater temperatures beginning at the Sandbian-Katian boundary. Elrick et al., (2013) argue that the changes in $\delta^{18}O_{PO4}$ in mixed carbonate-siliciclastic sequences are cyclic and likely orbitally forced. They ascribe the changes in $\delta^{18}O_{PO4}$ to combined shifts in temperature and ice volume. Quinton & MacLeod (2014) argue, however, there is no statistical evidence for an increase in $\delta^{18}O_{PO4}$ through the Katian, in direct disagreement with Trotter et al. (2008). Quinton & MacLeod also identify taxon-specific offsets in $\delta^{18}O_{PO4}$. More comprehensive spatial sampling of conodonts in more continuous sections may elucidate the current discrepancies in $\delta^{18}O_{PO4}$ records. Similar treatment of $\delta^{13}C_{carb}$ was able to resolve apparent spatial offsets in isotope values (Chapters 2,3) suggesting that diagenesis or miscorrelation between sections may be a current confounding factor for interpreting the $\delta^{18}O_{PO4}$ record. Clumped isotope (Δ^{47}) data for the Katian are consistent with the presence of terrestrial ice (Finnegan et al., 2011), but there is only one sample in the early Katian, preventing any strong conclusions. We interpret the temperature records as ambiguous in their current state.

6. CONCLUSIONS

The depositional pattern observed during the study interval is consistent with a eustatic sea level change driven by a glacial cycle. Various other sedimentological, geochemical, and paleontological trends are also consistent with, but not unique to, cooling and/or glaciation and some evidence is contradictory (e.g., $\delta^{18}O_{PO4}$). Many geochemical and geological signals in the

early Katian appear to be similar, but less dramatic versions of the same signals seen in the Hirnantian. The erosional unconformity at the base of the Katian-aged Trenton group, which could represent sea level fall during initial glaciation, is not as severe an unconformity as the one at the base of the Hirnantian. This is in agreement with the estimated sea level drop during the early Katian being lower than that during the Hirnantian (Haq & Trotter, 2008; Loi et al. 2013). The inferred temperature and/or ice volume changes in the early Katian are smaller in magnitude than those calculated for the Hirnantian (Finnegan et al., 2011; Elrick et al., 2013). Similarly, the extinction event at the base of the Katian is minor compared to the Hirnantian (Shourd, 1972; Webby et al., 2004). It appears that if glaciation occurred in the early Katian, then it was less severe than that of the Hirnantian glacial maximum.

The key points of this chapter are:

1. Seven high precision U-Pb ages were obtained for K-bentonites in two Late Ordovician locations in Missouri, USA. The Deicke and Millbrig beds are analytically indisinguishable at 453.40 ± 0.11 and Ma 452.35 ±0.13 Ma, respectively.
2. The stratigraphic position of K-bentonites ages is consistent with a linear sedimentation rate during the Guttenberg isotopic carbon excursion (GICE) in Missouri. The duration of the GICE is estimated to be ~370-450 kyr with a preferred intermediate duration of 400 kyr.
3. Cross-sections and isopachs based on $\delta^{13}C_{carb}$ correlation reveal a major shift in sedimentation locus during the latest Sandbian-early Katian. This is interpreted as a rapid shift in sea level. The sea level curve proposed within is generally consistent with other Laurentian and Gondwannan sea level curves, as well as the eustatic curve of Haq & Shutter (2008).

4. The stratigraphic trends outlined here along with multiple lines of evidence from previous studies are consistent with a glacial episode during this time. Future high-resolution temperature/ice volume data from $\delta^{18}O_{PO4}$ and Δ_{47} would complement the results of this study.

7. ACKNOWLEDGEMENTS

A majority of the data presented were collected as part of the Utica Shale Research Consortium. Thanks to all the members and partners for funding, materials, and thoughtful discussion. Specifically, Kris Karter (PA-DNR), James Leone (NYSM), and Matthew Erenpreiss (OH-DNR). J.G.M. would like to thank Taury Smith for first inspiring him to take on this project and for his many intellectual contributions. Thanks to Kun Wang (Harvard), Rachel Folkerts, and Claire Beaudoin for assistance with K-bentonite sampling. Thanks to Brandon Mahan, Chun Soo Park (Washington University), Patricia Chen (Washington University), and Ryan Talk (Washington University) for sample preparation. Thanks to Dwight McCay (Washington University) for assistance with isotope analyses. Thanks to Prof. Robert Criss (Washington University) for use of the MAT 252.

8. REFERENCES

Baird, G. C., Brett, C.E., 2002, Indian Castle Shale: late synorogenic siliciclastic succession in an evolving Middle to Late Ordovician foreland basin, eastern New York State: Physics and Chemistry of the Earth, v. **27**, p. 203-230.

Bergström, S. M., Chen, X., Gutiérrez-Marco, J.C., Dronov, A.,, 2009, The new chronostratigraphic classification of the Ordovician System and its relations to major regional series and stages and to $\delta^{13}C$ chemostratigraphy: Lethaia, v. **42**, p. 97-107.

Brenchley, P. J., 2004, End Ordovician glaciation, *in* Webby, B. D., Droser, M.L., Paris, F., Percival, I., ed., The Great Ordovician Biodiversification Event: New York, New York, Columbia University Press, p. 81-83.

Bowring, J. F., McLean, N.M., Walker, J.D., Bowring, S.A., 2008, Building cyberinfrastructure for geochronology; software engineering meets geochemistry, Geological Society of America, Volume **40**, Geological Society of America, p. 136.

Brenchley, P. J., Marshall, J.D., Carden, G.A.F., Robertson, D.B.R., Long, D.G.F., Meidla, T., Hints, L., Anderson, T.F., 1994, Barthymetric and isotopic evidence for a short-lived Late Ordovician glaciation in a greenhouse period: Geology, v. **22**, p. 295-298.

Brett, C. E., Baird, G.C., 2002, Revised stratigraphy of the Trenton Group in its type area, central New York State: sedimentology and tectonics of a Middle Ordovician shelf-to-basin succession: Physics and Chemistry of the Earth, v. **27**, p. 231-263.

Coates, J. W., Ettensohn, F.R., Rowe, H.D., 2010, Correlations across a facies mosaic within the Lexington Limestone of central Kentucky, USA, using whole-rock stable isotope compositions, *in* Finney, S. C., Berry, W.B.N., ed., GSA Special Paper **466**, p. 177-193.

Coe, A. L., Church, K.D., 2007, Sequence stratigraphy, *in* Coe, A. L., ed., The Sedimentary Record of Sea-Level Change: Cambridge, UK, Cambridge University Press, p. 287.

Conrad, C. P., 2013, The solid Earth's influence on sea level: Geological Society of America Bulletin, v. **125**, p. 1027-1052.

Denis, M., Buoncristiani, Konaté, Ghienne, J.-F., Guiraud, M., 2007, Hirnantian glacial and deglacial record in SW Djado Basin (NE Niger): Geodinamica Acta, v. **20**, p. 177-194.

Eiler, J. M., 2007, "Clumped-isotope" geochemistry- The study of naturally-occuring multiply-substituted isotopologues: Earth and Planetary Science Letters, v. **262**, p. 309-327.

Elrick, M., Reardon, D., Labor, W., Martin, J., Desrochers, A., Pope, M., 2013, Orbital-scale climate change and glacioeustasy during the early Late Ordovician (pre-Hirnantian) determined from $\delta^{18}O$ values in marine apatite: Geology, v. **41**, p. 775-778.

Ettensohn, F. R., 1994, Tectonic control on formation and cyclicity of major Appalachian unconformities and associated stratigraphic sequences, *in* Dennison, J. M., Ettensohn, F.R., ed., Tectonic and Eustatic Controls on Sedimentary Cycles, Volume **4**: Tulsa, Oklahoma, SEPM, p. 217-242.

Ettensohn, F. R., 2010, Origin of Late Ordovician (mid-Mohawkian) temperate-water conditions on southeastern Laurentia: Glacial or tectonic?, *in* Finney, S. C., Berry, W.B.N., ed., GSA Special Paper **466**, p. 163-175.

Finnegan, S., Bergmann, K., Eiler, J.M., Jones, D.S., Fike, D.A., Eisenman, I., Hughes, N.C., Tripati, A.K., Fischer, W.W., 2011, The Magnitude and Duration of Late Ordovician–Early Silurian Glaciation: Science, v. **331**, p. 903-906.

Finnegan, S., Fike, D.A., Jones, D., Fischer, W.W., 2012a, A temperature-dependent feedback on the magnitude of carbon isotope excursions: Geoscience Canada, v. **39**, p. 122-131.

Finnegan, S., Heim, N.A., Peters, S.E., Fischer, W.W., 2012, Climate change and the selective signature of the Late Ordovician mass extinction: Proceedings of the National Academy of Sciences, v. **109**, p. 6829-6834.

Frakes, L. A., Francis, J.E., Syktus, J.I., 1992, Climate Modes of the Phanerozoic, Great Britian, Press Syndicate of the University of Cambridge.

Hamoumi, N., 1999, Upper Ordovician glaciation spreading and its sedimentary record in Moroccan North Gondwana margin: Acta Universitatis Carolinae, v. **43**, p. 111-114.

Haq, B. U., Schutter, S.R., 2008, A chronology of Paleozoic sea-level changes: Science, v. **322**, p. 64-68.

Herrmann, A. D., Haupt, B.J., Patzkowsky, M.E., Seidov, D., Slingerland, R.L., 2004, Response of Late Ordovician paleoceanography to changes in sea level, continental drift, and atmospheric pCO_2: potential causes for long-term cooling and glaciation: Palaeogeography Palaeoclimatology Palaeoecology, v. **210**, p. 385-401.

Holland, S. M., Patzkowsky, M.E., 1997, Distal orogenic effects on peripheral bulge sedimentation: Middle and Upper Ordovician of the Nashville Dome: Journal of Sedimentary Research, v. **67**, p. 250-263.

Holland, S. M., Patzkowsky, M.E., 1998, Sequence stratigraphy and relative sea-level history of the Middle and Upper Ordovician of the Nashville Dome, Tennessee: Journal of Sedimentary Research, v. **68**, p. 684-699.

Holmden, C., Panchuk, K., Finney, S.C., 2012, Tightly coupled records of Ca and C isotope changes during the Hirnantian glaciation even in an epeiric sea setting: Geochimica et Cosmochimica Acta, v. **98**, p. 94-106.

Imbrie, J., Berger, A., Boyle, A.E., Clemens, S.C., Duffy, A., Howard, W.R., Kukla, G., Kutzbach, J., Martinson, D.G., McIntyre, A., Mix, A.C., Molfino, B., Morley, J.J., Peterson, L.C., Pisias, N.G., Prell, W.L., Raymo, M.E., Shackleton, N.J., Toggweiler, J.R., 1993, On the structure and origin of major glaciation cycles 2. The 100,000-year cycle: Paleoceanography, v. **8**, p. 699-735.

Jones, B., Desrochers, A., 1992, Shallow platform carbonates, *in* Walker, R. G., James, N.P., ed., Facies Models: Response to Sea Level Change: St. John's, Newfoundland, Geological Association of Canada, p. 277-302.

Keith, B. D., 1989, Regional facies of Upper Ordovician Series of eastern North America, *in* Keith, B. D., ed., The Trenton Group (Upper Ordovician Series) of eastern North America, Volume **29**, American Association of Petroleum Geologists, p. 1-16.

Kiessling, W., Flügel, E., Golonka, J., 2003, Patterns of Phanerozoic carbonate platform sedimentation: Lethaia, v. **36**, p. 195-226.

Kolata, D. R., Huff, W.D., Bergström, S.M., 1996, Ordovician K-bentonites of eastern North America: GSA Special Paper, v. **313**, p. 84.

Kolata, D. R., Huff, W.D., Bergström, S.M., 1998, Nature and regional significance of unconformities associated with the Middle Ordovician Hagan K-bentonite complex in the North American midcontinent: GSA Bulletin, v. **110**, p. 723-739.

Kolata, D. R., Huff, W.D., Bergström, S.M., 2001, The Ordovician Sebree Trough: An oceanic passage to the Midcontinent United States: GSA Bulletin, v. **113**, p. 1067-1078.

Krogh, T. E., 1973, A low-contamination method for hydrothermal decomposition of zircon and extraction of U and Pb for isotopic age determinations: Geochimica et Cosmochimica Acta, v. **37**, p. 485-494.

Kump, L. R., Arthur, M.A., Patzkowsky, M.E., Gibbs, M.T., Pinkus, D.S., Sheehan, P.M., 1999, A weathering hypothesis for glaciation at high atmospheric pCO_2 during the Late Ordovician: Palaeogeography Palaeoclimatology Palaeoecology, v. **152**, p. 173-187.

Lees, A., 1975, Possible influence of salinity and temperature on modern shelf carbonate sedimentation: Marine Geology, v. **19**, p. 159-198.

Lehmann, D. B., C.E., Cole, R., Baird, G., 1995, Distal sedimentation in a peripheral foreland basin: Ordovician black shales and associated flysch of the western Taconic foreland, New York State and Ontario: Geological Society of America Bulletin, v. **107**, p. 708-724.

Lehmann, D., Brett, C.E., Cole, R., 1994, Tectonic and eustatic influences upon the sedimentary environments of the Upper Ordovician strata of New York and Ontario, *in* Dennison, J. M., Ettensohn, F.R., ed., Tectonic and Eustatic Controls on Sedimentary Cycles, Volume **4**: Tulsa, Oklahoma, SEPM, p. 181-202.

Loi, A., Ghienne, J.L., Dabard, M.P., Paris, F., Botquelen, A., Christ, N., Elaouad-Debbaj, Z., Gorini, A., Vidal, M., Videt, B., Destombes, J., 2010, The Late Ordovician glacio-eustatic record from a high-latitude storm-dominated shelf-succession: The Bou Ingarf section (Anti-Atlas, Southern Morocco): Palaeogeography Palaeoclimatology Palaeoecology, v. **296**, p. 332-358.

Macdonald, F. A., Ryan-Davis, J., Crowley, J.L., Karabinos, P., 2014, A newly identified Gondwanan terrange in the northern Appalachian Mountains: Implications for the Taconic orogeny and closure of the Iapetus Ocean: Geology, v. **42**, p. 539-542.

Mattinson, J. M., 2005, Zircon U/Pb chemical abrasion (CA-TIMS) method: combined annealing and multi-step partial dissolution analysis for improved precision and accuracy of zircon ages: Chemical Geology, v. **220**, p. 47-66.

Mclean, N. M., Bowring, J.F., Bowring, S.A., Schoene, R.B., 2008, More than just an age; quantitative analyis of geochronological data and uncertainty, Geological Society of America, Volume **40**, Geological Society of America, p. 134.

Melchin, M. J., Mitchell, C.E., Holmden, C., Storch, P., 2013, Environmental changes in the Late Ordovician-early Silurian: Review and new insights from black shales and nitrogen isotopes: GSA Bulletin, v. **125**, p. 1635-1670.

Metzger, J. G., Fike, D.A., **2013**, Techniques for assessing spatial heterogeneity of carbonate $\delta^{13}C$ values: Implications for craton-wide isotope gradients: Sedimentology, v. 60, p. 1405-1431.

Metzger, J. G., Fike, D.A., Smith, L.B., 2014, Applying C-isotope Stratigraphy using Well Cuttings for High-Resolution Chemostratigraphic Correlation of the Subsurface *in* Smith,

L. B., ed., AAPG Bulletin Special Volume in Honor of Fred Read, v. **98**, AAPG, p. 1551-1576.

Min, K. W., Renne, P. R., and Huff, W. D., 2001, Ar-40/Ar-39 dating of Ordovician K-bentonites in Laurentia and Baltoscandia: Earth and Planetary Science Letters, v. **185**, p. 121-134.

Munnecke, A., Calner, M., Harper, D. A. T., and Servais, T., 2010, Ordovician and Silurian sea-water chemistry, sea level, and climate: A synopsis: Palaeogeography Palaeoclimatology Palaeoecology, v. **296**, no. 3-4, p. 389-413.

Nelson, C. S., 1988, An introductory perspective on non-tropical shelf carbonates: Sedimentary Geology, v. **60**, p. 3-14.

Page, A. A., Zalasiewicz, J.A., Williams, M., Popov, L.E., 2007, Were transgressive black shales a negative feedback modulating glacioeustasy in the Early Palaeozoic Icehouse?, *in* Williams, M., Haywood, A.M., Gregory, F.J., Schmidt, D.N., ed., Deep-Time Perspectives on Climate Change: Marrying the Signal from Computer Models and Biological Proxies: London, The Geological Society of London, p. 123-156.

Patchen, D. G., Hickman, J.B., Harris, D.C., Drahovzal, J.A., Lake, P.D., Smith, L.B., Nyahay, R., Schulze, R., Riley, R.A., Baranoski, M.T., Wickstrom, L.H., Laughrey, C.D., Kostelnick, J., Harper, J.A., Avary, K.L., Bocan, J., Hohn, M.E., McDowell, R., 2006, A geologic play book for Trenton-Black River Appalachian Basin exploration: West Virginia Geological Survey, p. 601.

Patzkowsky, M. E., Slupik, L.M., Arthur, M.A., Pancost, R.D., Freeman, K.H.,, 1997, Late Middle Ordovician environmental change and extinction: Harbinger of the Late Ordovician or continuation of Cambrian patterns?: Geology, v. **25**, p. 911-914.

Pope, M., Read, J.F., 1998, Ordovician metre-scale cycles: implications for climate and eustatic fluctuations in the central Appalachians during a global greenhouse, non-glacial to glacial transition: Palaeogeography Palaeoclimatology Palaeoecology, v. **138**, p. 27-42.

Pope, M., Steffan, J.B., 2003, Widespread, prolonged late Middle to Late Ordovician upwelling in North America: A proxy record of glaciation?: Geology, v. **31**, p. 63-66.

Quinton, P. C., MacLeod, K.G., 2014, Oxygen isotopes from conodont apatite of the midcontinent, US: Implications for Late Ordovician climate evolution: Palaeogeography Palaeoclimatology Palaeoecology, v. **404**, p. 57-66.

Rosenau, N., A., Herrmann, A.D., Leslie, S.A., 2012, Conodont apatite $\delta^{18}O$ values from a platform margin setting, Oklahoma, USA: Implications for initiation of Late Ordovician icehouse conditions: Palaeogeography Palaeoclimatology Palaeoecology, v. **315-316**, p. 172-180.

Saltzman, M. R., Young, S.A., 2005, Long-lived glaciation in the Late Ordovician? Isotopic and sequence-stratigraphic evidence from western Laurentia: Geology, v. **33**, p. 109-112.

Schourd, M. L., 1972, A paleoecological study of the Decorah Subgroup (Middle Ordovician) in the middle Mississippi Valley [Ph.D.]: Washington University, 222 p.

Schlesinger, W. H., 1997, Biogeochemistry: An analysis of global change, San Diego, CA, Academic Press, p. 588.

Sell, B., Ainsaar, L., and Leslie, S., 2013, Precise timing of the Late Ordovician (Sandbian) super-eruptions and associated environmental, biological, and climatological events: Journal of the Geological Society, v. **170**, p. 711-714.

Sepkoski, J. J., 1996, Patterns of Phanerozoic Extinction: A Perspective from Global Data Bases, *in* Walliser, O. H., ed., Global Events and Event Stratigraphy in the Phanerozoic: Berlin, Springer, p. 35-52.

Sheehan, P. M., 2001, History of marine biodiveristy: Geological Journal, v. **36**, p. 231-249.

Swezey, C. S., 2008, Regional stratigraphy and petroleum systems of the Michigan Basin, North America: United States Geological Survey, Scientific Investigations Map 2978.

Trotter, J. A., 2008, Did cooling oceans trigger Ordovician biodiversification? Evidence from conodont thermometry (vol 321, pg 550, 2008): Science, v. **321**, p. 1295-1295.

Tucker, R. D., Krogh, T.E., Ross, R.J.Jr, Williams, S.H., 1990, Time-scale calibration of high-precision U-Pb zircon dating of interstratified volcanic ashes in the Ordovician and Lower Silurian stratotypes of Britain: Earth and Planetary Science Letters, v. **100**, p. 51-58.

van Staal, C. R., Barr, S.M., 2012, Lithospheric architecture and tectonic evolution of the Canadian Appalachians and associated Atlantic Margin, *in* Percival, J. A., Cook. F.A., Clowes, R.M., ed., Tectonic Styles in Canada: the LITHOPROBE Perspective, Special Paper **49**, Geological Association of Canada, p. 41-97

Webby, B. D., Droser, M.L., Paris, F., Percival, I., 2004, The Great Ordovician Biodiversification Event, New York, New York, Columbia University Press.

Young, S. A., Saltzman, M.R., Bergström, S.M., 2005, Upper Ordovician (Mohawkian) carbon isotope ($\delta^{13}C$) stratigraphy in eastern and central North America: Regional expression of a perturbation of the global carbon cycle: Palaeogeography, Palaeoclimatology, Palaeoecology, v. **222**, p. 53-76.

Chapter 5

The Source of the Guttenberg $\delta^{13}C$ Excursion

J. Garrecht Metzger and David A. Fike

1. ABSTRACT

A carbon isotope box model was employed to constrain the mechanisms driving the Late Ordovician Guttenberg isotopic carbon excursion (GICE). The excursion is thought to be coincident with glaciation and a regressive-transgressive cycle. Two plausible mechanisms that could drive the GICE are increased organic carbon burial ($F_{b,org}$) and an increase in the isotopic signature of the weathering flux to the ocean (δ_w). The amount of excess organic carbon estimated to drive the excursion is ~$1.1 \bullet 10^{18}$ moles, equivalent to ~30% the size of the marine dissolved inorganic carbon reservoir (M_o) and a 50% increase in $F_{b,org}$ over 200 kyrs. Physically unrealistic changes in sedimentation rate and organic carbon content are required to bury sufficient organic carbon in Laurentian seas, suggesting that organic carbon burial may have been most important in deltas and marginal marine settings, consistent with modern organic carbon burial patterns. Changes in $F_{b,org}$ may have been due to the temperature-dependent microbial oxidation of organic matter in the oceans. Increases in δ_w will only result in substantial changes to $\delta^{13}C_{carb}$ if they reflect an increase in carbonate weathering at the expense of the flux of oxidized organic carbon to the ocean. A change in δ_w alone from -5 to -1.75‰ could drive the GICE. This δ_w shift represents a 22-35% increase in the fraction of weathering from carbonates with a concomitant 60-75% drop in the relative fraction of organic carbon

oxidation, depending on whether volcanic flux was constant or zero. Increased carbonate weathering during sea level lowstand is consistent with geologic interpretations and sea level curves for the study interval.

Absolute time constraints allowed us to invert the temporal trend in $\delta^{13}C_{carb}$ to stratigraphic height to understand the timing and rate of forcing change. The GICE, apparently, was deposited during an apparent constant rate of sedimentation. Both the rising and falling limbs of the excursion are concave ($\equiv d\delta^{13}C_{carb}{}^2/d^2\text{height} < 0$). A model was constructed that converts temporal changes $\delta^{13}C_{carb}$ to height under different sedimentation rates. Our results strongly suggest that $\delta^{13}C_{carb}$ excursions that are purely or strongly concave with respect to time are not likely the result of declining sedimentation rate except when changes in sedimentation rate are extreme (e.g., highly condensed beds). The stratigraphic expression of $\delta^{13}C_{carb}$ is interpreted as a more gradual change in forcing during the end of the GICE than in the beginning.

2. INTRODUCTION

The carbon cycle is intimately linked to the biosphere as carbon is the backbone of all organic molecules. Changes in the abundance and types of organisms through time have profoundly impacted the global carbon cycle, climate, and the redox state of the ocean-atmosphere system (e.g., Canfield, 2005; D'Hondt, 2005; Maloof et al., 2010a; Schulte et al., 2010). One of the principal ways to study the biogeochemical carbon cycle over geologic time scales is to measure changes in the stable isotopes of marine carbonate carbon ($\delta^{13}C_{carb}$) (e.g., Kump & Arthur, 1999; D'Hondt, 2005; Saltzman & Young, 2005; Maloof et al., 2006; Hurtgen et al., 2009; Maloof et al., 2010b; Bowen & Zachos, 2011). Changes in $\delta^{13}C_{carb}$ correspond to changes in the fluxes or isotope ratios of the various sources and sinks of carbon to and from the

ocean (Kump & Arthur, 1999). The most common way to mathematically model the carbon cycle is to view the ocean-atmosphere system as a box model (Figure 1). The simple parameterization of inputs and outputs allows quantitative testing of hypotheses that seek to explain the origin of deviations in $\delta^{13}C_{carb}$ from stable long-term values. The main advantages to this approach is the ability to eliminate certain mechanisms as possible drivers of carbon isotope excursion based on the directionality of change in $\delta^{13}C_{carb}$ and by placing constraints on the magnitude of change in fluxes and $\delta^{13}C$ values of the inputs and outputs. This approach has been used to evaluate possible changes in the burial of organic matter (Pancost et al., 1999; Katz et al., 2005; Saltzman & Young, 2005; Maloof et al., 2010b; Jones & Fike, 2013), pCO_2 (Kump & Arthur, 1999; Saltzman & Young, 2005; Young et al., 2008; Young et al., 2009; Pancost et al., 2013), and weathering (Kump et al., 1999; Page et al., 2007) over geologic time. The application of a box model in tandem with stratigraphic and geochemical context can provide further insights into carbon cycle dynamics during important intervals of Earth history. Here, we use a box model to understand the environmental changes that occurred during the Late Ordovician Guttenberg isotopic carbon excursion (GICE).

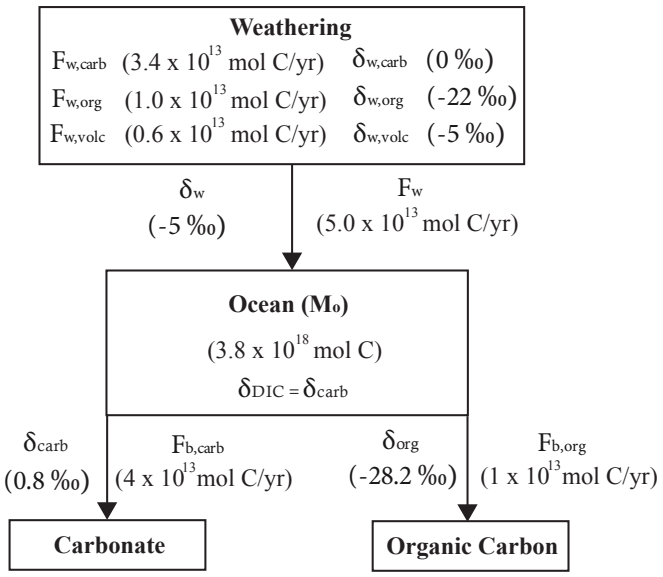

Figure 1. Biogeochemical carbon box model (*after* Kump & Arthur, 1999). Values given are for pre-excursion steady-state and are best-guesses for Paleozoic values. Fractionation (Δ) between carbonate carbon (δ_{carb}) and organic carbon (δ_{org}) being buried is 29‰ ($\Delta = \delta_{carb} - \delta_{org}$). Weathering flux ($F_w$) is composite of carbonate weathering, organic carbon oxidation, and volcanic CO_2 emissions.

The Guttenberg carbon isotope excursion (GICE) is a ~3‰ positive $\delta^{13}C_{carb}$ excursion which occurred in the latest Sandbian and earliest Katian Stages of the Late Ordovician Period (~453.4 Ma). It has been identified in carbonate strata from around the world including numerous parts of the United States (Patzkowsky et al., 1997; Young et al., 2005; Pancost et al., 1999; Chapter 2; Chapter 3; Ludvigson et al., 2004; Coates et al., 2010), China (Young et al., 2005; Bergström et al. 2009; Munnecke et al, 2011), Malaysia (Bergström et al., 2010), Estonia (Martma, 2005; Kaljo et al, 2007), and Sweden (Bergström et al., 2004). The duration of the excursion is likely ~400 kyr (Chapter 4). The first portion of the excursion correlates with an initial sea level fall and the falling limb of the excursion with subsequent sea level rise (*see* Chapter 4). To-date, no consensus has been reached on the origin of the excursion. The most prevalent theory suggests the excursion was driven by an increase in organic carbon burial

(Pancost et al., 1999; Saltzman & Young, 2005) associated with either upwelling of nutrient rich waters (causing increased primary production, Patzkowsky et al., 1997; Young et al., 2005; Young et al., 2008) or, alternatively, by decreased oxygen levels (causing increased organic matter preservation). Other mechanisms that could drive the excursion include a decrease in $\delta^{13}C$ of the organic matter being buried (Pancost et al., 1999), an increase in the $\delta^{13}C$ value of the material entering the ocean (*sensu* Kump et al., 1999; Page et al., 2007), and a decrease in pCO_2, which could change the fractionation (Δ) between organic matter and dissolved inorganic carbon (Kump & Arthur, 1999; Young et al., 2008; Young et al., 2009). It is important to constrain which mechanisms are the most likely because each one of them has different implications for environmental change over Earth history. For example, Saltzman & Young (2005) argue that increased organic carbon burial may have drawn down atmospheric CO_2 levels to the threshold of glaciation, but recent evidence suggests that glaciation was coincident with the GICE (Chapter 4).

In this chapter we use numerical box models coupled with geochemical and stratigraphic data to evaluate the contributions that each of these mechanisms might play in driving the Guttenberg $\delta^{13}C$ excursion. We evaluate the geologic evidence for different drivers of the excursion by examinating the type and magnitude of forcings required to reproduce the GICE and interpret them in a geologic context. The apparent constant sedimentation rate across the GICE allows the direct conversion of time to stratigraphic height. This imposes an additional constraint on the nature and timing of possible forcings responsible for driving the $\delta^{13}C_{carb}$ excursion, as the $\delta^{13}C_{carb}$ morphology of the model results must match that of the stratigraphic expression of $\delta^{13}C_{carb}$.

3. METHODS

The biogeochemical carbon cycle can be modeled by parameterizing the reactive pools of carbon at the surface of the Earth (see Kump & Arthur (1999) for further discussion of each parameter). The majority of reactive carbon is found in the form of dissolved inorganic carbon (DIC) in the ocean. Atmospheric CO_2 equilibrates with the DIC pool at a geologically rapid rate (Broecker & Peng, 1974), which means changes in DIC record a combined change in the oceanic and the atmospheric carbon cycle. Therefore, the main reservoir of reactive carbon is referred to collectively as the ocean-atmosphere system (Figure 1). The main sources of carbon into the ocean are volcanic CO_2 and weathering inputs from oxidized organic matter and carbonates. Each flux (F_i) has an associated isotopic composition (δ_i). A combined term, F_w, is used to represent the total weathering flux, while δ_w is used for its isotope value. Silicate weathering is ignored in the weathering flux because it does not contribute new carbon to the ocean-atmosphere system; rather, it converts CO_2 to HCO_3^-.

$$F_{in} = F_{volcanic} + F_{w,org} + F_{w,carb} \qquad \text{Eq. (1)}$$

The outputs of the system are the burial of carbonate carbon ($F_{b,carb}$) and organic carbon ($F_{b,org}$).

$$F_{out} = F_{b,carb} + F_{b,org} \qquad \text{Eq. (2)}$$

The offset between $\delta^{13}C_{carb}$ and $\delta^{13}C_{org}$ in the marine record is large (~20-30‰), predominantly due to the isotopic fractionation during photosynthetic uptake of DIC (Freeman & Hayes, 1992). This assumes organic carbon is dominated by the remains of marine

photosynthetic organisms (e.g., algae and cyanobacteria) as well as those of heterotrophic organisms that utilize organic matter derived from photosynthetic organisms without any substantial additional fractionation. Because this photosynthesis-derived organic carbon is sourced from DIC, an increase in $F_{b,org}$ will result in simultaneous increase in $\delta^{13}C_{DIC}$ of the ocean as more ^{13}C-depleted organic matter is removed from the ocean-atmosphere system. This is one example of a "lever" that is used to perturb the model.

The following is a mathematical description of biogeochemical carbon cycle box model. The model is developed using δ notation rather than the more exact R notation because doing so does not result in an errors larger than analytical uncertainty and is easier to relate model results to data. Knowing that

$$\left(\frac{dM_o}{dt}\right) = \left(F_{in} - F_{out}\right) \qquad \text{Eq. (3)}$$

where M_o is the mass of DIC in the ocean (in moles) and F values are fluxes (in moles/yr). The isotopic signature of the reservoir also changes with respect to time as a function of the isotopic values and fluxes of the inputs and outputs (Equation 4).

$$\left(\frac{dM_o\delta_{carb}}{dt}\right) = F_{in}\delta_{in} - F_{out}\delta_{out} \qquad \text{Eq. (4)}$$

Using the product rule of calculus on Equation (4) results in

$$M_o\left(\frac{d\delta_{carb}}{dt}\right) + \delta_{carb}\left(\frac{dM_o}{dt}\right) = F_{in}\delta_{in} - F_{out}\delta_{out} \qquad \text{Eq. (5)}$$

and

$$\left(\frac{d\delta_{carb}}{dt}\right)=\left(\frac{1}{M_o}\right)\left[F_{in}\delta_{in}-F_{out}\delta_{out}-\delta_{carb}\left(\frac{dM_o}{dt}\right)\right] \quad \text{Eq. (6)}$$

Substituting Equation (3) into Equation (6) yields

$$\left(\frac{d\delta_{carb}}{dt}\right)=\left(\frac{1}{M_o}\right)\left[F_{in}\delta_{in}-F_{out}\delta_{out}-F_{in}\delta_{carb}-F_{out}\delta_{carb}\right] \quad \text{Eq. (7)}$$

and

$$\left(\frac{d\delta_{carb}}{dt}\right)=\left(\frac{1}{M_o}\right)\left[F_{in}\left(\delta_{in}-\delta_{carb}\right)-F_{out}\left(\delta_{out}-\delta_{carb}\right)\right] \quad \text{Eq. (8)}$$

Using the δ values for each associated flux portion in equations (1) and (2) produces

$$\left(\frac{d\delta_{carb}}{dt}\right)=\left(\frac{1}{M_o}\right)\left[F_{w}\left(\delta_{w}-\delta_{carb}\right)-F_{b,org}\left(\delta_{b,org}-\delta_{carb}\right)-F_{b,carb}\left(\delta_{b,carb}-\delta_{carb}\right)\right] \quad \text{Eq. (9)}$$

Because $\delta^{13}C_{DIC} \approx \delta^{13}C_{carb}$, Equation (9) can be reduced to

$$\left(\frac{d\delta_{carb}}{dt}\right) = \left(\frac{1}{M_o}\right)\left[F_w\left(\delta_w - \delta_{carb}\right) - F_{b,org}\left(\delta_{b,org} - \delta_{carb}\right)\right] \quad \text{Eq. (10)}$$

The isotopic offset between organic matter being buried and carbonate carbon can be expressed as

$$\Delta = \left(\delta_{b,org} - \delta_{carb}\right) \quad \text{Eq. (11)}$$

Substituting Equation (11) into Equation (10) yields

$$\left(\frac{d\delta_{carb}}{dt}\right) = \frac{F_w\left(\delta_w - \delta_{carb}\right) - F_{b,org}\Delta}{M_o} \quad \text{Eq. (12)}$$

Equation (12) shows how the $\delta^{13}C$ of marine carbonates changes through time as a function of the isotopic signature and fluxes of inputs and outputs, the fractionation between organic and inorganic carbon, and the size of the reservoir. This model can be used to develop a quantitative understanding of how the carbon system responds to changes in these parameters. The directionality and magnitude of these changes can then be discussed in a geological context to exclude certain mechanisms as possible causes of the Guttenberg excursion.

One variable, δ_w, is a composite variable and can be written as a function of weathering fluxes of carbonate, volcanic input, and organic matter oxidation. This is to allow more direct investigation of the effects of changing sources during weathering on δ_w. F_w is free to increase

or decrease without changing any other fluxes. This is described as unbalanced weathering where an increase in one component of F_w does not require a change in the other F_w components.

$$\delta_w = \frac{F_{w,carb}}{F_w}\left(\delta_{w,carb}\right) + \frac{F_{w,volc}}{F_w}\left(\delta_{w,volc}\right) + \frac{F_{w,org}}{F_w}\left(\delta_{w,org}\right) \quad \text{Eq. (13)}$$

Weathering fluxes can also be written as relative fluxes (f_w) where a change in one weathering component is balanced by opposite changes in one or more of the other components and because of this, it is described as balanced weathering. During balanced weathering, each of the weathering components can be described as a relative fraction of f_w in the following manner:

$$f_{w,carb} = \frac{F_{w,carb}}{\left(F_{w,carb} + F_{w,volc} + F_{w,org}\right)} \quad \text{Eq. (14)}$$

$$f_{w,volc} = \frac{F_{w,volc}}{\left(F_{w,carb} + F_{w,volc} + F_{w,org}\right)} \quad \text{Eq. (15)}$$

$$f_{w,org} = \frac{F_{w,org}}{\left(F_{w,carb} + F_{w,volc} + F_{w,org}\right)} \quad \text{Eq. (16)}$$

where F_i are fluxes in moles/yr and

$$\sum f_w = \left(f_{w,carb} + f_{w,volc} + f_{w,org}\right) = 1 \quad \text{Eq. (17)}$$

δ_w can then be described in terms of f_w where

$$\delta_w = f_{w,carb}\left(\delta_{w,carb}\right) + f_{w,volc}\left(\delta_{w,volc}\right) + f_{w,org}\left(\delta_{w,org}\right) \quad \text{Eq. (18)}$$

Changes in δ_w as a function of $f_{w,carb}$ can by accompanied by proportional changes in the opposite direction of $f_{w,org}$ and $f_{w,volc}$. Alternatively, two-end-member scenarios can be used to constrain the maximum changes in each f_w component because a change in one f_w component results in a change in only one other f_w component. In the first scenario, changes in $f_{w,carb}$ affect only $f_{w,org}$ and in the second scenario changes in $f_{w,carb}$ affect only $f_{w,volc}$. Restating Equation (17) in a different form yields

$$f_{w,org} = \left(1 - f_{w,carb} - f_{w,volc}\right) \quad \text{Eq. (19)}$$

and substituting Equation (19) into Equation (18) yields

$$\delta_w = f_{w,carb}\left(\delta_{w,carb}\right) + f_{w,volc}\left(\delta_{w,volc}\right) + \left(1 - f_{w,carb} - f_{w,volc}\right)\left(\delta_{w,org}\right) \quad \text{Eq. (20)}$$

and

$$f_{w,carb} = \frac{\left(\delta_w - \delta_{w,org} - f_{w,volc}\left(\delta_{w,volc} - \delta_{w,org}\right)\right)}{\left(\delta_{w,carb} - \delta_{w,org}\right)} \quad \text{Eq. (21)}$$

Equation (20) shows how δ_w can be calculated independently of $f_{w,org}$ while Equation (21) shows how $f_{w,carb}$ can be calculated independently of $f_{w,org}$. By assuming $f_{w,volc}$ and $\delta_{w,carb}$, $\delta_{w,org}$, and $\delta_{w,volc}$ are constant in Equation (20), changes in δ_w are now a function of the balance between $f_{w,carb}$ and $f_{w,org}$ so that an increase in $f_{w,carb}$ results in an equal magnitude decrease in $f_{w,org}$. This is a useful arrangement to use as volcanism is likely less variable over the time scales investigated here compared to organic carbon weathering. Equation (21) is then used to calculate $f_{w,carb}$ while $f_{w,org}$ is solved for from Equation (19). The same method can be used to make δ_w a function of $f_{w,carb}$ and $f_{w,volc}$ (holding $f_{w,org}$ constant) so that an increase in $f_{w,carb}$ results in an equal magnitude decrease in $f_{w,volc}$. Rearranging Equation (17) in terms of $f_{w,volc}$ yields

$$f_{w,volc} = \left(1 - f_{w,carb} - f_{w,org}\right) \qquad \text{Eq. (22)}$$

which, when substituted into Equation (18) yields

$$\delta_w = f_{w,carb}\left(\delta_{w,carb}\right) + \left(1 - f_{w,carb} - f_{w,org}\right)\left(\delta_{w,volc}\right) + f_{w,org}\left(\delta_{w,org}\right) \qquad \text{Eq. (23)}$$

and

$$f_{w,carb} = \frac{\left(\delta_w - \delta_{w,volc} - f_{w,org}\left(\delta_{w,org} - \delta_{w,volc}\right)\right)}{\left(\delta_{w,carb} - \delta_{w,volc}\right)} \qquad \text{Eq. (24)}$$

For the present discussion, $\delta_{w,carb}$, $\delta_{w,volc}$, and $\delta_{w,org}$ are assumed to be constant and given values of 0‰, -5‰, and -22‰, respectively (Kump & Arthur, 1999). With all other variables defined, a

change in δ_w can now be quantified as the result of changes F_w or f_w. The most general form of the box model does not assume balanced weathering:

$$\left(\frac{d\delta_{carb}}{dt}\right) = \frac{F_w\left[\left(\frac{F_{w,carb}}{F_w}\left(\delta_{w,carb}\right) + \frac{F_{w,volc}}{F_w}\left(\delta_{w,volc}\right) + \frac{F_{w,org}}{F_w}\left(\delta_{w,org}\right)\right) - \delta_{carb}\right] - F_{b,org}\Delta_B}{M_o} \quad \text{Eq. (25)}$$

Assuming balanced weathering, the two end member f_w scenarios from Equations (21,24) can be modeled as:

$$\left(\frac{d\delta_{carb}}{dt}\right) = \frac{F_w\left[\left(f_{w,carb}\left(\delta_{w,carb}\right) + f_{w,volc}\left(\delta_{w,volc}\right) + \left(1 - f_{w,carb} - f_{w,volc}\right)\left(\delta_{w,org}\right)\right) - \delta_{carb}\right] - F_{b,org}\Delta_B}{M_o} \quad \text{Eq. (27)}$$

and

$$\left(\frac{d\delta_{carb}}{dt}\right) = \frac{F_w\left[\left(f_{w,carb}\left(\delta_{w,carb}\right) + \left(1 - f_{w,carb} - f_{w,org}\right)\left(\delta_{w,volc}\right) + f_{w,org}\left(\delta_{w,org}\right)\right) - \delta_{carb}\right] - F_{b,org}\Delta_B}{M_o} \quad \text{Eq. (28)}$$

4. RESULTS

Changes in fluxes and isotope signatures of material into and out of the ocean can drive $\delta^{13}C_{carb}$ excursions. A change in isotope signatures will produce an identical result in steady state (fixed M_o) and dynamic state (free M_o) assuming the initial reservoir sizes are the same. However, changes in fluxes will produce different responses, as changes in $\delta^{13}C_{carb}$ are

dependent in part on M_o (Figure 2A). A smaller M_o (as would result from increased $F_{b,org}$ in dynamic state) will allow $\delta^{13}C_{carb}$ to change faster than in steady state. The opposite is true when M_o increases, such as during increased F_w in dynamic state. This is demonstrated in Figure 2A where the longer elevated $F_{b,org}$ proceeds, the greater the divergence in results between steady state and dynamic state. These effects are generally small when M_o is not significantly altered. The equations above do not assume steady state and are valid for a variable M_o. The following results and discussion focus on modeling in a dynamic state unless otherwise noted.

The burial of the same amount of organic carbon for different durations will produce a different peak $\delta^{13}C_{carb}$ value and a different excursion morphology with the longer durations displaying a lower slope due to the smaller distance from equilibrium (Figure 2B). Different parameters can produce a 3‰ excursion, but with different $\delta^{13}C_{carb}$ morphologies and effects on M_o (Figure 2C). Both reduced F_w and increased $F_{b,org}$ will drive $\delta^{13}C_{carb}$ up and M_o down, but an excursion driven by decreased F_w results in a much larger drop in M_o. This is caused by the differences between δ_w and $\delta_{b,org}$ relative to $\delta^{13}C_{carb}$. The greatly reduced M_o during an excursion driven by F_w allows $\delta^{13}C_{carb}$ to change much faster. Large changes in M_o are not considered to be physically reasonable.

Changes in $F_{b,org}$, δ_w, and F_w can produce the observed 3‰ excursion, while no change in Δ can produce the required excursion magnitude as the theoretical maximum for Δ (32‰; Kump & Arthur, 1999) produces only a 0.5‰ excursion (Figure 2C).

Excursion morphology can be differentiated by whether the rising limb and falling limb are concave or convex (Figure 3). The following descriptions and discussion deal only with positive excursions driven by the forcings of $F_{b,org}$ and δ_w. The rising limb of the excursion will only be purely concave (i.e., $d^2\delta^{13}C_{carb}/dt^2$ always < 0) if forcing onset is sufficiently fast relative

to the residence time of C in the ocean. In this model, the change in forcing occurs across a single time step (5,000 yrs). The falling limb responds differently to a similar change in forcing. A rapid change in forcing (both on and off) changed across a single time step will produce a purely concave rise and a purely convex fall (Figure 3A). A gradational drop in forcing back to initial values will produce an initially concave fall, but shift to convex towards the end of the excursion (Figure 4). The exception to this case is when $F_{b,org}$ is changed gradationally to baseline values in such a way as to decrease M_o to <10 % initial values (Figure 3B, 4F). This cannot happen in steady state conditions as M_o is fixed (Figure 3B).

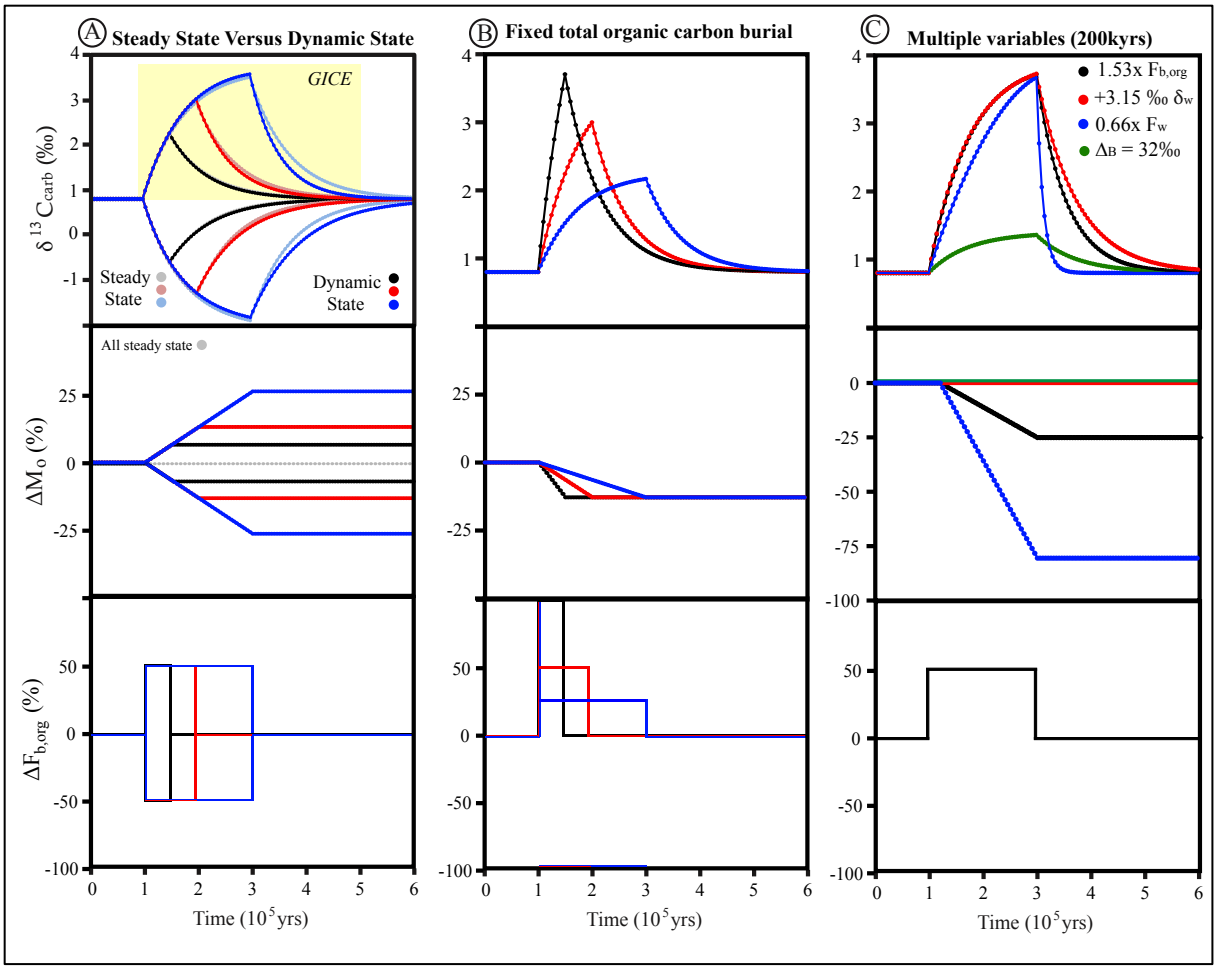

Figure 2. Box model results (lines) for various scenarios. Baseline variable values are given in Figure 1. A) Changing $F_{b,org}$ in steady state (SS) and dynamic state (DS) for three different forcing durations. This changes the absolute flux ($F_{b,org}$) equally (+50% for all positive runs and -50% for all negative runs), but yields different relative fluxes of organic carbon burial ($f_{b,org}$) depending on steady state or dynamic state assumptions (i.e., in steady state $F_{b,carb}$ decreases to balance increase increases in $F_{b,org}$ while $F_{b,carb}$ is constant in dynamic state). Yellow box represents the magnitude and inferred duration of GICE. B) Model results showing the same total organic carbon buried, but over different durations. Change in forcing was instantaneous for indicated duration. C) Four different variables with instantaneous forcing over 200 kyr in dynamic state. Δ_B increased from Phanerozoic average (~28.2‰) to theoretical maximum of 32‰ (Kump & Arthur, 1999).

A rapid, but gradational drop in forcing to *below* baseline values will produce a purely concave falling limb in both steady and dynamic states (Figure 4). Specifically, falling limbs are most concave when forcing drop is also concave, near linear when drop in forcing is linear, and slightly convex when forcing drop is convex (Figure 4).

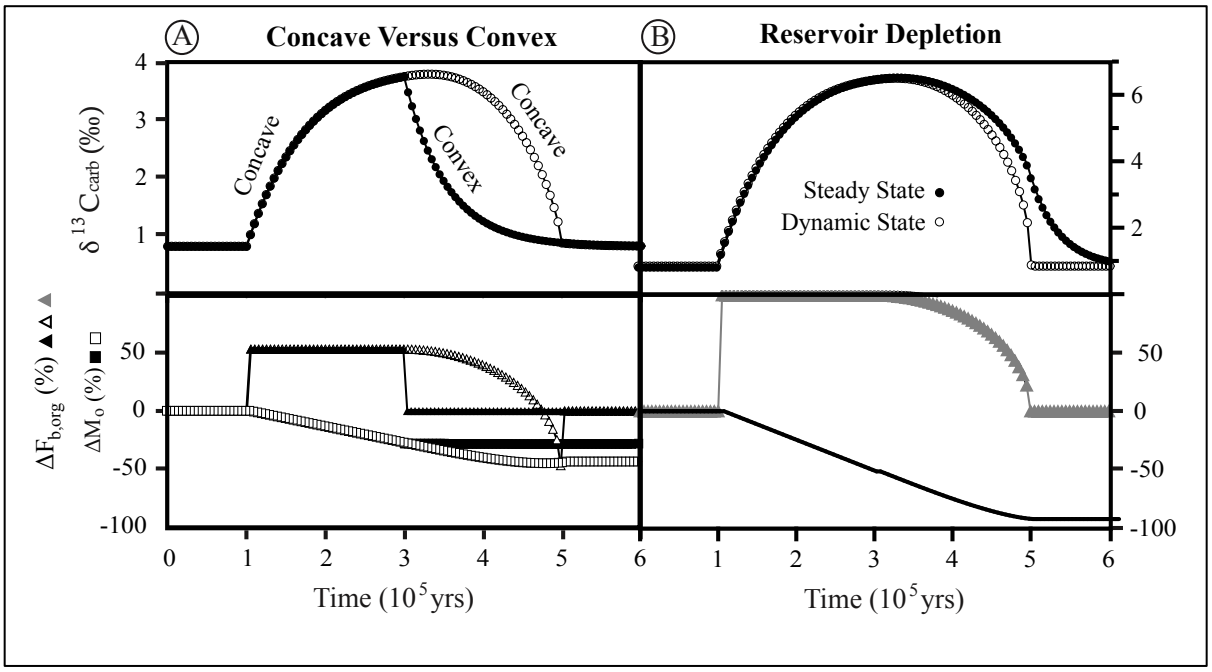

Figure 3. A) Box model results showing the difference in concave and convex rising and falling limbs of the $\delta^{13}C_{carb}$ excursion. Lower panels shows changes in relative forcing of $F_{b,org}$ and the size of the marine inorganic carbon reservoir (M_o). B) Box model results showing how dynamic state can produce a concave falling limb when the reservoir (M_o) has been significantly depleted (here to 8% of the original value). Less extreme reservoir depletions do not produce a concave excursion and further depletion of M_o results in complete depletion of the reservoir.

Simultaneous changes in $F_{b,org}$ and δ_w can also produce concave excursions. The falling limb will only be concave if $F_{b,org}$ and δ_w gradationally change together (Figure 5). An instantaneous change in $F_{b,org}$ and δ_w that is offset in time by a single time step will produce a purely convex falling limb. A gradational change in one parameter coupled with an instantaneous change in another will produce a linear or mixed concave/convex falling limb depending the how $F_{b,org}$ and δ_w are changed. Only a select set of $F_{b,org}$ and δ_w forcing combinations are shown here, but they capture important features. In general, $F_{b,org}$ and δ_w must gradationally change together and the more concave the forcing change is the more concave $\delta^{13}C_{carb}$ will be.

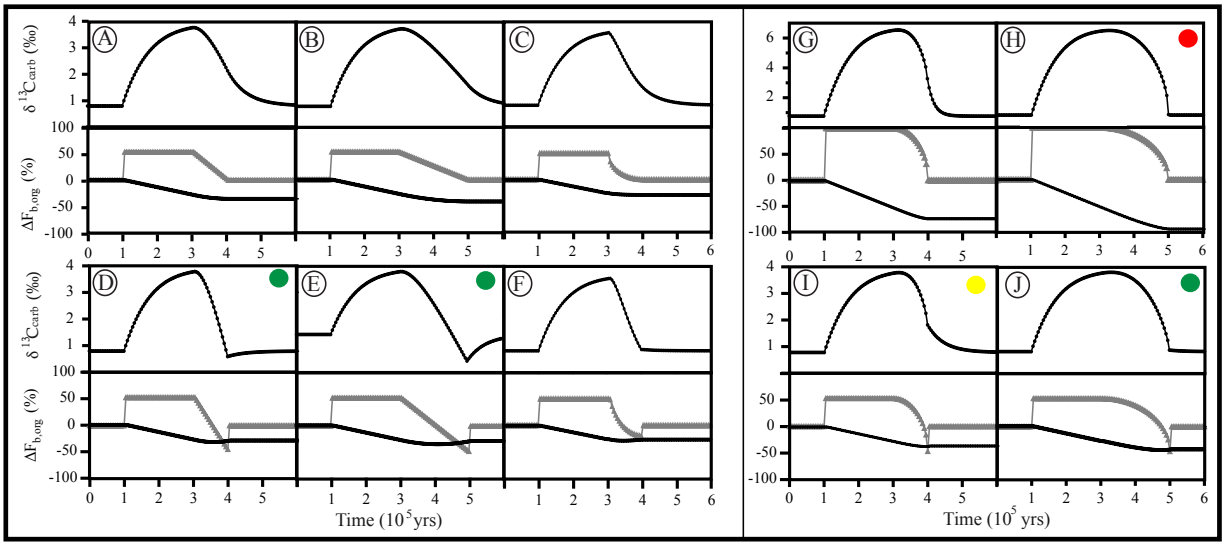

Figure 4. Model runs showing effect of changes in $F_{b,org}$ on $\delta^{13}C_{carb}$ and M_o. All models run in dynamic state. Model runs showing effect of a linear, concave, or convex drop in $F_{b,org}$ to baseline (top row) or below baseline (bottom row) values over 100 kyr (A,C,D,F,G,I) or 200 yrs (B,E,H,J). The only excursions that are purely concave (green dots) during the falling limb are those that drop $F_{b,org}$ to below baseline values or when the reservoir (M_o) is depleted to <10% of it's original value (red dot). (Yellow dots) Falling limbs that are not purely concave because of insufficient organic carbon burial before forcing was removed. Note differences in scale bar of $\delta^{13}C_{carb}$ plots.

If sedimentation rate is not constant then the morphology of $\delta^{13}C_{carb}$ through time will differ from the stratigrpahic expression of $\delta^{13}C_{carb}$. This was investigated using a model that produces a synthetic stratigraphic column with different sedimentation rates during the falling limb of the excursion. The modeled excursion was a 200 kyr pulse of increased $F_{b,org}$ (1.53x baseline). This duration and forcing magnitude was chosen because it produces a 3‰ excursion that lasts ~400 kyr. It was also chosen because it is the most concave excursion that can be produced using $F_{b,org}$ and therefore represents an endmember scenario. For a $\delta^{13}C_{carb}$ excursion

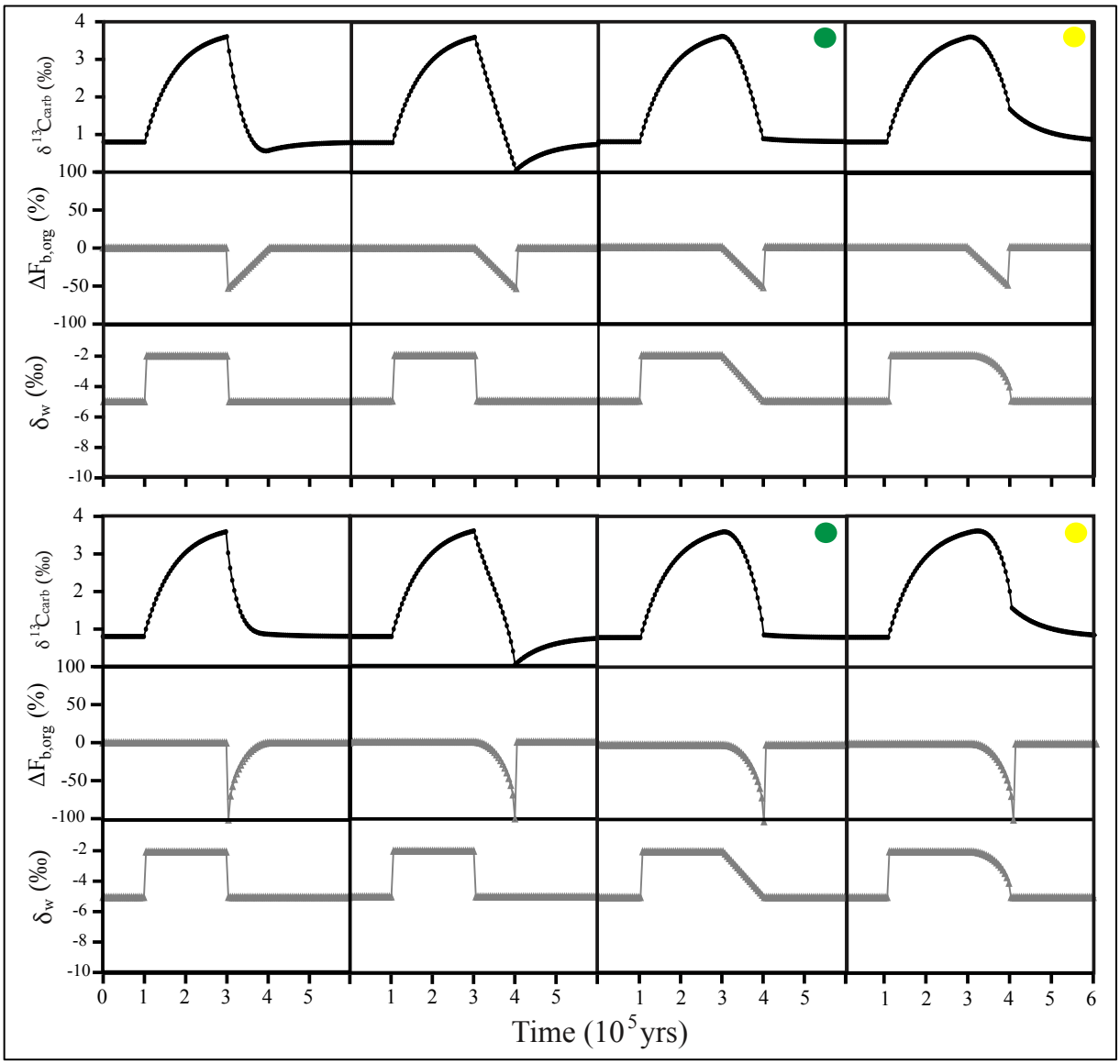

Figure 5. Box model results showing changes in $\delta^{13}C_{carb}$ due to changes in $F_{b,org}$ and δ_w. All excursions beging with a step-change in forcing and end with a step-change, linear, or exponential drop in both forcings. The falling limb of the $\delta^{13}C_{carb}$ excursion is only purely concave (i.e., $d\delta^{13}C_{carb}^2/dt^2 < 0$) when $F_{b,org}$ and δ_w decline gradationally together (green dots). Samples with yellow dots represent concave falling limbs where forcing was of insufficient magnitude to return to baseline levels before forcing was removed. Different combinations of gradiational decline in forcing produce similar results as shown here. Specifically, the more concave a forcing is, the more concave the $\delta^{13}C_{carb}$ falling limb will be.

that is convex with respect to time to appear concave with respect to height, sedimentation rate must decline at a greater rate with each time step (Figure 6). The drop in sedimentation rate means that all $\delta^{13}C_{carb}$ excursions with convex character that appear concave with respect to stratigraphic height are condensed. The sedimentation rate used was calculated from U-Pb ages of bentonites and was 1.84×10^{-2} mm/yr (Chapter 4). For the chosen $\delta^{13}C_{carb}$, sedimentation rate must exponentially decline so that the falling limb of the GICE is only 1.04 m at New London, Missouri (Chapter 2). The boundary between concave and convex is explicitly defined as when $(d\delta^{13}C_{carb}^2/dh^2) < 0$. The observed thickness of the falling limb at New London is 3.23 m.

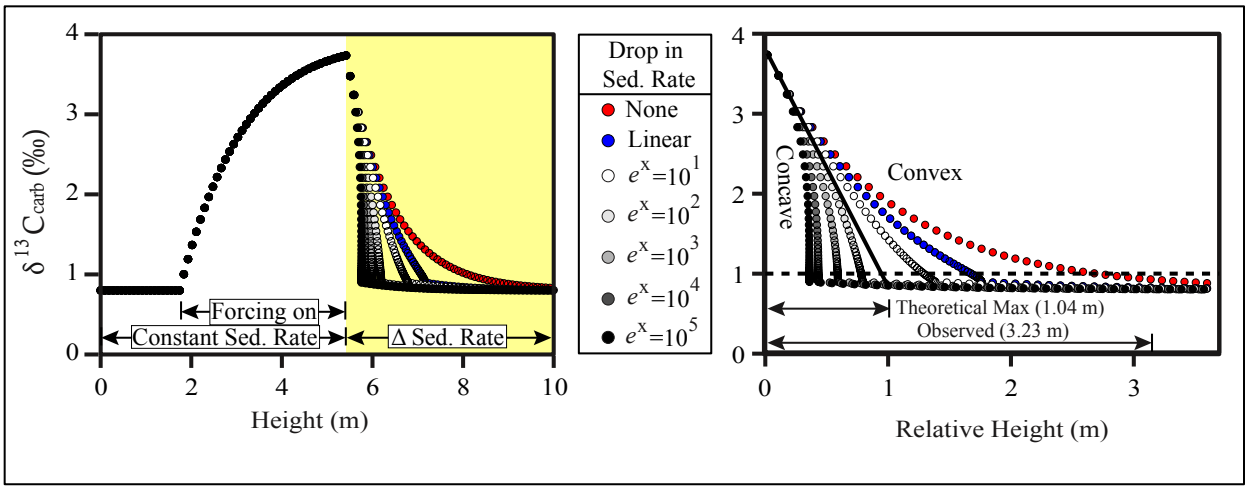

Figure 6. Guttenberg excursion modeled by increasing $F_{b,org}$ 53% for 200 kyr. Forcing was turned on and off in single time steps. Time was converted directly to height using a linear sedimentation rate calculated for New London (see text). Sedimentation rate is constant until the forcing is turned off. Different colors correspond to different sedimentation rates during falling limb of excursion. Data points show different falling limb of excursion in yellow displayed in right panel. Exponential rates (e^x = y) refer to maximum value obtained for normalization. For example, $e^x = 10^3$ refers to an exponential function that had a maximum y value of 1,000. Exponential curves with larger y values means the normalization values will represent an exponential curve with a higher proportion of large slopes. Solid line shows inflection point (linear), to the right of which is convex and to the left of which is concave. This upper limit of concavity (1.04 m) is significantly less than that observed falling limb width at study location New London. Similarly, the theoretical maximum at study location HM is 0.81 m while the observed distance is 1.6 m.

5. DISCUSSION

Model results show the GICE could be driven by changes in $F_{b,org}$, and δ_w, but exclude a changing fractionation factor (Δ) as a significant driver. Biological changes in primary producers (cell growth rate, cell geometry, cell size) that influence Δ and environmental controls on Δ (pCO_2) therefore did not drive or were only a minor influence on the GICE. Environmental shifts (e.g., CO_2) that affect $F_{b,org}$ cannot be ruled out. The remaining possible drivers of the excursion, $F_{b,org}$ and δ_w, are evaluated below.

5.1 Organic carbon burial ($F_{b,org}$)

Upwelling of nutrient-rich waters in the midcontinent of Laurentia has been hypothesized to have caused abundant phosphorite and chert deposits in the Middle and Late Ordovician (Kolata et al., 1998; Pope & Read, 1998; Pope and Steffan, 2009; Ettensohn, 2010). Upwelling has been invoked to explain the GICE as the result of increased organic carbon burial (Saltzman & Young, 2005; Young et al., 2005; Patzkowsky et al., 1997). The question then is can organic carbon burial in epeiric seas and epicontinental foreland basins drive a global $\delta^{13}C_{carb}$ excursion? To address this question we used geological data that estimate the area of Ordovician oceans (Kiessling et al., 2003) coupled with geochemical data estimating organic carbon concentration and burial rates (Berner, 1982; Kump & Arthur, 1999; Table 1). Sedimentation rates and organic carbon burial were also calculated for the study area using geochemical data (Chapters 2-4). The average sedimentation rate was calculated using sedimentation rates representative of the foreland basin calculated using U-Pb ages from Chapter 4. The average sedimentation rate (0.02 mm/yr) was obtained by an area-weighted average of three environments: the foreland basin (10% area, 0.18 mm/yr), intermediate platform and basin environments (25% area and 0.01mm/yr) and the cratonic interior (50% area and 0.00055 mm/yr. Kiessling et al. (2003) estimated that the average global extent of carbonate platforms was 1.1 x 10^7 km^2. For simplicity we used 1 x 10^7 km^2 and this is likely a significant overestimate of the sedimentary marine basins of Laurentia. Organic carbon content was chosen from modern carbonate sediments (1%, Berner, 1982) and is also likely an overestimate. If the excursion was driven by organic carbon burial alone then ~1.1 • 10^{18} extra moles of organic carbon would need to buried, equivalent to ~30% the size of the marine dissolved inorganic carbon reservoir (M_o). Table 1 shows that sedimentation rate, C_{org}, or area must increase by 10-100x to bury sufficient organic

carbon despite using parameter estimates that favor high organic carbon burial rates. It is unlikely that organic carbon concentration increased more than 5x across the platforms on average as 5% C_{org} is much higher than is commonly observed in most of the study interval (Chapter 2, Figure 6; Chapter 3, Figure 5; Young, *personal communication*). Seafloor area for carbon burial likely *decreased* during the GICE as a result of regression (Chapter 4). Sedimentation rate also could not have increased much on average across the platform as many areas do not contain the lower portions of the GICE during the sea level lowstand (Chapter 4). Therefore, current geological and geochemical data suggest that organic carbon in Laurentian cratonic seas is an untenable mechanism to drive the GICE.

The estimates used in this study are a first pass in quantifying organic carbon burial rates using stratigraphic $\delta^{13}C_{carb}$ data. The shortcomings of the estimates notwithstanding, it seems that upwelling in the Midcontinent and the proposed organic carbon burial (Pope & Steffan, 2009; Patzkowsky et al., 1997; Saltzman & Young, 2005; Young et al., 2005) are unlikely to have been the cause of organic carbon burial simply because of their low organic carbon content and low sedimentation rates. Furthermore, the most organic-rich deposits (the ones in which economically viable oil and gas deposits are found, (Kirschbaum et al., 2012; *unpublished data*) are found immediately *after* the GICE and are coincident with lower (but still positive) $\delta^{13}C_{carb}$ values of 0-1‰. This provides more geological evidence that organic carbon burial on the Laurentian platform is not the dominant control on the GICE. The uncoupled nature of platform

BASELINE	Area (10^6 km^2)	Sed Rate (mm/yr)	C_{org} (wt.%)	$F_{b,org}$ (mol/yr)	% Global burial	Target $F_{b,org}$ extra (mol/yr)	Target duration (years)
	10	0.02	1	1.92E11	1.9	1.1E18	2.0E5

EXCURSION	Multiplier	Parameter	$F_{b,org}$ (mol/yr)	Exra $F_{b,org}$ (mol/yr)	% Global burial	Time to bury extra (years)	Time to bury (Multiples)
	2	SR,C_{org}, or Area	3.8E11	1.9E11	3.8	5.7E6	27.7
	10	SR,C_{org}, or Area	1.9E12	1.9E12	19.2	6.4E5	2.2
	100	SR,C_{org}, or Area	1.9E13	1.9E13	192.0	5.8E4	-0.7
	2	SR + C_{org}	7.7E10	5.8E10	7.7	1.9E6	8.6
	5	SR + C_{org}	4.8E12	4.6E12	47.2	2.4E5	0.2
	10	SR + C_{org}	1.9E13	1.9E13	192.0	5.8E4	-0.7
	2 (SR + C_{org})	0.5 (Area)	9.6E11	7.7E11	10.0	1.4E6	6.2

Table 1. Area approximately equivalent to mean global carbonate platform area in Ordovician (Kiessling et al., 2003). Sedimentation rate (SR) calculated from different sections (see Discussion). C_{org} wt. % from Berner, (1982). Extra $F_{b,org}$ calculated from 3‰ excursion in Figure 2A. Percent global burial referes to organic carbon burial relative to estimated global flux of 1 x 10^{13} moles/yr (Kump & Arthur, 1999).

organic carbon burial and global $\delta^{13}C_{carb}$ could in part be due to the fact that in the modern ocean the majority of organic carbon burial occurs in deltas (Berner, 1982). While carbonate platforms may have served as primary repositories for the body fossils of metazoa, but they were not similarly important in storing the organic components of life.

5.2 Weathering ($F_{b,org}$ and δ_w)

The GICE is coincident with an initial regression during the rising limb of the excursion and a transgression during the falling limb (Chapter 4). These sea level changes may have had great effects on weathering fluxes and their isotopic signatures (δ_w). This is the result of the extremely low slope of the basin (often 0.01-0.001°) and the widespread carbonate deposits that underlie much of the equatorial and subequatorial oceans (Ronov, 1994; Kiessling et al., 2003).

A small sea level fall would result in the exposure of massive regions of carbonate. Because δ_w is controlled, in part, by carbonate weathering, an increase in the fraction of weathering derived from carbonates will drive an increase in δ_w (Equation 19). Loi et al. (2010) use a backstripping procedure to argue that there was an ~25-75 m eustatic sea level fall, likely glaciogenic, in Gondwana that was concurrent with the GICE. Large regions of carbonate would then be exposed for weathering. However, an increase δ_w will be accompanied by an increase in F_w as carbonate weathering proceeds rapidly. When all the components of F_w have $\delta < \delta^{13}C_{carb}$ (as is the case in this model) then an increase in F_w will result in a *drop* in $\delta^{13}C_{carb}$ or a negligible change in $\delta^{13}C_{carb}$. This is because all the components of F_w have $\delta < \delta^{13}C_{carb}$ in this model. Therefore, if there is no synchronous decrease in the weathering of other components then no increase in $F_{w,carb}$ can drive a positive $\delta^{13}C_{carb}$ excursion (Figure 9). If the weathering is balanced (i.e., fixed absolute total F_w, variable relative total f_w) then an excursion can be easily driven by an increase in $F_{w,carb}$ (Figure 7). If the GICE was driven by elevated δ_w during sea level lowstand, the weathering flux would have had to be balanced and balanced weathering has been proposed to explain the End Ordovician Hirnantian isotope excursion (Kump et al., 1999).

Increases in the absolute weathering flux (driven by increases in $F_{b,carb}$) may significantly alter ocean chemistry in such a way as to alter $F_{b,carb}$, $F_{b,org}$, or Δ. We have not quantitatively evaluated how the ocean would response to such a flux, but more sophisticated models that track carbonate saturation states and detailed biological feedbacks may help in discriminating between whether F_w or f_w is a more realistic parameter to use.

As mentioned above, it has been proposed that the Hirnantian glaciation may have driven a large $\delta^{13}C_{carb}$ excursion as a result of increased δ_w (Kump et al., 1999). Sea level during the recent Pleistocene glacial-interglacial cycles is thought to vary > 100 m. The relative dearth of

carbonate platforms in the Pleistocene means a change in sea level is unlikely to produce the same magnitude increase in $F_{w,carb}$ as predicted for the Ordovician. Rather, large drops in sea level during the Pleistocene glacials partially exposed coastal deltas (e.g., southeastern Asia, Louisiana), environments that are thought to store the majority of organic carbon (Berner, 1982), which may have increased $F_{w,org}$ and driven negative $\delta^{13}C_{carb}$ excursions. Small (0.5-1.0‰) negative excursions are in fact coincident with decreases in temperature and/or increases in ice volume (Raymo et al., 1997). This is consistent with significant variations in $F_{w,org}$ over short time scales, but could also be due to other processes such as changes in ocean mixing patterns (Raymo et al., 1997; Sigman & Boyle, 2000).

5.3 Excursion Morphology

Like many other positive $\delta^{13}C_{carb}$ excursions (e.g., Gill et al., 2007; Keller et al., 2004; Mitchell et al., 1996; Maloof et al., 2010; Zachos et al., 2001; Cramer et al., 2010; Sabatino et al., 2013; Burns & Matter, 1993), both the rising and falling limbs of the GICE are concave with respect to stratigraphic height (Figure 7). Assuming that the constant sedimentation rate calculated for New London reasonably represents the actual sedimentation history of New London, the $\delta^{13}C_{carb}$ excursion morphology can be interpreted to constrain mechanisms and the tempo of the forcing that drove the excursion. The rising limb at New London is interpreted to be concave, although moderate alteration during the rising limb of the GICE requires some extrapolation from noisy data (Chapter 2). The qualitative fit drawn in Figure 7 is based on the highest $\delta^{13}C_{carb}$, which are those believed to be least-altered (Chapter 2). Many unambiguous GICE sections in Laurentia show a concave rising limb (Patzkwosky et al., 1997; Young et al., 2005; Chapter 3; Chapter 4) in areas of low and high sedimentation rates. The continuous (but

noisy) rising limb suggests that no large gap in time is present. Acknowledging the imperfect record during the rising limb at New London, the sedimentation rate calculated for New London and shape of the rising limb suggest a rapid change in forcing.

An equal drop in forcing does not produce a $\delta^{13}C_{carb}$ drop that mirrors the rise (Figure 3), requiring that the change in forcing during the falling limb be different than that of the rising limb to generate a similar morphology. If only a single parameter is changing during the falling limb then the purely concave shape must result from a *gradational* change in forcing to *below* the pre-excursion baseline. The two exceptions to this are an increase in $F_{b,org}$ or a decrease in F_w that deplete the carbon reservoir to <10% of its initial values. We see no evidence to suggest a near complete depletion of the carbon reservoir (which would likely result in a major extinction and drop in carbonate deposition) and exclude this as a possibility.

If the GICE was driven by increased δ_w during balanced weathering, then δ_w must briefly drop farther below baseline values during the end of the excursion than it increased above baseline during the peak of the excursion (Figure 7). The carbonate weathering hypothesis predicts the exposure of carbonate platforms during sea level lowstand which are rapidly weathered into the ocean (*sensu* Kump et al., 1999). The sea level curve proposed in Chapter 4 is consistent with this hypothesis; however, the concave shape requires that δ_w decouple from the sea level curve and no mechanism is known that would drop δ_w to the necessary values. Alternatively, this decoupling could be the result of a sea level curve that does not accurately reflect true sea level change. If the excursion were driven by $F_{b,org}$ then a ~50% increase in organic burial must be followed by a drop to ~25% below baseline values. $F_{b,org}$ could be related to temperature where the microbially mediated oxidation of organic matter is sensitive to temperature while primary production is less so, resulting in increased organic carbon burial

efficiency during colder periods (Finnegan et al., 2012). This hypothesis suggests a coupling of $F_{b,org}$ and temperature. If sea level in this interval is also a function of temperature-dependent ice volume, then $F_{b,org}$ should also be roughly correlated with sea level. The drop in $F_{b,org}$ below baseline at the end of the GICE is consistent with a larger increase in respiration rate for a rise in temperature than drop in respiration rate for an equal drop in temperature (Finnegan et al., 2012). This mechanism could be tested by establishing high-resolution temperature and/or ice volume proxies (e.g., $\delta^{18}O_{PO4}$, Δ^{47} through the study interval.

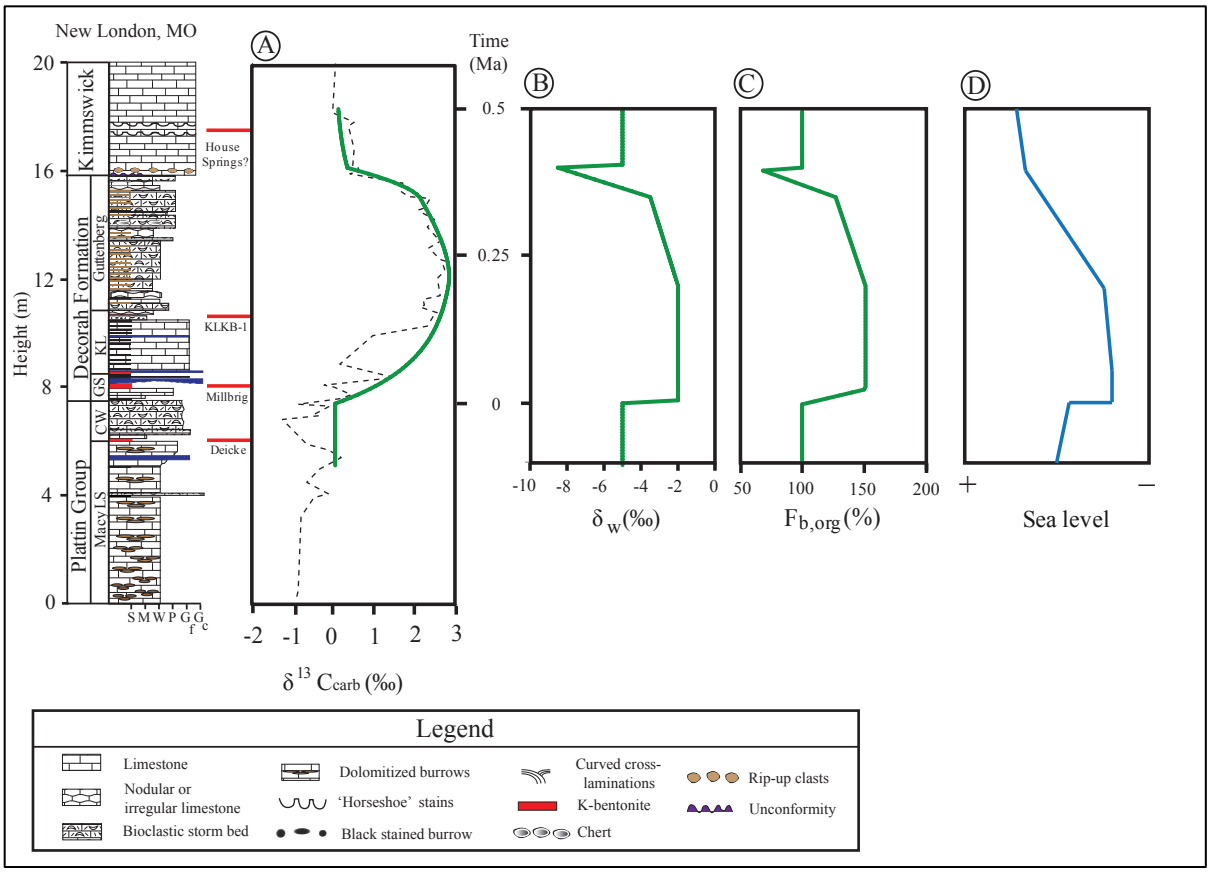

Figure 7. Qualitative fit for model results (A-C) in dynamic state assuming a change in only a single parameter δ_w and $F_{b,org}$. Data fit to match least-altered $\delta^{13}C_{carb}$ values in altered zone (~6m-10m). δ_w is plotted during "balanced" weathering where F_w is constant, but f_w is not. Sea level curve (D) based on facies changes correlates closely with the sea level curve determined for the Taconic Foreland Basin (Chapter 4). A step-change in sea level at ~7m corresponds to facies change associated with sea level drop. Time is estimated based on linear sedimentation rate where time = 0 half way between the Deicke and Millbrig K-bentonites (two lowermost K-bentonites) and the House Springs K-bentonite is ~0.5 Myr younger. This is done because the Deicke and Millbrig yield statistically indistinguishable ages and the House Springs in this section is a very thin (<1 cm) clay parting and correlated with the confirmed House Springs K-bentonite at Highway MM location (Chapter 2). The bentonite at ~11m was previously correlated to the Bentonite KLKB-1, which was dated to be ~0.25 Myr younger than the Deicke and Millbrig K-bentonites (Chapter 2). The offset between the calculated 0.25 Myr mark using a continuous, constant sedimentation rate and KLKB-1 does not significantly change interpretations of this figure. B and C show changes in parameters δ_w and $F_{b,org}$ that produce the same $\delta^{13}C_{carb}$ signal in (A). CW = Castlewood Limestone, GS = Glencoe Shale, KL = Kings Lake Limestone, LS = Limestone. See Chapter 2 for discussion of geology and global stratigraphic correlations.

A change in both $F_{b,org}$ and δ_w can also drive an excursion. If both parameters track sea level and co-vary back to baseline during the falling limb of the excursion the coeval change in both parameters reduces the magnitude of change in both parameters when compared to each

changing alone, but it will not produce a purely concave falling limb of the excursion. Therefore, the same problem remains as when one parameter drives the excursion, namely, at least one parameter must drop below baseline for a brief period. The sedimentation rate model may offer some insight into this problem. It was shown that conversion of a purely convex $\delta^{13}C_{carb}$ trend vs. time to a purely concave trend vs. height requires extensive stratigraphic condensation (Figure 6). However, many different forcing patterns produce $\delta^{13}C_{carb}$ signals that are concave until near the end of the excursion (e.g., Figure 4A,B,E). The rate of change in $\delta^{13}C_{carb}$ with respect to height is greatest near the end of the excursion. The Guttenberg Limestone does not show obvious signs of condensation except perhaps during the last meter (where $d\delta^{13}C_{carb}/dh$ is greatest), where beds thin. This interval at New London correlates to a series of five thin beds of different facies cemented together and bearing rip-up clasts (Chapter 2; Figure 4G). No consensus on the nature of the contact between the Guttenberg Limestone and the overlying Kimmswick exists. It may be a submarine unconformity showing signs of submarine scour during transgression (Kolata et al., 1998; D.R. Kolata, 2011, *personal communicati*on; Chapter 4). Rapid transgression can starve sediments, resulting in condensation as has been argued for this time interval in the midcontinent (Kolata et al., 1998). Condensation could also occur during regression/lowstand due to a decrease in accommodation space (Coe et al., 2005).

The apparent constant sedimentation rate during the GICE suggests that no large hiatuses in deposition or changes in sedimentation rate are present unless they are balanced by opposite changes in sedimentation rate. The general morphology of the $\delta^{13}C_{carb}$ curve at New London is similar to that of rapidly subsiding sections of the Taconic Foreland Basin (Young et al., 2005; Chapter 3), which is also consistent with a relatively constant sedimentation rate. Nevertheless,

condensation may occur during the last meter or so of the excursion. If the last meter of the excursion were nearly completely condensed to ~0 m, this would represent only ~10% of the duration of the interval. Such a process could explain the strong linear agreement in U-Pb ages and stratigraphic height, but also the $\delta^{13}C_{carb}$ morphology. The forcing exercises from this chapter and geologic evidence suggest that the majority of the excursion is coincident with a relatively constant sedimentation rate accompanied by a minor condensation event at the end. Therefore, no unique evidence exists supporting any one specific pattern in forcing(s). Rather, the results of this study suggest that the falling limb of the excursion was driven by a gradual change in forcing while change during the rising limb may have been more rapid.

6. CONCLUSIONS

A carbon cycle box model and recent chronological constraints were used to constrain the source of the Guttenberg isotopic carbon excursion (GICE). The conclusions below apply to the GICE, but also have broader implications for the biogeochemical carbon cycle and the interpretation of the $\delta^{13}C_{carb}$ record.

1. If the GICE represents only organic carbon burial ($F_{b,org}$), then an additional ~1.1 x 10^{18} moles of carbon were buried, equivalent to ~30% of the marine inorganic carbon reservoir.
2. Organic carbon burial likely occurred in deltas and marginal marine settings. Upwelling and organic carbon burial within epeiric seas is not a likely mechanism for the GICE.
3. $F_{b,org}$ may be strongly influenced by global changes in temperature-dependent marine microbial respiration rates.

4. An increase in the isotopic signature of the weathering flux due to increased weathering during sea level lowstand is consistent with our sea level curve, but requires balanced weathering.
5. A sedimentation rate model that converts $\delta^{13}C_{carb}$ signals through time to stratigraphic height strongly suggests that the change in forcing during the falling limb was gradual. The change in forcing is interpreted to have been more gradual that the rising limb of the excursion.

7. ACKNOWLEDGEMENTS

This work benefited from discussions with Alex Bradley (Washington University in Saint Louis), Steven Chemtob (Washington University in Saint Louis), Catherine Rose (Trinity College Dublin), Francis Macdonald (Harvard University), and Seth Young (Florida State University). Thanks to Washington University's Graduate School of Arts and Sciences for a Dissertation Fellowship.

8. REFERENCES

Achab, A., Asselin, E., Desrochers, A., Riva, J.F., Farley, C., 2011, Chitinozoan biostratigraphy of a new Upper Ordovician stratigraphic framework for Anticosti Island, Canada: GSA Bulletin, **v. 123**, p. 186-205.

Bergström, S. M., Xu, C., Schmitz, B., Young, S., Jia-Yu, R., Saltzman, M.R., 2009, First documentation of the Ordovician Guttenberg $\delta^{13}C$ excursion (GICE) in Asia: chemostratigraphy of the Pagoda and Yanwashan formations in southeastern China: Geological Magazine, **v. 146**, no. 1, p. 1-11.

Bergström, S. M., Huff, W.D., Saltzman, M.R., Kolata, D.R., Leslie, S.A., 2004, The greatest volcanic ash falls in the Phanerozoic: Trans-Atlantic relations of the Ordovician Millbrig and Kinnekulle K-bentonites: The Sedimentary Record, **v. 2**, no. 4, p. 4-8.

Bergstrom, S. M., Agematsu, S., Schmitz, B., 2010, Global Upper Ordovician correlation by means of $\delta^{13}C$ chemostratigraphy: implications of the discovery of the Guttenberg $\delta^{13}C$ excursion (GICE) in Malaysia: Geological Magazine, **v. 147**, no. 5, p. 641-651.

Berner, R. A., 1982, Burial of organic carbon and pyrite sulfur in the modern ocean: Its geochemical and environmental significance: American Journal of Science, v. **282**, p. 251-473.

Bintanja, R., van de Wal, R.S.W., Oerlemans, J., 2005, Modeled atmospheric temperatures and global sea levels over the past million years: Nature, **v. 437**, p. 125-128.

Brenchley, P. J., Carden, G.A.F., Hints, L., Kaljo, D., Marhsall, J.D., Martma, T., Meidla, T., Nolvak, J., 2003, High-resolution stable isotope stratigraphy of Upper Ordovician sequences: Constraints on the timing of bioevents and environmental changes associated with mass extinction and glaciation: GSA Bulletin, **v. 115**, p. 89-104.

Burns, S. J., Matter, A., 1993, Carbon isotopic record of the latest Proterozoic from Oman: Eclogae Geologicae Helvetiae, **v. 86**, p. 595-607.

Bowen, G. J., Zachos, J.C., 2010, Rapid carbon sequestration at the termination of the Palaeocene-Eocene Thermal Maximum: Nature Geoscience, v. **3**, p. 866-869.

Broecker, W. S., Peng, T.H., 1974, Gas exchange rates between air and sea: Tellus, **v. 26**, p. 22-35.

Canfield, D. E., 2005, The early history of atmospheric oxygen: Homage to Robert M. Garrels: Annual Review of Earth and Planetary Sciences, v. **33**, p. 1-36.

Coe, A. L., 2005, The Sedimentary Record of Sea-Level Change, Cambridge, UK, Cambridge University Press, p. 287.

Cramer, B. D., Loydell, D.K., Samtleben, C., Munnecke, A., Kaljo, D., Maennik, P., Martma, T., Jeppsson, L., Kleffner, M.A., Barrick, J.E., Johnson, C.A., Emsbo, P., Joachimski, M.M., Bickert, T., Saltzman, M.R., 2010, Testing the limits of Paleozoic chronostratigraphic correlation via high-resolution (<500 k.y.) integrated conodont, graptolite, and carbon isotope ($\delta^{13}C_{carb}$) biochemostratigraphy across the Llandovery-Wenlock (Silurian) boundary: Is a unified Phanerozoic time scale achievable?: GSA Bulletin, **v. 122**, p. 1700-1716.

Ettensohn, F. R., 2010, Origin of Late Ordovician (mid-Mohawkian) temperate-water conidtions on southeastern Laurentia: Glacial or tectonic?, *in* Finney, S. C., Berry, W.B.N., ed., GSA Special Paper **466**, p. 163-175.

Frakes, L. A., Francis, J.E., Syktus, J.I., 1992, Climate Modes of the Phanerozoic, Great Britian, Press Syndicate of the University of Cambridge.

Finnegan, S., Bergmann, K., Eiler, J.M., Jones, D.S., Fike, D.A., Eisenman, I., Hughes, N.C., Tripati, A.K., Fischer, W.W., 2011, The Magnitude and Duration of Late Ordovician–Early Silurian Glaciation: Science, **v. 331**, p. 903-906.

Finnegan, S., Fike, D.A., Jones, D., Fischer, W.W., 2012, A temperature-dependent feedback on the magnitude of carbon isotope excursions: Geoscience Canada, **v. 39**, p. 122-131.

Freeman, K. H., Hayes, J. M., 1992, Fractionation of carbon isotopes by phytoplankton and estimates of ancient CO_2 levels: Global Biogeochemical Cycles, **v. 6**, p. 185-198.

Gill, B. C., Lyons, T.W., Saltzman, M.R., 2007, Parallel, high-resolution carbon and sulfur isotope records of the evolving Paleozoic marine sulfur reservoir: Palaeogeography Palaeoclimatology Palaeoecology, **v. 256**, p. 156-173.

Hatch, J. R., Jacobson, S. R., Witzke, B. J., Risatti, J. B., Anders, D. E., Watney, W. L., Newell, K. D., and Vuletich, A. K., 1987, Possible late Middle Ordovician organic-carbon isotope excursion - Evidence from Ordovician oils and hydrocarbon source rocks, midcontinent and east-central United States: American Association of Petroleum Geologists Bulletin, **v. 71**, p. 1342-1354.

Hurtgen, M., Pruss, S.B., Knoll, A.H., 2009, Evaluating the relationship between the carbon and sulfur cycles in the later Cambrian ocean: An example from the Part au Port Group, western Newfoundland, Canada: Earth and Planetary Science Letters, v. **281**, p. 288-297.

Jones, D. S., Fike, D.A., 2013, Dynamic sulfur and carbon cycling through the end-Ordovician extinction revealed by paired sulfate-pyrite $\delta^{34}S$: Earth and Planetary Science Letters, **v. 363**, p. 144-155.

Kaljo, D., Martma, T., Saadre, T., 2007, Post-Hunnebergian Ordovician carbon isotope trend in Baltoscandia, its environmental implications and some similarities with that of Nevada: Palaeogeography Palaeoclimatology Palaeoecology**, v. 245**, p. 138-155.

Katz, M. E., Wright, J.D., Miller, K.G., Cramer, B.S., Fennel, K., Falkowski, P.G., 2005, Biological overprint of the geological carbon cycle: Marine Geology, **v. 217**, p. 323-338.

Keller, G., Berner, Z., Adatte, T., Stueben, D., 2004, Cenomanian-Turonian and $\delta^{13}C$, and $\delta^{18}O$, sea level and salinity variations at Pueblo, Colorado, **v. 211**, p. 19-43.

Kiessling, W., Flügel, E., Golonka, J., 2003, Patterns of Phanerozoic carbonate platform sedimentation: Lethaia, **v. 36**, p. 195-226.

Kirschbaum, M. A., Schenk, C.J., Cook, Ryder, R.T., Charpentier, R.R., Klett, T.R., Gaswirth, S.B., Tennyson, M.E., Whidden, K.J., 2012, Assessment of Undiscovered Oil and Gas Resources of the Ordovician Utica Shale of the Appalachian Basin Province, 2012: U.S. Geological Survey, 3116.

Kolata, D. R., Huff, W.D., Bergström, S.M., 1998, Nature and regional significance of unconformities associated with the Middle Ordovician Hagan K-bentonite complex in the North American midcontinent: GSA Bulletin, **v. 110**, p. 723-739.

Kump, L., R., Arthur, M.A., 1999, Interpreting carbon-isotope excursions: carbonates and organic matter: Chemical Geology, v. **161**, p. 181-198.

Kump, L. R., Arthur, M.A., Patzkowsky, M.E., Gibbs, M.T., Pinkus, D.S., Sheehan, P.M., 1999, A weathering hypothesis for glaciation at high atmospheric pCO_2 during the Late Ordovician: Palaeogeography Palaeoclimatology Palaeoecology, **v. 152**, p. 173-187.

Lefebvre, V., Servais, T., Francois, L., Averbuch, O., 2010, Did a Katian large igneous province trigger the Late Ordovician glaciation? A hypothesis tested with a carbon cycle model: Palaeogeography Palaeoclimatology Palaeoecology, **v. 296**, p. 310-319.

Loi, A., Ghienne, J.L., Dabard, M.P., Paris, F., Botquelen, A., Christ, N., Elaouad-Debbaj, Z., Gorini, A., Vidal, M., Videt, B., Destombes, J., 2010, The Late Ordovician glacio-eustatic record from a high-latitude storm-dominated shelf-succession: The Bou Ingarf section (Anti-Atlas, Southern Morocco): Palaeogeography Palaeoclimatology Palaeoecology, **v. 296**, p. 332-358.

Ludvigson, G. A., Jacobson, S.R., Witzke, B.J., Gonzàlez, L.A., 1996, Carbonate component chemostratigraphy and depositional history of the Ordovician Decorah Formation, Upper Mississippi Valley: Geological Society of America Special Paper, **v. 306**, p. 67-86.

Ludvigson, G. A., Witzke, B.J., Gonzàlez, L.A., Carpenter, S.J., Schneider, C.L., Hasiuk, F., 2004, Late Ordovician (Turnian-Chatfieldian) carbon isotope excursions and their stratigraphic and paleoceanographic significance: Palaeogeography, Palaeoclimatology, Palaeoecology, **v. 210**, p. 187-214.

Maloof, A. C., Schrag, D.P., Crowley, J.L., and Bowring, S.A., 2005, An expanded record of Early Cambrian carbon cycling from the Anti-Atlas Margin, Morocco: Canadian Journal of Earth Science, v. **42**, p. 2195-2216.

Maloof, A. C., Porter, S. M., Moore, J. L., Dudas, F. O., Bowring, S. A., Higgins, J. A., Fike, D. A., and Eddy, M. P., 2010a, The earliest Cambrian record of animals and ocean geochemical change: Geological Society of America Bulletin, v. **122**, no. 11-12, p. 1731-1774.

Maloof, A. C., Ramezani, J., Bowring, S.A., Fike, D.A., Porter, S.M., Mazouad, M., 2010b, Constraints on early Cambrian carbon cycling from the duration of the Nemakit-Daldynian—Tommotian boundary $\delta^{13}C$ shift, Morocco: Geology, **v. 38**, p. 623-626.

Schulte, P., Alegret, L., Arenillas, I., Arz, J. A., Barton, P. J., Bown, P. R., Bralower, T. J., Christeson, G. L., Claeys, P., Cockell, C. S., Collins, G. S., Deutsch, A., Goldin, T. J., Goto, K., Grajales-Nishimura, J. M., Grieve, R. A. F., Gulick, S. P. S., Johnson, K. R., Kiessling, W., Koeberl, C., Kring, D. A., MacLeod, K. G., Matsui, T., Melosh, J., Montanari, A., Morgan, J. V., Neal, C. R., Nichols, D. J., Norris, R. D., Pierazzo, E., Ravizza, G., Rebolledo-Vieyra, M., Reimold, W. U., Robin, E., Salge, T., Speijer, R. P., Sweet, A. R., Urrutia-Fucugauchi, J., Vajda, V., Whalen, M. T., and Willumsen, P. S., 2010, The Chicxulub Asteroid Impact and Mass Extinction at the Cretaceous-Paleogene Boundary: Science, v. **327**, no. 5970, p. 1214-1218.

Martma, T., 2005, Ordovician carbon isotopes: Estonian Geological Sections, Kerguta (564) Drill Core: Geological Survey of Estonia Bulletin, **v. 7**, p. 25-30.

Metzger, J. G., Fike, D.A., 2013, Techniques for assessing spatial heterogeneity of carbonate $\delta^{13}C$ values: Implications for craton-wide isotope gradients: Sedimentology, **v. 60, p**. 1405-1431.

Metzger, J. G., Fike, D.A., Smith, L.B., 2014, Applying C-isotope Stratigraphy using Well Cuttings for High-Resolution Chemostratigraphic Correlation of the Subsurface *in* Smith, L. B., ed., AAPG Bulletin Special Volume in Honor of Fred Read, **v. 98**, American Association of Petroleum Geologists, p. 1551-1576.

Mitchell, S. F., Paul, C.R.C., Gale, A.S., 1996, Carbon isotopes and sequence stratigraphy, *in* Howell, J. A., Aitken, J.F., ed., Geological Society Special Publication No. 104: High Resolution Sequence Stratigraphy: Innovations and Applications: London, The Geological Society.

Munnecke, A., Zhang, Y. L., Cheng, J., 2011, Stable carbon isotope stratigraphy in the Ordovician of South China: Palaeogeography Palaeoclimatology Palaeoecology, **v. 307**, p. 17-43.

Page, A. A., Zalasiewicz, J.A., Williams, M., Popov, L.E., 2007, Were transgressive black shales a negative feedback modulating glacioeustasy in the Early Palaeozoic Icehouse?, *in* Williams, M., Haywood, A.M., Gregory, F.J., Schmidt, D.N., ed., Deep-Time Perspectives on Climate Change: Marrying the Signal from Computer Models and Biological Proxies: London, The Geological Society of London, p. 123-156.

Pancost, R. D., Freeman, K. H., and Patzkowsky, M. E., 1999, Organic-matter source variation and the expression of a late Middle Ordovician carbon isotope excursion: Geology, **v. 27**, no. 11, p. 1015-1018.

Pancost, R. D., Freeman, K.H., Herrmann, A.D., Patzkowsky, M.E., Ainsaar, L., Martma, T., 2013, Reconstructing Late Ordovician carbon cycle variations: Geochimica et Cosmochimica Acta, **v. 104**, p. 433-454.

Patzkowsky, M. E., Slupik, L.M., Arthur, M.A., Pancost, R.D., Freeman, K.H., 1997, Late Middle Ordovician environmental change and extinction: Harbinger of the Late Ordovician or continuation of Cambrian patterns?: Geology, **v. 25**, p. 911-914.

Pope, M., Read, J.F., 1998, Ordovician metre-scale cycles: implications for climate and eustatic fluctuations in the central Appalachians during a global greenhouse, non-glacial to glacial transition: Palaeogeography Palaeoclimatology Palaeoecology, **v. 138**, p. 27-42.

Pope, M., Steffan, J.B., 2009, Widespread, prolonged late Middle to Late Ordovician upwelling in North America: A proxy record of glaciation?: Geology, **v. 31**, p. 63-66.

Raymo, M. E., Oppo, D.W., Curry, W., 1997, The mid-Pleistocene climate transition: A deep sea carbon isotopic perspective: Paleoceanography, v. **12**, p. 546-559.

Ronov, A. B., 1994, Phanerozoic transgressions and regressions on the continents: A quantitative approach based on areas flooded by the sea and areas of marine and continental deposition: American Journal of Science, **v. 294**, p. 777-801.

Sabatino, N., Vlahović, Jenkyns, H.C., Scopelliti, G., Neri, R., Prtoljan, B., Velić, I., 2013, Carbon-isotope record and palaeoenvironmental changes during the early Toarcian oceanic anoxic event in shallow-marine carbonates of the Adriatic Carbonate Platform in Croatia: Geological Magazine, **v. 150**, p. 1085-1102.

Saltzman, M. R., Young, S.A., 2005, Long-lived glaciation in the Late Ordovician? Isotopic and sequence-stratigraphic evidence from western Laurentia: Geology, **v. 33**, no. 2, p. 109-112.

Sigman, D. M., Boyle, E.A., 2000, Glacial/interglacial variations in atmospheric carbon dioxide: Nature, v. **407**, p. 859-869.

Young, S. A., Saltzman, M.R., Bergström, S.M., 2005, Upper Ordovician (Mohawkian) carbon isotope ($\delta^{13}C$) stratigraphy in eastern and central North America: Regional expression of a perturbation of the global carbon cycle: Palaeogeography, Palaeoclimatology, Palaeoecology, **v. 222**, p. 53-76.

Young, S. A., Saltzman, M. R., Bergstrom, S. M., Leslie, S. A., and Xu, C., 2008, Paired $\delta^{13}C_{carb}$ and $\delta^{13}C_{org}$ records of Upper Ordovician (Sandbian-Katian) carbonates in North America and China: Implications for paleoceanographic change: Palaeogeography Palaeoclimatology Palaeoecology, **v. 270**, no. 1-2, p. 166-178.

Young, S. A., Saltzman, M.R., Foland, K.A., Linder, J.S., Kump, L.R., 2009, A major drop in seawater $^{87}Sr/^{86}Sr$ during the Middle Ordovician (Darriwilian): Links to volcanism and climate?: Geology, **v. 37**, no. 10, p. 951-954.

Zachos, J., Pagani, M. Sloan, L., Thomas, E., Billups, K., 2001, Trends, Rhythms, and Aberrations in Global Climate 65 Ma to Present: Science, **v. 292**, p. 686-693.